Wind speed and wind energy potentials over Europe: Regionalisation, decadal predictability, and long-term future changes

Inaugural-Dissertation

zur

Erlangung des Doktorgrades

der Mathematisch-Naturwissenschaftlichen Fakultät

der Universität zu Köln

vorgelegt von

Julia Mömken

aus Köln

Karlsruhe, 2018

Berichterstatter:	Prof. Dr. Joaquim Pinto
	Prof. Dr. Yaping Shao
Tag der mündlichen Prüfung:	17. November 2017

Abstract

The mitigation of climate change demands a fundamental conversion of our energy system, from a mainly fossil fuel-driven system to one with a higher share of renewable sources. For Europe, wind has emerged as an important renewable energy source with high potential. However, wind energy production is strongly influenced by weather and climate conditions, and hence subject to day-to-day, seasonal and long-term climate change. The analysis and estimation of the impact of these changes on the future wind energy production is of high importance for the development of an energy system with higher renewable energy content. The overall objective of this thesis is to investigate regional scale wind speeds and wind energy potentials over Europe at different timescales, focussing on the near-term and long-term future. With this aim, three studies are performed. The first study estimates future changes of wind energy output (*Eout*) of an exemplary wind turbine over Europe in a large multi-model ensemble. For this purpose, model output from 22 global climate models (GCMs) from CMIP5 is regionalised using a statistical-dynamical downscaling (SDD) approach. This method is based on a combination of circulation weather type (CWT) analysis and regional climate modelling with COSMO-CLM. Mean annual *Eout* is projected to increase over Northern and Central Europe and decrease over Southern Europe in the ensemble mean. However, the individual ensemble members can differ both in terms of magnitude and sign of change. Simulated future changes are more robust in seasonal terms, in which *Eout* generally increases for winter and decreases in summer. These changes lead to an enhancement of the intra-annual variability of *Eout* for most parts of Europe, which in turn results in a higher volatility of wind energy production under future climate conditions. Regarding changes in the inter-annual variability, results for the individual models vary strongly and the spatial patterns are not coherent between future periods and scenarios. The study clearly reveals an impact of climate change on wind energy potentials over Europe, but in some aspects results depend strongly on the choice of GCM. This highlights the large uncertainties between different GCMs and the importance to analyse multi-model ensembles.

The second study evaluates future changes of regional wind speed and wind energy output over Europe, this time in a dynamically downscaled ensemble. The high resolution EURO-CORDEX ensemble is based on nine GCM-RCM chains at 12 km spatial and three-hourly temporal resolution. The ensemble mean projects a weak decrease of mean annual *Eout* for most parts of Europe and a small but robust increase for the Baltic and the Aegean Sea. Differences to the previous study are primarily based on the model choice. Regarding

variability, small robust changes are simulated for inter-daily variability, while changes are larger but more uncertain for inter- and intra-annual variability of *Eout*. Both inter-daily and intra-annual variability are projected to increase for Northern, Central and Eastern Europe. In terms of wind speed characteristics relevant for wind energy production, an increased occurrence of low wind speeds is detected. The study reveals that regions like the Baltic and the Aegean Sea could profit from climate change due to a combination of increasing mean annual *Eout* and decreasing intra-annual variability. On the other hand, negative impacts are projected for regions like Germany, France and Iberia with decreasing mean *Eout* and a higher intra-annual variability.

The third study examines the decadal predictability of wind speed and wind energy potentials over Central Europe in three generations of the decadal prediction system developed within the German MiKlip ('Mittelfristige Klimaprognosen') project. The prediction system is based on the global Max-Planck-Institute Earth System Model (MPI-ESM). Uninitialised historical and yearly-initialised hindcast experiments are downscaled applying the same SDD approach as used in the first study to assess the decadal forecast skill. The three ensemble generations show some decadal forecast skill for both mean annual wind speed and *Eout*. This skill is mainly limited to the first years (1-4) after initialisation. In seasonal terms, skill scores are generally lower than for annual means with lowest values in summer and highest values in autumn. In general, differences between the individual ensemble generations are small. The regionalisation is able to preserve and sometimes increase the forecast skill from the global model, and it often improves the ensemble spread. The study identifies a dominant westerly weather type with strong pressure gradients over Central Europe as potential source for the forecast skill, showing similar MSE-based skill scores as *Eout*. Overall, results are encouraging for the installation of a decadal prediction system for Central Europe and for the utilization of such a system for wind energy applications.

This thesis extends the current knowledge on wind speed and wind energy potentials over Europe. The outcomes show that climate change affects future wind energy generation at different timescales. Future responses depend on the analysed ensembles, which consider different models and downscaling approaches. Differences arise mainly from the model choice, while the different downscaling methods provide similar climate change signals. The results proved to be important for an advanced impact study, which analysed climate change impacts on a European renewable energy system. The results on decadal predictability are encouraging for the establishment of a decadal prediction system for wind energy applications. Overall, outcomes of this thesis may be relevant for the successful integration of wind energy into our electric power system.

Zusammenfassung

Der Klimaschutz erfordert einen grundlegenden Umbau unseres Stromnetzes, von einem vorwiegend mit fossilen Brennstoffen angetriebenen System zu einem System mit höheren Anteilen an erneuerbaren Energien. In Europa hat sich Wind als wichtige und vielversprechende erneuerbare Energiequelle erwiesen. Allerdings wird die Windenergieproduktion stark von vorherrschenden Wetter- und Klimabedingungen beeinflusst und unterliegt dadurch dem Klimawandel auf täglichen, saisonalen und langfristigen Zeitskalen. Die Analyse und Abschätzung der Auswirkungen des Klimawandels auf die zukünftige Windenergieproduktion ist somit von großer Bedeutung für die Entwicklung eines Energiesystems mit einem höheren Anteil an erneuerbaren Energien.

Das Ziel dieser Arbeit ist die Untersuchung von Windgeschwindigkeiten und Windenergiepotentialen auf der regionalen Skala für Europa auf verschiedenen Zeitskalen. Der Fokus liegt dabei auf der näheren und der langfristigen Zukunft. Mit diesem Ziel werden drei Studien durchgeführt. Die erste Studie untersucht zukünftige Änderungen der Windenergieleistung (*Eout*) für eine Beispiel-Windkraftanlage in Europa in einem großen Multimodell-Ensemble. Zu diesem Zweck wurde der Modelloutput von 22 globalen Klimamodellen (GCMs) aus CMIP5 mit einem statistisch-dynamischen Downscaling-Verfahren (SDD) regionalisiert. Dieses Verfahren basiert auf einer Kombination der Analyse von „Circulation Weather Types“ (CWTs) und regionaler Klimamodellierung mit COSMO-CLM. Für den mittleren jährlichen *Eout* wird im Ensemblemittel eine Zunahme über Nord- und Mitteleuropa und eine Abnahme über Südeuropa simuliert. Allerdings können sich die einzelnen Ensemblemitglieder sowohl in der Größenordnung als auch dem Vorzeichen der Veränderung unterscheiden. Für die einzelnen Jahreszeiten sind die simulierten Änderungen robuster, mit einem generellen Anstieg von *Eout* im Winter und einer Verminderung im Sommer. Diese saisonalen Änderungen führen zu einer Verstärkung der intra-annuellen Variabilität für große Teile von Europa. Daraus resultiert wiederum eine erhöhte Unbeständigkeit der Windenergieproduktion unter künftigen Klimabedingungen. In Bezug auf Änderungen der inter-annuellen Variabilität variieren die Ergebnisse der einzelnen Modelle stark und die räumlichen Muster der verschiedenen Zeiträume und Szenarien sind nicht kohärent. Die Studie zeigt einen deutlichen Einfluss des Klimawandels auf Windenergiepotentiale über Europa. Allerdings hängen die Ergebnisse in mancher Hinsicht stark von der Wahl der GCMs ab. Dies unterstreicht die Unsicherheiten zwischen verschiedenen GCMs und die Notwendigkeit Multimodell-Ensembles zu untersuchen.

Die zweite Studie analysiert zukünftige Änderungen der regionalen Windgeschwindigkeit und Windenergieleistung über Europa, diesmal in einem dynamisch regionalisierten Ensemble. Das hochaufgelöste EURO-CORDEX Ensemble basiert auf neun GCM-RCM Modellketten mit einer Auflösung von 12 km und drei Stunden. Das Ensemblemittel simuliert eine schwache Abnahme des mittleren jährlichen *Eout* für große Teile Europas und eine schwache aber robuste Zunahme für die Ostsee und die Ägäis. Unterschiede zur vorhergehenden Studie beruhen in erster Linie auf der Auswahl der Modelle. In Bezug auf die Variabilität von *Eout* werden kleine robuste Änderungen für die Variabilität zwischen einzelnen Tagen simuliert, während die Änderungen für die inter- und intra-annuelle Variabilität stärker aber unsicherer sind. Sowohl für die zwischentägliche als auch die intra-annuelle Variabilität wird ein Anstieg über Nord-, Mittel- und Osteuropa erwartet. Außerdem ist ein vermehrtes Auftreten von Schwachwindphasen erkennbar. Die Studie zeigt, dass Regionen wie die Ostsee und die Ägäis vom Klimawandel profitieren könnten da der mittlere jährliche *Eout* zunimmt und gleichzeitig die intra-annuelle Variabilität schwächer wird. Auf der anderen Seite zeigen sich negative Auswirkungen für Regionen wie Deutschland, Frankreich und die iberische Halbinsel, wo weniger *Eout* und zeitgleich eine steigende Variabilität simuliert wird.
Die dritte Studie untersucht die dekadische Vorhersagbarkeit von Windgeschwindigkeit und Windenergiepotentialen für Mitteleuropa in drei Generationen des dekadischen Vorhersagesystems, das im Rahmen des deutschen MiKlip-Projekts („Mittelfristige Klimaprognosen“) entwickelt wurde. Das Vorhersagesystem basiert auf dem globalen Max-Planck-Institute Earth System Model (MPI-ESM). Das gleiche SDD-Verfahren wie in der ersten Studie wird genutzt, um nicht-initialisierte historische Läufe und jährlich-initialisierte Hindcast-Läufe zu regionalisieren und den dekadischen Vorhersage-Skill zu bewerten. Die drei Ensemble-Generationen zeigen eine dekadische Vorhersagbarkeit für mittlere Windgeschwindigkeiten und *Eout*. Diese Vorhersagbarkeit ist im Allgemeinen auf die ersten Jahre nach der Initialisierung (1-4) beschränkt. Für die Jahreszeiten ist der Vorhersage-Skill generell schwächer ausgeprägt als für jährliche Mittelwerte. Die schwächsten Werte zeigen sich im Sommer und die höchsten Werte im Herbst. Die Unterschiede zwischen den einzelnen Ensemble-Generationen sind allgemein klein. Die Regionalisierung ist in der Lage den Vorhersage-Skill des globalen Modells zu bewahren und in einigen Fällen zu verbessern. Außerdem wird oftmals der Ensemble-Spread verbessert. In der Studie wird eine dominante westliche Wetterklasse mit starken Druckgradienten über Mitteleuropa als mögliche Quelle für die Vorhersagbarkeit identifiziert. Diese Wetterklasse zeigt ähnliche MSE-basierte Skill Scores wie *Eout*. Insgesamt sind die Ergebnisse vielversprechend für den Aufbau eines dekadischen

Vorhersagesystems für Mitteleuropa und dessen Nutzung für Windenergie-Anwendungen. Diese Arbeit erweitert den momentane Wissensstand zu Windgeschwindigkeit und Windenergiepotentialen in Europa. Die Ergebnisse zeigen, dass der Klimawandel die zukünftige Windenergieproduktion auf verschiedenen Zeitskalen beeinflusst. Die Zukunftsprojektionen hängen dabei von den betrachteten Ensembles ab, die unterschiedliche Modelle und Regionalisierungsansätze berücksichtigen. Unterschiede ergeben sich überwiegend aus der Wahl des Modells, während die verschiedenen Regionalisierungsverfahren ähnliche Klimaänderungssignale liefern. Die Ergebnisse sind für eine weiterführende Studie von Bedeutung, die den Einfluss des Klimawandels auf ein europäisches Stromnetz, das zu 100% mit erneuerbaren Energien angetrieben wird, untersucht. Die Resultate zur dekadischen Vorhersagbarkeit sind vielversprechend für die Etablierung eines dekadischen Vorhersagesystems für Windenergie-Anwendungen. Insgesamt können die Ergebnisse dieser Arbeit für eine erfolgreiche Einbindung von Windenergie in unser bestehendes Stromnetz relevant sein.

Contents

1 Introduction

The IPCC (2013) demands a considerable reduction of greenhouse gas emissions to limit climate change. At present, the energy supply sector accounts for a large amount of global greenhouse gas emissions affecting the earth's climate (Bruckner et al., 2014). The control and reduction of these emissions through an increased share of renewable and ecologically sustainable energy sources in the global energy mix plays a key role for a successful mitigation of climate change (e.g. Solomon et al., 2007). Still, the transition from a fossil fuel-driven energy system to one with a higher share of renewables remains one of the main challenges for decision makers in politics and economy (Manwell et al., 2009). Although the potential of renewable energies exceeds the energy demand worldwide (Fischedick et al., 2011), individual renewable energy sources are restricted to certain regions due to specific weather and climate conditions. In Europe, wind energy production has a large potential as an alternative to fossil fuel sources, while other sources, like e.g. hydropower are limited in terms of application (Wiser et al., 2011). To tap the full potential of wind energy generation, the successful integration of the highly volatile wind energy into the electric system (von Bremen and Lange, 2011) and the installation of an effective network of wind power plants (Manwell et al., 2009; Wilkes et al., 2012) are of high importance. Additionally, storage and backup facilities are required to maintain electricity supply in times with low wind energy production (e.g. Rodriguez et al., 2014).

Wind energy generation depends on several factors: geographical parameters (e.g. land use; Vautard et al., 2014), economical and technical parameters (Manwell et al., 2009), as well as weather and climate conditions (e.g. atmospheric circulation, near-surface wind conditions; Pryor and Barthelmie, 2010, 2013). Hence, the energy generation is strongly fluctuating on different timescales, which has a large impact on the operation of the energy system (e.g. Huber et al., 2014; Bloomfield et al., 2016). Highly resolved forecasts and predictions of regional and local scale wind speeds and wind energy potentials are required for the actual state, the near-term future, and the long-term future. Short-term forecasts enable an estimation of the electricity supply generated from wind power plants hours and

days in advance, thus allowing to compensate fluctuations and avoiding high losses or excesses (von Bremen and Lange, 2011). These forecasts are also relevant for energy trading. Near-term forecasts on seasonal to decadal timescales fall within the planning horizon of politics and economy (e.g. Meehl et al., 2009) and are therefore of particular interest for the future development of wind energy production. Finally, climate change projections are important for long-term planning and the analysis of the potential impact of a changing climate on wind energy potentials (e.g. Pryor and Barthelmie, 2010). Several studies over the last decades have shown that both wind speeds and wind energy are sensitive to climate change (e.g. Pryor et al., 2005a,b; Barstad et al., 2012; Hueging et al., 2013; Tobin et al., 2015). These studies use different global and regional climate models (GCMs and RCMs) with different emission scenarios and downscaling techniques focussing on different parts of Europe. A shortcoming of most of these studies is that they use large-scale parameters and boundary conditions from a limited number of GCMs, often only one, for the regionalisation of the global model output. To account for uncertainties arising from the choice of GCM/RCM, it is advisable to analyse simulations from multi-model ensembles. In addition, the projected long-term trends and future changes for wind speed and wind energy are relatively small compared to temperature trends (IPCC, 2012), while the natural variability of wind on inter-annual to decadal timescales is quite large and could thus conceal potential long-term trends.

The idea for this thesis originated within the German MiKlip project (Marotzke et al., 2016) and from a previous cooperation with the German Climate Service Center (HZG/GERICS, formerly CSC). Together with GERICS, a prototype database was developed to provide the wind energy sector and the public with information on wind energy resources for Germany. Special focus was given to potential climate change impacts. To prove beneficial for user applications, the database should contain data for different future periods and emission scenarios considering output from different models to take model uncertainties into account. However, the database currently stores data from a single RCM for the present and the future climate focussing only on long-term trends. Thus, one aim of this thesis is to extend the current analyses of regional scale wind speed and wind energy potentials over Europe for the near-term and the long-term future. Focus is given to different timescales (from sub-daily to multi-year means), different downscaling techniques (dynamical vs. statistical-dynamical) and different model ensembles. With this aim, a unique ensemble is created, considering both GCMs and RCMs. The objective of MiKlip is among others the prediction of potentially user-relevant variables (e.g. wind energy potentials, temperature extremes) at the regional scale over Europe up to ten years ahead

(near-term future). However, the field of research dealing with decadal climate predictions is still relatively new. So up to now most studies analyse the potential predictive skill of existing decadal prediction systems focussing on global meteorological parameters like temperature and precipitation. For the first time, this thesis analyses the MiKlip decadal prediction system with regard to regional wind energy potentials.
Overall, results from this thesis should help to achieve a better understanding of the potential impact of climate change for the near-term and the long-term future. This is important to adjust planning strategies concerning climate change adaptation, e.g. to meet the European Commission's aim to produce 14.9% of the European electricity demand from wind energy resources by 2020 (Moccia et al., 2014). In addition, results may be relevant for stakeholders in politics and economy and the planning of a future renewable energy system (e.g. Wohland et al., 2017). Three scientific publications form the basis for the investigation of two main research objectives:

1. Estimation of future changes of wind speed and wind energy potentials over Europe at the regional scale for the middle and the end of the 21st century, considering
   a) Future climate projections for two emission scenarios of a large CMIP5 multi-model ensemble (22 GCMs) downscaled with a statistical-dynamical downscaling approach (Paper I; Reyers et al., 2016).
   b) An ensemble of nine climate simulations with GCM-RCM model chains from EURO-CORDEX (dynamical downscaling of CMIP5) following two emission scenarios (Paper II; Moemken et al., 2018).
2. Analysis of the decadal predictability of wind speed and wind energy potentials over Central Europe in three generations of the MiKlip ('Mittelfristige Klimaprognosen') decadal prediction system downscaled with the same statistical-dynamical downscaling approach as in Paper I (Paper III; Moemken et al., 2016).

The three publications are linked with each other (see also Figure 9.2, chapter 9), either through the analysed datasets or through the used downscaling approach (for details see chapters 2.3 and 3). Paper I provides an overview of the ensemble mean responses to climate change and quantifies the uncertainties between the individual models in terms of regional wind energy potentials. Focus is given to changes of mean annual wind energy output (*Eout*), changes of mean seasonal *Eout* (including intra-annual variability), and changes in the inter-annual variability. Paper II investigates future changes of wind energy potentials at a very high temporal resolution, thus allowing insights on several timescales and addressing stakeholder needs. Focus is given to mean changes (annual and seasonal),

changes in variability (inter-annual to inter-daily), and changes in the occurrence of wind speeds relevant for wind energy production. The comparison of Papers I and II could provide a better understanding on the impact of different model ensembles and different downscaling techniques on the estimation of future changes of wind energy potentials. Paper III examines the decadal predictability of wind energy potentials over Central Europe. Focus is given to the analysis of decadal forecast skill for different lead times and seasons, and to the estimation of the added value of regionalisation.

Furthermore, the main results from three additional publications are presented, including the development and evaluation of the statistical-dynamical downscaling method for wind energy applications (Reyers et al., 2015) as applied in Papers I and III, the impact of climate change on a wind-dominated European power system (Weber et al., 2018), and the development and prospects of a regional MiKlip decadal prediction system (Reyers et al., 2017).

This thesis is organised as follows. Chapter 2 gives an overview of the meteorological background, including climate conditions for wind speed and wind energy potentials over Europe (2.1), decadal climate predictions (2.2), and the downscaling of global climate model data (2.3). Chapter 3 provides a detailed description of the used downscaling methods for wind energy applications: dynamical downscaling as applied in Paper II (3.1), and statistical-dynamical downscaling (Reyers et al., 2015) as applied in Papers I and III (3.2). Chapters 4, 5 and 7 supply the relevant publications (Paper I – III), which form the core of this thesis. Chapter 6 gives an overview of the main results from Weber et al. (2018), while results from Reyers et al. (2017) are presented in chapter 8. A summary and discussion of the main findings as well as an outlook of possible future work is given in chapter 9.

2 Background

Compensatory processes are the main drivers for atmospheric circulation. Thus, a balanced system would have no circulation in the atmosphere. At the earth, particularly two processes lead to global atmospheric circulation: the uneven heating of the earth-atmosphere-system by solar radiation, and the rotation of the earth (e.g. Kraus, 2004). The input of solar energy is highest at the equator (positive net radiation), while the earth loses energy at the poles through thermal radiation (negative net radiation). This uneven heating leads to temperature differences across the earth's surface on all spatial scales (Emeis, 2013). Simplified, warm air rises at the equator and is transported to the poles. The air is cooled along the way, sinks at the poles and is transported back to the equator. This causes semi-permanent pressure systems at the surface, marked by low-pressure systems at the equator and high-pressure systems at the poles. In upper levels, the distribution is vice versa with high-pressure systems at the equator and low-pressure systems at the poles. These distributions lead to a north-south pressure gradient between the warm subtropics and the cold polar regions. In order to compensate these pressure differences, air is transported from areas with high pressure to regions with low pressure. The rotation of the earth modifies this circulation by the Coriolis force leading to a deflection of moving air. Thus, three circulation cells are formed: the Hadley cell, the Ferrel cell and the polar cell. These cells produce mainly meridional winds (e.g. from North to South), while the Coriolis force adds a westerly component to winds towards the poles and an easterly component to winds towards the equator (Emeis, 2013). Besides this global wind system, smaller scale systems develop due to e.g. temperature differences between land and sea or between mountains and valleys.

In addition to the Coriolis force and the pressure gradient force, horizontal winds in the atmosphere depend on the centrifugal force and the frictional force (due to surface friction and turbulent viscosity of air). The frictional force can be neglected under idealised conditions outside the planetary boundary layer. A scale analysis shows that the centrifugal force is also negligible compared to the pressure gradient force and the Coriolis force. The

equilibrium of pressure gradient and Coriolis force is described by the so-called geostrophic winds, which flow parallel to the isobars. The wind speed of these geostrophic winds is proportional to the pressure gradient (e.g. Peixoto and Oort, 1992). In reality, the equilibrium is never achieved, since the sun radiates continuously and the earth stays a rotating system. Therefore there are always winds, which can potentially be used as energy source.

2.1 Wind speed and wind energy

Wind is used as operating power since thousands of years, when humans first started to built sailboats and sailing ships for transportation. Later on, wind powered mills were built to pump water and ground grain. In 1887, the first windmill for the production of electric power was developed (Price, 2005). Finally, the oil crisis during the 1970's intensified the investigation of non-fossil fuel energy sources (Manwell et al., 2009) and lead among others to the development of wind turbines and a new industry segment. Modern wind power plants generate electric power by using the buoyant force caused by air flowing along the rotors. This generated electricity depends on the size, the efficiency and the location of the wind turbine. Modern wind turbines can convert up to 45% of the wind's kinetic energy into mechanical energy and thus generate electric power. In Europe, the currently installed wind power capacity (on- and offshore) covers up to 11.4% of the EU's electricity demand (EWEA, 2016). In the German power system, the share of wind energy is 12.3% (*www.strom-report.de*, 2017). By 2020, the European Commission aims at producing 14.9% of the European electricity demand from wind energy resources (Moccia et al., 2014).
Like any other energy source, the use of wind energy has advantages and disadvantages. Wind is practically available worldwide without any limits since it is formed from solar radiation and is replenished by it continuously (Emeis, 2013). The transition from solar radiation to wind energy does not include the carbon cycle except for production, transportation, installation and maintenance of wind power plants (Emeis, 2013), which makes the generation of energy from wind comparatively low-emission. Modern wind power plants have a positive ecological balance after approximately two years since their start of operation. Additionally, wind energy still has a large potential through the expansion of wind farms both onshore and offshore. The main challenge for the usage of wind as energy source is its high volatility on different timescales. This can lead to strong fluctuations and the need for compensation with other energy sources (e.g. Huber et al., 2014; Bloomfield et al., 2016). In addition, there is currently no direct way to store energy produced by wind power plants.

2.1.1 Historical and current climate conditions

Wind is a highly variable quantity on both spatial and temporal scales. On the spatial scale, the large-scale pressure gradient between the Icelandic Low and the Azores High generates westerly winds over Europe. It is connected to the phase of the North Atlantic Oscillation (NAO). The pressure gradient between land and sea surfaces leads to relatively higher wind speeds along the European coastlines. Additionally, orographic barriers like the Alps or the Scandinavian mountain chain influence the wind at the local scale, leading to e.g. föhn effects (Troen and Petersen, 1989). In temporal terms, wind speeds over Europe vary at different timescales. The diurnal cycle of wind speed is related to the diurnal cycle of the planetary boundary layer (e.g. Stull, 1988) with higher winds around noon and a minimum during night. On seasonal scales, wind speed variability in Western Europe is influenced by the NAO (e.g. Hurrell and van Loon, 1997; Yan et al., 2002; Trigo et al., 2002). This influence is more pronounced during the winter months. The decadal variability of wind speeds over Europe is large (Bett et al., 2013) with up to 30% estimated for historical periods (Petersen et al., 1998).

Several studies investigated wind speeds over Europe in reanalysis data for both 10m-winds and upper-air winds relevant for wind energy production with somewhat inconsistent results. Bett et al. (2013) analysed 140 years of reanalysis data (Compo et al., 2011) finding no clear long-term trend of wind speed over Europe. Bakker et al. (2007) found a small decrease of mean annual geostrophic wind speeds over the Baltic Sea and a small increase for the Mediterranean Sea in the 40-year ERA-40 reanalysis dataset (Uppala et al., 2005). However, this trend is very small compared to the inter-annual variability. Pryor and Barthelmie (2003) investigated upper-air wind speeds (in 850 hPa) in the NCEP reanalysis (Kalnay et al., 1996). They discovered a significantly increasing trend for 1953-1999 over the Baltic region, which seems to be associated with increases in the upper quartile of the wind distribution. Vautard et al. (2010) observed a stilling trend in 10m-wind speeds that is not visible at higher levels. The stilling could be explained by an increase in surface roughness. Regions with pronounced stilling overlap with regions where vegetation has increased over the last 30 years, supporting the assumption that vegetation can have a slowing down effect on 10m-winds.

The potential of wind energy can be described through the wind energy density (WED) and the wind energy output (*Eout*) of an exemplary wind turbine. WED depends on the air density and the wind speed (often in 10m), while *Eout* takes specific wind turbine characteristics (e.g. cut-in and cut-out velocities, rotor diameter) into account. Both parameters are proportional to the cube of wind speed (e.g. Manwell et al., 2009). Therefore, higher

WED and *Eout* should be available in regions with generally higher wind speeds, e.g. the North Sea, while the wind energy potential should be lower in areas with lower wind speeds (e.g. Southern Europe). This is confirmed by several studies: Troen and Petersen (1989) gave the first detailed overview of potential wind energy sources in Europe in their European Wind Atlas, which is based on observational data. The Atlas provides an overview of mean wind speeds and energy densities for several European countries. Large energy sources are depicted for the British Isles, the western coast of Central Europe, the eastern North Atlantic, the North Sea, and the Aegean. Lu et al. (2009) analysed the global wind energy potential for individual countries based on reanalysis data. Inconsistent with Troen and Petersen (1989) and Hueging et al. (2013) they found higher wind energy potentials over land (onshore) than over sea (offshore) for most European countries. Mean annual *Eout* of 3000 TWh is depicted for Germany, Poland and Norway, while higher *Eout* (up to 5000 TWh) is depicted for Spain and Great Britain. Hueging et al. (2013) investigated the ability of different regional climate models (RCMs) to simulate the present wind energy indices. With this aim, they used two RCMs (CCLM and REMO), which are driven by a control simulation for the present climate. The simulated annual *Eout* of a 2.5 MW wind turbine shows a spatial pattern with distinct regional structures and a strong land-sea gradient (Figure 2.1). Highest values of 14000 MWh can be found in the North Atlantic to the northwest of the British Isles, while *Eout* of 12000 MWh is depicted for the North and Baltic Sea and along the western coast of Europe. Over the European continent, there is a strong north-south gradient with *Eout* values between 2000 and 8000 MWh. Lowest *Eout* is found over mountainous regions, where uncertainties due to the representation of orography in the models are highest (Hueging et al., 2013).

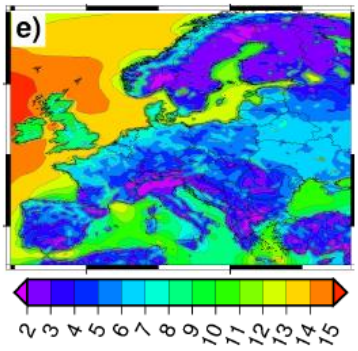

Fig. 2.1: Annual *Eout* of a 2.5 MW wind turbine in 10^3 MWh obtained from CCLM-20C (1961-2000). Source: Hueging et al. (2013), Figure 1e. ©American Meteorological Society. Used with permission.

2.1.2 Future climate conditions

Several studies indicated an influence of climate change on the atmospheric circulation and the surface pressure systems (e.g. Pryor and Barthelmie, 2010; Hueging et al., 2013). These changes can also influence the wind distribution and the wind energy potential in future decades (Pryor and Barthelmie, 2010).
Hueging et al. (2013) investigated changes in the mean sea level pressure (MSLP) and the MSLP gradients for the end of the 21st century in a global climate model (GCM) focussing on the different seasons. They discovered a decrease of MSLP in the northern North Atlantic during winter, which is associated with an intensification and displacement of the Icelandic Low. At the same time, MSLP is increasing in the south-eastern North Atlantic and over Southern Europe, resulting in an intensification and eastward shift of the Azores High. This combination causes a larger pressure gradient over the North Atlantic and Europe. Projected changes for summer are weaker, with a decrease (increase) of MSLP over the subtropics and high latitudes (North-western Europe).
Changes in regional scale wind speeds and wind energy potentials over Europe were addressed in several studies over the last years. Most of these studies agree on a small increase of wind energy potentials over Northern Europe and a small decrease over Southern Europe under future climate conditions. However, there can be differences regarding the magnitude and sometimes the sign of the projected changes. Räisänen et al. (2004) depicted a significant increase of mean wind speeds over Northern Europe, which is in agreement with the MSLP changes discovered by Hueging et al. (2013) and is confirmed by Kjellström et al. (2011). However, the changes can differ strongly between different GCMs and emission scenarios. Bloom et al. (2008) found a strong seasonal dependence of the projected changes. Pryor et al. (2005a) discovered an increase of wind energy density during winter over Northern Europe for 2071-2100. At the same time, future changes can affect the wind distribution in different ways: while mean wind speeds are projected to decrease, the 90th percentile is projected to increase (Pryor et al., 2005b). Pryor et al. (2012) found an increase in the magnitude of wind gusts in Scandinavia and an increasing intra-annual variability. Again, projected changes are sensitive to the model choice (Pryor et al., 2005a) due to different initial conditions and model parameterisations (Pryor et al., 2012). Hueging et al. (2013) analysed changes in the regional-scale wind energy potential over Europe using high-resolution data of two RCMs (CCLM and REMO, driven by the same GCM ECHAM). They focussed on changes in wind energy density and wind energy output of a 2.5 MW wind turbine. The projected changes are related to simulated changes in the large-scale pressure pattern, surface winds and synoptic activity over Europe and

the North-Atlantic. Hueging et al. (2013) found an increase of mean annual *Eout* over Northern and North-eastern Europe (Figure 2.2), which is in line with changes in mean wind speeds depicted in Räisänen et al. (2004). At the same time, a decrease is detected

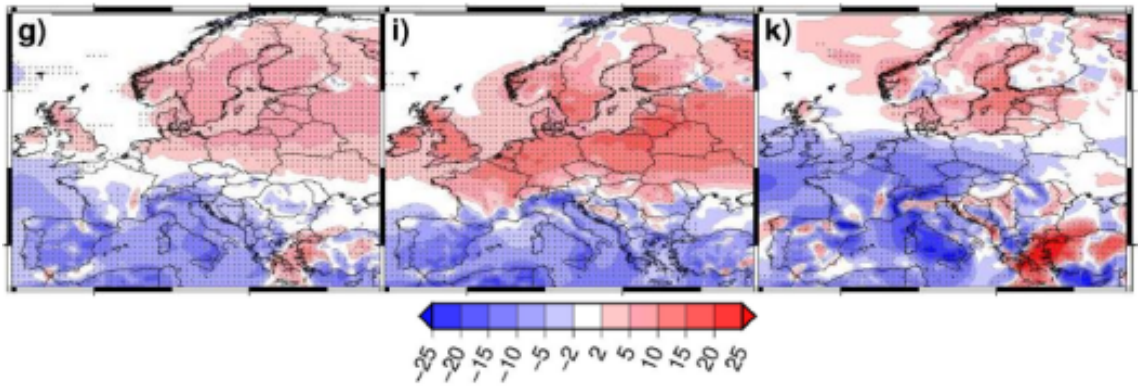

Fig. 2.2: Changes in annual *Eout* of a 2.5 MW wind turbine in % between the RCM-A1B and RCM-20C for CCLM for all year (g), winter (DJF; i), and summer (JJA; k). Reference periods are 1961-2000 and 2061-2100. Source: Hueging et al. (2013), Figure 3. ©American Meteorological Society. Used with permission.

for Southern Europe except the Aegean region, with highest values for Spain and the Mediterranean Sea. Changes are more pronounced for the different seasons (Figure 2.2): a significant increase of *Eout* is simulated for Northern and Central Europe during winter, together with a strong decrease over Southern Europe. Changes for summer are different, with decreasing *Eout* for large parts of Southern and Central Europe and increases for the Baltic and Aegean regions. The seasonal changes depicted in Hueging et al. (2013) lead to a higher intra-annual variability. Tobin et al. (2016) investigated climate change impacts on the wind power generation in an RCM ensemble conducted within EURO-CORDEX focussing on a European mid-century wind farm scenario. They found that the annual energy yield remains stable throughout the next decades. Nevertheless, changes at the local scale can reach up to 15%.

Additionally, climate change could alter the environmental context for operation, maintenance and design of wind power plants (Pryor and Barthelmie, 2010). For example, wind extremes can lead to critical loads on wind turbines resulting in more frequent power-downs or even damages. Several studies found evidence for increasing magnitudes of wind speed extremes for Northern Europe (e.g. Pryor et al., 2005a; Haugen and Iversen, 2008) and Central Europe (Leckebusch et al., 2008) in future decades.

All studies reveal a connection between a changing climate and the wind energy potential

under future climate conditions. This link is of high importance for future wind energy production. However, the demand for forecasts/predictions on timescales from one year up to one decade has strongly increased over the last years, especially in politics and economy (Goddard et al., 2013). These decadal predictions are introduced in the next chapter.

2.2 Decadal climate predictions

Decadal climate predictions focus on short-term climate change and natural climate variability on timescales from one year to one decade (Meehl et al., 2009). These timescales are of high importance for decision makers in ecology, economy, politics and society (Meehl et al., 2009; Chikamoto et al., 2013; Goddard et al., 2013) and thus are of particular interest for the short-term development and planning of wind energy production. One of the main challenges for decadal predictions is the initialisation of the climate system (Meehl et al., 2009). While long-term climate projections depend mostly on the boundary conditions, decadal predictions depend on both realistic initial and boundary conditions (Figure 2.3; van Oldenborgh et al., 2012) for example from observational data.

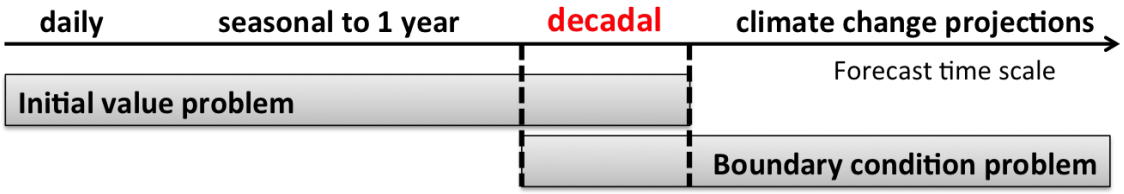

Fig. 2.3: Schematic illustration of different forecast/prediction timescales. Adapted from: Meehl et al. (2009).

Additionally, the predictability is prone to model uncertainties and systematic model biases (e.g. used physics or climatology; Chikamoto et al., 2013). The forecast skill of decadal predictions depends on the ability of the employed GCMs to realistically simulate the decadal variability, both in terms of pattern and magnitude (Meehl et al., 2009). Therefore they need to account for internal generated variability as well as variability forced by external processes (e.g. volcanic eruptions).
Within the German consortium MiKlip ('Mittelfristige Klimaprognosen', decadal climate predictions; Marotzke et al., 2016) a model system based on the Max-Planck-Institute Earth System Model (MPI-ESM) is developed to produce skilful decadal predictions on global and regional scales. The first generation of this model system contributes to the Coupled Model Intercomparison Project Phase 5 (CMIP5; Taylor et al., 2012). Through

CMIP5, a set of global coordinated climate model experiments has been made available, comprising simulations for the recent past, decadal simulations and climate change projections. The decadal simulations are divided into two kinds of experiments: hindcasts (initialised forecasts of past cases) and predictions (near future projections starting from current climate conditions). The initial conditions for these runs are taken from assimilation runs that use reanalysis data from the past and the present, either ocean-only or ocean-atmosphere. Only observed CO_2 values are used as boundary conditions. Some models also consider effects due to volcanic eruptions or changes in the solar activity. Ensembles are generated through an initialisation at different time steps of the assimilation run (usually 1-day-lagged initialisation; e.g. Müller et al., 2012). The hindcast experiments enable the analysis of decadal predictability for different parameters through a comparison with observations or reanalysis data (e.g. Smith et al., 2007). This is usually realised by calculating skill scores. Simplified, these scores estimate whether the initialisation of the hindcasts improves the decadal predictability compared to a reference simulation (e.g. Müller et al., 2012; Goddard et al., 2013). Typically, either uninitialised historical runs (for past cases) or the climatology serve as reference. Skill scores are calculated for different lead times (e.g. yr1-4: first to fourth year after initialisation) to quantify how far ahead the initialisation provides predictive skill.

Over the last years, several studies assessed the decadal forecast skill of existing forecast systems. These systems are based on individual model ensembles (e.g. Müller et al., 2012, 2014; Goddard et al., 2013; Marotzke et al., 2016) or multi-model ensembles (e.g. van Oldenborgh et al., 2012; Doblas-Reyes et al., 2013; Eade et al., 2014). All of these studies found some predictive skill, but the results differ strongly for different parameters, regions and lead times. Importantly, Eade et al. (2014) pointed out that the potential forecast skill is often underestimated due to a lower predictable component in the models compared to observations. While focus is given mostly on the global scale and primary meteorological parameters like temperature (e.g. Smith et al., 2007; Müller et al., 2012) and precipitation (e.g. van Oldenborgh et al., 2012), only few studies deal with the decadal predictability at the regional scale and of user-relevant variables. For example, Kruschke et al. (2014) analysed the forecast skill of decadal predictions conducted within MiKlip for cyclone activity over the Northern Hemisphere. For intense cyclones, they found some regions in the North Atlantic with positive predictive skill. Mieruch et al. (2014) considered dynamically downscaled MiKlip hindcasts to evaluate the decadal predictability of seasonal temperature anomalies and precipitation sums over Europe. While the positive forecast skill for summer temperatures could be preserved by the regionalisation, the predictive

skill of precipitation sums could be improved by the downscaling. Haas et al. (2016) used a statistical-dynamical downscaling approach to estimate the decadal forecast skill of peak winds in MPI-ESM at the regional scale. Results from their study showed highest skill scores for short lead times (1-4) and upper wind percentiles (75^{th}-90^{th}).
Results on both the global and the regional scale are promising for the decadal prediction of different variables. However, the results for the regional prediction systems depend not only on parameters, regions or lead times but also on the downscaling technique applied for regionalisation. The differences between the different downscaling methods and their advantages and disadvantages are described in the next section.

2.3 Downscaling of global climate model data

GCMs are a useful tool for climate change projections and decadal predictions. But for applications to the regional or even the local scale, the resolution of the GCM simulations (typically 100-300 km) is insufficient. Therefore, a downscaling of the global model data is necessary to provide information at a higher resolution. Several methods have been developed and applied in recent years. All downscaling methods belong to one of the following three categories: statistical/empirical downscaling, dynamical downscaling, and statistical-dynamical downscaling (e.g. Hewitson and Crane, 1996; Wilby and Wigley, 1997; Fuentes and Heimann, 2000; Maraun et al., 2010).
The statistical downscaling (SD) consists of two steps. First, a statistical relationship between the local climate variable of interest (e.g. temperature or wind speed) and the large-scale parameter (e.g. MSLP field) is developed based on observational or reanalysis data. This relationship is applied to the GCM output in the second step to simulate local climate characteristics. The SD is computationally inexpensive (cost efficient), easy to use, and can be applied very fast to large GCM ensembles (Wilby et al., 2004). However, the approach assumes a stationary statistical relationship and does not include sub-grid-scale processes like e.g. land and sea breeze. Pryor et al. (2005c) used a SD approach to analyse the impact of climate change on wind speed and wind energy densities over Europe for the end of the 21^{st} century. The approach includes relative vorticity and MSLP gradients as large-scale predictors and parameters of the wind speed probability distribution function (PDF) as predictants. Devis et al. (2013) developed a SD method to downscale GCM output to the wind speed distribution at the hub height of wind turbines using local-scale hub height wind speed PDF parameters as predictants and PDF parameters of large-scale atmospheric parameters as predictors.

The dynamical downscaling (DD) is based on the modelling of atmospheric processes at the regional scale. A high-resolution RCM is nested into the coarser resolution GCM using the GCM output as boundary conditions (e.g. Räisänen et al., 2001). The RCM has a physically-based dynamical core, which allows the resolution of synoptic patterns. Different physical parameterisations account for sub-grid-scale-processes like convection, turbulence or radiation (Teixeira et al., 2008). Additionally, the RCM provides information at very high spatial and temporal resolution. However, the DD is computationally very expensive, thus typically only small ensembles can be generated. Accordingly, most studies using DD for climate change studies are restricted to single GCMs and single emission scenarios. For example, Hueging et al. (2013) investigate regional scale changes in wind energy potentials using two RCMs driven with the same GCM for a single emission scenario.
The statistical-dynamical downscaling (SDD) combines the advantages of SD and DD. SDD approaches are often based on the classification of weather types from large-scale parameters (e.g. MSLP). In a next step, representatives for each weather type are simulated with a RCM. The results are analysed statistically, in which the frequency of the individual weather classes determines the corresponding weights. Pinto et al. (2010) developed a SDD approach to estimate the impact of winter storms over Western Europe under future climate conditions. Haas and Pinto (2012) developed a SDD approach to reproduce dynamically downscaled wind gust speeds in a cost efficient way. A further approach for wind energy application by Reyers et al. (2015) is described in detail in the next chapter.

3 Downscaling for wind energy applications

In this thesis, two downscaling approaches are considered to analyse wind energy potentials on the regional scale over Europe: dynamical downscaling and statistical-dynamical downscaling.

3.1 Dynamical downscaling

Chapters 5 and 6 are based on regional climate projections from the European branch within the CORDEX framework (EURO-CORDEX, *http://www.euro-cordex.net*). The CORDEX initiative (WCRP Coordinated Regional Downscaling Experiment; Giorgi et al., 2009) aims at dynamically downscaling the CMIP5 global climate projections to generate multi-model ensembles of regional projections for different regions all over the globe. Therefore several RCMs are nested into different GCMs.
The GCMs provide simulated large-scale atmospheric fields (surface pressure, temperature, humidity) as boundary conditions, and soil moisture, sea surface temperature and sea ice as initial conditions to the RCMs. The RCMs incorporate more complex topography and coastlines, heterogeneous landscapes, and detailed descriptions/parameterisations of physical processes to generate realistic climate information at spatial resolutions of usually 20 to 50 km. However, the quality of the dynamically downscaled data depends on the accuracy and biases of the GCMs (Seaby et al., 2013).
Within EURO-CORDEX, historical and climate change simulations are provided for approximately 27°N - 72°N and 22°W - 45°E with a resolution of 12 km (0.11°) and 50 km (0.44°). More details on e.g. the used GCM-RCM chains can be found in Paper II (chapter 5).

3.2 Statistical-dynamical downscaling

In chapters 4 and 7, a statistical-dynamical downscaling approach is used to regionalise a large GCM ensemble from CMIP5 (chapter 4) and the MiKlip decadal prediction system (chapter 7). The SDD methodology was developed in Mömken (2014) and Reyers et al. (2015) and is described in the following, according to the two references.

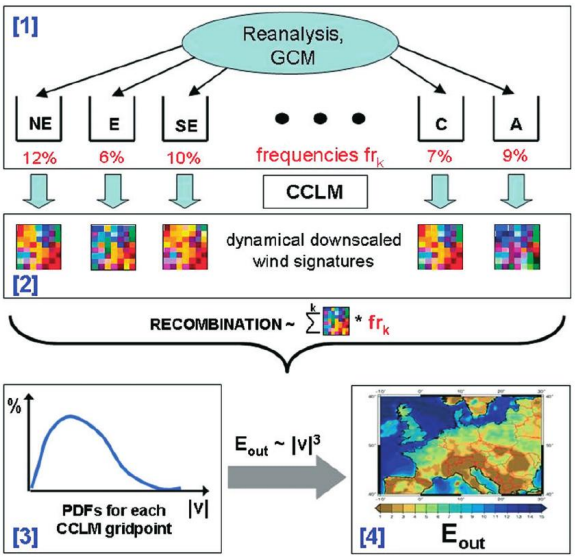

Fig. 3.1: Schematic illustration of the SDD with its four steps. Source: Reyers et al. (2015), Figure 1. ©Royal Meteorological Society. Used with permission.

The SDD approach consists of four steps (Figure 3.1). In the first step, the large-scale circulation is analysed and characterised for each day using a weather type classification. For this purpose, an extended version of the circulation weather type (CWT) method by Jones et al. (1993) is employed. The CWT method follows the objective Lamb weather types (Lamb, 1972; Jenkinson and Collinson, 1977) and has been used in a wide range of studies (e.g. Jones et al., 2012). Daily global MSLP fields interpolated on a regular 2.5° grid are used as input data for the classification. By considering instantaneous MSLP values at 16 grid points around the central point at 50°N 10°E (Frankfurt, Germany) the direction and strength of the geostrophic flow and the vorticity are calculated based on pressure gradients. The near-surface atmospheric flow is then assigned to one of ten basic CWTs: northeast (NE), east (E), southeast (SE), south (S), southwest (SW), west (W), northwest (NW), north (N), cyclonic (C), anti-cyclonic (A). Additionally, the mixed type anti-cyclonic/west (AW) is considered since it is the most frequent mixed type. For

wind energy production, the strength of the geostrophic flow is a crucial factor. This strength is described by the f-parameter, which represents the current MSLP gradient at the central point. Depending on the CWT, the f-parameter ranges from values slightly above 0 hPa/1000km (weak gradient) to ca. 45 hPa/1000km (strong gradient). Each of the 11 CWTs is subdivided into classes of f-parameters with 5 hPa/1000km intervals (0-5 to 45-50 hPa/1000km) to capture the complete range of wind speeds within a CWT. This results in a maximum of 110 classes, but only 77 of them are assigned. In addition, the frequency of occurrence for each of these classes is estimated. Figure 3.2 shows exemplarily the climatological MSLP fields for classes W and C, both with a low and a high f-parameter.

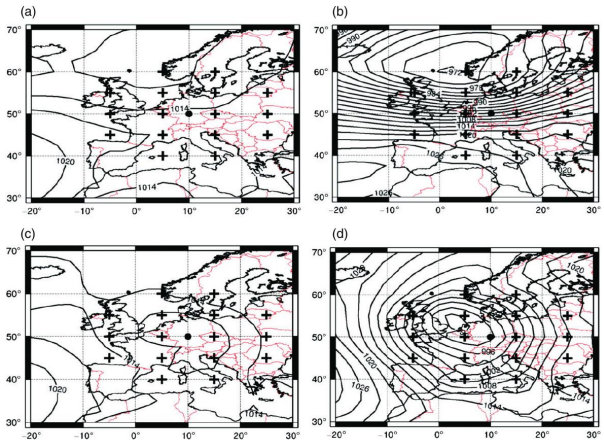

Fig. 3.2: Climatological mean of MSLP fields for two exemplary CWTs obtained from ERA-Interim. Source: Reyers et al. (2015), Figure 2. ©Royal Meteorological Society. Used with permission.

In the second step, representative days for each of the 77 classes are simulated with the RCM COSMO of the German Weather Service (Deutscher Wetterdienst, DWD) in its Climate Mode (version 4.8, hereafter CCLM; e.g. Rockel et al., 2008). CCLM simulations with a horizontal resolution of 0.22° are performed using the domain of the EURO-CORDEX project (roughly 20°N - 70°N and 30°W - 50°E). ERA-Interim data serves as initial and boundary conditions. For each class, up to ten representative days are selected. The choice of representatives within a class is random, but data from all four seasons is included if possible. The ERA-Interim-driven representatives are used for the downscaling of all global datasets, assuming that the wind characteristics of the individual CWTs are similar in model and reanalysis.

In the third step, the simulated hourly 10m-wind speeds for the representative days are

recombined to wind velocity PDFs at each CCLM grid point. Therefore the occurrence of a given wind speed (in 0.1 m/s intervals) is calculated as the sum of the contributions from all classes weighted by the respective class frequency and the number of representative days.

In the last step, the wind speed PDFs are used to calculate gridded *Eout* for an exemplary wind turbine. First, the hourly 10m-wind velocities are extrapolated to the average hub height of a wind turbine using a vertical wind profile. This is a standard procedure in wind energy applications (e.g. Manwell et al., 2009; Hueging et al., 2013). Here, the power law is used:

$$\frac{U(z)}{U(z_r)} = \left(\frac{z}{z_r}\right)^{\alpha} \tag{3.1}$$

where *U(z)* and *U(z_r)* are the wind speeds at hub height z and a reference height z_r (usually 10 m). α is the power law exponent, which is set to 0.2 for onshore areas (IEC, 2005a) and 0.14 for offshore sites (IEC, 2005b). The extrapolated wind velocities are used for the computation of *Eout*, following the characteristics of the exemplary wind turbine:

1. No *Eout* is produced below the cut-in velocity (around 3 m/s) and above the cut-out velocity (ca. 25 m/s).

2. Between the cut-in velocity and the rated velocity (around 13 m/s), *Eout* can be determined as:

$$E_{out} = c_p \frac{1}{2} \rho \pi R^2 U^3 \tag{3.2}$$

   with the power coefficient c_p (0.35), the air density ρ (constant value of 1.225 kg/m^3), the rotor radius R (50m), and the wind speed at hub height *U(z)*.

3. Between the rated velocity and the cut-out velocity, a constant maximum *Eout* of 2.5 MW is assumed.

Finally, gridded *Eout* is calculated by assuming that a wind turbine is placed at every grid point. Spatial distributions of mean annual *Eout* are obtained by integrating *Eout* over all wind speed ranges with the respective climatological velocity frequencies as weighting factors. Figure 3.3a shows the spatial distribution of mean annual *Eout* downscaled from ERA-Interim reanalysis data (climatology for 1979-2010).

The SDD method is easily applicable to different datasets like reanalysis data or climate change projections and different time periods. Only the weather type analysis (step 1) has

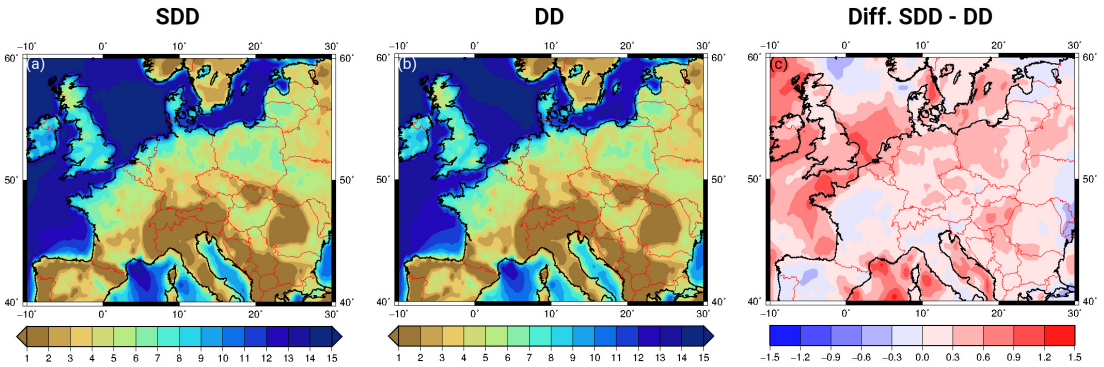

Fig. 3.3: (a) Climatological mean of annual *Eout* in 10^3 MWh for ERA-Interim (1979-2010) as obtained by SDD. (b) as (a), but obtained by DD. (c) Difference between annual *Eout* from SDD and DD in 10^3 MWh obtained from ERA-Interim. Adapted from: Reyers et al. (2015), Figure 7. ©Royal Meteorological Society. Used with permission.

to be recalculated. Reyers et al. (2015) used the SDD approach for the regionalisation of three different datasets. For evaluation, they applied the SDD to ERA-Interim reanalysis (Dee et al., 2011) and compared the results to a purely DD method and wind data from the German Weather Service (DWD). The SDD is able to simulate realistic near-surface wind distributions for most stations in Germany with largest discrepancies for coastal stations. Additionally, the results for simulated *Eout* show a good agreement between SDD and DD (Figure 3.3b) for Central Europe and a reduced agreement over areas like the North Sea and the Mediterranean region (Figure 3.3c). Reyers et al. (2015) also tested the applicability of SDD to decadal hindcasts from the MiKlip consortium (see section 2.2) and climate change projections. Regarding the application to decadal hindcasts, a good accordance between SDD and DD is found for Germany and nearby areas, especially the Benelux region, Czech Republic and Poland, while correlations to DD are lower for other European countries (Figure 3.4). In terms of climate change projections, the SDD approach performs well for the entire European sector. Reyers et al. (2015) concluded that the SDD method is a suitable and inexpensive alternative to a purely DD approach and that it can easily be applied to large ensembles of global data.

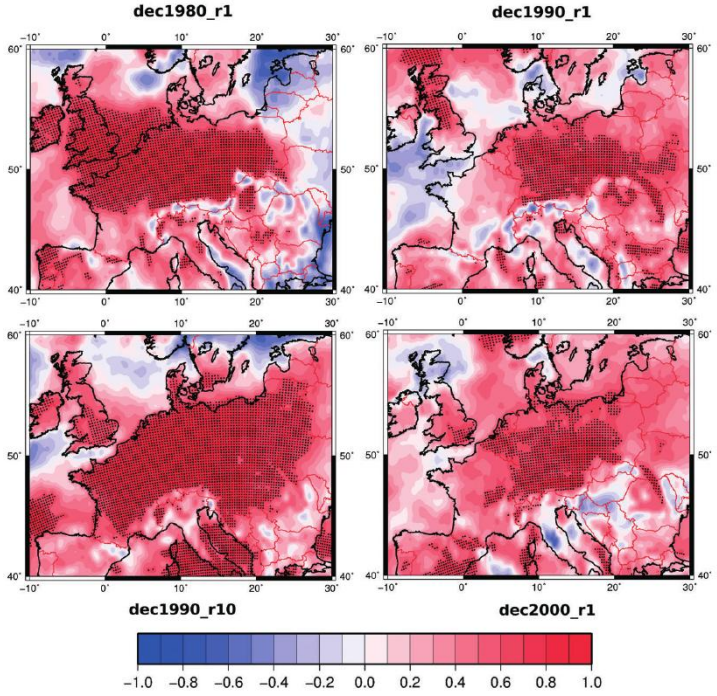

Fig. 3.4: Correlation per grid point between annual *Eout* time series simulated by SDD and DD for four exemplary hindcasts. Grid points with a significant correlation are dotted. Source: Reyers et al. (2015), Figure 11. ©Royal Meteorological Society. Used with permission.

4 Future changes of wind energy potentials over Europe in a large CMIP5 multi-model ensemble

---

Reference:

Reyers, M., Moemken, J., and Pinto, J. G. (2016). Future changes of wind energy potentials over Europe in a large CMIP5 multi-model ensemble. *Int. J. Climatol.*, 36:783–796. doi:10.1002/joc.4382

Page numbers are as published in *International Journal of Climatology*.

INTERNATIONAL JOURNAL OF CLIMATOLOGY
Int. J. Climatol. **36**: 783–796 (2016)
Published online 1 June 2015 in Wiley Online Library
(wileyonlinelibrary.com) DOI: 10.1002/joc.4382

RMetS
Royal Meteorological Society

Future changes of wind energy potentials over Europe in a large CMIP5 multi-model ensemble

Mark Reyers,[a]* Julia Moemken[a] and Joaquim G. Pinto[a,b]
[a] *Institute for Geophysics and Meteorology, University of Cologne, Germany*
[b] *Department of Meteorology, University of Reading, UK*

ABSTRACT: A statistical-dynamical downscaling method is used to estimate future changes of wind energy output (*Eout*) of a benchmark wind turbine across Europe at the regional scale. With this aim, 22 global climate models (GCMs) of the Coupled Model Intercomparison Project Phase 5 (CMIP5) ensemble are considered. The downscaling method uses circulation weather types and regional climate modelling with the COSMO-CLM model. Future projections are computed for two time periods (2021–2060 and 2061–2100) following two scenarios (RCP4.5 and RCP8.5). The CMIP5 ensemble mean response reveals a more likely than not increase of mean annual *Eout* over Northern and Central Europe and a likely decrease over Southern Europe. There is some uncertainty with respect to the magnitude and the sign of the changes. Higher robustness in future changes is observed for specific seasons. Except from the Mediterranean area, an ensemble mean increase of *Eout* is simulated for winter and a decreasing for the summer season, resulting in a strong increase of the intra-annual variability for most of Europe. The latter is, in particular, probable during the second half of the 21st century under the RCP8.5 scenario. In general, signals are stronger for 2061–2100 compared to 2021–2060 and for RCP8.5 compared to RCP4.5. Regarding changes of the inter-annual variability of *Eout* for Central Europe, the future projections strongly vary between individual models and also between future periods and scenarios within single models. This study showed for an ensemble of 22 CMIP5 models that changes in the wind energy potentials over Europe may take place in future decades. However, due to the uncertainties detected in this research, further investigations with multi-model ensembles are needed to provide a better quantification and understanding of the future changes.

KEY WORDS wind energy; future changes; Europe; CMIP5; multi-model ensemble; statistical-dynamical downscaling ; circulation weather types

Received 20 August 2014; Revised 5 March 2015; Accepted 22 April 2015

1. Introduction

The observed anthropogenic climate change and the projected global warming due to increasing greenhouse gas emissions have raised the necessity of an increase in renewable energy production in the upcoming decades. Because of its geographical position, wind energy is a promising renewable energy source for Europe, while other alternative energy sources such as hydropower are limited (Wiser *et al.*, 2011). By 2020, the European Commission aims to produce 15.7% of the EU's electricity from wind (Moccia *et al.*, 2011). A further increase of wind power capacity is expected for the upcoming decades (Capros *et al.*, 2013). Wind energy production in future decades may in turn also be influenced by the changing climate, because near-surface wind conditions are linked to the synoptic scale variability on different time-scales (Pryor and Barthelmie, 2010). The impact of climate change on regional wind speeds and wind energy potentials in Europe has been investigated in several recent studies (e.g. Barstad *et al.*, 2012; Cradden *et al.*, 2012; Nolan *et al.*, 2012, 2014; Pryor *et al.*, 2012; Hueging *et al.*, 2013; Tobin *et al.*, 2015). Most of these studies, which use different models and downscaling methods and focus on different parts of Europe, agree on a general increase in wind energy potentials over Northern Europe, especially during winter, and a general decrease over Southern Europe. However, there are some differences both in the magnitude and the sign of the projected changes. For example, several studies found that the changes in wind speed and wind energy are sensitive to the choice of the global climate model (GCM) and may be influenced by their internal variability and initial conditions (e.g. Pryor *et al.*, 2005, 2012; Tobin *et al.*, 2015). Additionally, evidence is given that future projections of synoptic activity may strongly differ between individual GCMs, which is mainly due to different model parameterisations or uncertainties in the simulated ocean circulation changes (Woollings *et al.*, 2012; Zappa *et al.*, 2013).

A shortcoming of most studies dealing with future projections of wind energy potentials is that they often use large-scale parameters, such as wind speed or wind direction, and boundary conditions of a limited number of GCMs, sometimes only one, for the downscaling

* Correspondence to: M. Reyers, University of Cologne, Institute for Geophysics and Meteorology, Pohligstrasse 3, 50969 Cologne, Germany.
E-mail: mreyers@meteo.uni-koeln.de

procedure. In order to take into account the uncertainties arising from the choice of the GCM, it is recommended to downscale future scenarios from large multi-model ensembles. A large ensemble of GCMs and Earth System Models (ESMs) has been recently made available through the Coupled Model Intercomparison Project Phase 5 (CMIP5; Taylor *et al.*, 2012). Studies that aim to assess future changes of the synoptic activity (to some extent linked to wind energy potentials) over Europe in the CMIP5 models mostly consider large-scale features like storm tracks or cyclones (e.g. Chang *et al.*, 2012; Zappa *et al.*, 2013). For example, Zappa *et al.* (2013) analysed the responses of cyclones over the European sector to climate change in 19 CMIP5 models. The ensemble mean response shows an increase in the number of winter cyclones over Central Europe and a decrease in the number of North Atlantic cyclones in summer for 2070–2099. However, the future changes in the individual models may differ or even show opposite trends. Based on such GCM results, it is not possible to directly draw conclusions from their findings for regional changes of wind energy potentials, because wind energy production is strongly influenced by local topographic characteristics (e.g. Ouammi *et al.*, 2012) and not only depends on mean wind conditions but on changes in the full spectrum of wind speeds. As a consequence, there is still a lack of knowledge about future projections of regional wind energy potentials in a CMIP5 multi-model ensemble.

In this study, we use a statistical-dynamical downscaling (SDD) method following Reyers *et al.* (2015) to assess regional changes of wind energy potentials over Europe in an ensemble of 22 CMIP5 models. The objective is to provide an overview of the ensemble mean responses to climate change and to quantify the uncertainties between the individual models. An overview of the 22 models as well as a description of the downscaling method is given in Section 2. The main results of this study are shown in Section 3, including an evaluation of the CMIP5 ensemble (Section 3.1), future projections of mean annual wind energy output (Section 3.2), and changes of the inter- and intra-annual variability of wind energy production (Section 3.3). Conclusions and a discussion of the results are given in Section 4.

2. Methods and data

In this study, an SDD approach (e.g. Fuentes and Heimann, 2000; Pinto *et al.*, 2010) is used to downscale wind energy potentials over Europe for present day and future climate conditions. SDD approaches combine weather type analysis and regional climate model simulations for selected representative episodes of relevant weather types. The adaption of SDD for wind energy applications is given in detail in Reyers *et al.* (2015), and thus only a short summary is presented here. SDD consists of four crucial steps:

In the first step, a circulation weather type (CWT) analysis following Jones *et al.* (1993) is applied to daily mean sea level pressure (MSLP) fields to assign the large-scale atmospheric flow into directional (e.g. west) or rotational (e.g. cyclonic) CWTs (see Reyers *et al.*, 2015 for more details). With this aim, daily MSLP fields of global data sets (e.g. reanalysis for evaluation purposes; historical and future scenarios of GCMs for present day and future climate conditions, respectively) are first interpolated on a regular 2.5° grid. Further, the CWTs are subdivided into classes with different pressure gradients, ranging from ca. 45 hPa per 1000 km to values below 5 hPa per 1000 km (5 hPa per 1000 km intervals, see Reyers *et al.*, 2015) at the central point, which for this study is situated at 10°E, 50°N (near Frankfurt, Germany). The CWT classification is based on the orientation and the gradient of the isobars at the central point, using MSLP at 16 neighbouring grid points (Reyers *et al.*, 2015; their Figure 1). Altogether, 77 large-scale weather classes are considered.

Second, representative days for each of these 77 classes are simulated with the regional COSMO model of the German Weather Forecast Service Deutscher Wetterdienst (DWD, http://www.cosmo-model.org) in its *CL*imate *M*ode (version 4.8, hereafter CCLM; see e.g. Rockel *et al.*, 2008). Reanalysis data from the European Centre for Medium-Range Weather Forecasts (ERA-Interim; Dee *et al.*, 2011) are used as initial and boundary conditions. The model domain comprises the region of the EURO-CORDEX project (Giorgi *et al.*, 2006) with a horizontal resolution of 0.22°. Up to ten representative days for each of the 77 classes have been simulated (altogether 669 simulated representatives) to ensure that the full spectrum of potential representatives is covered.

Third, at each CCLM grid point simulated, hourly 10 m wind speeds of the representative days are recombined to probability density functions (PDFs) by weighting the contributions of all 77 weather classes by the respective class frequency (e.g. frequency of a class in a future time period) and the number of simulated representative days. Finally, the gridded PDFs of the 10 m wind speed are used to determine highly resolved gridded wind energy output (*Eout*) of an example wind turbine. Note that these PDFs are based on hourly wind speeds. Therefore, sub-daily wind variations and extremes are considered in the downscaling approach. Following Reyers *et al.* (2015), characteristics of a 2.5 MW wind turbine from General Electric (2010) with an assumed average turbine hub height of 80 m are employed. Here, we use the power law to extrapolate hourly 10 m wind speeds to the hub height (wind speed in 80 m, v_{80}). In general, *Eout* of the example turbine is proportional to v_{80} cubed:

$$E_{\text{out}} = c_{\text{p}} \frac{1}{2} \rho \pi R^2 v_{80}^3 \tag{1}$$

where c_{p} is the power coefficient (constant value of 0.35 for the idealized turbine), ρ is the air density (constant value of 1.225 kg m^{-3}), and R the rotor radius of the idealized turbine (50 m). For $v_{80} < 3.5$ m s^{-1} (cut-in velocity) and $v_{80} > 25$ m s^{-1} (cut-out velocity), no energy output is produced. Between wind speeds of 12.5 m s^{-1} (rated velocity) and 25 m s^{-1} (cut-out velocity), the maximum value of *Eout* of 2.5 MW is reached. The computed *Eout* is

integrated over all wind velocity ranges and weighted with the corresponding climatological velocity frequencies to obtain distributions of mean annual energy output for each grid point. To apply the SDD approach to different data sets or time periods, only the weather type analysis (step 1) has to be repeated and eventually calibrated, while the subsequent steps remain unchanged (see Reyers *et al.*, 2015).

Reyers *et al.* (2015) evaluated the results of the SDD approach for wind energy potentials against purely dynamical downscaling methods applied to reanalysis and CMIP3 models (e.g. Hueging *et al.*, 2013) and concluded that they agree particularly well for Central Europe. This is the case for simulated *Eout* on the annual time-scale and for long-term future projections. Over other areas, the agreement is reduced, but the general pattern coincides. In this study, the SDD approach is used to determine the climate change response of *Eout* in an ensemble of 22 CMIP5 models. The names and institutions of the 22 models as well as their original horizontal and vertical resolutions are listed in Table 1. The ensemble comprises

Table 1. List of the 22 CMIP5 models used in this study, including information on model name, respective institution, and the horizontal and vertical resolution.

Model name	Institution	Horizontal resolution	Vertical levels
ACCESS1.3 (Australian Community Climate and Earth System Simulator, coupled model, version 1.3)	Centre for Australian Weather and Climate Research (CAWCR), Australia	192 × 145	38
CanESM2 (Second Generation Canadian Earth System Model)	Canadian Centre for Climate Modelling and Analysis (CCCma), Canada	T63 (128 × 64)	35
CCSM4 (Community Climate System Model, version 4)*	National Center for Atmospheric Research (NCAR), United States	288 × 192	26
CNRM-CM5 (CNRM Coupled Global Climate Model, version 5)	Centre National de Recherches Mètèorologiques (CNRM), France	TL127 (256 × 128)	31
CSIRO-Mk3.6.0 (CSIRO Mark, version 3.6.0)	Commonwealth Scientific and Industrial Research Organisation (CSIRO), Australia	T63 (192 × 96)	18
EC-EARTH (EC-Earth Consortium)	European Consortium (EC)	TL159 (320 × 160)	62
FGOALS-g2 (Flexible Global Ocean-atmosphere-Land System Model gridpoint, second spectral version)*	State Key Laboratory of Numerical Modelling for Atmospheric Sciences and Geophysical Fluid Dynamics (LASG), China	128 × 60	26
GFDL-CM3 (GFDL global Coupled Model, version 3)	Geophysical Fluid Dynamics Laboratory (GFDL), United States	144 × 90	48
GFDL-ESM2G (GFDL Earth System Model with GOLD ocean component)	GFDL, United States	144 × 90	24
GFDL-ESM2M (GFDL Earth System Model with MOM4 ocean component)	GFDL, United States	144 × 90	24
HadGEM2-CC (Hadley Centre Global Environment Model, version 2, Carbon Cycle)	Met Office Hadley Centre, United Kingdom	192 x 145	38
HadGEM2-ES (Hadley Centre Global Environment Model, version 2, Earth System)	Met Office Hadley Centre, United Kingdom	192 × 145	38
INM-CM4 (INM Coupled Model, version 4.0)*	Institute of Numerical Mathematics (INM), Russia	180 × 120	21
IPSL-CM5A-LR (IPSL Coupled Model, version 5, coupled with NEMO, low resolution)	L'Institut Pierre-Simon Laplace (IPSL), France	96 × 96	39
IPSL-CM5A-MR (IPSL Coupled Model, version 5, coupled with NEMO, medium resolution)	IPSL, France	144 × 143	39
MIROC5 (MIROC, version 5)	Model for Interdisciplinary Research on Climate (MIROC), Japan	T85 (256 × 128)	56
MIROC-ESM (MIROC, Earth System Model)	MIROC, Japan	T42 (128 × 64)	80
MIROC-ESM-CHEM (MIROC, Earth System Model, Chemistry Coupled)	MIROC, Japan	T42 (128 × 64)	80
MPI-ESM-LR (MPI Earth System Model, low resolution)	Max Planck Institute (MPI) for Meteorology, Germany	T63 (192 × 96)	47
MPI-ESM-MR (MPI Earth System Model, medium resolution)	MPI, Germany	T63 (192 × 96)	95
MRI-CGCM3 (MRI Coupled Atmosphere-ocean General Circulation Model, version 3)*	Meteorological Research Institute (MRI), Japan	TL159 (320 × 160)	48
NorESM1-M (Norwegian Earth System Model, version 1, intermediate resolution)	Norwegian Climate Centre (NCC), Norway	144 × 96	26

*Models without wind data are marked.

both coupled GCMs as well as ESMs. While some of the individual model ensembles comprise up to 12 realisations per scenario, others have only one realisation. To ensure an equal contribution to the ensemble mean, we decided to use the first available realisation of each model simulation. Two future periods (2021–2060 and 2061–2100) are compared to the historical period 1961–2000. For the historical period, the CMIP5 models are forced with observed greenhouse gas concentrations. For the future periods, two scenarios are considered in this study: RCP4.5 and RCP8.5 (Meinshausen *et al.*, 2011). In the RCP4.5, fossil CO_2 emissions are assumed to increase until 2040 and permanently decrease thereafter. Nevertheless, a moderate permanent increase of CO_2 concentration is simulated in this scenario reaching 543 ppm in 2100. This results in an additional anthropogenic radiative forcing of $4.5\,W\,m^{-2}$ at the end of the 21st century. In contrast, the fossil CO_2 emissions in the RCP8.5 strongly rise until 2100. This leads to a CO_2 concentration of ca. 2000 ppm and a strong anthropogenic radiative forcing of $8.5\,W\,m^{-2}$ by 2100. For comparison and validation purposes, SDD is also applied to ERA-Interim (see Reyers *et al.*, 2015).

In this study, future climate change responses of *Eout* in the CMIP5 ensemble are analysed with respect to the following three focal points:

(i) changes of mean annual *Eout*
(ii) changes of mean seasonal *Eout* (winter: December–February; summer: June–August)
(iii) changes of inter-annual variability (in terms of the standard deviation of annual *Eout*).

Future changes are determined as difference of *Eout* in the future period (2021–2060 or 2061–2100) minus *Eout* under present day conditions (1961–2000). For (i) and (ii), significances of the changes are calculated using the Student's *t*-test method. For ensemble mean changes, signal-to-noise ratios are quantified by dividing mean changes by the standard deviation between the changes of the individual ensemble members. For the evaluation of the inter-annual variability, focus is given on selected regions over Central Europe, for which the approach produces comparable results to dynamical downscaling (Reyers *et al.*, 2015).

Regional changes of *Eout* are related to changes in large-scale atmospheric circulation, namely the mean 10 m wind speeds and MSLP fields in the CMIP5 models. Because wind data are not available for all models, this analysis is restricted to 18 models, comprising the same model ensemble as shown in Table 1 minus CCSM4, FGOALS-g2, INM-CM4, and MRI-CGCM3.

3. Results

3.1. Evaluation of historical CMIP5 runs

The SDD approach is used to estimate *Eout* based on the CMIP5 ensemble for Europe. The study focuses on Central Europe, because the considered weather typing approach is representative for the large-scale flow conditions over Germany and surrounding countries (cf. Section 2 and Reyers *et al.*, 2015). First, we analyse how well the CWT frequencies for the historical runs of the CMIP5 models agree to those in ERA-Interim. Aside from the rotational CWTs (cyclonic and anti-cyclonic), the westerly weather types dominate the near-surface atmospheric flow over Central Europe (see also Reyers *et al.*, 2015). Global circulation models tend to overestimate the zonal flow in the North Atlantic/European Sector (e.g. Sillmann and Croci-Maspoli, 2009). Accordingly, Zappa *et al.* (2013) have shown that CMIP5 models overestimate the number of winter cyclones in a zonal band between the subtropical North Atlantic and Central Europe. In terms of the CWTs, this typical bias is reflected by an overestimation of the frequencies of the westerly weather types over Europe in the GCMs. Table 2 shows the frequencies of all CWTs west (W; flow direction 67.5°–112.5°W), of CWTs west with a strong pressure gradient of more than 15 hPa per 1000 km (W+), and of the combined westerly types southwest, west, and northwest (SW, W, NW; 22.5°–157.5°W) in ERA-Interim and the respective deviations for the historical runs of the 22 models. In ERA-Interim, on ca. 10% of the period 1979–2010, the atmospheric flow can be assigned to CWT W. Nearly half of these CWTs (4.54%) have a gradient of more than 15 hPa per 1000 km (W+). Altogether, the westerly types (SW, W, NW) account for 27.61% of all days. As expected, most of the CMIP5 models clearly overestimate the frequencies of the westerly

Table 2. Frequency of CWT west (W, second column), CWT west with a pressure gradient of more than 15 hPa per 1000 km (W+, third column), and the sum of frequencies of CWT southwest, west, and northwest (SW, W, NW, fourth column) in ERA-Interim and the respective deviations for the historical runs of the 22 CMIP5 models.

Model	W	W+ ($f > 15$)	SW, W, NW
ERA-Interim	9.58	4.54	27.61
ACCESS1.3	+1.00	+1.97	−0.35
CanESM2	+3.02	+3.45	+6.06
CCSM4	+7.47	+7.36	+13.10
CNRM-CM5	−0.05	+0.59	+0.44
CSIRO-MK3.6.0	−2.02	−1.21	−4.46
EC-EARTH	+0.51	+1.06	+0.21
FGOALS-g2	−1.67	−1.52	−2.58
GFDL-CM3	+1.88	+1.85	+4.39
GDFL-ESM2G	+3.56	+2.86	+8.16
GFDL-ESM2M	+2.31	+2.01	+4.80
HadGEM2-CC	−0.68	0	−2.67
HadGEM2-ES	−0.62	−0.06	−2.56
INM-CM4	+2.67	+2.94	+4.30
IPSL-CM5A-LR	+4.58	+4.08	+9.34
IPSL-CM5A-MR	+4.24	+4.03	+10.24
MIROC5	−3.83	−2.37	−7.84
MIROC-ESM	+3.62	+3.11	+9.13
MIROC-ESM-CHEM	+2.84	+2.82	+7.38
MPI-ESM-LR	+1.65	+1.56	+5.22
MPI-ESM-MR	+3.22	+2.50	+8.07
MRI-CGCM3	+3.56	+4.01	+6.56
NorESM1-M	+6.54	+5.38	+12.43

All numbers are given in absolute %.

types, in particular for W+. For example, the frequency of W+ in IPSL-CM5A-LR and IPSL-CM5A-MR is nearly twice as much as in ERA-Interim (+4.08% and +4.03%, respectively). Altogether, 15 (14) of the 22 CMIP5 models show a distinct higher frequency for W (SW, W, NW). Nevertheless, some other models clearly underestimate the westerly types. MIROC5 for instance simulates approximately only half as much CWTs W+ as observed in ERA-Interim (−2.37%). Four models are identified, which show a good agreement with ERA-Interim in terms of the frequencies of the westerly weather types: CNRM-CM5, EC-EARTH, HadGEM2-CC, and HadGEM2-ES. CNRM-CM5 reveals an only slight overestimation of W+ and SW, W, NW, while the deviation for W compared to ERA-Interim is nearly zero. A positive but weak bias is observed for EC-EARTH. HadGEM2-CC and HadGEM2-ES simulate too few CWTs SW, W, NW, while the frequencies of W and W+ match the frequencies in ERA-Interim. A realistic representation of the zonal flow in the historical runs does not necessarily mean that the future projections are more reliable than in the other models. However, for sensitivity studies, this small ensemble of four GCMs is also analysed separately.

As expected, the overestimation of W and W+ in most of the models results in a general overestimation of *Eout* in the historical runs when compared to *Eout* as simulated for ERA-Interim. Figure 1(a) shows the climatological mean of annual *Eout* for the reanalysis. Highest *Eout* is simulated for the offshore regions of the North and the Baltic Sea. Over land, a north–south gradient can be observed, with strong *Eout* along the coastal areas of the North and Baltic Sea and low values over Iberia, the Alps, and Southeast Europe. High magnitudes are also simulated for the British Isles, while *Eout* is weaker over Scandinavia. In particular over Northern Germany and Poland, the ensemble mean of the historical CMIP5 runs clearly overestimates *Eout*, where the annual mean is more than 10^3 MWh higher than in ERA-Interim (Figure 1(b)).

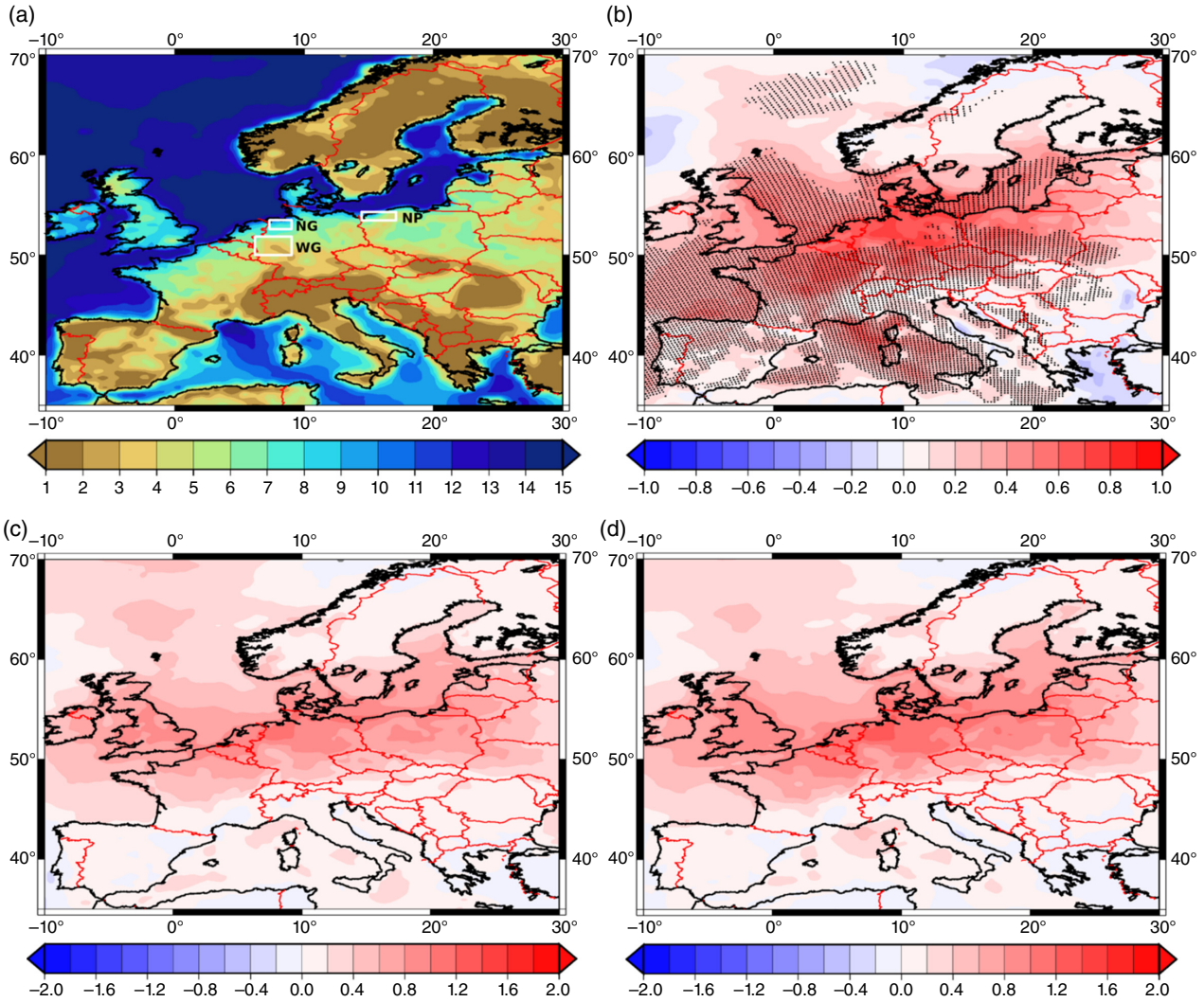

Figure 1. (a) Climatological mean of annual *Eout* in 10^3 MWh for ERA-Interim (1979–2010). (b) Difference of ensemble mean annual *Eout* for the historical runs of the 22 CMIP5 models (1961–2000) minus annual *Eout* of ERA-Interim in 10^3 MWh. The dotted regions indicate grid points, where at least 18 models overestimate *Eout* of ERA-Interim. (c) Difference of *Eout* for winter (December–February) minus *Eout* for summer (June–August) for ERA-Interim in 10^3 MWh. (d) as (c) but for the ensemble mean of the historical runs of the 22 CMIP5 models. The white boxes in (a) indicate the subdomains Northern Germany (NG), Western Germany (WG), and Northern Poland (NP) for detailed analyses.

Only in Southeast Europe and over Northern Scandinavia, the CMIP5 ensemble underestimates *Eout*. Over most parts of Western and Central Europe and the Mediterranean, at least 18 models simulate too high values of *Eout* (Figure 1(b)). The *Eout* biases of the historical runs of the 22 individual models are presented in Figure S1 (Supporting Information). However, despite these biases, the spatial distributions of mean annual *Eout* of all individual models agree well to the spatial pattern of ERA-Interim (not shown). If the CWT frequencies are bias corrected towards the frequencies of ERA-Interim, the magnitudes of annual *Eout* are also similar to the reanalysis (not shown; see also Section 3.2).

Because of more windy conditions in winter over Europe, *Eout* reveals a distinct seasonality in the reanalysis. Figure 1(c) shows the intra-annual variability in ERA-Interim, derived as the difference of winter (December–February) minus summer (June–August) *Eout*. Except from some regions in Southern Europe, *Eout* in winter exceeds the values for summer. Along the coastal areas of the North and the Baltic Sea, *Eout* for December–February is up to 2×10^3 MWh higher than for June–August. This intra-annual variability is captured well by the CMIP5 ensemble (Figure 1(d)). As for ERA-Interim, the ensemble mean *Eout* for winter is higher than for the summer season in most parts of Europe. Aside from the spatial pattern, also the magnitudes of the intra-annual variability in the ensemble mean agree well to ERA-Interim (cf. Figure 1(d) and (c)).

3.2. Future changes of mean annual *Eout*

After evaluating the historical runs of CMIP5, the future responses of mean annual *Eout* in the near future decades (2021–2060) and in the second half of the 21st century (2061–2100) are analysed. These changes are presented in Figure 2 for the ensemble mean of the RCP8.5 scenario. A slight increase of *Eout* in 2021–2060 is revealed for Germany, Scandinavia, and the Baltic States, while less *Eout* is simulated for France, Iberia, and the Mediterranean region (Figure 2(a)). Nevertheless, future

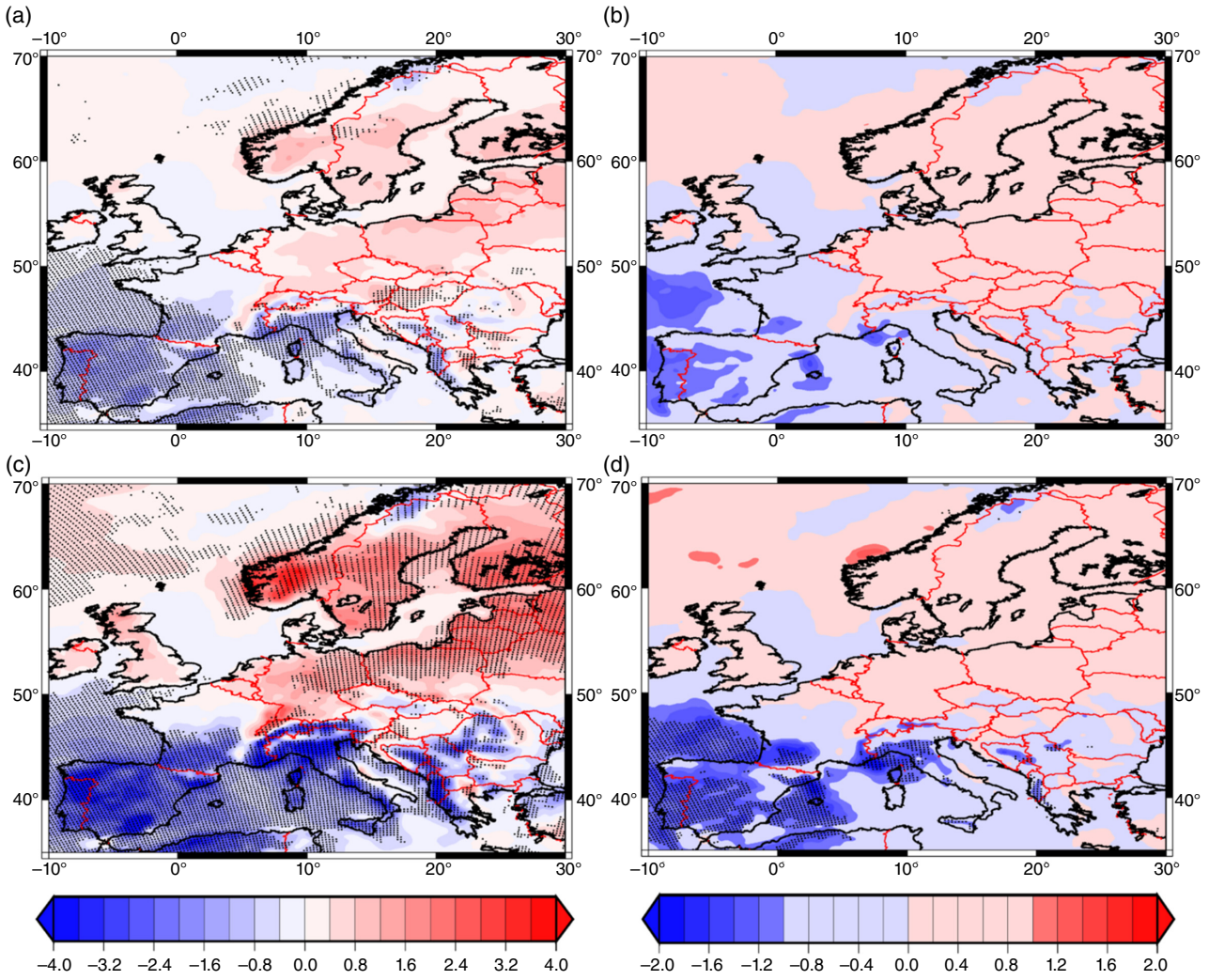

Figure 2. (a) Changes of annual *Eout* in % for the ensemble mean of RCP8.5 (2021–2060) minus the ensemble mean of historical (1961–2000). Dotted regions indicate grid points, where more than 15 models have the same sign as the ensemble mean. (b) Signal-to-noise ratio (mean change divided by standard deviation) for RCP8.5 (2021–2060) minus historical (1961–2000). Dotted regions indicate grid points where the changes are significant at the 95% confidence interval. (c) as (a) but for 2061–2100. (d) as (b) but for 2061–2100.

responses strongly differ between the individual CMIP5 ensemble members (see Figure S2 for the near future projections under the RCP8.5 scenario in all individual models). Accordingly, the signal-to-noise ratio is below 1 for nearly the entire European sector (Figure 2(b)), i.e. the standard deviation between the responses in the individual models is higher than the ensemble mean change. In Southwest Europe, the signal-to-noise ratio is above 1. In this region, more than 15 [thus meaning that the changes are probable according to the Intergovernmental Panel on Climate Change (IPCC) definition, in the following abbreviated as 15+] models show a decrease of *Eout*. Higher robustness of the future changes is found for 2061–2100 (Figure 2(c) and (d)). For large parts of Germany, Scandinavia, and Eastern Europe, 15+ models simulate higher *Eout* (see Figure S3 for individual models), resulting in an ensemble average increase of up to 4% (Figure 2(c)). However, the low signal-to-noise ratios again reveal that there is high uncertainty about the magnitude of the future changes between the individual ensemble members over this region (Figure 2(d)). As a result, the positive ensemble mean responses are not significant. Only the strong decrease over Southwestern Europe is significant at the 95% confidence level. Similar results but with slightly weaker trends are found for the RCP4.5 scenario, indicating that the spatial patterns of the future changes are only marginally sensitive to the radiative forcing in the different scenarios (see Figure S4).

In this study, we have used a 2.5 MW wind turbine from General Electric (2010, hereafter GE2.5) as a benchmark. As specifications may strongly differ between different turbines, the question arises if the identified future changes are sensitive to the choice of turbine. We have additionally considered the specific power curves of four operating turbines to estimate future changes of mean annual *Eout* for exemplary CMIP5 models with opposite trends. The characteristics of the turbines differ not only with regard to their cut-in and cut-out velocity but also in terms of the maximum energy output and the slopes of their power curves (not shown). Results indicate that the projected changes are very similar for all five turbines with respect to both, the magnitude and the spatial pattern. While some sensitivity is found for the choice of the cut-out velocity, the impact of the maximum energy output and the slope of the power curve on future changes is very small (not shown). In summary, the choice of the turbine has an only marginal impact on the estimated future changes. For the following investigations, we have therefore focused only on results of GE2.5.

In a sensitivity study, the future responses have been determined with SDD-simulated *Eout* using bias-corrected CWT frequencies. With this aim, the historical CWT frequencies of the 22 individual models have been corrected towards the respective frequencies of ERA-Interim, and the resulting empirical factors have then been applied to the CWT frequencies of the future scenarios. Nevertheless, because the CWT biases are systematic in both the historical runs and the future scenarios, the bias correction has an only weak impact on the future projections in terms of the climate change signal itself (see also Figure S5). The ensemble mean changes only slightly differ, and for most individual models, the sign of the future trend as derived from bias-corrected data is the same as for the uncorrected models. Therefore, we focus primarily on the original model datasets for the analyses.

In another sensitivity study, the four models with a realistic representation of the frequencies of the westerly weather types are considered (see Section 3.1). These four GCMs show an only weak or in some cases an opposite response to increased greenhouse gas forcing compared to other GCMs (Figures S2 and S3). However, no general sensitivity of the future changes to biases in the historical runs of the individual models is detectable for *Eout* (not shown).

To quantify the spread between the different individual 22 ensemble members particularly over Central Europe, Figure 3 shows box-whisker plots of the absolute *Eout* changes under both scenarios for three exemplary subdomains (cf. Figure 1(a)). The subdomains are located at the coastal area of the Baltic Sea in Northern Poland (NP), at the coastal area of the North Sea in Northern Germany (NG), and in Western Germany (WG), which is characterized by low mountain ranges. For WG, the majority of the models reveal a positive trend of mean annual *Eout* (Figure 3(a)). The median change is positive for both future periods and scenarios. More than 75% of the models simulate more *Eout* in 2061–2100 under the RCP8.5 scenario. Nevertheless, a distinct spread between the ensemble members is observed. For example, the future changes for the period 2021–2060 under RCP4.5 range from ca. +400 MWh to −200 MWh. A higher uncertainty between the ensemble members is found for NG (Figure 3(b)). Depending on the period and the scenario, the median change is either positive or negative. Again, the individual responses range from high positive to high negative values for both future periods and scenarios. For NP, a higher agreement between the individual models with respect to the sign of the future changes can be observed (Figure 3(c)). Most of the models show increasing *Eout* values for both future periods. A maximum increase of more than 400 MWh is simulated for 2061–2100 under RCP8.5. At the same time, a decrease of −100 MWh is detected within the CMIP5 ensemble for this period and scenario. Also for the near future decades (2021–2060), a distinct spread between the ensemble members is observed. In general, changes of mean annual *Eout* for the three subdomains are small when compared to the model-intern variability. For most individual GCMs, the future changes for both scenarios and time periods are below the historical inter-annual variability (see black box-whisker plots in Figure 3).

To summarize, an increase of mean annual *Eout* is found for the majority of the CMIP5 ensemble under future climate conditions for Central and Northern Europe (likely for the Baltic States in 2061–2100 under the RCP8.5 scenario), while decreasing values are found for Southern Europe (likely for the second half of the 21st century). As a consequence, positive ensemble mean changes in the former region and negative, significant changes in the latter

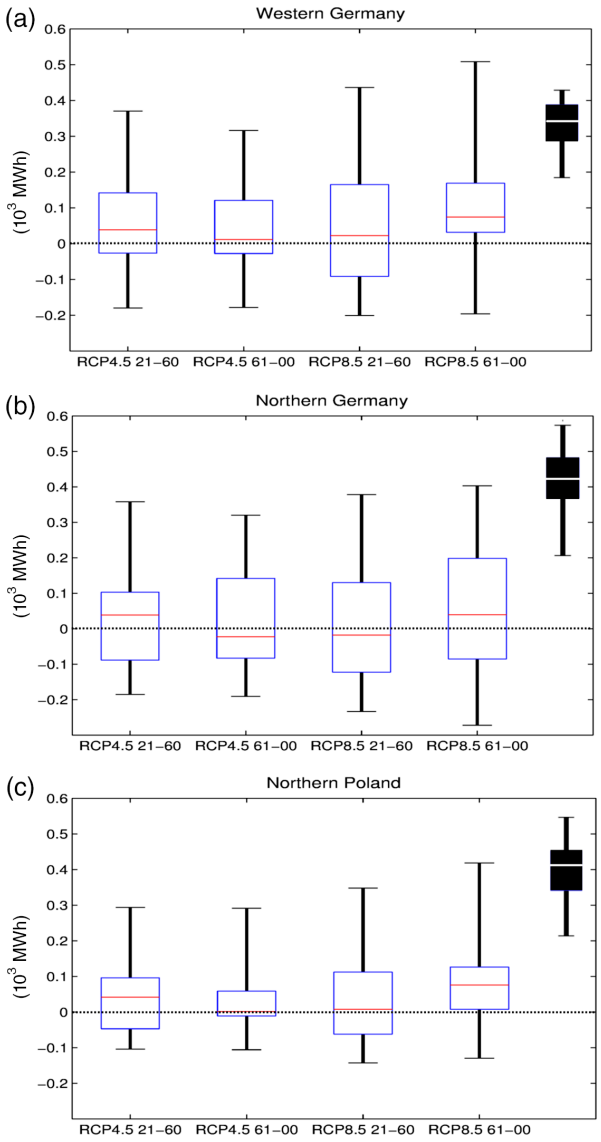

Figure 3. Box-whisker plots for the changes of mean annual *Eout* in 10^3 MWh in the 22 ensemble members for (a) Western Germany, (b) Northern Germany, and (c) Northern Poland. The whisker indicate the minimum and maximum changes, the boxes represent the 25th–75th percentile, and the middle line shows the median. From left to right: RCP4.5 2021–2060; RCP4.5 2061–2100; RCP8.5 2021–2060; RCP8.5 2061–2100. The black box-whisker plots at top right show ranges of the model-intern inter-annual variability in the historical runs. For the location of the subdomains please refer to Figure 1(a).

are simulated. However, large uncertainties between the ensemble members are detected, including opposite signs of the future trends in some regions.

The regional ensemble mean changes of annual *Eout* can be related to alterations of the large-scale atmospheric circulation under future climate conditions. Figure 4(a) and (b) shows the ensemble mean changes of large-scale MSLP and mean wind speed in the RCP8.5 scenario for the 18 available GCMs (see Table 1). An average decrease of MSLP for a band north of 60°N is found in future decades (isolines in Figure 4), and the change is stronger for 2061–2100 than for 2021–2060. These alterations result in general stronger MSLP gradients over Northern Europe and along the coastal areas of the North and Baltic Sea (not shown). As a consequence, higher large-scale mean wind speeds are detected over the North and Baltic Sea, Germany, and most parts of Scandinavia and the Baltic States (shading in Figure 4) particularly for the late 21st century. Further, an eastward shift of the Azores high pressure system is detected for both periods, leading to a weakening of mean wind speeds over Spain and the Mediterranean. The future changes of both MSLP and mean wind speed are similar for the RCP4.5 scenario but with lower magnitudes (not shown). The ensemble mean responses in large-scale mean wind speed correspond well to regional changes of *Eout* (cf. Figure 2). However, opposite trends are found for parts of the North Sea and Southeast Europe. Also for the individual models in most cases shifts in mean wind speed are in line with regional changes in *Eout*. On the other hand, discrepancies in the sign of the trends are found for some limited regions depending on the model (not shown).

3.3. Intra- and inter-annual changes

Aside from changes of mean wind energy potentials, possible changes in the intra- and inter-annual variability of *Eout* due to climate change are of crucial interest for future planning. While a decrease of the variability would benefit the wind energy sector due to more regularity of energy production, a higher variability can potentially lead to a lower reliability of wind energy as an alternative energy source.

As shown in Section 3.1, in both the reanalysis and the historical runs of the CMIP5 models, *Eout* of the sample turbine is higher during winter than for summer. Hence, increased *Eout* in winter with a simultaneously decline of summer *Eout* in the upcoming decades would result in a higher intra-annual variability. Figure 5(a) and (b) shows the ensemble mean changes of *Eout* in winter (December–February) for the RCP8.5 scenario. For both future periods (2021–2060 and 2061–2100), more *Eout* is simulated over Central and Northern Europe, while a decline can be observed for Southern Europe. These trends are likely and much stronger for the second half of the 21st century, where for the majority of Europe 15+ models show the same response as the ensemble means (Figure 5(b)). Accordingly, over the North Sea and for some Mediterranean regions, the signal-to-noise ratio is above 1 (not shown). A very different spatial pattern of change is detected for the summer season (Figure 5(c) and (d)). Except from some local regions, particularly over the Mediterranean, an overall decrease of *Eout* is simulated for 2021–2060 (more likely than not at most grid points) and, more robust, for 2061–2100 (likely at most grid points). As for the changes of mean annual *Eout* (see Section 3.2), future trends of seasonal *Eout* show a large spread between the individual models, as is illustrated in Figures S6 and S7 for 2021–2060 under the RCP8.5 scenario. For both scenarios, the seasonal changes (as shown in Figure 5(a)–(d) for RCP8.5) result in a strong ensemble mean amplification of the intra-annual variability of *Eout* over large parts

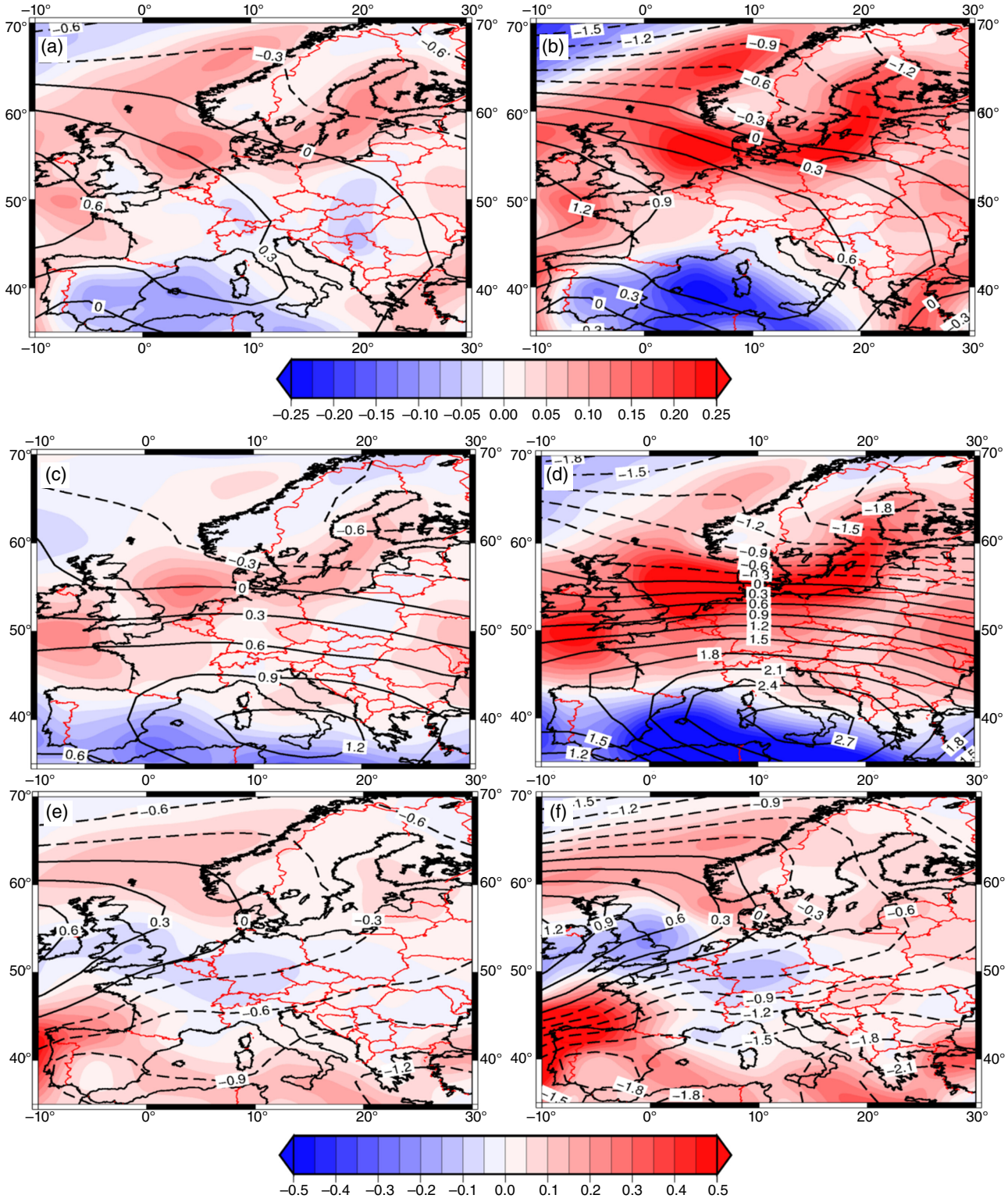

Figure 4. Changes of MSLP (isolines in hPa) and mean wind speed (shaded areas in $m\,s^{-1}$) for the ensemble mean of the RCP8.5 scenario minus the ensemble mean of the historical (1961–2000) for 2021–2060 (left) and 2061–2100 (right). (a, b) For the whole year, (c, d) for winter, (e, f) for summer. Only 18 ensemble members are considered (see text).

of Central and Northern Europe (see Figure 5(e) and (f) for the RCP8.5 scenario). For 2061–2100, the increase accounts for up to 30% for RCP8.5 (Figure 5(f)). For both scenarios and periods, this positive trend is probable, because 15+ models simulate an increase for most grid points in this domain. On the other hand, a decline of the variability is found for Southern Europe (Figure 5(e) and (f)). Note that the high percentages in this region are due to the comparable low intra-annual variability in the ensemble mean for the historical runs (cf. Figure 1(d)).

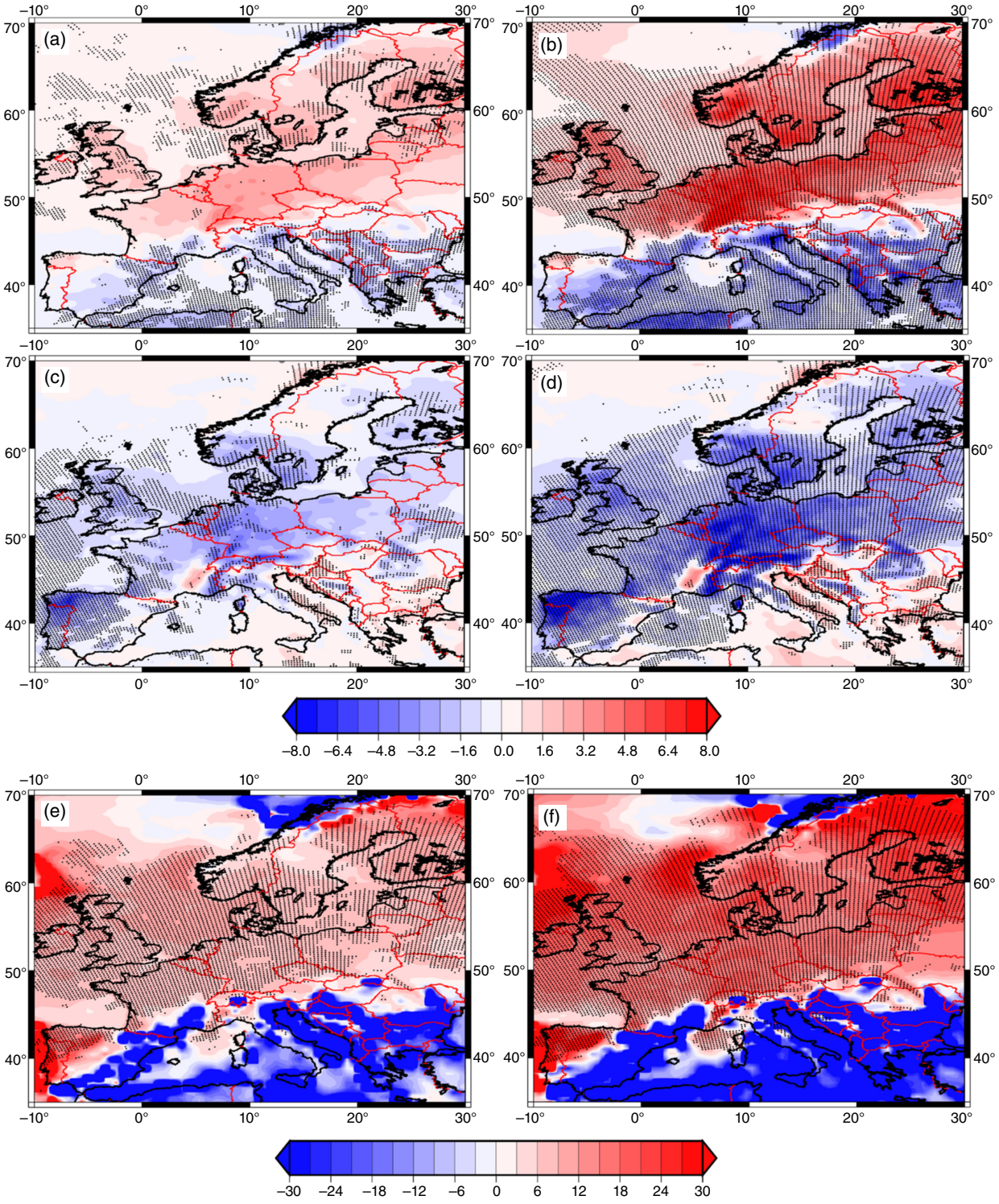

Figure 5. Changes of winter (December–February) *Eout* in % for the ensemble mean of RCP8.5 minus the ensemble mean of historical (1961–2000) for (a) 2021–2060 and (b) 2061–2100. Dotted regions indicate grid points where more than 15 models have the same sign as the ensemble mean. (c) as (a), but for summer. (d) as (b), but for summer. Changes of intra-annual variability (December–February minus June–August) of *Eout* in % for the ensemble mean of RCP8.5 minus the ensemble mean of historical (1961–2000) for (e) 2021–2060 and (f) 2061–2100. Dotted regions indicate grid points where more than 15 models show an increasing intra-annual variability.

As for the mean annual changes, future trends of *Eout* during winter are in line with shifts of the large-scale pressure fields and mean wind speeds in the CMIP5 models (cp. Figure 5(a) and (b) with Figure 4(c) and (d)). The changes in the large-scale ensemble mean (MSLP and mean wind speed) are similar to the annual changes (cf. Figure 4(a) and (b)), but with much stronger trends. Some discrepancies between changes of *Eout* and mean wind speed are revealed for the summer season (cf. Figure 5(c) and (d) with 4(e) and (f)). For instance, the mean wind

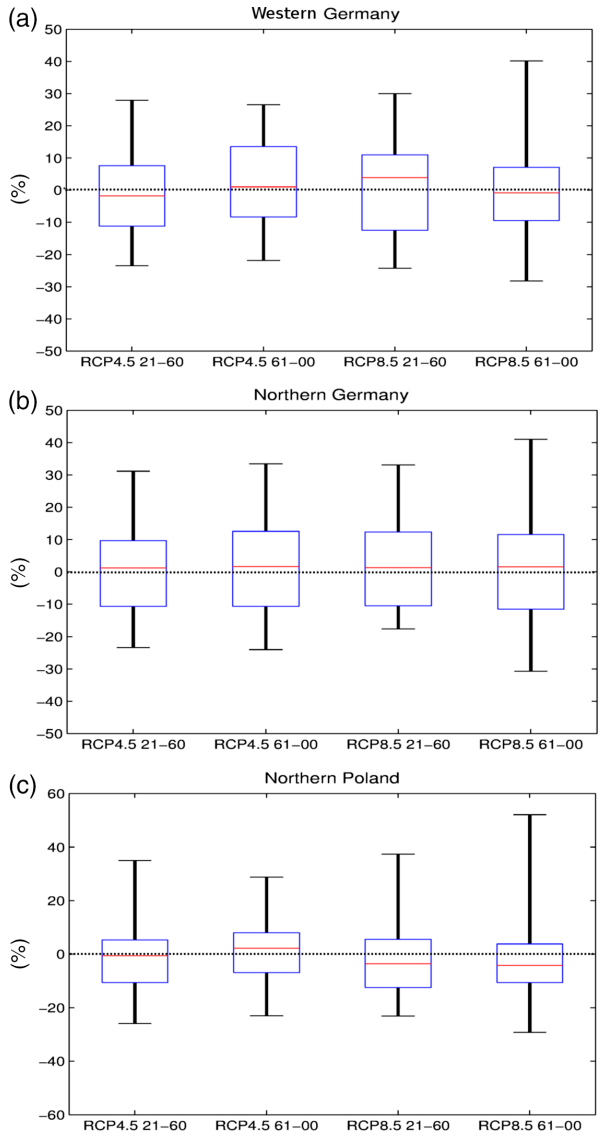

Figure 6. Box-whisker plots for the changes of inter-annual variability of *Eout* in % in the 22 ensemble members for (a) Western Germany, (b) Northern Germany, and (c) Northern Poland. The whisker indicate the minimum and maximum changes, the boxes represent the 25th–75th percentile, and the middle line shows the median. From left to right: RCP4.5 2021–2060; RCP4.5 2061–2100; RCP8.5 2021–2060; RCP8.5 2061–2100. For the location of the subdomains please refer to Figure 1(a).

speed slightly increases over the North and Baltic Sea, while *Eout* at the same time decreases.

Changes of the inter-annual variability of *Eout* are determined in terms of the standard deviation of annual *Eout* for each individual model, separately. On annual time-scales, the SDD used in this study is most reliable for Germany and the surrounding area due to the choice of the central point being located at 50°N, 10°W (see Section 2 and Reyers *et al.*, 2015). Therefore, we focus on the three selected domains over this area (cf. Figure 1(a)). Figure 6 shows box-whisker plots as derived from the relative changes of the inter-annual variability in the 22 individual CMIP5 models over the three subdomains. For both periods and scenarios, the median changes oscillate around zero and the trends reveal a large spread from strong positive to strong negative values. In particular for the second half of the 21st century, the changes under the RCP8.5 scenario vary between approximately −40 and +40% in all three subdomains. These results reflect that there is a high uncertainty about the changes of the inter-annual variability of *Eout* in a future climate in the CMIP5 ensemble.

The inter-annual variability in the historical runs of the 22 individual models as well as the respective future changes for the three subdomains are depicted in Tables S1–S3. There is apparently no relationship between the ability of the models to simulate realistic standard deviations and the future changes of the variability (see third–sixth column in Tables S1–S3). Future changes not only vary between the individual models but also between the scenarios and periods within single models. While in some models the sign of the trends are equal for both periods and scenarios (e.g. MIROC-ESM-CHEM in WG, Table S1), the trend shows opposite signs in other models, depending on the scenario and the period (e.g. HadGEM-CC in NP, Table S3).

We have compared the future changes of the inter-annual variability of regional *Eout* in the three subdomains with changes of the variability of large-scale mean wind speeds at the corresponding grid points of the 18 available individual CMIP5 models (not shown). As for *Eout*, the future changes of the variability for wind strongly differ between the individual models and/or scenarios/periods. For some of the models, projected changes have the same sign in 2021–2061 and in 2061–2100 under both scenarios (e.g. MIROC5 and MPI-ESM-MR in WG). On the other hand, there are also a few models which show opposite trends for both periods and both scenarios (e.g. GFDL-ESM2G in WG). Hence, the conclusions for the mean wind speed are the same as for local *Eout*: there is a high uncertainty with respect to future changes of the inter-annual variability for Central Europe in the CMIP5 ensemble.

4. Summary and discussion

In this study, an SDD method is used to estimate future changes of regional *Eout* of a benchmark turbine over Europe for an ensemble of 22 CMIP5 models. The changes are determined for near future conditions (2021–2060) and for the second half of the 21st century (2061–2100) following the two scenarios RCP4.5 and RCP8.5. The main findings of the study can be summarized as follows:

(i) The CMIP5 ensemble mean reveal an increase of mean annual *Eout* over Northern and Central Europe and a decrease over the Mediterranean area. According to the IPCC definition, the increase over Northern and Central Europe is more likely than not, while it is likely for the Baltic States and 2061–2100. The decrease over Southern Europe is likely over most of the area for both periods under the RCP8.5 scenario. However, there is some uncertainty about these projections with respect to both the magnitude and the sign of the changes.

(ii) More robust results are found in seasonal terms, in particular for the second half of the 21st century: increasing *Eout* is likely for winter and a decline is likely in summer for most parts of Europe. This leads to a stronger intra-annual variability of *Eout* over most of Europe and thus to a higher irregularity of wind energy production in future decades.
(iii) Analyses of the future changes of the inter-annual variability reveal a very high uncertainty between the models for Central Europe. Hence, it is not possible to conclude whether the wind energy sector will have to deal with changes in reliability of wind energy production in future decades over Central Europe.

The ensemble mean results found in this study are generally consistent with the findings of most recent analyses dealing with future changes of wind energy potentials. An increase of wind energy potentials (particularly in the winter season) over parts of Northern and Central Europe was also found by Cradden *et al.* (2012); Hueging *et al.* (2013); Nolan *et al.* (2012, 2014); and Tobin *et al.* (2015). However, this study identified quite wide-range future changes based on the 22 GCMs, which may in some cases strongly differ from the ensemble mean response (see also Tobin *et al.*, 2015). Some models predict a decrease of wind energy potentials over Northern Europe, which is in line with the findings of Pryor *et al.* (2005). On the other hand, a distinct significant increase of the inter-annual variability over Central Europe, as found by Hueging *et al.* (2013) based on ECHAM5 GCM simulations from the CMIP3 experiment, is not confirmed by the results of our multi-model ensemble analysis. This result shows how important it is to consider multi-model ensembles for impact studies as in this case for wind energy.

In contrast to other studies using single GCMs, most of future changes in terms of the ensemble mean analysed here are not significant. Even in the strong response during winter, only a few grid points in Southern Europe are significant at the 95% confidence interval. This is not only due to the ensemble spread in simulated *Eout* for the future decades but also due to the strong differences in the historical runs of the models, which both contribute to the ensemble mean changes. This is in line with Tobin *et al.* (2015), who concluded from an ensemble of CMIP3 RCM simulations that the changes in wind power potential will probably remain within a 20% range even in the late 21st century.

In most cases, results from the RCP8.5 scenario have been discussed, which is the most realistic scenario when regarding the actually recent emissions. Although the responses under the RCP4.5 are in some cases clearly weaker than in RCP8.5, this has no impact on the main findings of this study with respect to the sign of ensemble mean changes and only a small influence on the uncertainties. In fact, changes for RCP4.5 and RCP8.5 are very similar for 2021–2060.

The regional changes of *Eout* have been related to future shifts of large-scale mean wind speeds in the models. Despite a general agreement between responses of both *Eout* and wind, in some regions non-consistent trends are detected. This is not only the case for the ensemble mean but also for individual models (not shown). Further, changes of *Eout* for some models do not necessarily correspond to changes of the number of cyclones over the European sector found in Zappa *et al.* (2013; see their appendix). There are several possible reasons for these differences. First, *Eout* is strongly influenced by local topographic characteristics. In this study, we have used an RCM with a horizontal resolution of 0.22° for the downscaling of *Eout*, which enables a realistic representation of coast lines and mountain ranges. Because the resolutions of the CMIP5 models are much coarser (1.125° or coarser, see Table 1), these regional orographic effects are not captured in the large-scale fields of mean wind speed. Further, *Eout* of the sample turbine not only depends on mean or maximum wind conditions but also on the full spectrum of wind speeds in a certain time period. If (as an idealized example) in a future period only the low and high percentiles of the wind speed equally change, the trend of the mean wind speed is small or even nearly zero, while *Eout* may strongly increase because of the characteristics of the turbine (*Eout* proportional to v cubed).

The SDD approach uses simulated episodes from ERA-Interim. In case weather conditions occur in the GCM which feature pressure gradients higher than the strongest gradient in ERA-Interim, no simulated representatives are available. This could potentially be an issue for the westerly CWTs (SW, W, NW). We have quantified the number of days per decade with a gradient higher than 45 hPa per 1000 km (strongest gradient found in ERA-Interim) for these three CWTs. For 21 of the 22 GCMs, the number of days with these characteristics is always below 0.5 days per decade (MRI-CGCM3 features roughly 2.5 days per decade), both for the historical and the RCP8.5 scenario period. As these days are not removed from the analysis, but are assigned to the CWTs with the strongest pressure gradient in ERA-Interim (40–45 hPa per 1000 km), this issue leads only to negligible differences. Hence, we conclude that this simplification has nearly no influence on the analysed future projections and that the method is therefore appropriate for a multi-model assessment of future wind energy potentials.

Another simplification in our method is the use of a constant power law coefficient to obtain wind speeds in 80 m height (see Reyers *et al.*, 2015). Such simplifications (e.g. Hueging *et al.*, 2013) are necessary due to the large amount of data which needs to be handled in such a multi-model approach. Tobin *et al.* (2015) have addressed this issue and showed that the use of a dynamic power law coefficient instead of a constant coefficient has only a slight impact on the climate change projections of wind energy potentials based on CMIP3 models. Further, the resulting biases are mostly systematic in both present and future periods, and thus cancel each other out when computing future changes.

A challenge for future works is to identify the reasons for the uncertainties in the responses of *Eout* to climate change in the CMIP5 models. In some recent studies, the

uncertainties of projected changes of synoptic variability or of large-scale flow conditions in CMIP3 and CMIP5 models could be related to uncertainties in the response of the North Atlantic Ocean (e.g. Woollings *et al.*, 2012; Haarsma *et al.*, 2013). In terms of local changes of wind energy potentials in different European regions, a more detailed analysis is required, e.g. on how regional wind systems are affected by large-scale changes.

Regarding the findings of this study, we conclude that future projections of wind energy potentials over Europe strongly depend on the choice of the GCM. Therefore, it is advisable to perform multi-model assessments using large ensembles of GCMs in future works. Future work will also focus on the CORDEX Europe database to enable a more detailed analysis of future projections of wind energy potentials for Europe at the regional scale.

Acknowledgements

First of all, we acknowledge the World Climate Research Programme's Working Group on Coupled Modelling, which is responsible for CMIP, and we thank the climate modelling groups from all over the world (listed in Table 1) for producing and making available their model output. For CMIP, the US Department of Energy's Program for Climate Model Diagnosis and Intercomparison provides coordinating support and led development of software infrastructure in partnership with the Global Organization for Earth System Science Portals. This research is funded by collaboration with the Helmholtz-Zentrum Geesthacht/Climate Service Center (HZG/CSC). We thank the ECMWF for the ERA-Interim Reanalysis dataset and the German Climate Computer Centre (DKRZ, Hamburg) for computer and storage resources. We thank the Climate Limited-area Modelling Community (CLM-Community) for providing the COSMO-CLM model and for assistance. Finally, we thank the two anonymous reviewers for their helpful comments.

Supporting Information

The following supporting information is available as part of the online article:

Table S1. Inter-annual variability (10^{-3} σ mean^{-1}) of spatial mean of *Eout* for Western Germany (see Figure 1(a) of the main text) for ERA-Interim and the 22 models (second column), and the future changes in % (third–sixth column).

Table S2. Inter-annual variability (10^{-3} σ mean^{-1}) of spatial mean of *Eout* for Northern Germany (see Figure 1(a) of the main text) for ERA-Interim and the 22 models (second column), and the future changes in % (third–sixth column).

Table S3. Inter-annual variability (10^{-3} σ mean^{-1}) of spatial mean of *Eout* for Northern Poland (see Figure 1(a) of the main text) for ERA-Interim and the 22 models (second column), and the future changes in % (third–sixth column).

Figure S1. Differences of mean annual *Eout* for the historical runs of the 22 CMIP5 models (1961–2000) minus annual *Eout* of ERA-Interim in 10^3 MWh.

Figure S2. Changes of annual *Eout* in % for RCP8.5 (2021–2060) minus the historical runs (1961–2000) for the 22 CMIP5 models.

Figure S3. Changes of annual *Eout* in % for RCP8.5 (2061–2100) minus the historical runs (1961–2000) for the 22 CMIP5 models.

Figure S4. (a) Changes of annual *Eout* in % for the ensemble mean of RCP4.5 (2021–2060) minus the ensemble mean of historical (1961–2000). Dotted regions indicate grid points, where more than 15 models have the same sign as the ensemble mean. (b) Signal-to-noise ratio (mean change divided by standard deviation) for RCP4.5 (2021–2060) minus historical (1961–2000). Dotted regions indicate grid points where the changes are significant at the 95% confidence interval. (c) as (a) but for 2061–2100. (d) as (b) but for 2061–2100.

Figure S5. (a) Changes of annual *Eout* in % for the uncorrected ensemble mean of RCP8.5 (2061–2100) minus the ensemble mean of historical (1961–2000). Dotted regions indicate grid points, where more than 15 models have the same sign as the ensemble mean. (b) Signal-to-noise ratio (mean change divided by standard deviation) for uncorrected RCP8.5 (2061–2100) minus historical (1961–2000). Dotted regions indicate grid points where the changes are significant at the 95% confidence interval. (c) as (a) but for the bias-corrected ensemble. (d) as (b) but for the bias-corrected ensemble. For details, see main text.

Figure S6. Changes of winter (December–February) *Eout* in % for RCP8.5 (2021–2060) minus the historical runs (1961–2000) for the 22 CMIP5 models.

Figure S7. Changes of summer (June–August) *Eout* in % for RCP8.5 (2021–2060) minus the historical runs (1961–2000) for the 22 CMIP5 models.

References

Barstad I, Sorteberg A, dos-Santos Mesquita M. 2012. Present and future offshore wind power potential in Northern Europe based on downscaled global climate runs with adjusted SST and sea ice cover. *Renew. Energy* **44**: 398–405.

Capros P, De Vita A, Hoeglund-Isaksson L, Winiwarter W, Purohit P, Bottcher H, Frank S, Havlik P, Gusti M, Witzke HP. 2013. EU energy, transports and GHG emissions. Trends to 2050. Reference scenario 2013. European Commission, Luxembourg.

Chang EKM, Guo Y, Xia X. 2012. CMIP5 multimodel ensemble projection of storm track change under global warming. *J. Geophys. Res. Atmos.* **117**: D23118, doi: 10.1029/2012JD018578.

Cradden LC, Harrison GP, Chick JP. 2012. Will climate change impact on wind power development in the UK? *Clim. Change* **115**: 837–852.

Dee DP, Uppala SM, Simmons AJ, Berrisford P, Poli P, Kobayashi S, Andrae U, Balmaseda MA, Balsamo G, Bauer P, Bechtold P, Beljaars ACM, van de Berg L, Bidlot J, Bormann N, Delsol C, Dragani R, Fuentes M, Geer AJ, Haimberger L, Healy SB, Hersbach H, Holm EV, Isaksen L, Kallberg P, Kohler M, Matricardi M, McNally AP, Monge-Sanz BM, Morcrette JJ, Park BK, Peubey C, de Rosnay P, Tavolato C, Thepaut JN, Vitart F. 2011. The ERA-Interim reanalysis: configuration and performance of the data assimilation system. *Q. J. R. Meteorol. Soc.* **137**: 553–597.

Fuentes U, Heimann D. 2000. An improved statistical-dynamical downscaling scheme and its application to the Alpine precipitation climatology. *Theor. Appl. Climatol.* **65**: 119–135.

General Electric. 2010. 2.5 MW wind turbine series GEA17007B. http://site.ge-energy.com/prod_serv/products/wind_turbines/en/downloads/GEA17007A-Wind25Brochure.pdf (accessed 2 March 2015).

Giorgi F, Jones C, Asrar GR. 2006. Addressing climate information needs at the regional level: the CORDEX framework. *Bull. World Meteorol. Organ.* **58**: 175–183.

Haarsma RJ, Selten F, van Oldenburgh GJ. 2013. Anthropogenic changes of the thermal and zonal flow structure over Western Europe and Eastern North Atlantic in CMIP3 and CMP5 models. *Clim. Dyn.* **41**: 2577–2588, doi: 10.1007/s00382-013-1734-8.

Hueging H, Born K, Haas R, Jacob D, Pinto JG. 2013. Regional changes in wind energy potential over Europe using regional climate model ensemble projections. *J. Appl. Meteorol. Climatol.* **52**: 903–917, doi: 10.1175/JAMC-D-12-086.1.

Jones PD, Hulme M, Briffa KR. 1993. A comparison of lamb circulation types with an objective classification scheme. *Int. J. Climatol.* **13**: 655–663.

Meinshausen M, Smith SJ, Calvin K, Daniel JS, Kainuma MLT, Lamarque JF, Matsumoto K, Montzka SA, Raper SCB, Riahi K, Thomson A, Velders GJM, van Vuuren DPP. 2011. The RCP greenhouse gas concentrations and their extensions from 1765 to 2300. *Clim. Change* **109**: 213–241, doi: 10.1007/s10584-011-0156-z.

Moccia J, Arapogianni A, Wilkes J, Kjaer C, Gruet R. 2011. Pure power – wind energy targets for 2020 and 2030. European Wind Energy Association Report, EWEA, Brussels, 98 pp. http://www.ewea.org/fileadmin/files/library/publications/reports/Pure_Power_III.pdf (accessed 2 March 2015).

Nolan P, Lynch P, McGrath R, Semmler T, Wang SY. 2012. Simulating climate change and its effect on the wind energy resource of Ireland. *Wind Energy* **15**: 593–608, doi: 10.1002/we.489.

Nolan P, Lynch P, Sweeney C. 2014. Simulating the future wind energy resource of Ireland using the COSMO-CLM model. *Wind Energy* **17**: 19–37, doi: 10.1002/we.1554.

Ouammi A, Ghigliotti V, Robba M, Mimet A, Sacile R. 2012. A decision support system for the optimal exploitation of wind energy on regional scale. *Renew. Energy* **37**: 299–309.

Pinto JG, Neuhaus CP, Leckebusch GC, Reyers M, Kerschgens M. 2010. Estimation of wind storm impacts over West Germany under future climate conditions using a statistical-dynamical downscaling approach. *Tellus A* **62**: 188–201, doi: 10.1111/j.1600-0870.2009.00424.x.

Pryor SC, Barthelmie RJ. 2010. Climate change impacts on wind energy: a review. *Renew Sustain Energy Rev.* **14**: 430–437.

Pryor SC, Schoof JT, Barthelmie RJ. 2005. Climate change impacts on wind speeds and wind energy density in northern Europe: empirical downscaling of multiple AOGCMs. *Clim. Res.* **29**: 183–198, doi: 10.3354/cr029183.

Pryor SC, Barthelmie RJ, Claussen NE, Drews M, MacKellar N, Kjellström E. 2012. Analyses of possible changes in intense and extreme wind speeds over Northern Europe under climate change scenarios. *Clim. Dyn.* **38**: 189–208.

Reyers M, Pinto JG, Moemken J. 2015. Statistical-dynamical downscaling for wind energy potentials: evaluation and applications to decadal hindcasts and climate change projections. *Int. J. Climatol.* **35**: 229–244, doi: 10.1002/joc.3975.

Rockel B, Will A, Hense A. 2008. Special issue: regional climate modelling with COSMO-CLM (CCLM). *Meteorol. Z.* **17**: 347–348.

Sillmann J, Croci-Maspoli M. 2009. Present and future atmospheric blocking and its impact on European mean and extreme climate. *Geophys. Res. Lett.* **36**: L10702, doi: 10.1029/2009GL038259.

Taylor KE, Stouffer RJ, Meehl GA. 2012. An overview of CMIP5 and the experiment design. *Bull. Am. Meteorol. Soc.* **93**(4): 485–498, doi: 10.1175/BAMS-D-11-00094.1.

Tobin I, Vautard R, Balog I, Bréon F-M, Jerez S, Ruti PM, Thais F, Vrac M, Yiou P. 2015. Assessing climate change impacts on European wind energy from ENSEMBLES high-resolution climate projections. *Clim. Change* **128**: 99–112, doi: 10.1007/s10584-014-1291-0.

Wiser R, Yang Z, Hand M, Hohmeyer O, Infield D, Jensen PH, Nikolaev V, O'Malley M, Sinden G, Zervos A. 2011. Wind energy. In *IPCC Special Report on Renewable Energy Sources and Climate Change Mitigation*, Edenhofer O, Pichs-Madruga R, Sokona Y, Seyboth K, Matschoss P, Kadner S, Zwickel T, Eickemeier P, Hansen G, Schlömer S, von Stechow C (eds). Cambridge University Press: Cambridge, UK and New York, NY.

Woollings T, Gregory JM, Pinto JG, Reyers M, Brayshaw DJ. 2012. Response of the North Atlantic storm track to climate change shaped by ocean-atmosphere coupling. *Nat. Geosci.* **5**: 313–317, doi: 10.1038/ngeo1438.

Zappa G, Shaffrey LC, Hodges KI, Sansom PG, Stephenson DB. 2013. A multimodel assessment of future projections of North Atlantic and European extratropical cyclones in the CMIP5 climate models. *J. Clim.* **26**: 5846–5862, doi: 10.1175/JCLI-D-12-00573.1.

Supplementary Material

Tab.S 1: Inter-annual variability (10^{-3} σ/mean) of spatial mean of *Eout* for Western Germany (see Figure 1a of the main text) for ERA-Interim and the 22 models (second column), and the future changes in % (third-sixth column).

Model	Historical	RCP4.5 (2021-2060)	RCP4.5 (2061-2100)	RCP8.5 (2021-2060)	RCP8.5 (2061-2100)
ERA-Interim	64.06				
ACCESS1.3	74.07	-2.22	-0.90	-0.22	-14.11
CanESM2	74.49	-11.42	2.75	11.15	-17.22
CCSM4	69.04	-12.71	-7.05	13.77	-6.76
CNRM-CM5	60.82	7.61	13.51	9.65	6.34
CSIRO-Mk3.6.0	61.56	-3.86	-11.90	-15.36	-6.63
EC-EARTH	66.05	6.71	15.62	13.83	5.29
FGOALS-g2	50.01	4.37	20.17	6.20	40.17
GFDL-CM3	61.63	27.97	18.73	7.56	-6.49
GFDL-ESM2G	60.68	14.43	11.09	10.65	14.14
GFDL-ESM2M	79.85	-16.75	-12.80	-18.37	-28.26
HadGEM2-CC	67.38	10.11	6.40	-12.49	2.19
HadGEM2-ES	82.03	-4.41	-10.96	1.63	7.12
INM-CM4	65.79	6.56	13.60	-9.61	2.16
IPSL-CM5A-LR	75.07	-5.39	-8.31	-12.82	11.85
IPSL-CM5A-MR	78.23	-5.75	1.03	-6.73	31.10
MIROC5	51.17	-1.37	8.16	7.89	-3.86
MIROC-ESM	64.71	2.73	-7.85	10.94	-13.97
MIROC-ESM-CHEM	79.22	-23.50	-21.86	-24.24	-9.49
MPI-ESM-LR	57.87	27.72	26.56	29.96	30.16
MPI-ESM-MR	67.92	-21.97	-15.56	14.04	-18.03
MRI-CGCM3	65.70	9.59	-6.46	-1.79	2.67
NorESM1-M	76.80	-11.17	1.00	-15.72	-6.41

Tab.S 2: Inter-annual variability (10^{-3} σ/mean) of spatial mean of *Eout* for Northern Germany (see Figure 1a of the main text) for ERA-Interim and the 22 models (second column), and the future changes in % (third-sixth column).

Model	Historical	RCP4.5 (2021-2060)	RCP4.5 (2061-2100)	RCP8.5 (2021-2060)	RCP8.5 (2061-2100)
ERA-Interim	41.13				
ACCESS1.3	54.08	-7.46	-6.73	-9.88	-20.29
CanESM2	50.79	-10.66	3.53	6.04	-18.48
CCSM4	49.47	-20.11	-11.46	13.40	-11.40
CNRM-CM5	42.57	1.25	11.20	12.36	0.92
CSIRO-Mk3.6.0	45.15	-5.45	-20.55	-10.46	-10.10
EC-EARTH	45.61	2.75	12.88	10.31	2.81
FGOALS-g2	35.20	2.18	19.10	-4.48	41.06
GFDL-CM3	43.56	16.85	12.56	0.32	-14.02
GFDL-ESM2G	39.25	19.31	20.04	19.93	32.86
GFDL-ESM2M	57.98	-23.40	-13.65	-17.61	-30.68
HadGEM2-CC	49.71	11.19	1.58	-11.00	2.29
HadGEM2-ES	52.66	5.59	1.30	5.87	8.80
INM-CM4	46.92	0.39	12.25	-14.91	5.87
IPSL-CM5A-LR	52.43	2.47	1.71	-7.94	11.56
IPSL-CM5A-MR	60.47	-16.70	-10.65	-17.04	15.74
MIROC5	29.31	9.67	26.76	28.86	27.80
MIROC-ESM	47.29	1.17	-13.98	2.28	-18.22
MIROC-ESM-CHEM	55.15	-22.61	-24.06	-15.94	-5.04
MPI-ESM-LR	36.90	31.17	33.48	33.07	34.10
MPI-ESM-MR	45.03	-13.39	-10.13	18.71	-11.53
MRI-CGCM3*	43.06	11.70	4.60	9.26	6.20
NorESM1-M	53.28	-1.02	-2.75	-5.41	-6.35

Tab.S 3: Inter-annual variability (10^{-3} σ/mean) of spatial mean of *Eout* for Northern Poland (see Figure 1a of the main text) for ERA-Interim and the 22 models (second column), and the future changes in % (third-sixth column).

Model	Historical	RCP4.5 (2021-2060)	RCP4.5 (2061-2100)	RCP8.5 (2021-2060)	RCP8.5 (2061-2100)
ERA-Interim	59.66				
ACCESS1.3	73.88	-6.46	-10.14	-4.46	-20.86
CanESM2	67.12	-10.67	7.99	8.02	-10.64
CCSM4	65.76	-8.25	7.34	13.28	-5.07
CNRM-CM5	60.47	-5.89	17.04	2.55	4.27
CSIRO-Mk3.6.0	52.79	2.82	-8.92	-3.48	-5.61
EC-EARTH	65.07	6.75	8.00	-2.11	-10.32
FGOALS-g2	41.41	4.83	28.78	-2.91	52.08
GFDL-CM3	61.85	14.07	13.01	-5.41	-11.53
GFDL-ESM2G	60.04	6.53	7.79	9.14	7.39
GFDL-ESM2M	78.20	-18.21	-14.59	-20.46	-29.20
HadGEM2-CC	68.08	5.31	-5.12	-12.46	2.76
HadGEM2-ES	77.44	2.78	-3.93	-1.40	3.45
INM-CM4	69.48	-2.10	-0.33	-23.15	-9.42
IPSL-CM5A-LR	71.61	-5.27	-1.42	-15.37	3.79
IPSL-CM5A-MR	83.84	-19.56	-4.95	-17.48	17.19
MIROC5	52.51	-13.04	7.16	-4.82	2.09
MIROC-ESM	62.11	3.22	-11.13	-3.79	-18.64
MIROC-ESM-CHEM	75.31	-25.88	-22.97	-21.52	-17.29
MPI-ESM-LR	53.15	35.00	25.64	37.34	19.27
MPI-ESM-MR	59.75	-16.31	-6.94	17.47	-3.27
MRI-CGCM3*	62.52	8.86	4.76	5.53	2.42
NorESM1-M	73.17	0.90	4.72	-4.44	-8.92

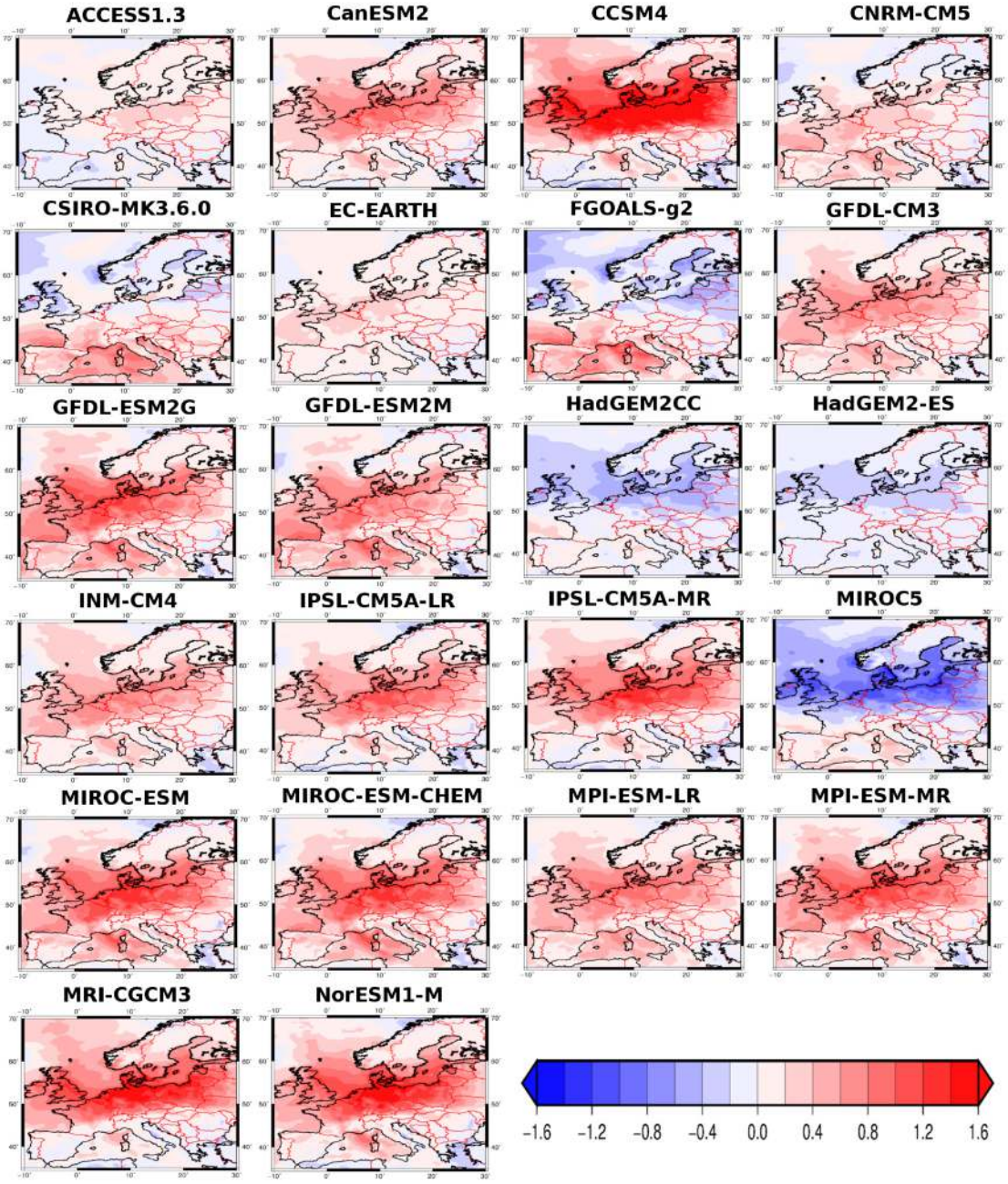

Fig.S 1: Differences of mean annual *Eout* for the historical runs of the 22 CMIP5 models (1961-2000) minus annual *Eout* of ERA-Interim in 10^3 MWh.

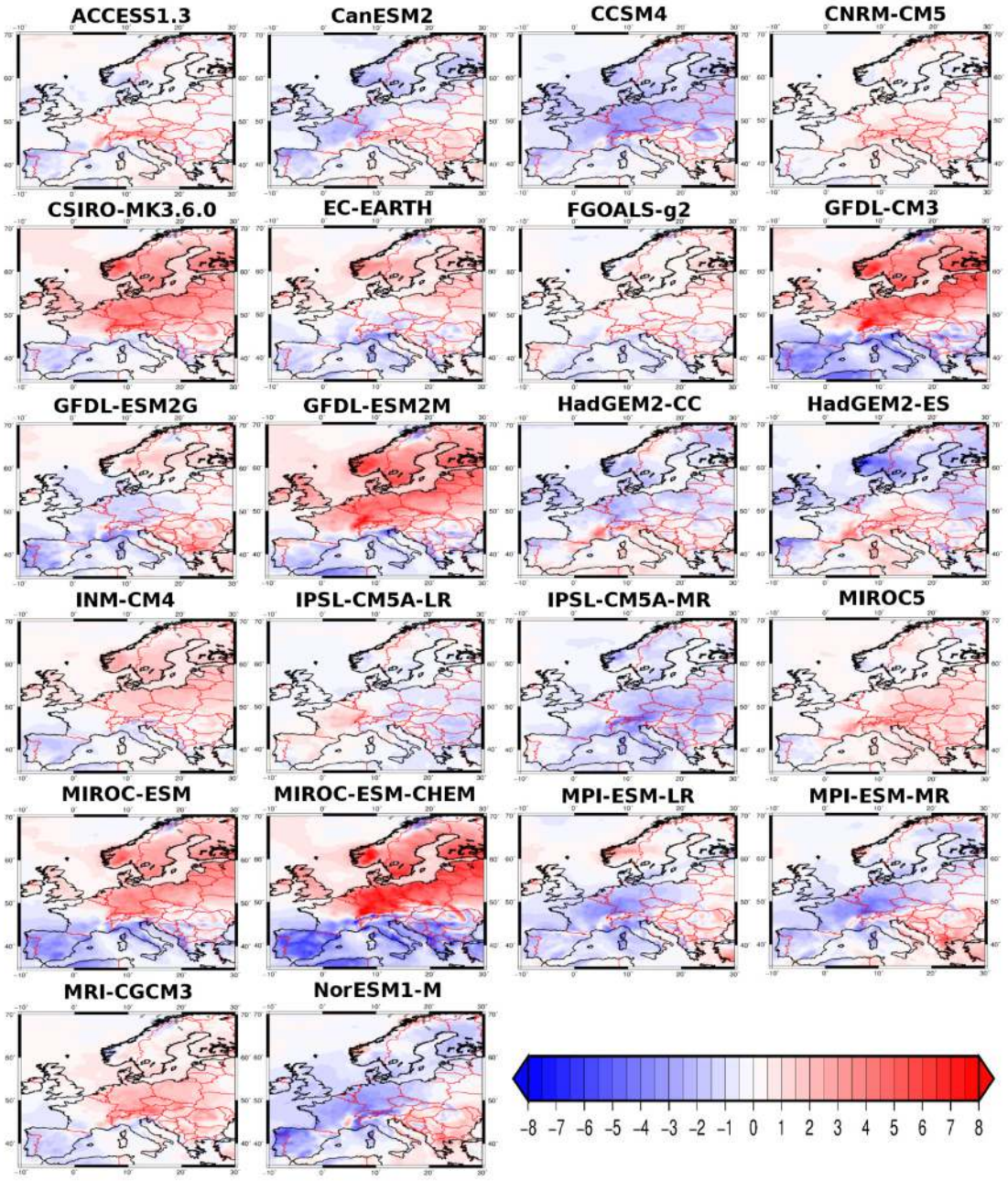

Fig.S 2: Changes of annual *Eout* in % for RCP8.5 (2021-2060) minus the historical runs (1961-2000) for the 22 CMIP5 models.

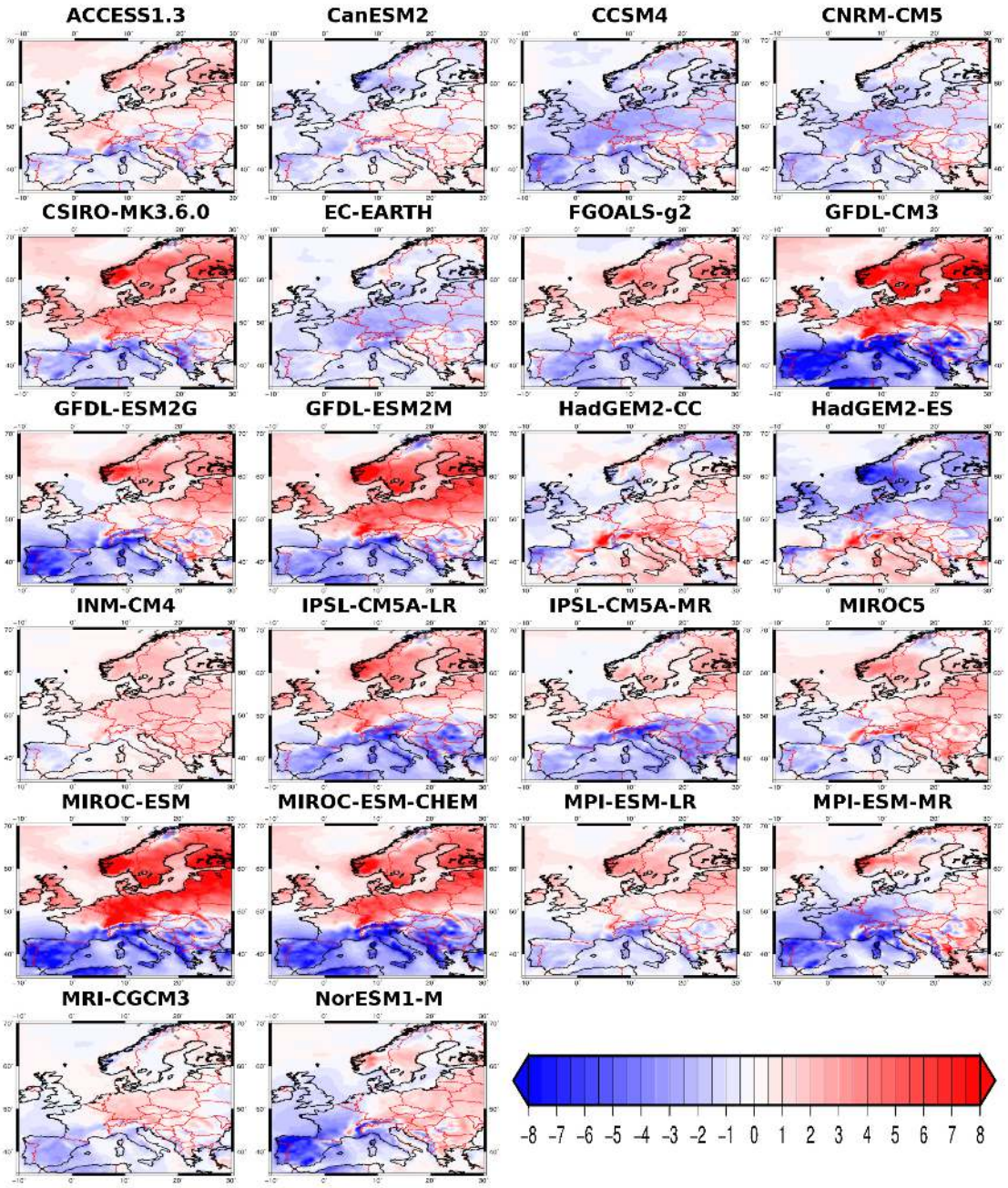

Fig.S 3: Changes of annual *Eout* in % for RCP8.5 (2061-2100) minus the historical runs (1961-2000) for the 22 CMIP5 models.

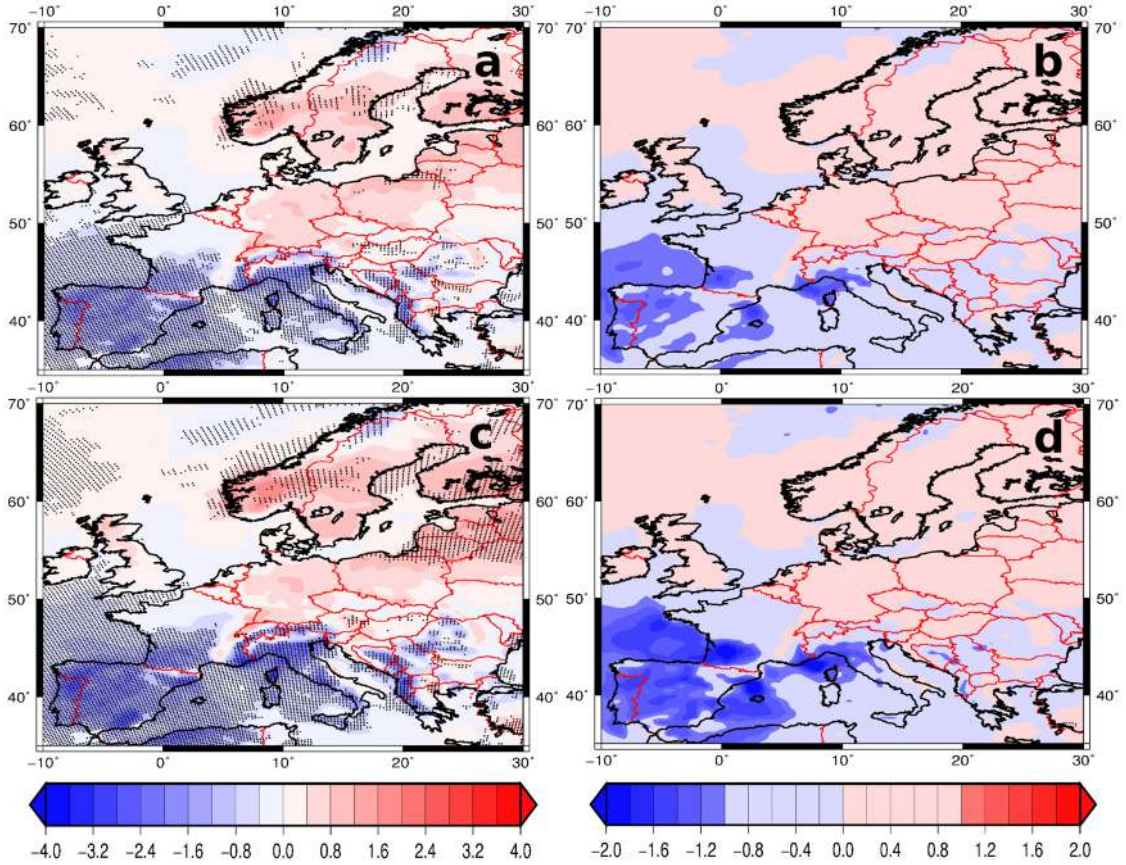

Fig.S 4: (a) Changes of annual *Eout* in % for the ensemble mean of RCP4.5 (2021-2060) minus the ensemble mean of historical (1961-2000). Dotted regions indicate grid points, where more than 15 models have the same sign as the ensemble mean. (b) Signal-to-noise ratio (mean change divided by standard deviation) for RCP4.5 (2021-2060) minus historical (1961-2000). Dotted regions indicate grid points where the changes are significant at the 95% confidence interval. (c) as (a) but for 2061-2100. (d) as (b) but for 2061-2100.

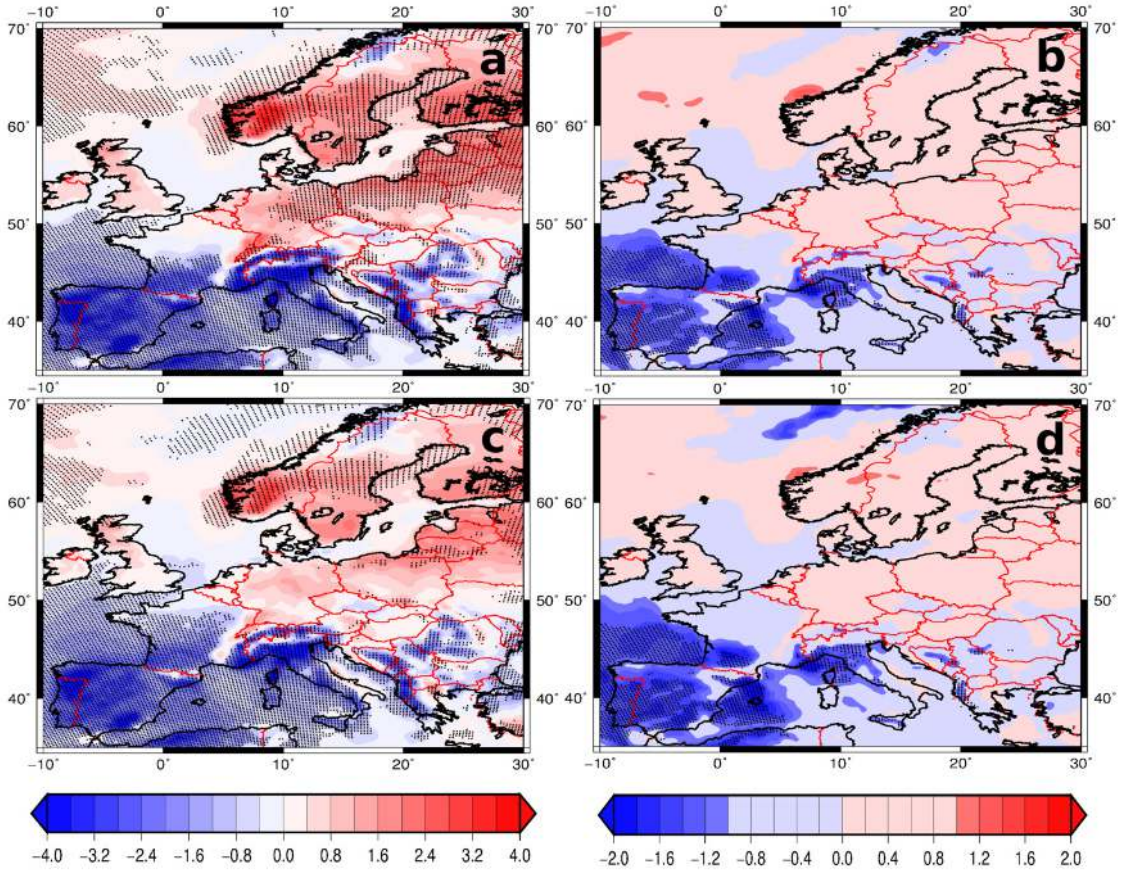

Fig.S 5: (a) Changes of annual *Eout* in % for the uncorrected ensemble mean of RCP8.5 (2061-2100) minus the ensemble mean of historical (1961-2000). Dotted regions indicate grid points, where more than 15 models have the same sign as the ensemble mean. (b) Signal-to-noise ratio (mean change divided by standard deviation) for uncorrected RCP8.5 (2061-2100) minus historical (1961-2000). Dotted regions indicate grid points where the changes are significant at the 95% confidence interval. (c) as (a) but for the bias-corrected ensemble. (d) as (b) but for the bias-corrected ensemble. For details, see main text.

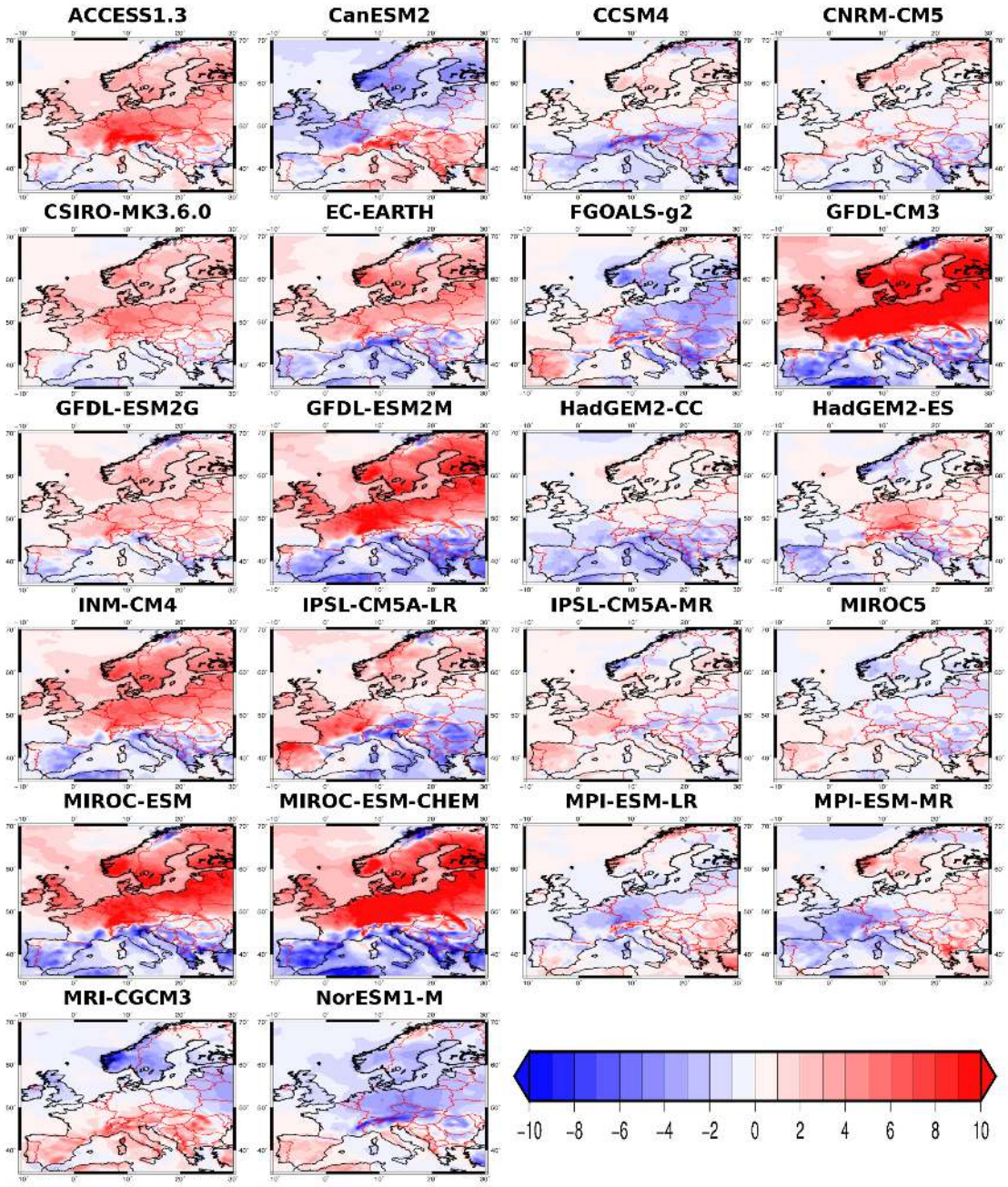

Fig.S 6: Changes of winter (December-February) *Eout* in % for RCP8.5 (2021-2060) minus the historical runs (1961-2000) for the 22 CMIP5 models.

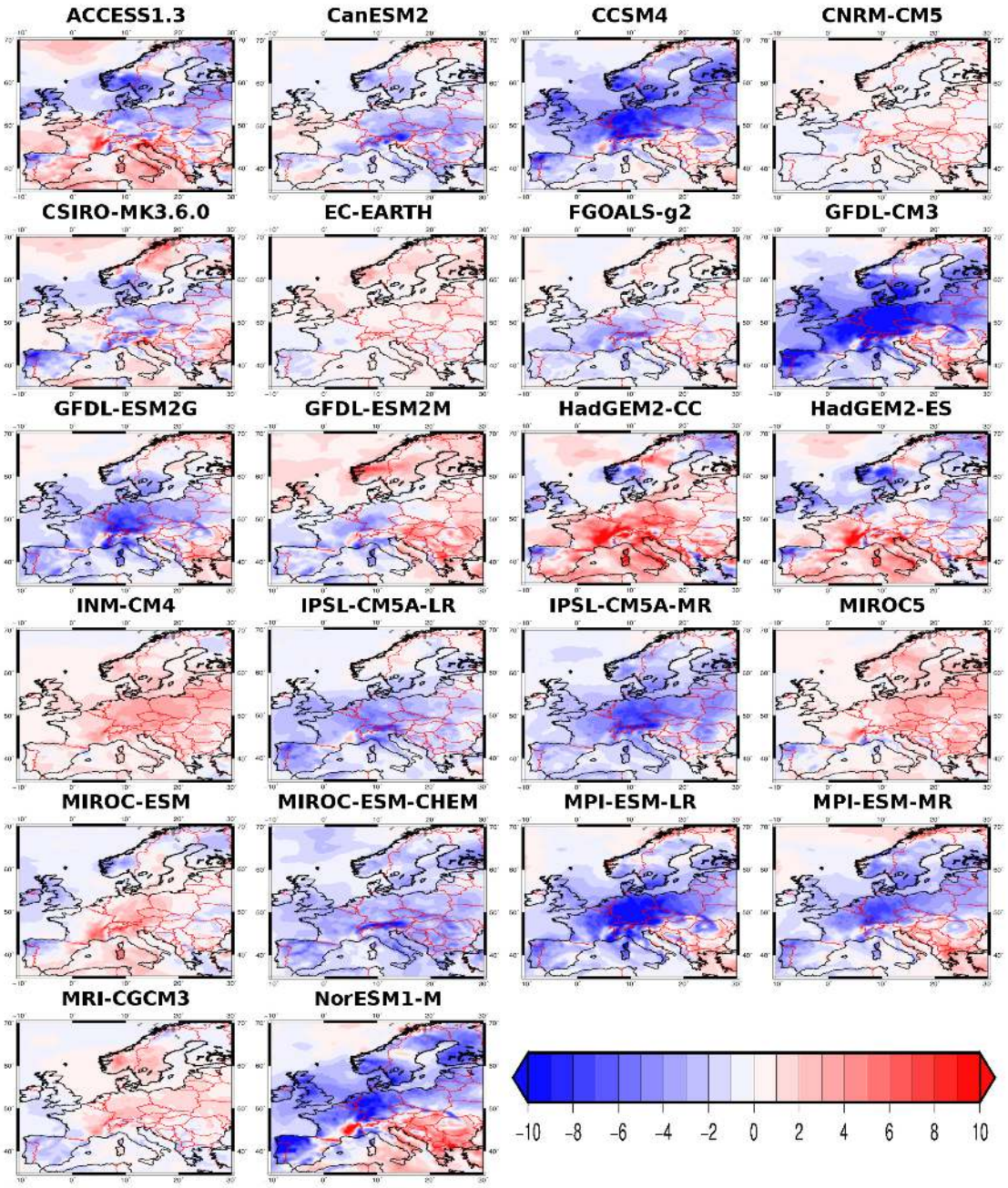

Fig.S 7: Changes of summer (June-August) *Eout* in % for RCP8.5 (2021-2060) minus the historical runs (1961-2000) for the 22 CMIP5 models.

5 Future changes of wind speed and wind energy potentials in EURO-CORDEX ensemble simulations

---

Reference:

Moemken, J., Reyers, M., Feldmann, H., and Pinto, J. G. (2018). Future changes of wind speed and wind energy potentials in EURO-CORDEX ensemble simulations. *J. Geophys. Res. Atmos.*, 123:6373–6389. doi:10.1029/2018JD028473

Page numbers are as published in *Journal of Geophysical Research: Atmospheres.*

Journal of Geophysical Research: Atmospheres

RESEARCH ARTICLE
10.1029/2018JD028473

Future Changes of Wind Speed and Wind Energy Potentials in EURO-CORDEX Ensemble Simulations

Julia Moemken[1,2], Mark Reyers[2], Hendrik Feldmann[1], and Joaquim G. Pinto[1]

[1]Institute of Meteorology and Climate Research, Karlsruhe Institute of Technology, Karlsruhe, Germany, [2]Institute for Geophysics and Meteorology, University of Cologne, Cologne, Germany

Key Points:
- Future changes of wind speed and wind energy output (Eout) over Europe are evaluated based on a high-resolution EURO-CORDEX ensemble
- Changes are robust for summer Eout and intraannual variability, and more uncertain for annual/winter Eout and interdaily variability
- The Baltic and Aegean Sea could profit from a changing climate, while negative impacts are projected for Germany, France, and Iberia

Supporting Information:
- Supporting Information S1

Correspondence to:
J. Moemken,
julia.moemken@kit.edu

Citation:
Moemken, J., Reyers, M., Feldmann, H., & Pinto, J. G. (2018). Future changes of wind speed and wind energy potentials in EURO-CORDEX ensemble simulations. *Journal of Geophysical Research: Atmospheres*, *123*, 6373–6389. https://doi.org/10.1029/2018JD028473

Received 2 FEB 2018
Accepted 25 MAY 2018
Accepted article online 5 JUN 2018
Published online 20 JUN 2018

Abstract Renewable energy production is strongly influenced by weather and climate. Regional climate projections can be useful to quantify climate change impacts on renewable energies. With this aim, we analyze future changes of wind speed and wind energy potentials using a multimodel ensemble of EURO-CORDEX simulations at 12 km and three-hourly resolution, considering nine different global and regional climate model chains. A comparison between modeled historical 10 m wind speeds and ERA-Interim-driven evaluation runs for the same regional climate models uncovers some substantial model biases. The bias-corrected 10 m wind speeds are extrapolated to the hub height of a wind turbine to derive gridded wind energy output (Eout). The ensemble mean responses project only small changes of mean annual and winter Eout for large parts of Europe in future decades, but a considerable decrease for summer Eout. In terms of variability, increasing intraannual and interdaily variabilities are projected for large parts of northern, central, and eastern Europe. While the ensemble spread is quite large for interdaily variability, results are more robust for intraannual variability. With respect to wind speed characteristics relevant for wind energy production, a robust increase in the occurrence of low wind speeds ($<$3 m/s) is detected. Due to a combination of higher annual mean Eout and lower intraannual variability, climate change could be beneficial for regions like Baltic and Aegean Sea. For large parts of Germany, France, and Iberia, a lower mean Eout and increased intraannual variability may imply larger temporal/spatial fluctuations in future wind energy production and therefore a more challenging wind energy management.

1. Introduction

The energy supply sector is one of the largest contributors to global greenhouse gas emissions (Bruckner et al., 2014), which affect the Earth's climate. In order to control and reduce these emissions, the need for a larger percentage of renewable energy in the energy mix has increased over the last decades. The global potential of renewable energies is larger than the global energy demand (Fischedick et al., 2011), but individual renewable energy sources are restricted to certain regions and specific weather conditions. In Europe, wind energy production has emerged as a promising alternative to fossil fuel sources. The total wind power capacity currently installed in Europe (onshore and offshore) has the potential to cover 11.4% of the European electricity consumption in a normal wind year (European Wind Energy Association, 2016). To meet the aim of the European Commission to produce 14.9% of the European Union's electricity demand in 2020 from wind energy resources (Moccia et al., 2014), the installation of an effective network of wind power plants is planned (Manwell et al., 2009; Wilkes et al., 2012). However, the successful integration into the electric energy system remains the main challenge for decision makers.

Wind energy production itself depends on the weather conditions and thus can be potentially affected by climate change. Changes, for example, in the large-to-local scale circulation, in the land cover, or changes in the intensity of storms can affect the near-surface wind conditions (Hueging et al., 2013; Pryor & Barthelmie, 2010, 2013; Tobin et al., 2016), leading to changing frequencies of calm and/or strong wind periods. Consequently, this would imply stronger fluctuations of generated electric power. Some previous studies have been investigating the impact of climate change on the European electricity sector (e.g., Dowling, 2013; Golombek et al., 2012; Wenz et al., 2017). At the same time, an increasing number of studies are addressing the impact of climate change on regional wind speeds and wind energy potentials over Europe (e.g., Barstad et al., 2012; Hueging et al., 2013; Reyers et al., 2016; Tobin et al., 2015, 2016). Most of these studies agree on a small increase in wind energy potentials on annual average over northern Europe and a small decrease over southern Europe under future climate conditions. However, there are differences in both sign and magnitude of the projected changes. These differences seem to result mostly from the

choice of the respective models (both global and regional climate models, GCM and RCM), including different initial conditions and model parameterizations, and from different downscaling approaches (e.g., Pryor et al., 2005, 2012; Reyers et al., 2016; Tobin et al., 2015).

In order to account for the uncertainties arising from the model choice, it is recommended to investigate a multimodel ensemble. On the global scale, such an ensemble has been made available through the Coupled Model Intercomparison Project Phase 5 (CMIP5; Taylor et al., 2012). Reyers et al. (2016) downscaled 22 CMIP5 models to investigate future changes of wind energy potentials over Europe, using a statistical-dynamical downscaling approach. They found an increase of annual wind energy output (Eout) over northern and central Europe and a decrease over the Mediterranean region in the ensemble mean. In seasonal terms, increases of Eout are likely for winter and a decrease is likely in summer for most parts of Europe. In general, climate change signals are more robust in seasonal terms. However, the single models in the ensemble may differ strongly from each other (Reyers et al., 2016; cf. their Figures S2 and S3). On the regional scale, the World Climate Research Program (WCRP) Coordinated Regional Downscaling Experiment (CORDEX, http://wrcp-cordex.jussieu.fr/; Giorgi et al., 2009) aims at dynamically downscaling the CMIP5 global climate projections to generate multimodel ensembles of regional climate projections for different regions worldwide. The European branch within the CORDEX framework (EURO-CORDEX, http://www.euro-cordex.net) provides regional climate projections for Europe at 50 km (EUR-44) and 12 km (EUR-11) resolution. These simulations complement coarser resolution data from other projects like PRUDENCE and ENSEMBLES (Hewitt & Griggs, 2004; Van der Linden & Mitchell, 2009). The first studies investigating EURO-CORDEX mainly focused on the evaluation of present-day climate runs (e.g., Kotlarski et al., 2014; Vautard et al., 2013), while recent studies also focus on future projections. Jacob et al. (2014) investigated future changes in mean temperature and precipitation in the EURO-CORDEX ensemble and compared the results to those achieved within the ENSEMBLES project. They found a good agreement for the overall spatial patterns, while the higher resolution of EURO-CORDEX influences the change pattern for heavy precipitation compared to ENSEMBLES. Tobin et al. (2016) investigated the impacts of climate change on the wind power generation potential in an ensemble of EURO-CORDEX with seven RCMs driven by five GCMs, focusing on a European midcentury wind farm scenario. They discovered that the annual energy yield of future European wind farms will remain stable (within ±5%) throughout the 21st century. However, changes at the local scale can reach 15% in magnitude.

The aim of this work is to investigate future changes of wind energy potentials over Europe in a regional multimodel ensemble at a very high temporal resolution, thus allowing insights on several timescales and addressing the stakeholder needs. We consider an ensemble of nine simulations with GCM-RCM model chains from EURO-CORDEX following the Representative Concentration Pathway (RCP) 4.5 and RCP8.5 scenarios to estimate future changes of wind characteristics relevant for wind energy production. Focus is given to mean changes in annual and seasonal wind energy production, changes in variability, and for the first time to changes in the occurrence of wind speeds relevant for wind energy production. We aim at providing an overview of the ensemble mean responses to climate change as well as quantifying the uncertainties between the individual models at the regional scale.

The paper is organized as follows. The EURO-CORDEX data sets are described in section 2 (section 2.1), followed by the description of the bias correction method (section 2.2), the extrapolation method, and the computation of wind energy potentials (section 2.3). The evaluation of the historical data sets is presented in section 3. Section 4 focuses on future changes of mean annual wind energy output and changes in variability, while section 5 focuses on future changes in specific wind speed characteristics. A short summary and discussion of the results concludes this paper in section 6.

2. Data and Methods

2.1. Data

In this study, we use a subset of nine GCM-RCM model chains conducted within the framework of EURO-CORDEX. The ensemble (Table 1) comprises the two RCMs COSMO-CLM (hereafter CCLM; Rockel et al., 2008) and RCA4 (Kupiainen et al., 2011; Samuelsson et al., 2011). They are driven by five different GCMs: CNRM-CM5, EC-EARTH, HadGEM2-ES, MPI-ESM-LR, and IPSL-CM5A-MR (not available for CCLM). We chose this particular ensemble to investigate both the differences between individual GCMs and the differences between different RCMs driven with the same GCM. Further, this ensemble enables us to analyze

Table 1
Overview of the Global and Regional Climate Models Used in This Study, Including Information on the Name, the Ensemble Member, and the Available Scenarios and Times

GCM	GCM member	RCM	Scenarios	Time
CNRM-CM5-LR	r1i1p1	RCA4	Historical	1970–2005
			RCP4.5, RCP8.5	2006–2100
EC-EARTH	r12i1p1	RCA4	Historical	1970–2005
			RCP4.5, RCP8.5	2006–2100
ERA-Interim	r1i1p1	RCA4	Evaluation	1980–2010
HadGEM2-ES	r1i1p1	RCA4	Historical	1970–2005
			RCP4.5, RCP8.5	2006–2100
IPSL-CM5A-MR	r1i1p1	RCA4	Historical	1970–2005
			RCP4.5, RCP8.5	2006–2100
MPI-ESM-LR	r1i1p1	RCA4	Historical	1970–2005
			RCP4.5, RCP8.5	2006–2100
CNRM-CM5-LR	r1i1p1	CCLM4-8-17	Historical	1970–2005
			RCP4.5, RCP8.5	2006–2100
EC-EARTH	r12i1p1	CCLM4-8-17	Historical	1970–2005
			RCP4.5	2006–2100
ERA-Interim	r1i1p1	CCLM4-8-17	Evaluation	1989–2008
HadGEM2-ES	r1i1p1	CCLM4-8-17	Historical	1970–2005
			RCP4.5, RCP8.5	2006–2100
MPI-ESM-LR	r1i1p1	CCLM4-8-17	Historical	1970–2005
			RCP4.5, RCP8.5	2006–2100

subdaily variations, as model output is available in three-hourly temporal resolution. The RCM simulations have a grid resolution of about 12 km (0.11°), and we use three-hourly 10 m wind speeds from the first available realization for each model simulation. The future climate projections were carried out for two emission scenarios, RCP4.5 and RCP8.5 (Meinshausen et al., 2011). The moderate RCP4.5 scenario results in an additional radiative forcing of 4.5 W/m^2 in 2100, while the stronger RCP8.5 scenario corresponds to 8.5 W/m^2 anthropogenic radiative forcing in 2100. Data for both scenarios are available for all model chains, except from EC-EARTH driven CCLM where the RCP8.5 data are missing. Two future periods (2021–2050 and 2071–2100) are compared to the historical period (1971–2000) to compute future changes. We use the model congruence/consistency as measure for the robustness and uncertainty of climate change signals, following the Intergovernmental Panel on Climate Change definition and Jacob et al. (2014). Thus, changes are defined as (non) likely/robust if (less) more than 66% of the ensemble members (corresponding to six out of nine members) agree on the sign of change.

To validate historical model simulations, observations or reanalysis data are usually used. Unlike for daily temperature and precipitation (E-OBS; Haylock et al., 2008), there is no consistent gridded data set of observations for wind speed or wind energy potentials available over Europe (e.g., Kjellström et al., 2011; Nikulin et al., 2011). The accessible wind speed data are station-based for every individual country, with diverse quality and spatial and temporal coverage. This results in a large inhomogeneity of the observed wind field (Nikulin et al., 2011). Several studies have investigated the performance of both RCMs (CCLM and RCA4, or its preceding version RCA3) to represent near surface wind speeds, typically focusing on individual countries with available wind observations. For example, Haas and Pinto (2012), Born et al. (2012), Haas et al. (2014), and Reyers et al. (2015) evaluated wind speeds and wind gusts from ERA-Interim-driven CCLM simulations against station-based observational data over Germany. These studies generally agree on a good representation of wind speed distributions in CCLM compared to observations. Larger discrepancies are primarily found for coastal regions and areas with complex topography. Since Germany is characterized by a wide range of different landscapes (from lowland coastal to high alpine regions), these results may be regarded as representative for other European countries (Haas & Pinto, 2012). Kjellström et al. (2005) and Nolan et al. (2012) evaluated wind gusts and wind speeds derived from RCA3 against observations for Sweden and Ireland, respectively. They agree on a good model performance in reproducing the wind speed climatology. However, the RCM tends to underestimate the wind speed and not to capture the high end of the wind speed distribution. Finally, Tobin et al. (2016) evaluated several EURO-CORDEX simulations (including RCA4 and CCLM) against ISDLite stations (Smith et al., 2011) and QuikSCAT satellite surface wind speed

observations (Ruti et al., 2008). Their results reveal generally good model skills. The lower correlations between observed and simulated values (especially over land) can mainly be attributed to the spatial scale differences between point measurements and grid-cell-averaged wind speeds (see also Born et al., 2012). In spite of these caveats, we conclude that both RCMs are suitable for the analysis of possible wind energy changes at the regional scale.

Here we compare the historical simulations to the respective ERA-Interim-driven (Dee et al., 2011) evaluation runs from EURO-CORDEX (for CCLM and RCA4). Since this evaluation uses model-specific reference data, it is only qualitative. That means the reanalysis-driven simulations provide a good representation of the temporal and spatial variabilities, but not necessarily for the absolute wind speeds. This seems to be sufficient for the presented study as it considers primarily relative changes rather than absolute changes. For CCLM, the ERA-Interim evaluation run is only available for 1989–2008, while the RCA4 evaluation run comprises the years 1981 to 2010. Therefore, we choose different validation periods for RCA4 (historical 1971–2000 versus evaluation 1981–2010) and CCLM (historical 1979–1998 versus evaluation 1989–2008). For the evaluation, we analyze both the 10 m wind speed climatology and the intraannual variability (estimated as difference of mean winter wind speeds [December–February] minus mean summer wind speeds [June–August]).

2.2. Bias Correction

The evaluation of the historical ensemble uncovered some substantial biases for surface wind speeds compared to ERA-Interim (see section 3). Since these biases may influence the climate change signal, in particular when analyzing wind speed thresholds relevant for wind energy production, a bias correction was applied to the three-hourly 10 m wind speeds from both the historical and the scenario runs. In a first step, theoretical Weibull distributions are fitted to the wind speed time series of the historical runs and the ERA-Interim evaluation runs (following, e.g., Haas et al., 2014). The cumulative distribution function:

$$F(x) = 1 - \exp\left[-\left({}^{x}/_{\alpha}\right)^{\beta}\right]$$

is used to estimate the scale (α) and shape (β) parameters. This results in two pairs of parameters: one pair for the ERA-Interim evaluation ($\alpha_{\mathrm{eval}}, \beta_{\mathrm{eval}}$) and one pair for the historical simulations ($\alpha_{\mathrm{hist}}, \beta_{\mathrm{hist}}$). In the next step, a probability mapping is carried out to adjust the simulated wind speeds to the evaluation runs (following Michelangeli et al., 2009). We obtain a transfer function by equalizing the theoretical Weibull distributions for evaluation and simulation:

$$F_{\mathrm{eval}}(x_{\mathrm{eval}}) = F_{\mathrm{sim}}(x_{\mathrm{sim.}})$$

Finally, the corrected simulations can be calculated:

$$x_{\mathrm{corr}} = F^{-1}_{\mathrm{eval}}(F_{\mathrm{sim}}(x_{\mathrm{sim}})) = \alpha_{\mathrm{eval}}\left(-\ln\left(1-\left(1-\exp\left({}^{x_{\mathrm{sim}}}/_{\alpha_{\mathrm{hist}}}\right)^{\beta_{\mathrm{hist}}}\right)\right)\right)^{{}^{1}/_{\beta_{\mathrm{eval}}}}$$

Please notice that the historical shape and scale parameters are used for the correction of both historical runs and future projections, thus maintaining coherence.

2.3. Wind Speed Extrapolation and Calculation of Wind Energy Potentials

The corrected 10 m wind speeds are used for the calculation of gridded Eout of an operational wind turbine. The calculation consists of two steps.

First, 10 m wind speeds are extrapolated to the average turbine hub height (here 100 m) using the power law (e.g., Hueging et al., 2013; Pryor et al., 2005; Tobin et al., 2015):

$$\frac{U(z)}{U(z_r)} = \left(\frac{z}{z_r}\right)^{\alpha}$$

where $U(z)$ is the wind speed at height z (e.g., hub height), $U(z_r)$ is the reference wind speed at height z_r (usually 10 m), and α is the power law exponent. The α is a highly variable quantity, which is influenced by,

for example, elevation, temperature, time of day, and various mixing parameters (Manwell et al., 2009). Several approximations exist for the power law exponent. Early work showed that under certain conditions (neutral conditions and flat terrain), α is equal to 1/7 (≈0.14; e.g., Schlichting, 1968; in the following referred to as type A). A more complex approximation was proposed by Justus (1978), where α depends on the reference height z_r and the velocity at reference height U (z_r):

$$\alpha = \frac{0.37 - 0.088\ \ln(U(z_r))}{1 - 0.088\ \ln\left({}^{z_r}/_{10}\right)}$$

(type B). The International Electrotechnical Commission suggests power law exponents of 0.2 for onshore areas (International Electrotechnical Commission, 2005a) and of 0.14 for offshore sites (International Electrotechnical Commission, 2005b; type C). The different extrapolation methods influence the wind speed characteristics at hub height. For example, the approximation by Justus (1978) shifts the wind probability density functions to higher wind speeds compared to the other mentioned methods (Figure S1). For this study, we follow the suggestion by the International Electrotechnical Commission, which was also applied in several other studies (e.g., Hueging et al., 2013; Moemken et al., 2016). Thus, we use the land-sea mask of the respective RCMs and apply a power law exponent of either 0.14 (water) or 0.2 (all land types).

In the second step, Eout is calculated from the wind speeds at hub height. The result is gridded three-hourly Eout in MWh. Eout depends not only on the velocity but also on the characteristics of the wind turbine (e.g., cut-in/cut-out velocity, maximum power, and rotor radius). This dependence is taken into account by using the characteristic power curve of a turbine. In this study, we used the operational wind turbine Nordex N117 (http://www.nordex-online.com/en/produkte-service/wind-turbines/n117-24-mw.html). The corresponding power curve (see Figure S2) is derived from manufacturer data. Nordex N117 has a cut-in velocity of 3 m/s and a cut-out velocity of 20 m/s. Its maximum power of 2.4 MW is reached at 11 m/s (rated velocity). Below the cut-in velocity and above the cut-out velocity, no Eout is produced. Between the rated and the cut-out velocity, the maximum value of Eout is assumed (2.4 MW). Finally, between the cut-in and the rated velocity, a fourth degree polynomial function is fitted to the power curve to calculate Eout. Gridded Eout is calculated by assuming that a wind turbine is placed at every single grid point. With this approach, we can assess the local potential for wind energy production under current and future climate conditions for every region in Europe, which may be of great importance for the future deployment of wind farms. However, this assumption cannot account for the actual wind farm capacity, its changes nor developments in wind turbine technology. For a sensitivity study, some calculations for the CCLM ensemble were repeated using a different operational wind turbine. Vestas V112 (https://en.wind-turbine-models.com/turbines/7-vestas-v-112-onshore) has a cut-in velocity of 3 m/s and is switched off at 25 m/s. The turbine reaches its maximum power of 3.075 MW at 13 m/s.

3. Comparison of Historical and Reanalysis-Driven EURO-CORDEX Simulations

The historical 10 m wind speeds are compared to ERA-Interim-driven evaluation runs of the respective RCMs (see also section 2.1). First, we analyze how well the wind climatology for the historical runs agrees to the ERA-Interim climatology. Figure 1a shows the surface wind climatology as derived from the ERA-Interim driven RCA4 simulation (hereafter RCA4-ERA) and Figure 1g the respective simulation with CCLM (hereafter CCLM-ERA). In both experiments, highest wind speeds are simulated for the offshore regions of North and Baltic Sea and the eastern North Atlantic. Over land, highest wind speeds are found over the British Isles, and for RCA4-ERA over the Norwegian coast and the Alps. Both simulations agree well over the oceans. However, wind speeds over land are typically lower (1 to 5 m/s) for CCLM-ERA compared to RCA4-ERA, which exhibits wind speeds between 3 and 6 m/s in the climatological mean. The largest differences between the simulations are found in regions with complex topography (e.g., western Scandinavia, the Alps, and the Pyrenees). Here RCA4-ERA simulates higher wind speeds compared to the surrounding areas, whereas CCLM-ERA simulates low mean wind speeds. This topography dependency seems to be specific to the choice of the RCM and not the forcing data, since the historical simulations for the different GCMs (Figures 1b and 1f for RCA4 and Figures 1h and 1k for CCLM) indicate no bias pattern related to topography.

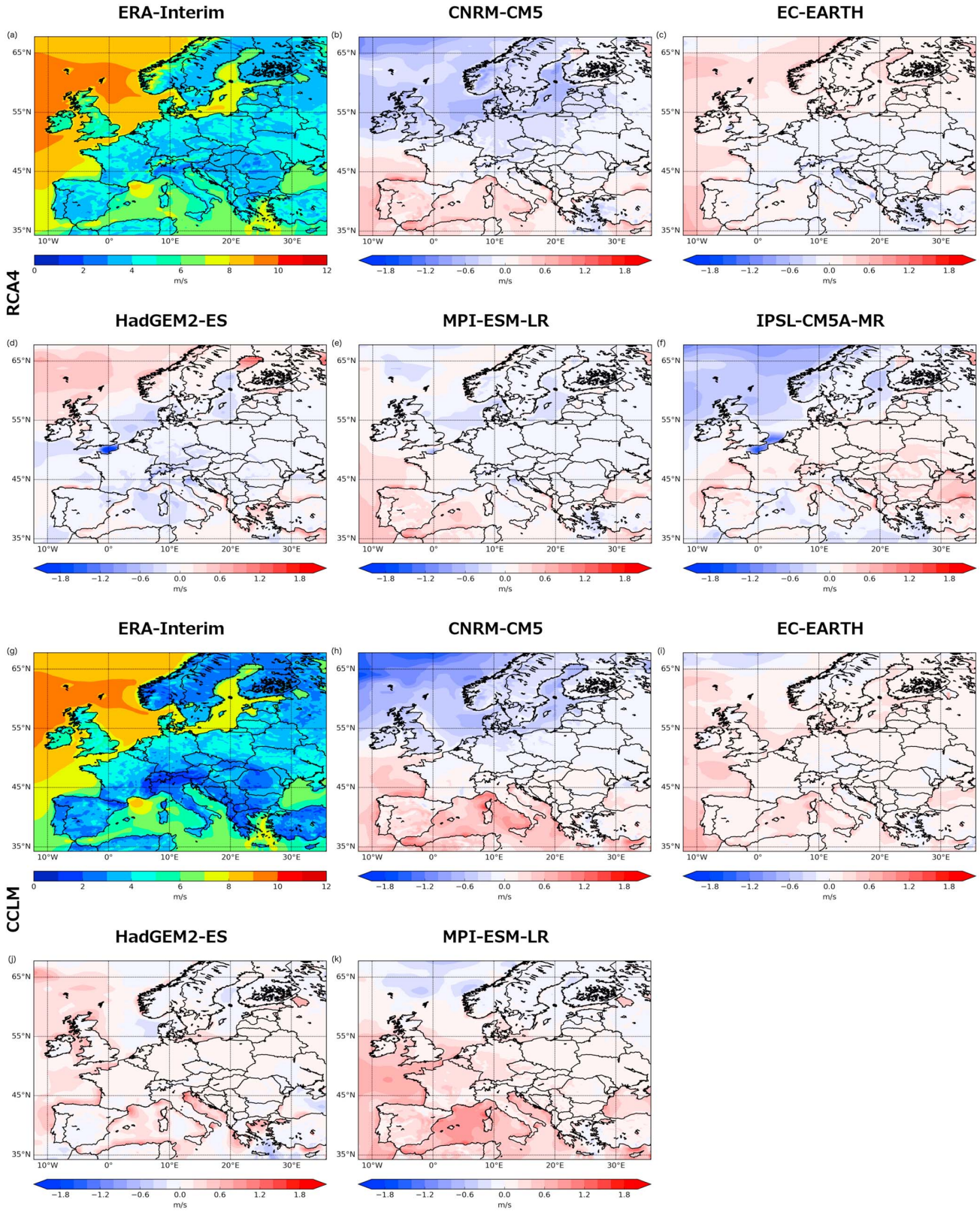

Figure 1. (a) Climatological mean of 10 m wind speed in m/s for ERA-Interim evaluation run of RCA4 (1981–2010). Difference between historical run (1971–2000) of (b) CNRM-CM5, (c) EC-EARTH, (d) HadGEM2-ES, (e) MPI-ESM-LR, and (f) IPSL-CM5A-MR and ERA-Interim evaluation run in m/s. (g–k) Same as (a)–(e) but for CCLM.

The GCM-driven historical simulations show substantial biases compared to the ERA-driven evaluation runs:

1. The CNRM-CM5-driven simulations (Figures 1b and 1h) show a general north-south anomaly pattern with too low wind speeds (up to 1.2 m/s) in the north and a positive bias in the Mediterranean area. For central Europe there is a small negative bias for both RCMs, which is slightly more pronounced for RCA4.
2. The biases in the simulations forced by EC-EARTH (Figures 1c and 1i) are generally weak, especially over land (±0.2 m/s).
3. The RCM simulations driven by HadGEM2-ES (Figures 1d and 1j) depict again low biases. These are negative for large parts of Europe in the RCA4 run and slightly positive for CCLM.
4. The bias pattern for the RCM simulations forced by MPI-ESM-LR (Figures 1e and 1k) shows a slight underestimation of wind speeds for northern and central Europe for RCA4, while the CCLM depicts an overestimation in these regions. Both simulations show positive biases for southern Europe.
5. The IPSL-CM5A-MR-driven run (Figure 1f; only available for RCA4) clearly underestimates 10 m wind speeds over northern Europe (especially over sea) and the Mediterranean Sea, while deviations are positive over central and southern Europe.

Despite these biases, the spatial distributions of climatological surface winds of the individual models for both RCMs agree well to the spatial pattern of the evaluation runs (not shown).

Due to windier conditions in winter over Europe, the surface wind speeds reveal a clear seasonality in the reanalysis data. We use the intraannual variability to analyze this seasonality. Generally, the patterns for RCA4-ERA and CCLM-ERA (Figures S3a and S3f) look similar, with slightly higher values over the ocean for CCLM-ERA and over land for RCA4-ERA. For both evaluation runs the surface wind speeds in winter clearly exceed the values for summer over most parts of Europe, except from some continental regions in southern Europe. Over sea and along the Norwegian coast, winter minus summer differences reach 5 m/s. Again, the GCM-driven historical runs show substantial biases. For RCA4, the ensemble mean clearly overestimates the intraannual variability over large parts of Europe (not shown). Negative anomalies are only visible over some parts of northern and southern Europe. The model biases of the intraannual variability strongly differ between the individual RCA4 simulations (Figures S3b–S3f), resulting in nonrobust differences for the entire European continent (not shown). The ensemble mean of the historical runs for CCLM shows an underestimation of intraannual variability over northern Europe (except from North and Baltic Sea) and an overestimation for central and southern Europe. As for RCA4, differences between the individual GCM-RCM chains are also large (Figures S3h–S3k).

To summarize, the historical runs show substantial biases compared to the ERA-Interim evaluation run. These biases result from both the driving GCM and the RCM, but differences between the GCMs are typically larger than those between the RCMs except for coastal areas and regions with complex topography. They may influence the climate change signal, in particular when investigating wind speed thresholds, which are relevant for the wind energy production. We therefore applied a bias correction to the three-hourly 10 m wind speeds from both the historical and the scenario runs (see section 2.2), before analyzing wind speed and Eout in a future climate.

4. Future Changes of Wind Energy Output

After evaluating the historical EURO-CORDEX ensemble, the future responses of Eout are analyzed on different timescales. First, we investigate future changes of mean annual and mean seasonal Eout, which could be relevant for the planning of future wind parks. Further, we analyze changes in the variability of Eout, ranging from interannual to interdaily timescales. These timescales are of high importance for the operation of the energy system and the integration of wind energy into the energy system. While interdaily timescales are relevant for the power system management (e.g., occurrence of ramping events and grid balancing) and energy trading, intraannual to interannual timescales are important for resource assessments and the planning of backup and storage facilities.

4.1. Changes in Mean Annual and Seasonal Eout

The changes of mean annual Eout are presented in Figure 2 for the ensemble mean projections of RCA4 (upper row) and CCLM (middle row). Changes are shown for both future scenarios (RCP4.5 and RCP8.5) and both future periods (2021–2050 and 2071–2100). In addition, Figure 2 depicts the number of models

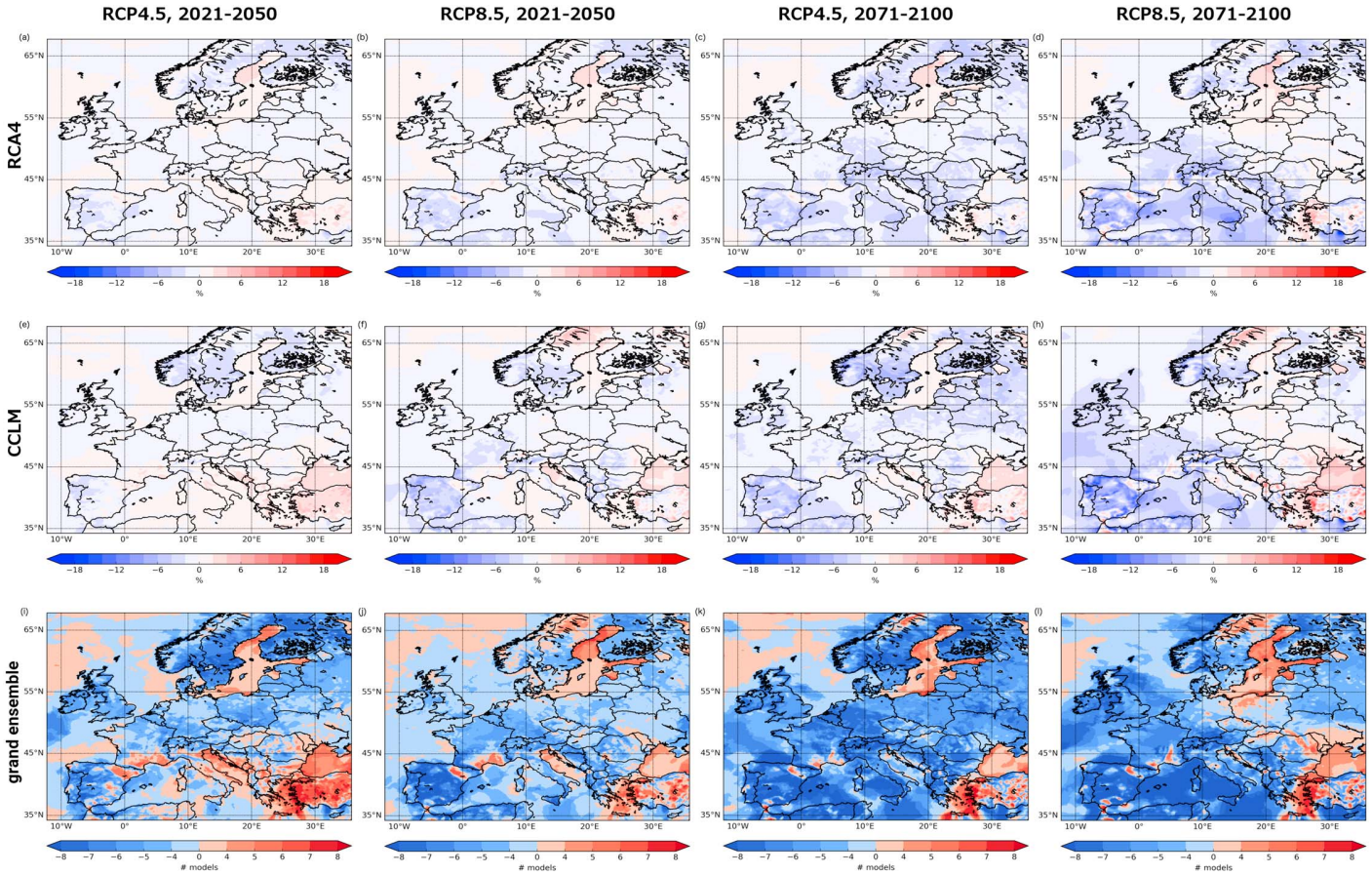

Figure 2. Changes of mean annual Eout in % for the ensemble mean of (a) RCP4.5 (2021–2050), (b) RCP8.5 (2021–2050), (c) RCP4.5 (2071–2100), and (d) RCP8.5 (2071–2100) minus the ensemble mean of historical (1971–2000) for RCA4. (e–h) Same as (a)–(d) but for CCLM. Number of model chains (from the grand ensemble) that agree on the sign of change for mean annual Eout for (i) RCP4.5 (2021–2050), (j) RCP8.5 (2021–2050), (k) RCP4.5 (2071–2100), and (l) RCP8.5 (2071–2100).

from the grand ensemble (all model chains) that agree on the sign of change (lower row). The RCA4 ensemble reveals a slight decrease of Eout (<5%) over Scandinavia and the Iberian Peninsula, and a slight increase for the Baltic Sea and the Aegean region for 2021–2050 in RCP4.5. For most of the investigation area, changes range between −2% and +2% (Figure 2a). Similar patterns can be found for the CCLM ensemble (Figure 2e). For RCP8.5 (Figures 2b and 2f), future responses exhibit higher magnitudes than for RCP4.5, while the climate change pattern is similar. The climate change signal is stronger and more robust for the end of the century (2071–2100) in both ensembles for RCP4.5 (Figures 2c and 2g), where reduced Eout (up to 8%) is simulated for large parts of Europe. Only for the Aegean region, the Black Sea, and the Baltic Sea, Eout is projected to increase. For southern Europe, the British Isles, and parts of Scandinavia, six or more ensemble members (meaning 66% for RCP4.5, respectively, 75% for RCP8.5) agree on the sign of change (Figures 2k and 2l). Nevertheless, differences between the individual models can be large for certain regions (cf. Figure S4). While the CNRM-CM5-driven simulations predict a small increase of Eout for central Europe, northern France, the British Isles, and Scandinavia, EC-EARTH, HadGEM2-ES, and IPSL-CM5A-MR project a decrease of Eout over large parts of Europe. On the other hand, all downscaled GCMs agree on increasing Eout over the Baltic Sea and Aegean region, with only different magnitudes of change. For RCP8.5, the decrease of Eout over the Iberian Peninsula and the Mediterranean region reaches up to 14% (Figures 2d and 2h). The individual GCMs contributing to the ensemble mean differ more distinct from each other than for RCP4.5 (cf. Figure S5). For example, the MPI-ESM-LR-driven simulations show a strong increase of Eout (up to 10%) for central and eastern Europe, while EC-EARTH and HadGEM2-ES show decreasing Eout for the same regions. This results in nonrobust signals in these regions (see also Figure 6a). It is obvious that the differences

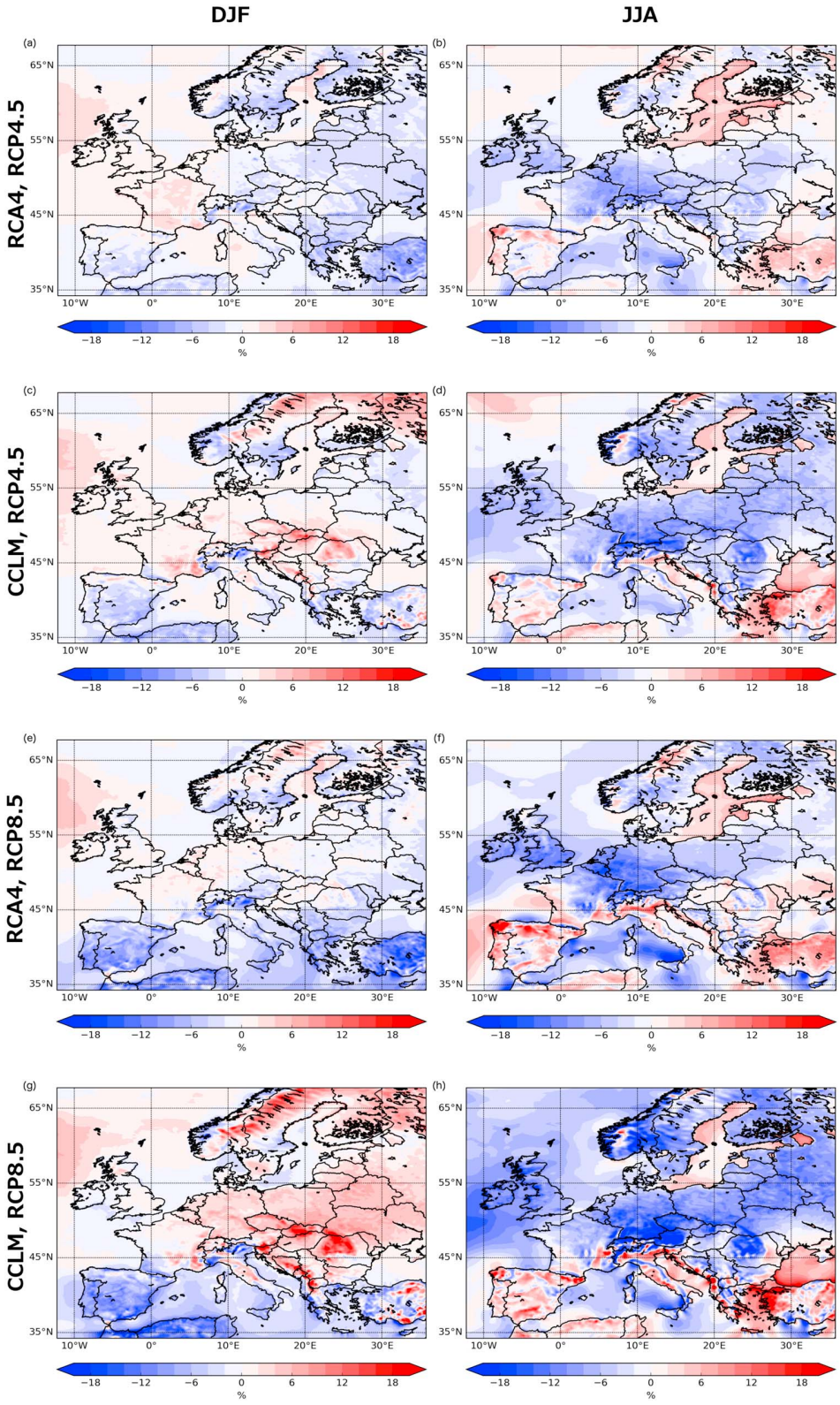

Figure 3. Changes of seasonal Eout in % for the ensemble mean of RCP4.5 (2071–2100) minus the ensemble mean of historical (1971–2000) for RCA4 for (a) winter (December–February) and (b) summer (June–August). (c and d) Same as (a) and (b) but for CCLM. (e and f) Same as (a) and (b) but for RCP8.5 (2071–2100). (g and h) Same as (e) and (f) but for CCLM.

between the ensemble means of the two RCMs are highest for 2071–2100 of the RCP8.5 scenario (compare Figures 2d and 2h). This is due to the different ensemble sizes (three GCMs for CCLM; five GCMs for RCA4).

Next we analyze future changes for winter and summer Eout since opposite trends in the two seasons would lead to a higher intraannual variability of Eout and therefore to a higher irregularity of wind energy production within the year. On the other hand, similar future trends in winter and summer would benefit the wind energy sector due to a higher regularity of wind energy production throughout the year. Figure 3 shows the changes in mean winter (December–February) and summer (June–August) Eout for the ensemble mean of RCA4 and CCLM, for the end of the century (2071–2100) and in both scenarios. Both ensembles reveal different spatial change patterns for winter and summer. For the RCA4 ensemble, increasing Eout is simulated for the North Atlantic, central Europe (including France, parts of Germany, and Poland), and parts of Scandinavia and the Baltic region during winter (Figure 3a). A decrease of Eout in winter can be found for southern Europe and most parts of eastern Europe. Changes range from −15% to +8%. The change pattern for summer reveals a strong decrease of Eout for central Europe, the Mediterranean Sea, the British Isles, and large parts of Scandinavia (Figure 3b). The Aegean region, the Baltic Sea, and parts of southern Europe are projected to experience an increase of Eout in summer in future decades. In general, changes for RCP8.5 are stronger than for RCP4.5. The future responses of the individual GCMs differ again strongly from each other (see Figure S6 for RCP8.5). For winter, three of the five model chains (CNRM-CM5, MPI-ESM-LR, and IPSL-CM5A-MR) agree on increasing Eout over central and western Europe, while the HadGEM2-ES-driven simulation projects decreasing Eout of up to 20% for the whole continent. For summer the agreement is better, at least for central Europe, the British Isles, and the Mediterranean region. The future changes simulated with the CCLM ensemble show similar change patterns but with higher magnitudes, especially in regions with complex topography. Differences to RCA4 can be found for winter over eastern Europe, where Eout is projected to increase in CCLM. In general, changes range from −20% to +20% with higher values for RCP8.5. Again, the differences between the two ensembles seem to result primarily from the different ensemble sizes (cf. Figure S6).

4.2. Changes in Variability

For both ensembles and future scenarios, the seasonal changes of Eout (as shown in Figure 3) lead to an ensemble mean amplification of the intraannual variability of Eout (calculated as mean winter minus mean summer Eout) in future decades over large parts of the North Atlantic region and Europe, namely, central Europe and parts of Scandinavia (see Figures 4 and S7, top row). This amplification is strongest for RCP8.5 and the end of the century. On the other hand, a decrease in variability can be found for the Iberian Peninsula, the Baltic and Black Seas, and parts of eastern Europe. Again, changes are strongest for 2071–2100 and RCP8.5. The agreement between the two ensembles is very good, with similar spatial patterns and magnitude (compare Figures 4 and S7).

The interannual variability is simply calculated as the standard deviation of annual Eout values in a given period. Changes in the interannual variability are depicted in Figure 4 (middle row) for RCA4 and Figure S7 for CCLM, for both scenarios and both future periods. The change pattern is less distinct than that of the intraannual variability. While some regions (e.g., Germany, northern France, and eastern North Atlantic) experience an increase in interannual variability of up to 30%, other regions like the Iberian Peninsula or the Black Sea show a decreasing variability. The spatial pattern is somewhat messy and less coherent between periods and scenarios. Nevertheless, climate change signals are quite robust for certain regions (e.g., Germany, Iberian Peninsula, or Scandinavia), especially for the end of the 21st century (see also Figure 6e).

A clearer pattern of future changes is revealed for the interdaily variability of Eout (standard deviation of daily integrated three-hourly Eout values). Figure 4 shows the future projections for the RCA4 and Figure S7 for the CCLM ensemble mean, for both scenarios and periods. An increase of variability is simulated for central Europe, the North Atlantic, Scandinavia, and large parts of eastern Europe. While these changes are rather small for midcentury, this increase can reach 5% in 2071–2100. A declining variability is projected for the Iberian Peninsula and the countries surrounding the Mediterranean Sea. Here changes of more than 8% are projected for the end of the century. Interestingly, the changes of interdaily variability agree well for both the RCA4 and CCLM ensemble, and thus seem to be quite robust (see also Figure 6f).

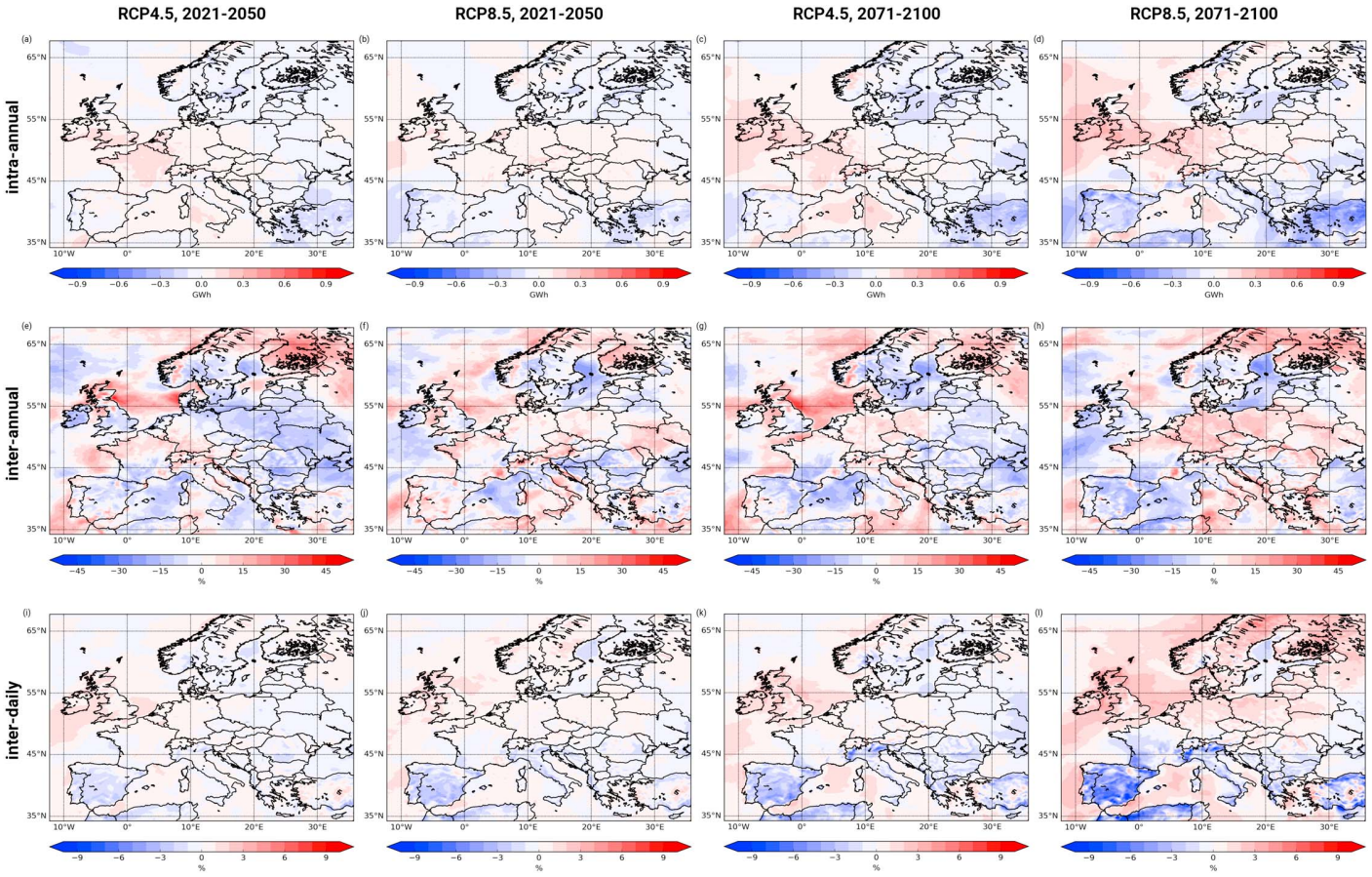

Figure 4. Changes of intraannual variability of Eout in GWh for the ensemble mean of (a) RCP4.5 (2021–2050), (b) RCP8.5 (2021–2050), (c) RCP4.5 (2071–2100), and (d) RCP8.5 (2071–2100) minus the ensemble mean of historical (1971–2000) for RCA4. (e–h) Same as (a)–(d) but for changes in interannual variability of Eout in %. (i–l) Same as (a)–(d) but for changes in interdaily variability of Eout in %.

5. Future Changes in Specific Wind Speed Characteristics

The impact of the future changes on wind speed characteristics relevant for wind energy production is now investigated in details. We analyze the occurrence of wind speeds at 100 m (turbine hub height) that are below the cut-in velocity, above the cut-out velocity, and between rated and cut-out velocity (range with maximum Eout) of the chosen wind turbine. Figure 5 shows the projected changes in the number of three-hourly dates per year, which fulfill these criteria. Depicted are the ensemble mean changes of RCA4 and CCLM for RCP8.5 and the end of the century. Both ensembles simulate an increase of three-hourly dates per year with wind speeds below 3 m/s (cut-in velocity for N117; see section 2.3) for large parts of Europe. Over some regions, for example, in the Mediterranean or in Scandinavia, this increase accounts for up to 140 dates per year (about 5%), particularly in the CCLM ensemble. Only for the Baltic Sea, the Black Sea (only CCLM), and the Aegean region a decrease is detected (Figures 5a and 5d). On the other hand, the number of three-hourly dates with wind speeds above 20 m/s (cut-out for N117) is projected to decline over the Mediterranean Sea and the North Atlantic, while the number will remain stable (±1%) for most of continental Europe. A strong decrease is projected for 100 m winds between 11 and 20 m/s over the North Atlantic and surrounding coastal areas, the Mediterranean region, and the Iberian Peninsula. An increase is only simulated for the Baltic Sea and the Aegean, while the number of three-hourly dates per year is nearly unchanged for central and eastern Europe. Again, the signals shown in Figure 5 are quite robust between the two RCM ensembles (see also Figures 6g and 6i). The seasonal trends (cf. Figure S8 for the RCA4 ensemble) show similar spatial patterns to the annual trends (Figure 5). However, the magnitudes are typically higher, and small differences can be found between the individual seasons. For example, the increase of three-hourly dates

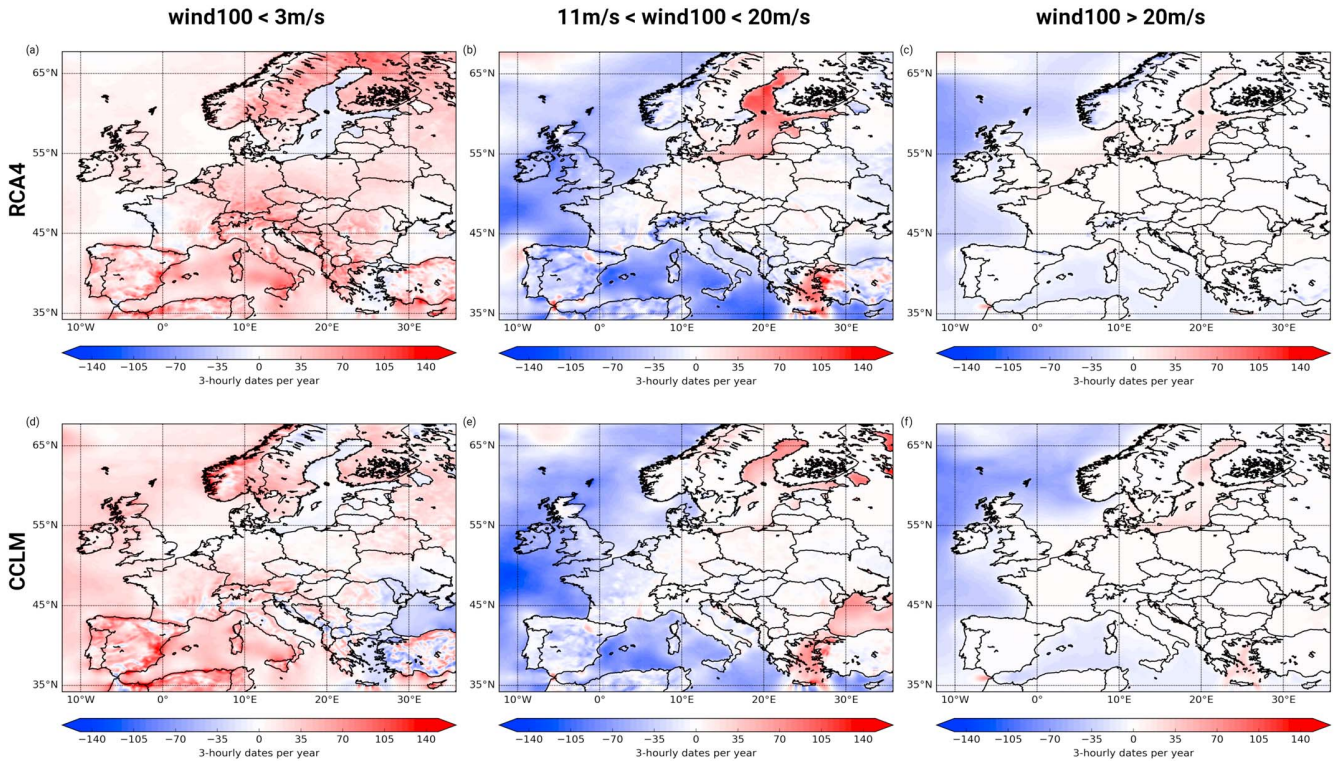

Figure 5. Changes in the number of three-hourly dates per year with (a) 100 m wind speed <3 m/s, (b) 11 m/s <100 m wind speed <20 m/s, and (c) 100 m wind speed >20 m/s for the ensemble mean of RCP8.5 (2071–2100) minus the ensemble mean of historical (1971–2000) for RCA4. (d–f) Same as (a)–(c) but for CCLM.

with wind speeds below 3 m/s over central Europe and the decrease of the rated velocity over the North Atlantic are strongest for summer. As these presented results imply more periods with calm conditions and less periods with optimal wind speeds for wind energy production, the projected changes would impede the operation of the wind energy system in a future climate.

6. Summary and Discussion

In this study, we used an ensemble of nine GCM-RCM model chains from EURO-CORDEX at 12 km resolution to estimate future changes of wind speed and wind energy output at the regional scale. The potential changes were estimated for the near future decades (2021–2050) and the end of the 21st century (2071–2100) using two climate change scenarios, RCP4.5 and RCP8.5. The main results of this study are summarized in the following and in Figure 6, which displays the coherence of climate change signals for the whole ensemble:

1. The historical EURO-CORDEX runs show substantial biases in 10 m wind speed. These biases depend primarily on the choice of the driving GCM. The choice of the RCM also plays a role for the annual mean and diurnal cycle biases, while differences between the RCMs are small regarding the intraannual variability. A bias correction was performed before computing future climate change signals.
2. The ensemble mean projections reveal a decrease of average annual Eout for most of Europe in future decades, while increases are found for the Baltic and Aegean Seas. Changes are generally more pronounced for the end of the century and the RCP8.5 scenario. The climate change signals are robust (in the sense that six or more model chains agree on the sign of change; see also section 2.1) for most parts of southern Europe, and parts of the Aegean and the Baltic region (see Figure 6a). On the other hand, the ensemble spread can be quite large for central and eastern Europe and parts of Scandinavia, where signals are not robust.
3. In seasonal terms, a general decrease of Eout is identified for the summer months, particularly for central Europe, while an increase is detected for western and central continental Europe for the winter season.

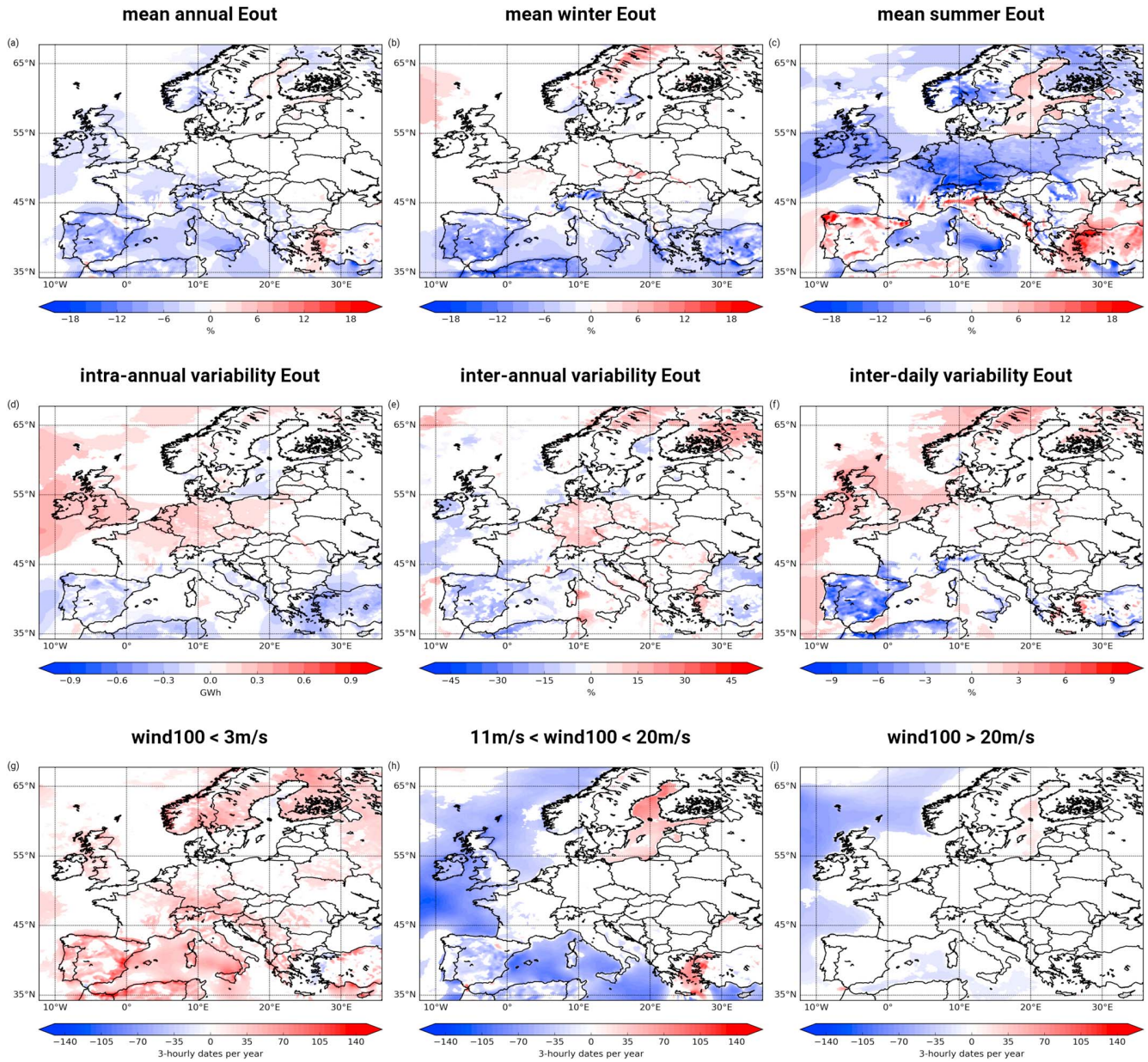

Figure 6. Changes for the grand ensemble mean (all model chains) of RCP8.5 for 2071–2100 for (a) mean annual Eout in %, (b) mean winter Eout in %, (c) mean summer Eout in %, (d) intraannual variability of Eout in GWh, (e) interannual variability of Eout in %, and (f) interdaily variability of Eout in %; number of three-hourly dates per year with (g) 100 m wind speed <3 m/s, (h) 11 m/s <100 m wind speed <20 m/s, and (i) 100 m wind speed >20 m/s. Depicted are only changes with six or more ensemble members agreeing on the sign of change.

This increase in winter is not robust, whereas most model chains agree on a simultaneous decrease for southern Europe (Figure 6b). In general, the agreement between models is better for summer (cp. Figures 6b and 6c), where climate change signals are robust for nearly all of Europe.

4. In terms of variability, both intraannual and interdaily variability of Eout are projected to increase over northern, central, and parts of eastern Europe in future decades, leading to a higher irregularity of wind energy production. The climate change signal for interdaily variability is robust for the British Isles, Scandinavia, and most of continental southern Europe (Figure 6f), while climate change signals for intraannual variability are robust everywhere except eastern Europe, the Mediterranean Sea, and parts of the North Sea (Figure 6d).

5. Finally, the RCM ensembles simulate a higher occurrence of 100 m wind speeds below the cut-in velocity (here 3 m/s) for all of Europe, except the Baltic Sea. This increase is robust for large parts of Europe (Figure 6g). At the same time, a robust decrease of 100 m wind speeds between 11 and 20 m/s is simulated for the North Atlantic, the North Sea, the Mediterranean Sea, and surrounding coastal areas (Figure 6h).

The climate change signals identified in the analyzed GCM-RCM chains are generally weaker compared to some previous studies (e.g., Hueging et al., 2013; Reyers et al., 2016). Moreover, for mean annual Eout the ensemble mean changes have different signs of change for northern and central Europe. On the other hand, changes in mean annual Eout show similar magnitudes and signs as changes in mean wind power generation potential as identified by Tobin et al. (2016) in a different subset of EURO-CORDEX simulations. The differences to the study of Reyers et al. (2016) seem to be primarily attributed to the choice of GCMs. Reyers et al. (2016) examined 22 CMIP5 models, and the GCMs used in this study are among the models with the weakest signals (cf. their Figures S2 and S3). Further differences may arise from the different downscaling methods and/or assumptions regarding the wind profile in the boundary layer. For example, Reyers et al. (2016) used a statistical-dynamical approach for a large multimodel ensemble, while in the present study we have analyzed results from a purely dynamical downscaling approach and a smaller data set (for EURO-CORDEX only simulations with boundary conditions from five GCMs are available). However, the presented approach enables the estimation of climate change signals on a very high temporal resolution like interdaily timescales, thus giving novel insights in timescales, which could not be addressed with the statistical-dynamical downscaling approach. Tobin et al. (2016) also performed similar investigations (e.g., changes in mean values and variability) for a 2050 wind farm scenario, which assumed an increase in installed capacity over many European regions by 100–300%, depending on the energy policy projections (see also Vautard et al., 2014). Their results show smaller magnitudes of climate change signals for mean annual and mean seasonal energy yield and similar magnitudes for variability compared to Eout values from our simplified approach, where a wind turbine is placed at every model grid point. However, the signs of climate change signals can differ for some regions like France (for mean annual energy yield) or Germany and Benelux (for intraannual variability).

Tobin et al. (2016) concluded that the climate change impacts on wind energy generation should be small compared to the expected growth in installed capacity and improvements in technology (e.g., increasing hub heights and rotor diameters).

Generally, we could demonstrate that mean changes of annual wind speed and Eout are small compared to future changes of the interannual and intraannual variabilities, which agree with the results of, for example, Reyers et al. (2016) and Tobin et al. (2016). In particular, an enhancement of the intraannual variability would affect a wind-driven energy system in a future climate due to a higher irregularity of wind energy production within a year. The combined changes of mean annual Eout and intraannual variability (Figures 2 and 4) show areas where future changes are generally positive for the wind energy sector (e.g., Baltic Sea, Aegean Sea; with higher mean Eout and lower seasonal variability). For other areas, changes are mostly negative (e.g., most land areas in France, Germany, and the British Isles; with lower mean Eout and an increasing seasonal variability). Further, our results indicate a strong increase of situations with low wind speeds, which are below the cut-in velocity of typical wind turbines. This could result in enhanced backup and storage needs and therefore impede the operation of a wind-driven energy system (Wohland et al., 2017).

In line with previous studies like Reyers et al. (2016) and Tobin et al. (2016), there is some uncertainty in future projections on the impact of climate change on wind energy production arising from the choice of the model. In contrast to Tobin et al. (2016), this model uncertainty is more pronounced between the individual GCMs than between the different RCMs. It is identified here for interannual and intraannual variabilities and mean annual Eout, while we found rather robust results for interdaily variability as well as mean seasonal Eout (see also Tobin et al., 2016). Moreover, the projected changes in the occurrence of certain wind speeds relevant for wind energy production are quite robust, where often six or more of the nine GCM-RCM chains agree on the sign of change. However, these results depend strongly on the region. While the Baltic and Aegean area show robust results for nearly all analyses, uncertainties are much more pronounced for central and eastern Europe.

In a sensitivity study, some calculations for the CCLM ensemble were repeated using a different operational wind turbine (see section 2.3) to investigate in how far the climate change signal is sensitive to the choice of

turbine. For example, we estimated the future responses for mean annual Eout and intraannual variability (see Figure S9) for the RCP8.5 scenario. For both parameters, results are very similar for both turbines with respect to magnitude and spatial pattern. So we conclude that the choice of the turbine has a negligible impact on the projected future changes.

Our results for the regional scale can be related to changes in the large-scale atmospheric conditions in future decades. Several studies agree on the general changes in the mean sea level pressure and circulation patterns over Europe and the North Atlantic (e.g., Woollings et al., 2012; Zappa et al., 2015). Winter storminess is projected to increase over western Europe (e.g., Feser et al., 2015; Ulbrich et al., 2008) due to an extension of the eddy-driven jet stream toward the British Isles and an intensification of cyclones during winter. This leads to enhanced wind speeds over central and western Europe (cf. Donat et al., 2010; Pinto et al., 2012). For summer, decreasing wind speeds are projected, especially over southern Europe (e.g., Hueging et al., 2013; Reyers et al., 2015). This leads to an amplification of intraannual variability for wind speed and wind energy production as was also detected in our study.

For future work, wind power generation statistics should be analyzed by taking the wind farm distribution and installed power into account (e.g., Cannon et al., 2015; Drew et al., 2015; Tobin et al., 2016), also with a stronger focus on subdaily variability. Additionally, focus should be given to the impact of the projected changes of Eout on the energy system at the European scale (cf. Wohland et al., 2017), also taking projected changes in other renewable energy sources like solar (Jerez et al., 2015) into account toward an optimal energy mix. This is of high importance for a successful integration of wind energy into the existing energy system and an adaptation of the energy system to climate change.

Acknowledgments
We acknowledge the World Climate Research Programme's Working Group on Regional Climate and the Working Group on Coupled Modeling, former coordinating body of CORDEX and responsible panel for CMIP5. We also thank the climate modeling groups for producing and making available their model output. We acknowledge the Earth System Grid Federation infrastructure, an international effort led by the U.S. Department of Energy's Program for Climate Model Diagnosis and Intercomparison, the European Network for Earth System Modeling, and other partners in the Global Organisation for Earth System Science Portals (GO-ESSP). We thank the German Climate Computer Centre (DKRZ, Hamburg) and the Regional Computing Centre (RRZK, University of Cologne) for computer and storage resources. We also thank Klaus Keuler (BTU Cottbus) for help assessing the CCLM data. We thank Larisa Seregina and Sven Ulbrich (both University of Cologne) for help with the bias correction. This study was partially funded by the Helmholtz-Zentrum Geesthacht/German Climate Service Center (HZG/GERICS). J. G. P. thanks the AXA Research Fund for support. The 10 m wind speed data from EURO-CORDEX are available from the ESGF data center (e.g., on the node of LIU, https://esg-dn1.nsc.liu.se/projects/esgf-liu/; project: CORDEX; domain: EUR-11; variable: sfcWind; time frequency: 3 hr). All other data are available at the long-term archive CERA of the DKRZ upon request. We thank the reviewers for their comments on an earlier version of this manuscript.

References

Barstad, I., Sorteberg, A., & dos-Santos Mesquita, M. (2012). Present and future offshore wind power potential in northern Europe based on downscaled global climate runs with adjusted SST and sea ice cover. *Renewable Energy*, *44*, 398–405. https://doi.org/10.1016/j.renene.2012.02.008

Born, K., Ludwig, P., & Pinto, J. G. (2012). Wind gust estimation for mid-European winter storms: Towards a probabilistic view. *Tellus A*, *64*(1), 17471. https://doi.org/10.3402/tellusa.v64i0.17471

Bruckner, T., Bashmakov, I. A., Mulugetta, Y., Chum, H., de la Vega Navarro, A., Edmonds, J., et al. (2014). Energy systems. In O. Edenhofer, et al. (Eds.), *Climate Change 2014: Mitigation of Climate Change. Contribution of Working Group III to the Fifth Assessment Report of the Intergovernmental Panel on Climate Change* (516 pp.). Cambridge, United Kingdom and New York: Cambridge University Press.

Cannon, D. J., Brayshaw, D. J., Methven, J., Coker, P. J., & Lenaghan, D. (2015). Using reanalysis data to quantify extreme wind power generation statistics: A 33 year case study in Great Britain. *Renewable Energy*, *75*, 767–778. https://doi.org/10.1016/j.renene.2014.10.024

Dee, D. P., Uppala, S. M., Simmons, A. J., Berrisford, P., Poli, P., Kobayashi, S., et al. (2011). The ERA-Interim reanalysis: Configuration and performance of the data assimilation system. *Quarterly Journal of the Royal Meteorological Society*, *137*(656), 553–597. https://doi.org/10.1002/qj.828

Donat, M. G., Leckebusch, G. C., Pinto, J. G., & Ulbrich, U. (2010). European storminess and associated circulation weather types: Future changes deduced from a multi-model ensemble of GCM simulations. *Climate Research*, *42*(1), 27–43. https://doi.org/10.3354/cr00853

Dowling, P. (2013). The impact of climate change on the European energy system. *Energy Policy*, *60*, 406–417. https://doi.org/10.1016/j.enpol.2013.05.093

Drew, D. R., Cannon, D. J., Brayshaw, D. J., Barlow, J. F., & Coker, P. J. (2015). The impact of future offshore wind farms on wind power generation in Great Britain. *Resources Policy*, *4*(1), 155–171. https://doi.org/10.3390/resources4010155

European Wind Energy Association (2016). Wind in power—2015 European Statistics European Wind Energy Association Report, EWEA (12 pp.). Retrieved from https://windeurope.org/wp-content/uploads/files/about-wind/statistics/EWEA-Annual-Statistics-2015.pdf, (accessed 12 December 2016).

Feser, F., Barcikowska, M., Krueger, O., Schenk, F., Weisse, R., & Xia, L. (2015). Storminess over the North Atlantic and northwestern Europe—A review. *Quarterly Journal of the Royal Meteorological Society*, *141*(687), 350–382. https://doi.org/10.1002/qj.2364

Fischedick, M., Schaeffer, R., Adedoyin, A., Akai, M., Bruckner, T., Clarke, L., et al. (2011). Mitigation potential and costs. In O. Edenhofer, et al. (Eds.), *IPCC Special Report on Renewable Energy Sources and Climate Change Mitigation. Prepared by Working Group III of the Intergovernmental Panel on Climate Change* (840 pp.). Cambridge, United Kingdom and New York: Cambridge University Press.

Giorgi, F., Jones, C., & Asrar, G. R. (2009). Addressing climate information needs at the regional level: The CORDEX framework. *Bulletin - World Meteorological Organization*, *58*, 175–183.

Golombek, R., Kittelsen, S. A. C., & Haddeland, I. (2012). Climate change: Impacts on electricity markets in Western Europe. *Climatic Change*, *113*(2), 357–370. https://doi.org/10.1007/s10584-011-0348-6

Haas, R., & Pinto, J. G. (2012). A combined statistical and dynamical approach for downscaling large-scale footprints of European windstorms. *Geophysical Research Letters*, *39*, L23804. https://doi.org/10.1029/2012GL054014

Haas, R., Pinto, J. G., & Born, K. (2014). Can dynamically downscaled wind-storm footprints be improved by observations through a probabilistic approach? *Journal of Geophysical Research: Atmospheres*, *119*, 713–725. https://doi.org/10.1002/2013JD020882

Haylock, M. R., Hofstra, N., Klein Tank, A. M. G., Klok, E. J., Jones, P. D., & New, M. (2008). A European daily high-resolution gridded dataset of surface temperature and precipitation. *Journal of Geophysical Research*, *113*, D20119. https://doi.org/10.1029/2008JD010201

Hewitt, C. D., & Griggs, D. J. (2004). Ensembles-based predictions of climate changes and their impacts. *Eos*, *85*(52), 566. https://doi.org/10.1029/2004EO520005

Hueging, H., Born, K., Haas, R., Jacob, D., & Pinto, J. G. (2013). Regional changes in wind energy potential over Europe using regional climate model ensemble projections. *Journal of Applied Meteorology and Climatology*, *52*(4), 903–917. https://doi.org/10.1175/JAMC-D-12-086.1

International Electrotechnical Commission (2005a). *Wind turbines—Part 1: Design requirements. IEC 61400–1* (p. 179). Geneva, Switzerland: International Electrotechnical Commission.

International Electrotechnical Commission (2005b). *Wind turbines—Part 3: Design requirements for offshore wind turbines. IEC 61400–3* (p. 263). Geneva, Switzerland: International Electrotechnical Commission.

Jacob, D., Petersen, J., Eggert, B., Alias, A., Christensen, O. B., Bouwer, L. M., et al. (2014). EURO-CORDEX: New high-resolution climate change projections for European impact research. *Regional Environmental Change*, *14*(2), 563–578. https://doi.org/10.1007/s10113-013-0499-2

Jerez, S., Tobin, I., Vautard, R., Montávez, J. P., López-Romero, J. M., Thais, F., et al. (2015). The impact of climate change on photovoltaic power generation in Europe. *Nature Communications*, *6*(1), 10014. https://doi.org/10.1038/ncomms10014

Justus, C. G. (1978). *Winds and wind system performance*. Philadelphia, PA: Franklin Institute Press.

Kjellström, E., Bärring, L., Hansson, U., Jones, C., Samuelsson, P., Rummukainen, M., et al. (2005). A 140-year simulation of European climate with the new version of the Rossby Centre regional atmospheric climate model (RCA3) (SMHI Reports Meteorology and Climatology, vol. 108, SMHI, SE-60176, 54 pp.). Norrköping, Sweden.

Kjellström, E., Nikulin, G., Hansson, U., Strandberg, G., & Ullerstig, A. (2011). 21st century changes in the European climate: Uncertainties derived from an ensemble of regional climate model simulations. *Tellus A*, *63*(1), 24–40. https://doi.org/10.1111/j.1600-080.2010.00475.x

Kotlarski, S., Keuler, K., Christensen, O. B., Déqué, M., Gobiet, A., Goergen, K., et al. (2014). Regional climate modelling on European scales: A joint standard evaluation of the EURO-CORDEX RCM ensemble. *Geoscientific Model Development*, *7*(4), 1297–1333. https://doi.org/10.5194/gmd-7-1297-2014

Kupiainen, M., Samuelsson, P., Jones, C., Jansson, C., Willén, U., Wang, S., & Döscher, R. (2011). Rossby Centre regional atmospheric model, RCA4. Rossby Centre Newsletter, June.

Manwell, J. F., McGowan, J. G., & Rogers, A. L. (2009). *Wind Energy Explained: Theory, Design and Application* (2nd ed.). Chichester, UK: John Wiley. https://doi.org/10.1002/9781119994367.index

Meinshausen, M., Smith, S. J., Calvin, K., Daniel, J. S., Kainuma, M. L. T., Lamarque, J.-F., et al. (2011). The RCP greenhouse gas concentrations and their extensions from 1765 to 2300. *Climatic Change*, *109*(1-2), 213–241. https://doi.org/10.1007/s10584-011-0156-z

Michelangeli, P.-A., Vrac, M., & Loukos, H. (2009). Probabilistic downscaling approaches: Application to wind cumulative distribution functions. *Geophysical Research Letters*, *36*, L11708. https://doi.org/10.1029/2009GL038401

Moccia, J., Wilkes, J., Pineda, I., & Corbetta, G. (2014). Wind energy scenarios for 2020. European Wind Energy Association Report, EWEA (3 pp.). Retrieved from http://www.ewea.org/fileadmin/files/library/publications/scenarios/EWEA-Wind-energy-scenarios-2020.pdf, (accessed 12 December 2016).

Moemken, J., Reyers, M., Buldmann, B., & Pinto, J. G. (2016). Decadal predictability of regional scale wind speed and wind energy potentials over Central Europe. *Tellus A*, *68*(1), 29199. https://doi.org/10.3402/tellusa.v68.29199

Nikulin, G., Kjellström, E., Hansson, U., Strandberg, G., & Ullerstig, A. (2011). Evaluation and future projections of temperature, precipitation and wind extremes over Europe in an ensemble of regional climate simulations. *Tellus A*, *63*(1), 41–55. https://doi.org/10.1111/j.1600-0870.2010.00466.x

Nolan, P., Lynch, P., McGrath, R., Semmler, T., & Wang, S. (2012). Simulating climate change and its effects on the wind energy resource of Ireland. *Wind Energy*, *15*(4), 593–608. https://doi.org/10.1002/we.489

Pinto, J. G., Karremann, M. K., Born, K., Della-Marta, P. M., & Klawa, M. (2012). Loss potentials associated with European windstorms under future climate conditions. *Climate Research*, *54*(1), 1–20. https://doi.org/10.3354/cr01111

Pryor, S. C., & Barthelmie, R. J. (2010). Climate change impacts on wind energy: A review. *Renewable and Sustainable Energy Reviews*, *14*(1), 430–437. https://doi.org/10.1016/j.rser.2009.07.028

Pryor, S. C., & Barthelmie, R. J. (2013). Assessing the vulnerability of wind energy to climate change and extreme events. *Climatic Change*, *121*(1), 79–91. https://doi.org/10.1007/s10584-013-0889-y

Pryor, S. C., Barthelmie, R. J., Claussen, N. E., Drews, M., MacKellar, N., & Kjellström, E. (2012). Analyses of possible changes in intense and extreme wind speeds over northern Europe under climate change scenarios. *Climate Dynamics*, *38*(1-2), 189–208. https://doi.org/10.1007/s00382-010-0955-3

Pryor, S. C., Schoof, J. T., & Barthelmie, R. J. (2005). Climate change impacts on wind speeds and wind energy density in northern Europe: Empirical downscaling of multiple AOGCMs. *Climate Research*, *29*, 183–198. https://doi.org/10.3354/cr029183

Reyers, M., Moemken, J., & Pinto, J. G. (2016). Future changes of wind energy potentials over Europe in a large CMIP5 multi-model ensemble. *International Journal of Climatology*, *36*(2), 783–796. https://doi.org/10.1002/joc.4382

Reyers, M., Pinto, J. G., & Moemken, J. (2015). Statistical-dynamical downscaling for wind energy potentials: Evaluation and applications to decadal hindcasts and climate change projections. *International Journal of Climatology*, *35*(2), 229–244. https://doi.org/10.1002/joc.3075

Rockel, B., Will, A., & Hense, A. (2008). Special issue: Regional climate modelling with COSMO-CLM (CCLM). *Meteorologische Zeitschrift*, *17*(4), 347–348. https://doi.org/10.1127/0941-2948/2008/0309

Ruti, P. M., Marullo, S., D'Ortenzio, F., & Tremant, M. (2008). Comparison of analysed and measured wind speeds in the perspective of oceanic simulations over the Mediterranean basin: Analyses, QuikSCAT and buoy data. *Journal of Marine Systems*, *70*(1-2), 33–48. https://doi.org/10.1016/j.jmarsys.2007.02.026

Samuelsson, P., Jones, C., Willén, U., Ullerstig, A., Gollvik, S., Hansson, U., et al. (2011). The Rossby Centre Regional Climate Model RCA3: model description and performance. *Tellus A*, *63*, 4–23. https://doi.org/10.1111/j.1600-0870.2010.00478.x

Schlichting, H. (1968). *Boundary layer theory* (6th ed.). New York: McGraw-Hill.

Smith, A., Lott, N., & Vose, R. (2011). The integrated surface database: Recent developments and partnerships. *Bulletin of the American Meteorological Society*, *92*(6), 704–708. https://doi.org/10.1175/2011BAMS3015.1

Taylor, K. E., Stouffer, R. J., & Meehl, G. A. (2012). An overview of CMIP5 and the experiment design. *Bulletin of the American Meteorological Society*, *93*(4), 485–498. https://doi.org/10.1175/BAMS-D-11-00094.1

Tobin, I., Jerez, S., Vautard, R., Thais, F., van Meijgaard, E., Prein, A., et al. (2016). Climate change impacts on the power generation potential of a European mid-century wind farms scenario. *Environmental Research Letters*, *11*(3), 034013. https://doi.org/10.1088/1748-9326/11/3/034013

Tobin, I., Vautard, R., Balog, I., Bréon, F.-M., Jerez, S., Ruti, P., et al. (2015). Assessing climate change impacts on European wind energy from ENSEMBLES high-resolution climate projections. *Climatic Change*, *128*(1-2), 99–112. https://doi.org/10.1007/s10584-014-1291-0

Ulbrich, U., Pinto, J. G., Kupfer, H., Leckebusch, G. C., Spangehl, T., & Reyers, M. (2008). Changing northern hemisphere storm tracks in an ensemble of IPCC climate change simulations. *Journal of Climate*, *21*(8), 1669–1679. https://doi.org/10.1175/2007JCLI1992.1

Van der Linden, P., & Mitchell, J. F. B. (Eds.) (2009). *ENSEMBLES: Climate change and its impacts: Summary of research and results from ENSEMBLES project*. Exeter: Met Office Hadley Centre.

Vautard, R., Gobiet, A., Jacob, D., Belda, M., Colette, A., Déqué, M., et al. (2013). The simulation of European heat waves from an ensemble of regional climate models within the EURO-CORDEX project. *Climate Dynamics*, *41*(9-10), 2555–2575. https://doi.org/10.1007/s00382-013-1714-z

Vautard, R., Thais, F., Tobin, I., Bréon, F.-M., Devezeaux de Lavergne, J.-G., Colette, A., et al. (2014). Regional climate model simulations indicate limited climatic impacts by operational and planned European wind farms. *Nature Communications*, *5*(1), 3196. https://doi.org/10.1038/ncomms4196

Wenz, L., Levermann, A., & Auffhammer, M. (2017). North-south polarization of European electricity consumption under future warming. *Proceedings of the National Academy of Sciences of the United States of America*, *144*(38), E7910–E7918. https://doi.org/10.1073/pnas.1704339114

Wilkes, J., Moccia, J., & Dragan, M. (2012). *Wind in power—2011 European Statistics European Wind Energy Association Report* (11 pp.). Brussels: EWEA.

Wohland, J., Reyers, M., Weber, J., & Witthaut, D. (2017). More homogeneous wind conditions under strong climate change decrease the potential for inter-state balancing of electricity in Europe. *Earth System Dynamics*, *8*, 1047–1060. https://doi.org/10.5194/esd-8-1047-2017

Woollings, T., Gregory, J. M., Pinto, J. G., Reyers, M., & Brayshaw, D. J. (2012). Response of the North Atlantic storm track to climate change shaped by ocean-atmosphere coupling. *Nature Geoscience*, *5*(5), 313–317. https://doi.org/10.1038/ngeo1438

Zappa, G., Hoskins, B. J., & Shepherd, T. G. (2015). Improving climate change detection through optimal seasonal averaging: The case of the North Atlantic jet and European precipitation. *Journal of Climate*, *28*(16), 6381–6397. https://doi.org/10.1175/JCLI-D-14-00823.1

Journal of Geophysical Research: Atmospheres

Supporting Information for

Future changes of wind speed and wind energy potentials in EURO-CORDEX ensemble simulations

Julia Moemken[1,2], Mark Reyers[2], Hendrik Feldmann[1], Joaquim G. Pinto[1]

[1] Institute of Meteorology and Climate Research, Karlsruhe Institute of Technology, Germany, [2] Institute for Geophysics and Meteorology, University of Cologne, Germany

Contents of this file

Introduction

This supporting information provides additional Figures as follows:

- Distribution of 100m-wind speed for selected grid points (Figure S1)
- Characteristic power curves (Figure S2)
- Intra-annual variability of 10m-wind speed for ERA-Interim driven RCMs and historical runs (Figure S3)
- Future changes of mean annual Eout in % for the individual GCM-RCM chains (Figures S4 and S5)
- Future changes of winter and summer Eout in % for the individual GCM-RCM chains (Figure S6)
- Future changes of variability of Eout (Figure S7)
- Changes in the number of three-hourly dates per season (Figure S8)
- Comparison of the two wind turbines N117 and V112 (Figure S9)

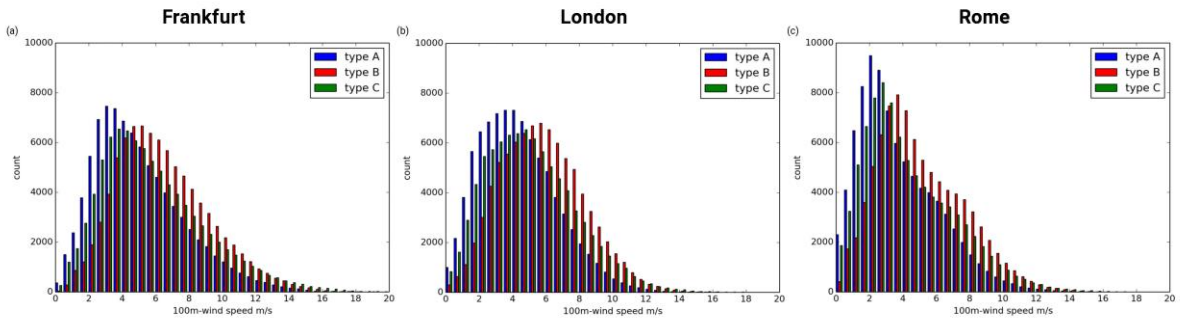

Figure S1: Distribution of 100m-wind speed for ERA-Interim driven RCA4 (1981-2010) for the grid point nearest to (a) Frankfurt, (b) London, and (c) Rome. Wind speeds are extrapolated from 10m-wind speeds using extrapolation approximations (see section 2.3): type A (blue), type B (red) and type C (green). For details, please refer to section 2.3 of the main document.

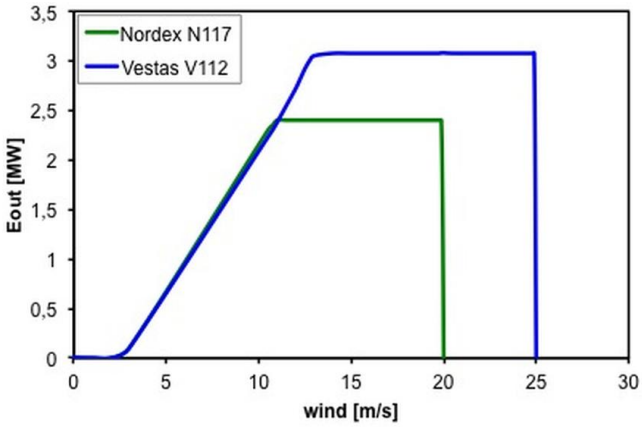

Figure S2: Characteristic power curves for the wind turbines Nordex N117 (green) and Vestas V112 (blue) as derived from manufacturer data. For more details please refer to the main document.

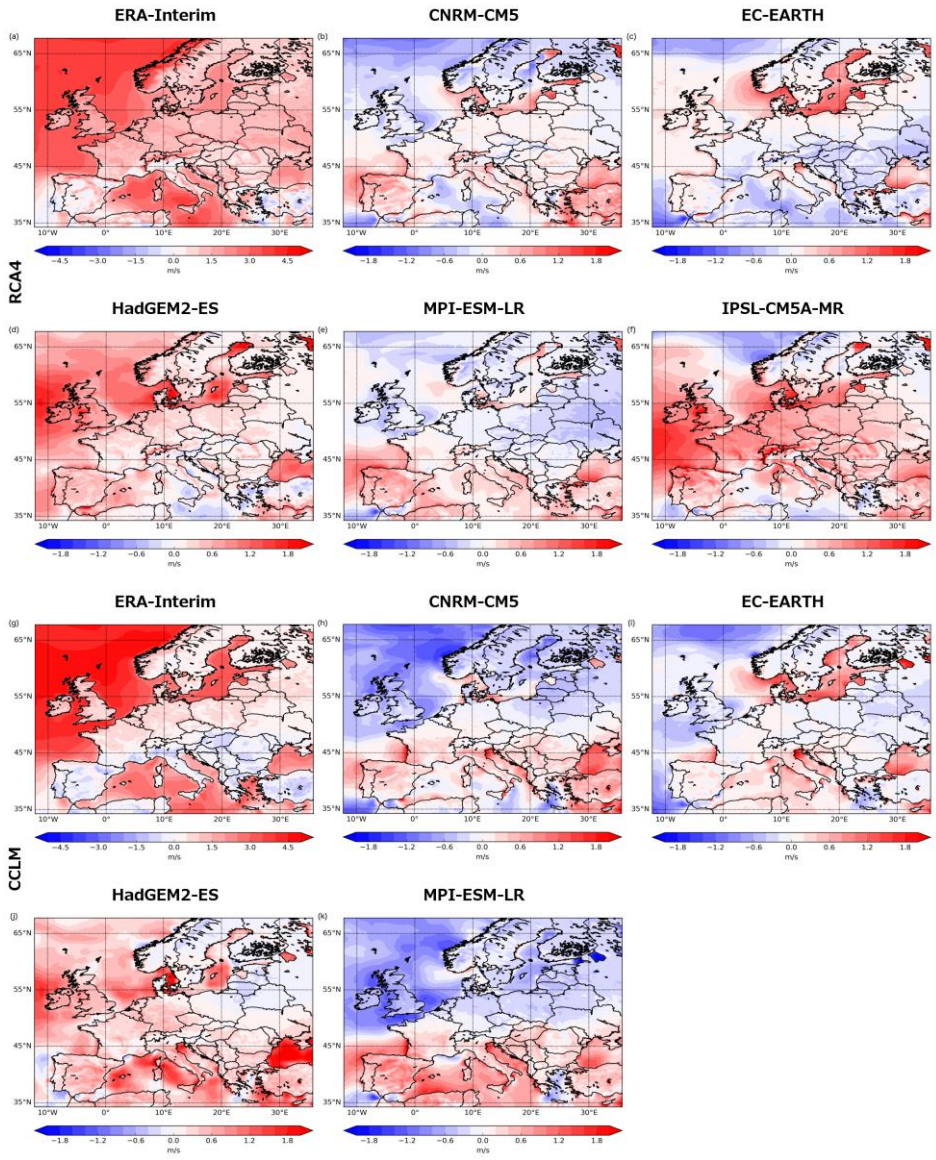

Figure S3: (a) Intra-annual variability of 10m-wind speed for ERA-Interim driven RCA4 (1981-2010) in m/s. (b) – (f) Difference of intra-annual variability of 10m-wind speed for the historical run of (b) CNRM-CM5, (c) EC-EARTH, (d) HadGEM2-ES, (e) MPI-ESM-LR, and (f) IPSL-CM5A-MR driven RCA4 (1971-2000) minus intra-annual variability of 10m-wind speed for ERA-Interim in m/s. (g) – (k) as (a) – (e), but for CCLM.

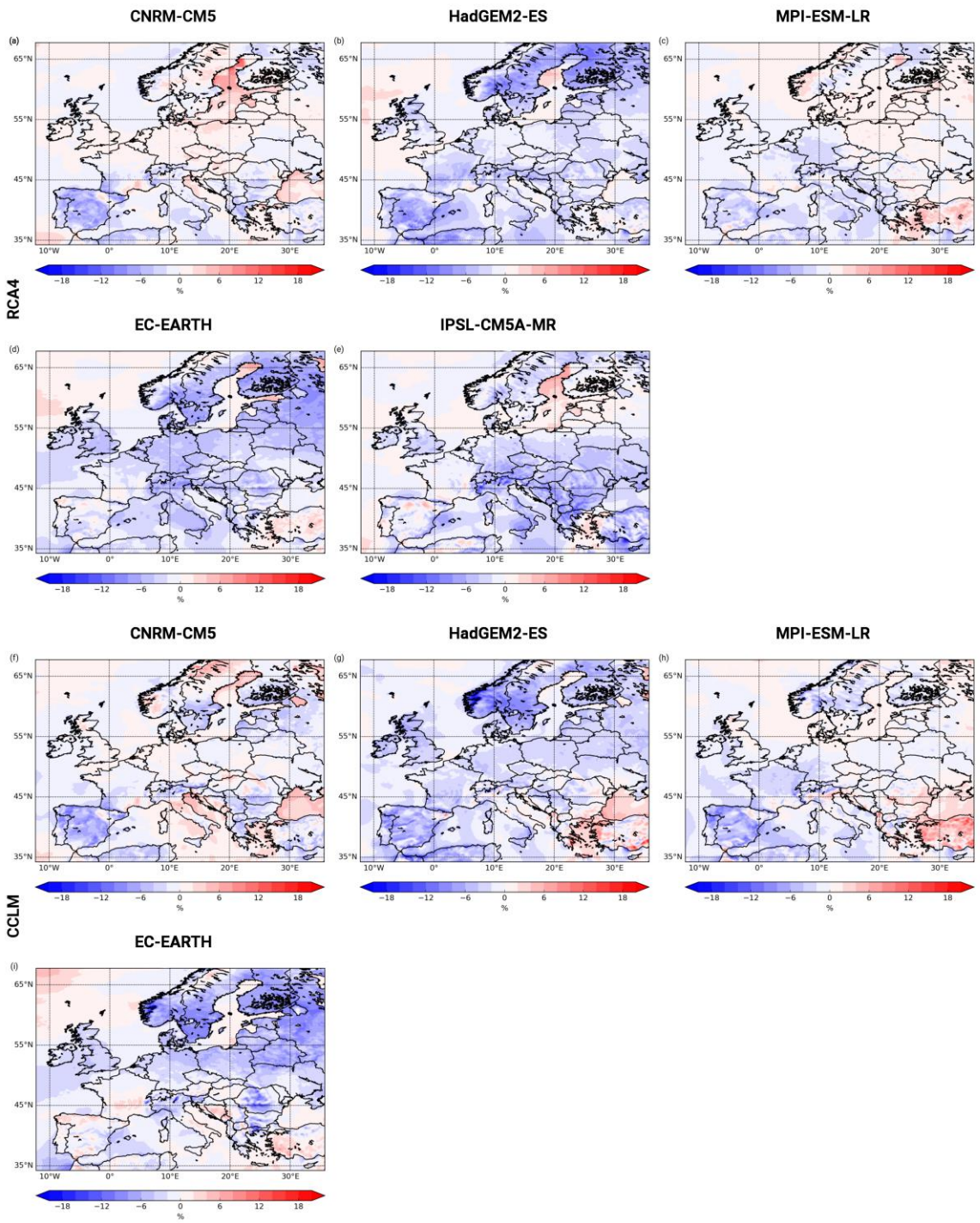

Figure S4: Changes of mean annual Eout in % for RCP4.5 (2071-2100) minus historical (1971-2000) for (a) CNRM-CM5, (b) HadGEM2-ES, (c) MPI-ESM-LR, (d) EC-EARTH, and (e) IPSL-CM5A-MR driven RCA4. (f) – (i) as (a) – (d), but for CCLM.

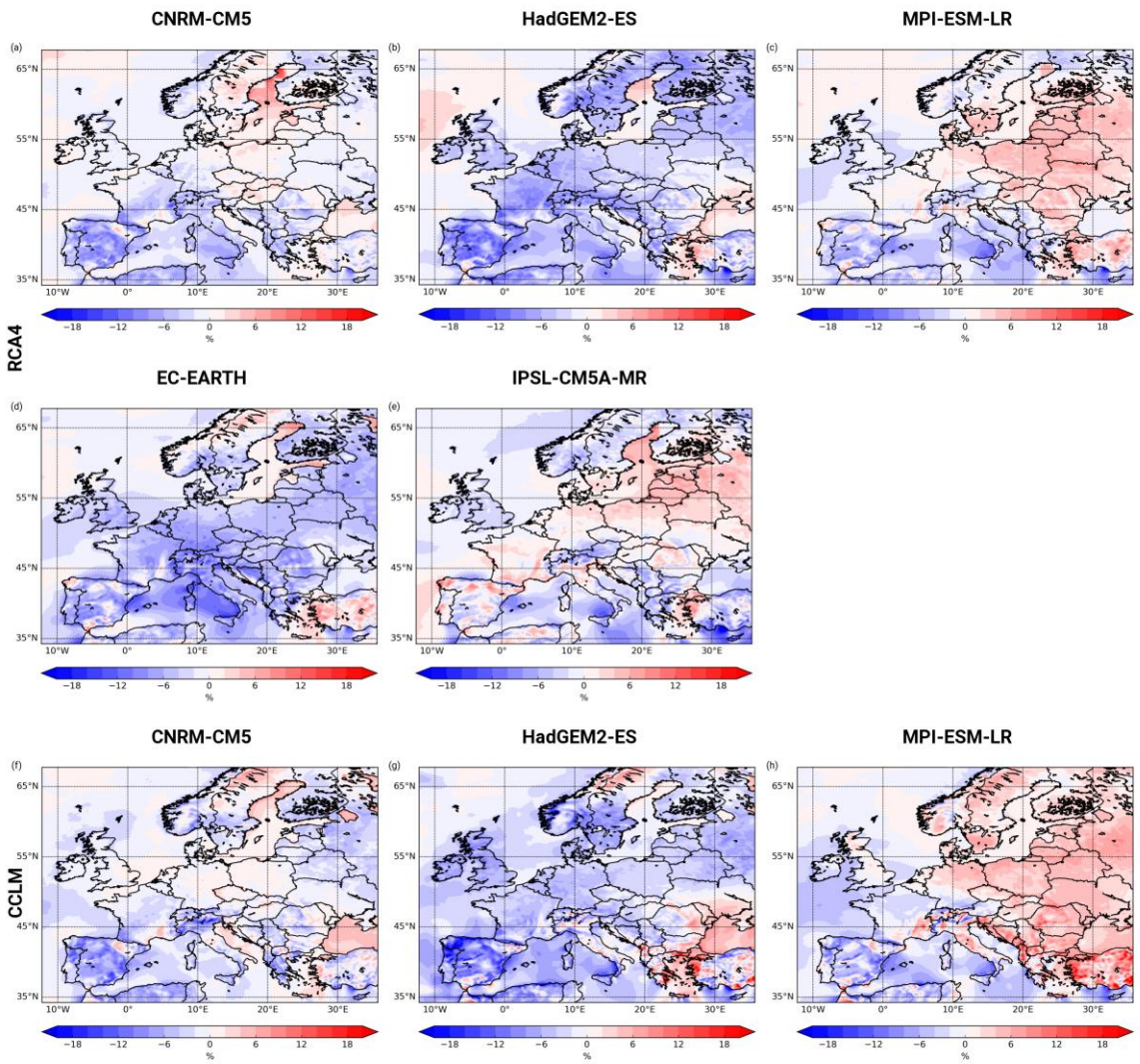

Figure S5: Changes of mean annual Eout in % for RCP8.5 (2071-2100) minus historical (1971-2000) for (a) CNRM-CM5, (b) HadGEM2-ES, (c) MPI-ESM-LR, (d) EC-EARTH, and (e) IPSL-CM5A-MR driven RCA4. (f) – (i) as (a) – (d), but for CCLM.

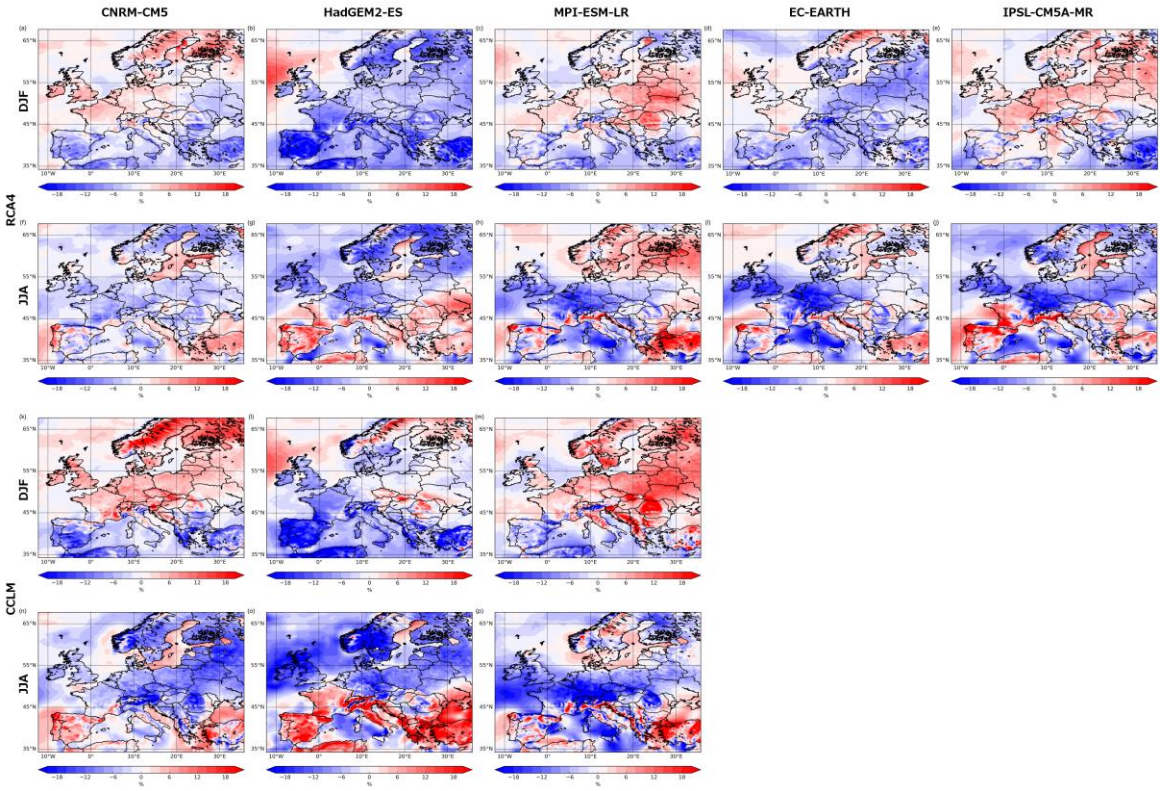

Figure S6: Changes of winter Eout in % for RCP8.5 (2071-2100) minus historical (1971-2000) for (a) CNRM-CM5, (b) HadGEM2-ES, (c) MPI-ESM-LR, (d) EC-EARTH, and (e) IPSL-CM5A-MR driven RCA4. (f) – (j) as (a) – (e), but for changes in summer Eout. (k) – (p) as (a) – (j), but for CCLM.

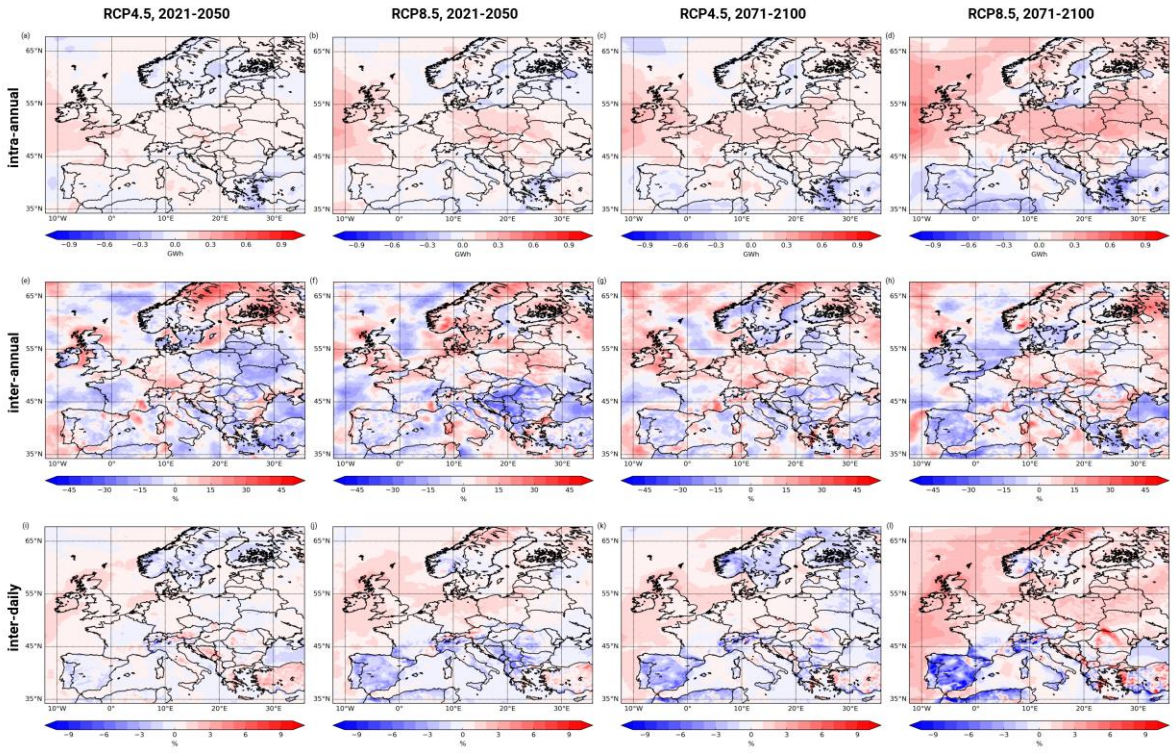

Figure S7: Changes of intra-annual variability of Eout in GWh for the ensemble mean of (a) RCP4.5 (2021-2050), (b) RCP8.5 (2021-2050), (c) RCP4.5 (2071-2100), (d) RCP8.5 (2071-2100) minus the ensemble mean of historical (1971-2000) for CCLM. (e) – (h) as (a) – (d), but for changes in inter-annual variability of Eout in %. (i) – (l) as (a) – (d), but for changes in inter-daily variability of Eout in %.

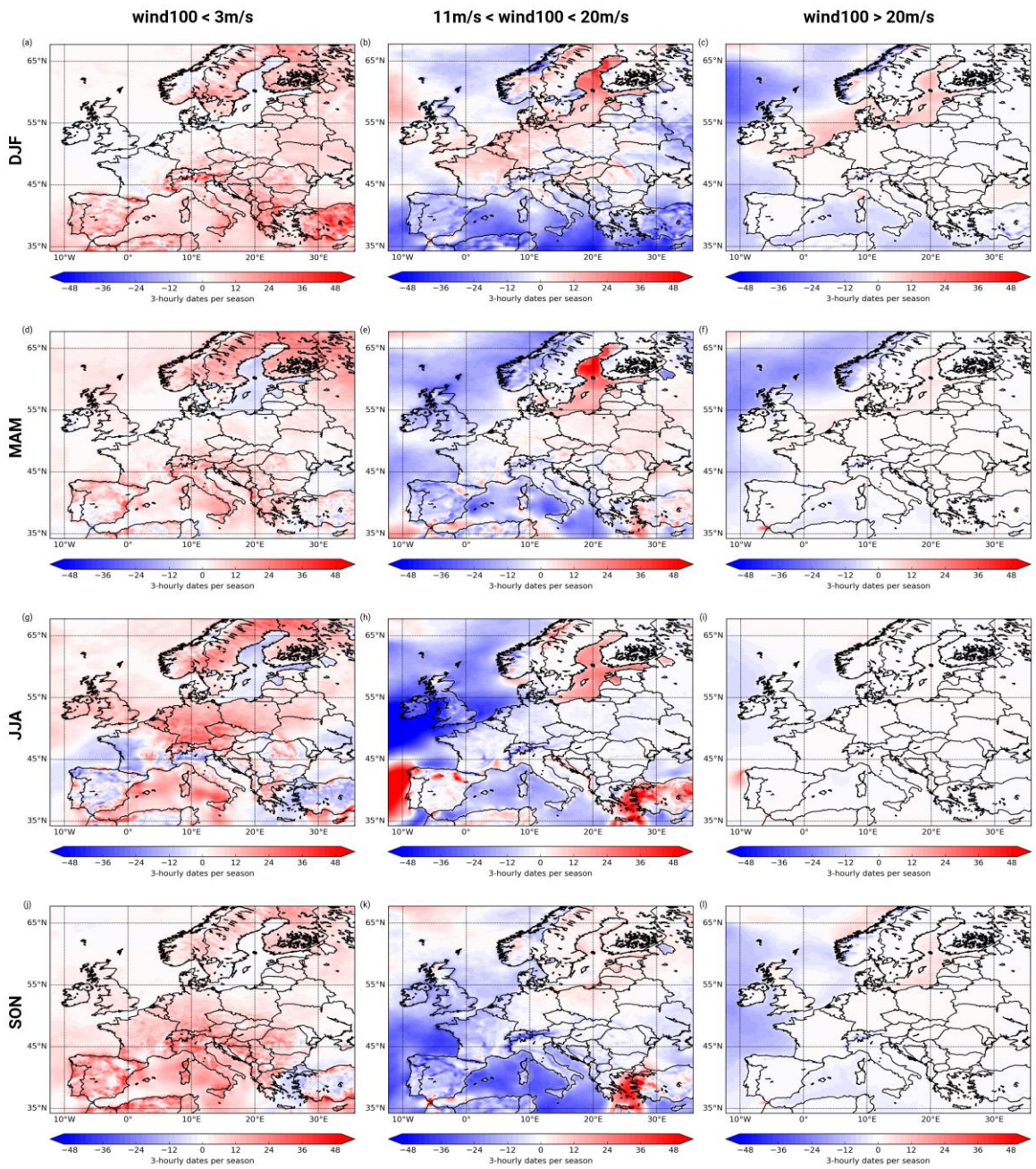

Figure S8: Changes in the number of three-hourly dates per winter (DJF) with (a) 100m-wind speed < 3 m/s, (b) 11 m/s < 100m-wind speed < 20 m/s, (c) 100m-wind speed > 20 m/s for the ensemble mean of RCP8.5 (2071-2100) minus the ensemble mean of historical (1971-2000) for RCA4. (d) – (f) as (a) – (c), but for spring (MAM). (g) – (i) as (a) – (c), but for summer (JJA). (j) – (l) as (a) – (c), but for autumn (SON).

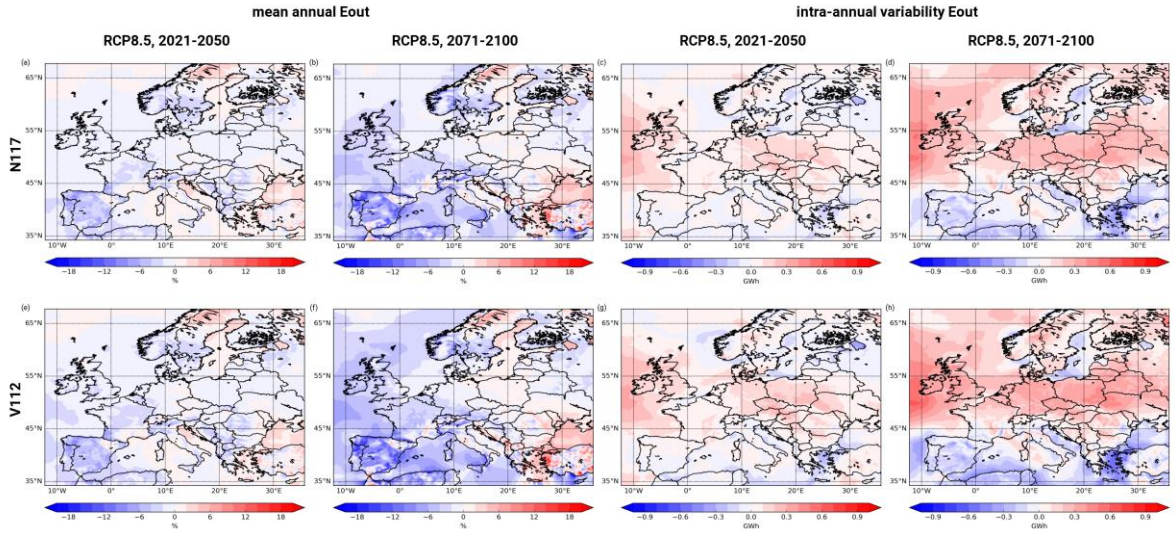

Figure S9: Changes of mean annual Eout in % for the ensemble mean of (a) RCP8.5 (2021-2050), and (b) RCP8.5 (2071-2100) minus the ensemble mean of historical (1971-2000) for CCLM for wind turbine N117. Changes of intra-annual variability of Eout in GWh for the ensemble mean of (a) RCP8.5 (2021-2050), and (b) RCP8.5 (2071-2100) minus the ensemble mean of historical (1971-2000) for CCLM for wind turbine N117. (e) – (h) as (a) – (d), but for the wind turbine V112. For details on the different turbines, please refer to Section 2.3 in the main text.

6 Impact of climate change on backup energy and storage needs in wind-dominated power systems in Europe

Based on the results of Moemken et al. (2018) and Reyers et al. (2016) and in cooperation with colleagues from Forschungszentrum Jülich, an advanced impact study was performed. This study deals with the influence of climate change on the temporal characteristics of wind power generation and the need for backup and storage infrastructures in a wind-dominated European power system. The results are published as Weber et al. (2018) in *PLOS ONE*. In this chapter, the analysed data and the main results are presented (see Appendix for full publication).

The operation of future renewable power systems with large contributions of wind is determined by weather and climate. Hence, the generated electric power is strongly fluctuating on different timescales, which is crucial for system operation. Backup and storage infrastructures are needed to guarantee supply also during periods of low wind generation. Weber et al. (2018) analysed how potential future changes of wind energy potentials in Europe as e.g. identified by Moemken et al. (2018) and Reyers et al. (2016) could impact a future renewable energy system, focussing on backup and storage needs. With this aim, a high-resolution ensemble of five GCM-RCM model chains from EURO-CORDEX is investigated. This ensemble consists of five different GCMs, which are dynamically downscaled with the RCM RCA4. It is thus a subsample of the nine GCM-RCM model chains considered in Moemken et al. (2018). Potential future changes are estimated for two future periods, 2030-2060 (mid-century) and 2070-2100 (end of century), considering

a strong (RCP8.5) and a medium emission scenario (RCP4.5). The analysis is based on near-surface wind speed at 0.11° horizontal and three-hourly temporal resolution. A characterisation based on circulation weather types of the large-scale atmospheric circulation over Central Europe in a large CMIP5 ensemble complements the results.

Backup needs are projected to increase for most parts of Central Europe (including Germany, Poland, Czech Republic, Switzerland, Austria, Belgium and the Netherlands), France, the British Isles and Scandinavia in the RCP8.5 scenario by the ensemble mean. This increase can reach up to 15% for the end of the century (Figure 6.1). At the same time, decreasing backup needs are simulated for the Iberian Peninsula, Greece and Croatia. Similar results are observed for the mid-century period and in the RCP4.5, but climate change signals are less pronounced and often not robust.

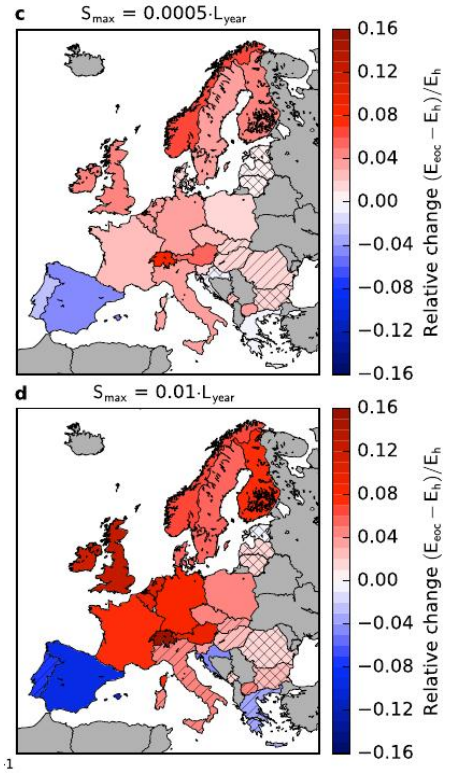

Fig. 6.1: Relative change of the average backup energy needs for 2070-2100 compared to 1970-2000 for 29 European countries, for two values of the storage capacity S_{max} and RCP8.5. The colours depict the ensemble mean response and the hatching indicates the robustness of the results. No hatching: 5/5 models agree on the sign of change, striped: 4/5 models agree, crossbred: 3/5 models agree. Source: Weber et al. (2018), Figure 2.

Furthermore, the same tendencies with slightly different magnitudes are detected for different storage sizes (cf. Figure 6.1c and d), different shares of renewables in the power system and a different siting of wind turbines (not shown).
Two processes are identified as main reasons for the increase in backup needs: an increased likelihood for long periods with low wind energy generation and a higher seasonal variability of wind speed. The duration distribution of periods with low wind power output is projected to shift to longer durations for large parts of Central Europe, France, the British Isles and Scandinavia, and to shorter durations for the Iberian Peninsula for the end of the century (Figure 6.2). For Eastern Europe, Italy, Greece and Norway, climate change signals are weaker and not robust. This part of the study is complemented with results from Reyers et al. (2016, chapter 4). The large CMIP5 ensemble confirms the shift to longer periods with low wind power generation. 19 out of 22 models simulate an increase in the mean duration of periods with low pressure gradients, which correspond to lower wind power yields in Central Europe.

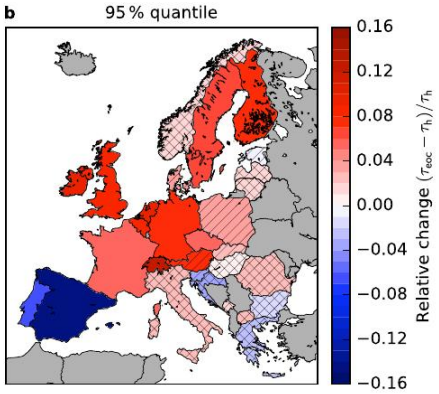

Fig. 6.2: Relative change of the duration assigned to the 95% quantile for 2070-2100 compared to 1970-2000 for 29 European countries and RCP8.5. The colours depict the ensemble mean response and the hatching indicates the robustness of the results. No hatching: 5/5 models agree on the sign of change, striped: 4/5 models agree, crossbred: 3/5 models agree. Source: Weber et al. (2018), Figure 5b.

At the same time, the winter-summer ratio of the wind power yield is simulated to increase for Central and North-western Europe and to decrease for the Iberian Peninsula, Greece and Croatia (Figure 6.3). In Northern Europe, climate change signals are small and not robust, thus here the increase of backup needs is primarily associated with a longer duration of low wind power generation.
Weber et al. (2018) showed that climate change is likely to impede the system integration of wind energy. The need for large backup and storage facilities increases in future decades

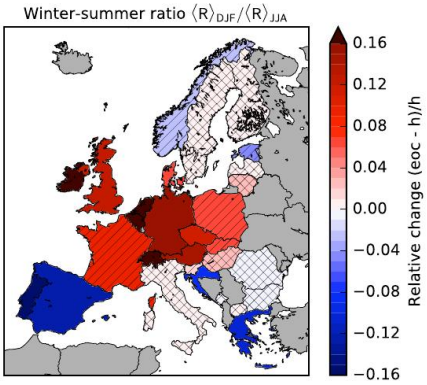

Fig. 6.3: Relative change of the winter-summer ratio of the average wind power yield for 2070-2100 compared to 1970-2000 for 29 European countries and RCP8.5. The colours depict the ensemble mean response and the hatching indicates the robustness of the results. No hatching: 5/5 models agree on the sign of change, striped: 4/5 models agree, crossbred: 3/5 models agree. Source: Weber et al. (2018), Figure 7.

to secure the electricity supply in periods with low wind energy generation. The main reasons for the increase in backup energies, namely the higher probability of long periods with low wind energy production and the increased seasonal variability, are also found in Moemken et al. (2018, see chapters 5 and 9.4). The results highlight the importance to combine energy and climate change research studies, and the necessity of integrated energy systems that account for other renewable sources like solar power.

7 Decadal predictability of regional scale wind speed and wind energy potentials over Central Europe

---

Reference:

Moemken, J., Reyers, M., Buldmann, B., and Pinto, J. G. (2016). Decadal predictability of regional scale wind speed and wind energy potentials over Central Europe. *TellusA*, 68:29199. doi:10.3402/tellusa.v68.29199

Page numbers are as published in *Tellus A*.

Tellus SERIES A DYNAMIC METEOROLOGY AND OCEANOGRAPHY
PUBLISHED BY THE INTERNATIONAL METEOROLOGICAL INSTITUTE IN STOCKHOLM

Decadal predictability of regional scale wind speed and wind energy potentials over Central Europe

By JULIA MOEMKEN[1]*, MARK REYERS[1], BENJAMIN BULDMANN[1] and JOAQUIM G. PINTO[1,2], [1]*Institute for Geophysics and Meteorology, University of Cologne, Cologne, Germany*; [2]*Department of Meteorology, University of Reading, Reading, United Kingdom*

(Manuscript received 20 July 2015; in final form 24 February 2016)

ABSTRACT

Decadal predictions on timescales from one year to one decade are gaining importance since this time frame falls within the planning horizon of politics, economy and society. The present study examines the decadal predictability of regional wind speed and wind energy potentials in three generations of the MiKlip ('Mittelfristige Klimaprognosen') decadal prediction system. The system is based on the global Max-Planck-Institute Earth System Model (MPI-ESM), and the three generations differ primarily in the ocean initialisation. Ensembles of uninitialised historical and yearly initialised hindcast experiments are used to assess the forecast skill for 10 m wind speeds and wind energy output (*Eout*) over Central Europe with lead times from one year to one decade. With this aim, a statistical-dynamical downscaling (SDD) approach is used for the regionalisation. Its added value is evaluated by comparison of skill scores for MPI-ESM large-scale wind speeds and SDD-simulated regional wind speeds. All three MPI-ESM ensemble generations show some forecast skill for annual mean wind speed and *Eout* over Central Europe on yearly and multi-yearly time scales. This forecast skill is mostly limited to the first years after initialisation. Differences between the three ensemble generations are generally small. The regionalisation preserves and sometimes increases the forecast skills of the global runs but results depend on lead time and ensemble generation. Moreover, regionalisation often improves the ensemble spread. Seasonal *Eout* skills are generally lower than for annual means. Skill scores are lowest during summer and persist longest in autumn. A large-scale westerly weather type with strong pressure gradients over Central Europe is identified as potential source of the skill for wind energy potentials, showing a similar forecast skill and a high correlation with *Eout* anomalies. These results are promising towards the establishment of a decadal prediction system for wind energy applications over Central Europe.

Keywords: decadal prediction, regionalisation, wind speed, wind energy, Central Europe, statistical-dynamical downscaling, MiKlip decadal prediction system, MPI-ESM, COSMO-CLM

To access the supplementary material to this article, please see Supplementary files under 'Article Tools'.

1. Introduction

The demand for renewable, ecologically sustainable energy sources as alternative to fossil sources has strongly increased in recent years (Solomon et al., 2007). In Europe, wind energy production has emerged as a promising renewable energy source to face the projected climate change due to increasing greenhouse gas emissions. The currently installed wind energy capacity in Europe has the potential to produce enough electricity to cover up to 8 % of the EU's electricity demand (Pineda et al., 2014). By 2020, the European Commission aims to produce 14.9 % of the EU's electricity from wind energy resources (Moccia et al., 2014). Wind energy production itself is influenced by weather and climate due to its dependence on near-surface wind conditions (e.g. Pryor and Barthelmie, 2010). In recent years, several studies investigated the impact of climate change on wind speeds and wind energy production over Europe on the regional scale for the middle and end of the 21st century (e.g. Barstad et al., 2012; Pryor et al., 2012; Hueging et al., 2013; Tobin et al., 2014; Reyers et al., 2016). These studies used different

*Corresponding author.
email: jmoemken@meteo.uni-koeln.de

Citation: Tellus A 2016, **68**, 29199, http://dx.doi.org/10.3402/tellusa.v68.29199

global and regional climate models (GCMs and RCMs) with different emission scenarios and downscaling techniques, and focused on different parts of Europe. Most of these studies agree on a general increase in wind energy potentials over Northern Europe and a general decrease over Southern Europe in future decades. Differences can be found regarding the magnitude and sometimes the sign of the projected changes. These differences seem to result not only from different initial conditions and model parameterisations but also from downscaling technique (e.g. Pryor et al., 2005, 2012; Tobin et al., 2014; Reyers et al., 2016). However, both potential long-term trends and future changes for wind speed and wind energy potentials are quite small compared to temperature trends (IPCC, 2012). At the same time, the natural variability of wind, especially on interannual to decadal timescales, is quite large and might conceal potential long-term trends.

Short-term climate predictions, which can assess this decadal variability, are of particular interest for the development of wind energy production, as their time frame of one year up to one decade falls within the planning horizon of politics and economy (e.g. Meehl et al., 2009). The German consortium MiKlip ('Mittelfristige Klimaprognosen', decadal climate predictions; Marotzke et al., submitted) developed a model system based on the Max-Planck-Institute Earth System Model (MPI-ESM) to provide skilful decadal predictions on global and regional scales. Therefore, the decadal predictions should represent natural variability as well as changes due to increasing greenhouse gas emissions (e.g. Solomon et al., 2011). The present study evaluates several generations of the MPI-ESM decadal prediction system recently conducted within MiKlip with respect to the decadal predictability of regional wind speed and wind energy production. The first generation of MPI-ESM decadal predictions (*baseline0*) contributes to the Coupled Model Intercomparison Project Phase 5 (CMIP5; Taylor et al., 2012). An overview over recent studies, especially from CMIP5, and the current state-of-the-art for decadal predictions can be found in Meehl et al. (2014). Through CMIP5, a set of global decadal hindcast experiments (initialised forecasts of past cases) and predictions (of future cases) has been made available. The initial conditions for these decadal runs are taken from assimilation runs, which use reanalysis data (ocean-only or ocean-atmosphere) from the past and the present (see Section 2.1). Ensembles are generated by initialising the simulations at different time steps of the assimilation run (usually 1-day-lagged initialisation; e.g. Müller et al., 2012). The hindcast experiments are used to analyse the decadal predictability for different parameters through a comparison to observations and reanalysis data (e.g. Smith et al., 2007).

Several publications assessed the decadal forecast skill of existing forecast systems, either for individual model ensembles (e.g. Müller et al., 2012, 2014; Goddard et al., 2013; Marotzke et al., submitted) or for multi-model ensembles (e.g. van Oldenborgh et al., 2012; Doblas-Reyes et al., 2013; Eade et al., 2014). Most of these studies focus on the global scale and on primary meteorological parameters like temperature (e.g. Smith et al., 2007; Müller et al., 2012) and precipitation (e.g. van Oldenborgh et al., 2012). Although all of these studies found some decadal forecast skill, their results differ for different parameters, regions and lead times. In particular, Eade et al. (2014) indicated that potential skill in decadal prediction systems may often be underestimated. Nevertheless, most of them agree that the North Atlantic is a key region for decadal climate predictions (e.g. Müller et al., 2012). So far, only few studies investigated decadal predictions on the regional scale, and to our knowledge, none is dealing with wind energy. Kruschke et al. (2014), for example, analysed the decadal forecast skill for cyclone activity over the Northern Hemisphere in the MPI-ESM and found some regions over the North Atlantic with positive predictive skill for intense cyclones. Mieruch et al. (2014) investigated the decadal forecast skill for seasonal temperature anomalies and precipitation sums in dynamically downscaled MPI-ESM hindcasts, focusing on Europe. They found a good predictive skill for summer temperature, which could be preserved by regionalisation. Predictive skill for precipitation sums could even be improved by the downscaling in their study. Haas et al. (2015) evaluated the decadal predictability of peak winds on the regional scale in the MPI-ESM, using a statistical-dynamical downscaling (SDD) approach for the regionalisation. Their results showed highest skill scores for short lead times and upper gust percentiles.

For the application to regional scales, the resolution of the global decadal predictions is insufficient. Therefore, a downscaling of the global datasets to the regional scale is necessary (e.g. Mieruch et al., 2014; Haas et al., 2015). In principle, it is possible to use a dynamical downscaling (DD) approach for the regionalisation of large ensembles, depending on available computing power, storage capacities and time. However, since most decadal prediction systems comprise multiple ensemble members of yearly initialised hindcasts, resulting in a total of several hundreds of simulations per ensemble generation (see Section 2.1), it is hardly possible to regionalise the entire hindcast ensemble using a purely DD method. The present study uses a SDD approach (following Fuentes and Heimann, 2000; Pinto et al., 2010) to investigate the decadal predictability of wind energy potentials over Central Europe, with special focus on Germany. SDD approaches combine a purely DD application with statistical approaches, for example weather type analysis (e.g. Reyers et al., 2015) or transfer functions (e.g. Najac et al., 2011; Haas and Pinto, 2012). This combination offers a good and cost-efficient alternative to DD. In this study, we

applied the SDD approach developed by Reyers et al. (2015) to the decadal hindcasts and predictions of the MPI-ESM and analysed the decadal forecast skill for different lead times and different seasons. The focus of this study is given to wind and wind energy potentials over Germany.

The paper is organised as follows. The decadal prediction and hindcast datasets are described in Section 2 (part 2.1). Additionally, Section 2 contains the methodology of SDD (2.2), bias and drift correction (2.3), and an explanation of the skill metrics (2.4). The results for wind speed are presented in Section 3: the added value of downscaling is addressed in Section 3.1, while Section 3.2 contains the forecast skill for different wind percentiles. The results for wind energy potentials are described in Section 4, focusing on the forecast skill over Central Europe (4.1), the seasonal dependence of forecast skill (4.2) and a potential source of forecast skill (4.3). A short summary and discussion of the results concludes this paper in Section 5.

2. Data and methods

2.1. Data

Three decadal prediction generations of the coupled model MPI-ESM performed in low-resolution mode (MPI-ESM-LR; Giorgetta et al., 2013) are analysed. The coupled model consists of the atmospheric model ECHAM6 (Stevens et al., 2013), the ocean model MPIOM (Jungclaus et al., 2013), the land-biosphere model JSBACH (Raddatz et al., 2007) and the ocean-biogeochemistry model HAMOCC (Ilyina et al., 2013), coupled by OASIS3 (Valcke et al., 2003). The atmospheric component is run with a T63 horizontal resolution (1.875°) and 47 vertical levels, and the MPIOM with a horizontal resolution of 1.5° and 40 vertical levels.

The three MPI-ESM ensemble generations differ in their initialisation (see Table 1; cf. also Marotzke et al., submitted). The first analysed generation of decadal hindcasts is called *baseline1* (second MiKlip ensemble generation). The initial conditions are taken from an assimilation experiment, where the model state is nudged towards ocean temperature and salinity anomalies of an MPIOM experiment forced with ORA-S4 ocean reanalysis (Balmaseda et al., 2013), and full atmospheric fields from ERA40 (Uppala et al., 2005) and ERA-Interim (Dee et al., 2011). The *baseline1* ensemble consists of 10 members of yearly initialised decadal hindcasts and predictions from the initialisation year 1960 (hereafter dec1960: comprising the 10-yr period 01 January 1961 to 31 December 1970) to 2011 (dec2011: comprising the 10-yr period 01 January 2012 to 31 December 2021), and is described in detail in Pohlmann et al. (2013). The latest MPI-ESM generation – named *prototype* – differs from *baseline1* in terms of full-field ocean initialisation and consists of two separate ensembles (see Table 1). The first *prototype* ensemble (hereafter *prototype1*) uses full-fields from ORA-S4 reanalysis, while the second *prototype* ensemble (hereafter *prototype2*) uses full-fields of GECCO2 ocean reanalysis (Köhl, 2015). Both *prototype1* and *prototype2* ensembles consist of 15 members of yearly initialised decadal hindcasts and predictions, from which 10 members are utilised here for the initialisation period 1960–2013 (dec1960 to dec2013). For all three generations, the ensemble members are generated through a 1-day-lagged initialisation (e.g. Müller et al., 2012). Further, uninitialised historical runs are used here as reference datasets to estimate the added value of initialisation (see also Section 2.4). They consist of 10 ensemble members and are started from a pre-industrial control simulation and consider aerosol and greenhouse gas concentrations for the period 1850–2005 (e.g. Müller et al., 2012). The first MiKlip ensemble generation *baseline0* is not discussed here due to the limited number of runs (10 members every 5 yr for the period 1960–1999, 10 members for the period 2000–2010 and only three members in every other year).

To evaluate the model performance in terms of the decadal forecast skill, observations or reanalysis datasets are usually used. In this study, we consider the ERA-Interim reanalysis dataset (Dee et al., 2011) for evaluation and for the computation of different forecast skill scores (see also Section 2.4). ERA-Interim is the third global reanalysis dataset of the European Centre for Medium-Range Weather Forecasts (ECMWF). It is available from 1979 onwards. In this study, we use ERA-Interim data for the period 1979–2010.

Table 1. Overview of the three MPI-ESM ensemble generations used in this study, including information on the name within the MiKlip consortium, the ocean initialisation, the atmosphere initialisation and the number of ensemble members.

Ensemble	Ocean initialisation	Atmosphere initialisation	# Ensemble member
baseline1	Anomalies from ORA-S4 reanalysis	Full-fields from ERA-Interim/ERA40	10
prototype1	Full-fields from ORA-S4 reanalysis	As above	10 (from 15)
prototype2	Full-fields from GECCO2 reanalysis	As above	10 (from 15)
historical	–	–	10 (from 15)

In order to enable a direct comparison between the different ensembles, 10 simulations are used for all datasets. All simulations correspond to the 'low-resolution' set up.

2.2. *Statistical-dynamical downscaling methodology*

We follow the SDD methodology by Reyers et al. (2015) to downscale the global MPI-ESM hindcasts and historical runs to derive regional wind speeds and wind energy production. Since the SDD approach for the application to wind energy potentials is described in detail in Reyers et al. (2015), only a short summary is given here. SDD consists of four steps:

In the first step, a circulation weather type (CWT) approach after Jones et al. (1993) is applied to daily mean sea level pressure (MSLP) fields, using the following global datasets as input data: ERA-Interim reanalysis for evaluation, 10 historical runs and three ensembles of MPI-ESM hindcasts for the analysis of decadal predictability. All datasets are interpolated on the same regular 2.5° grid for the computation of the CWTs. The large-scale atmospheric flow as represented by the instantaneous MSLP fields is characterised for each day for Central Europe using the central point at 10°E, 50°N (near Frankfurt, Germany; Fig. 1a). The patterns are assigned to 10 basic CWTs (eight directional and two rotational classes; e.g. west W or cyclonic C) and one mixed CWT (anti-cyclonic/west AW). The days corresponding to the AW type are not accounted for in the basic A or W types. In addition, the 11 CWTs are subdivided into classes with different pressure

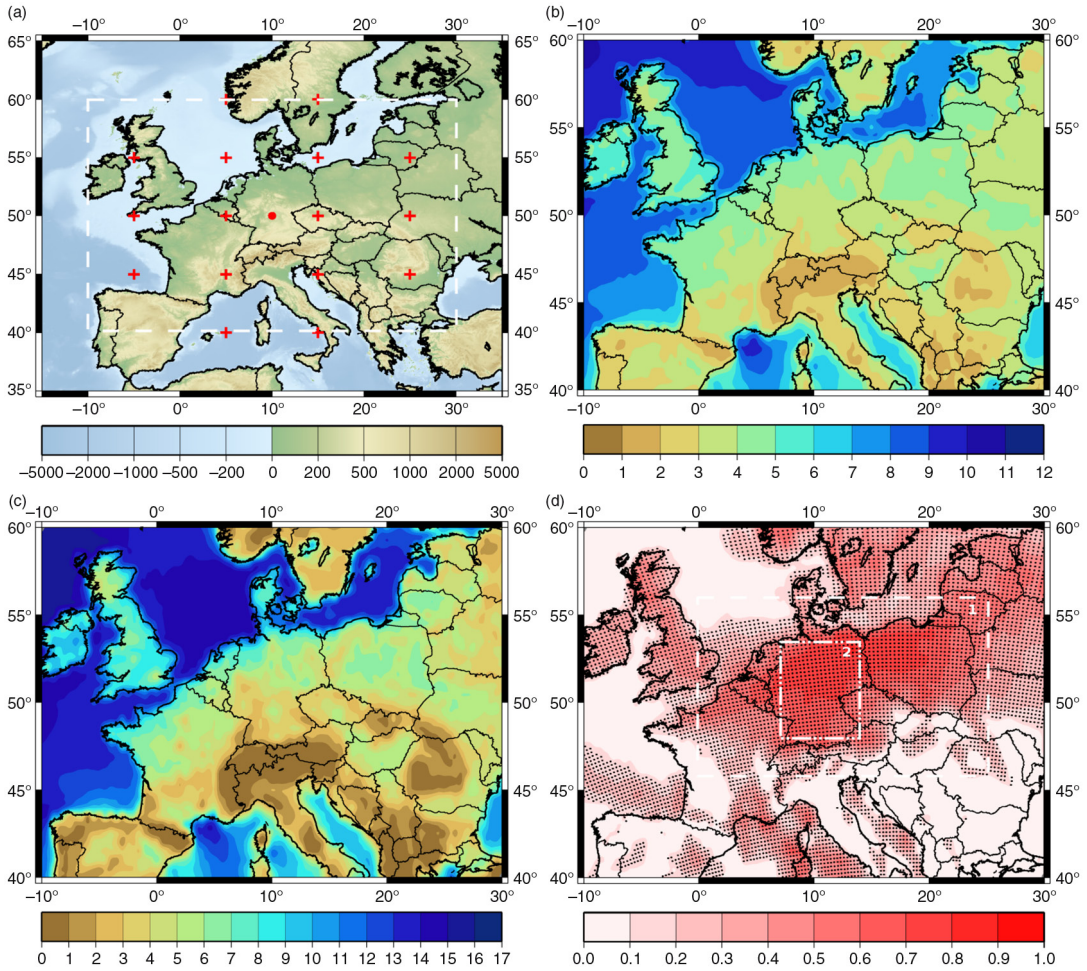

Fig. 1. (a) Topography of Europe in metre, and grid points for CWT analysis (step 1 of SDD). The red point represents the central point at 10°E, 50°N (near Frankfurt, Germany), and the red crosses represent the surrounding 16 grid points used for the computation of the CWTs. The white box represents the region for figures (b) to (d). (b) Climatological mean of mean 10 m wind speed in metre per second for ERA-Interim (1979–2010) as obtained by SDD. (c) Climatological mean of annual *Eout* in 10^3 MWh for ERA-Interim (1979–2010) as obtained by SDD. (d) Explained variance between annual *Eout* time series for ERA-Interim (1979–2010) as obtained by SDD and as obtained by DD (DD_{era}) per CCLM grid point. Grid points with significant correlation are dotted (*t*-test, 95% confidence level). Box 1 represents the subregion for the computation of the MSE skill scores as shown in Fig. 5 and Supplementary Figs. 2–5 (see also Section 4), and box 2 represents the subregion for the averages over Germany (7°E–14°E, 48°N–53°N) as shown in Figs. 2, 3, 4, 6, 7 and Supplementary Fig. 1.

gradients in 5 hPa per 1000 km intervals, ranging from below 5 hPa per 1000 km to ca. 45 hPa per 1000 km. Altogether, 77 weather classes are considered.

In the second step, representative days for each of the 77 classes are simulated with the regional climate model COSMO of the German Weather Service (Deutscher Wetterdienst, DWD) in its *Cl*imate *M*ode (version 4.8, hereafter CCLM; e.g. Rockel et al., 2008). CCLM simulations with a horizontal resolution of 0.22° are performed for the model domain of the EURO-CORDEX project (Giorgi et al., 2006), using ERA-Interim data as initial and boundary conditions. For each of the 77 weather classes, up to 10 representatives have been extracted. Note that the ERA-Interim-driven representatives are used for the regionalisation of all global datasets, assuming that the wind characteristics of the different CWTs are similar in both the model and the reanalysis (see Reyers et al., 2015).

In the third step, simulated hourly 10 m wind speeds of the representative days are recombined to probability density functions (PDFs) at each CCLM grid point. Therefore, we weighted the contributions of all 77 classes by the respective class frequency (e.g. frequency of a weather class in a certain decade) and the number of representative days.

The last step is subdivided into two separate substeps, one for wind speed and one for wind energy potentials. For wind speed, the PDFs of the hourly 10 m wind speeds are directly used to calculate different wind percentiles and the mean wind for each grid point. Figure 1b shows the spatial distribution of the mean wind for ERA-Interim (climatology for 1979–2010) as obtained by SDD. For wind energy applications, the PDFs of the hourly 10 m wind speeds are used to calculate gridded wind energy output (*Eout*) of a 2.5-MW wind turbine from General Electrics (2010). First, the hourly 10 m wind speeds are extrapolated to the average turbine hub height using a vertical wind profile, which is the standard procedure in wind energy applications from the 'large-scale' perspective (e.g. Hueging et al., 2013; Tobin et al., 2014). Here, the power law is used to extrapolate the 10 m wind speeds to a height of 80 m (*v80*; Reyers et al., 2015). The extrapolated wind speeds form the basis to compute *Eout*, following these characteristics: Below $v80 = 3.5$ m/s (cut-in velocity) and above $v80 =$ 25 m/s (cut-out velocity), no energy output is produced. Between the cut-in velocity (3.5 m/s) and the rated velocity (12.5 m/s), *Eout* is calculated as:

$$E_{out} = c_p \frac{1}{2} \rho \pi R^2 \nu_{80}^3, \quad (1)$$

with power coefficient c_p (constant value of 0.35 for the idealised turbine), air density ρ (constant value of 1.225 kg m^{-3}) and rotor radius R of the idealised wind turbine (50 m). Between wind velocities of 12.5 m/s (rated velocity) and 25 m/s (cut-out velocity), a constant maximum *Eout* of 2.5 MW is assumed. To obtain spatial distributions of mean annual wind energy output for each CCLM grid point, *Eout* is integrated over all wind speed ranges and weighted with the respective climatological velocity frequencies. Figure 1c shows the spatial distribution of mean annual *Eout* for the ERA-Interim data (climatology for 1979–2010) as obtained by SDD. For the application of SDD to the different MPI-ESM datasets and to different time periods, only the weather type computation (step 1) has to be recalculated.

Reyers et al. (2015) evaluated the results for the SDD approach for wind energy potentials against a purely DD method applied to ERA-Interim. The results show a good agreement for Central Europe (see also Fig. 1d; explained variance between annual *Eout* as obtained by SDD and annual *Eout* as obtained by DD), while agreement is reduced over other areas, like the North Sea or the Mediterranean region. They also tested the applicability of SDD to decadal hindcasts of the *baseline1* ensemble and concluded that SDD performs well for Germany, the Benelux region, the Czech Republic, and Poland (cf. Reyers et al., 2015; their figures 10 and 11). The lower performance of the SDD approach in other European countries is due to the considered CWT classification, which is centred over Germany and thus has a better performance over Germany and nearby countries (see Fig. 1a; Reyers et al., 2015).

2.3. Bias and potential drift correction

Several studies revealed a systematic bias in the MPI-ESM historical runs and hindcasts due to model drifts (e.g. Kruschke et al., 2014, 2015). This systematic bias is both dependent on the model generation and forecast time. The International CLIVAR Project Office (ICPO; 2011) suggests a bias correction for anomaly-initialised predictions and uninitialised simulations by subtracting a climatological bias, while a subtraction of lead time-dependent bias should be used for full-field initialised predictions. In a sensitivity study, we applied a bias correction to the CWT frequencies of the *baseline1* ensemble (first step of the SDD; see Section 2.2). In terms of our SDD approach, the systematic bias is reflected by an overestimation of the frequencies of some weather types, especially the westerly types over Europe (see Reyers et al., 2016; their table 2 and figure 1b). This is due to the typical overestimation of the zonal flow in the North Atlantic/European Sector in GCMs (e.g. Sillmann and Croci-Maspoli, 2009). Therefore, the climatological CWT frequencies for both decadal hindcasts and uninitialised historical runs were corrected towards the respective climatological frequencies of ERA-Interim. The resulting empirical factors have been applied to the decadal CWT frequencies for the different lead times, which were

then used for the computation of *Eout*. However, since the bias is systematic in CWT frequencies of both hindcasts and the historical runs as reference dataset, the bias correction has only negligible effects on our results (not shown).

Kharin et al. (2012) stated that it is problematic to assume a constant model drift, especially when differences between observed and modelled long-term climate trends are large. This is in particular the case for decadal predictions initialised by full-fields (e.g. *prototype*). We also analysed the potential model drift in the *prototype1* ensemble, focusing on CWT frequencies and 10 m wind speeds. In both cases, the consequences of the model drift are small for our approach (not shown). Therefore, we have chosen to use the original datasets for all analyses.

2.4. Forecast skill assessment

Three different metrics are used to identify a potential added value of downscaling and estimate whether the initialisation of the hindcasts improves the decadal predictability compared to the uninitialised historical runs: the mean square error skill score (MSESS) and the ranked probability skill score (RPSS) to quantify the accuracy of the hindcasts, and the reliability (REL) to assess the relation between ensemble spread and bias. The different skill metrics are calculated for seven different lead times for the whole year and the single seasons. Lead times corresponding to the first half of the decade (e.g. yr1-3: first to third year after initialisation; hereafter short lead times) represent skill that is supposed to originate from the initialisation. We also considered lead times corresponding to the second half of the decade (e.g. yr6-9: sixth to ninth year after initialisation; hereafter longer lead times) to see how far ahead the initialisation provides predictive skill. Moreover, one lead time covering nearly the whole decade (yr2-9) is analysed. As suggested by Goddard et al. (2013), lead times are temporally averaged. All three skill metrics compare the MPI-ESM ensembles to observations. Since no gridded observations for wind are available for Central Europe, we used a purely DD simulation of a reanalysis dataset instead as verification dataset. DD is simulated with CCLM, using ERA-Interim data for 1979–2010 as boundary conditions (hereafter DD_{era}; see Reyers et al., 2015). As DD_{era} is available for the period 1979–2010, we decided to use the decadal hindcasts dec1978 (1979–1988) to dec2000 (2001–2010) for the computation of the metrics in this study. Thereby, we ensure that the same number of yearly initialised hindcasts is considered for all lead times. The study focuses on Central Europe (box 1 in Fig. 1d) and Germany (box 2 in Fig. 1d; 7°–14°E and 48°–53°N), since the results of the CWT approach are primarily representative for the large-scale atmospheric conditions over Germany and surrounding countries (cf. Fig. 1d and Reyers et al., 2015). Temporal anomalies are used for the computations of the skill metrics rather than absolute values to remove systematic climatological biases. For Germany, anomalies are spatially averaged before computing the skill scores.

The MSESS (Goddard et al., 2013) is a deterministic skill score and defined as

$$MSESS = 1 - \frac{MSE_{dec}}{MSE_{hist}}, \tag{2}$$

where MSE_{dec} is the mean squared error (MSE) between the ensemble mean of the initialised hindcast experiments and the verification dataset (DD_{era}). MSE_{hist} is the MSE of a reference dataset, which is in this case the ensemble mean of the uninitialised historical runs. Therefore, a positive MSESS suggests that the initialised hindcasts are more accurate in representing the observed decadal climate variability than the uninitialised historical runs (Goddard et al., 2013), and a negative value indicates the opposite.

The probabilistic RPSS (Wilks, 2011; Kruschke et al., 2014) is defined as

$$RPSS = 1 - \frac{RPS_{dec}}{RPS_{hist}}, \tag{3}$$

where RPS_{dec} is the ranked probability score (RPS) of the initialised hindcast experiments, and RPS_{hist} is the RPS of the uninitialised historical runs. The RPS is an extension of the Brier score (scalar accuracy measure for binary events) to multi-category forecasts (Wilks, 2011). Following Kruschke et al. (2014), three categories are used here for the calculation of RPS: below normal, normal and above normal. The categories are defined using the 33.3 and 66.6 percentiles of *Eout* and wind speed anomaly time series. The RPS is based on the cumulative probabilities for the three categories (Wilks, 2011):

$$RPS_{\tau} = \frac{1}{I}\sum_{i=1}^{I}\sum_{k=1}^{K}\left(F_{\tau,i,k} - O_{t(i,\tau),k}\right)^2. \tag{4}$$

$F_{\tau,i,k}$ is the cumulative probability of the 10 ensemble members within category k (here $K=3$), derived from the forecast ensemble of initialisation i (with a total number of $I=23$, for dec1978–dec2000) for a certain lead time τ. $O_{t(i,\tau),k}$ is the cumulative probability within category k derived from observations (here DD_{era}) for time t, which corresponds to the time of initialisation i and the lead time τ. $O_{t(i,\tau),k}$ is the Heaviside step function with $O_{t(i,\tau),k}=1$ if the event occurs in category k or lower or else $O_{t(i,\tau),k}=0$ if a category higher than k is observed. A positive RPSS therefore indicates that the initialised hindcasts have a higher probability to predict an observed anomaly category than the uninitialised historical runs, and vice versa for a negative RPSS. Following Kruschke et al. (2014), we corrected the RPS for biases due to finite ensemble sizes

(see also Ferro, 2007). RPSSs are calculated for different wind percentiles as well as for *Eout*.

The reliability (REL; Weigel et al., 2009) is defined as

$$REL = \frac{RMSE_{dec} - \sqrt{\langle \sigma^2_{ensemble} \rangle_t}}{RMSE_{dec}}, \quad (5)$$

where $RMSE_{dec}$ is the root mean square error between the ensemble mean of the initialised hindcasts and the verification dataset DD_{era}, and $\sqrt{\langle \sigma^2_{ensemble} \rangle_t}$ is the time-mean ensemble spread. The reliability quantifies if the ensemble spread is able to cover the model uncertainties (Mieruch et al., 2014). The ensemble is well calibrated for REL values around zero. The ensemble is called underconfident if $REL < 0$, and overconfident if $REL > 0$.

3. Decadal predictability of wind speed

3.1. The added value of downscaling

We first analyse the added value of downscaling by comparing large-scale MPI-ESM wind speed to SDD-simulated regional wind speed. With this aim, we calculate skill metrics for both variables. Figure 2 shows the RPSS and the reliability for annual wind speeds averaged over Germany (see box 2 in Fig. 1d) for the three ensemble generations (*baseline1*, *prototype1* and *prototype2*). All generations exhibit forecast skill, both for large-scale and regional scale wind speeds. The RPSSs are positive for most lead times, with highest skill scores for short lead times (e.g. yr1-3). The regionalisation is able to preserve the decadal forecast skill of the global runs for almost all lead times and in all three ensembles. For some lead times, the downscaling increases the predictive skill. This added value of downscaling is particularly apparent for *baseline1* (e.g. yr1-3, yr4-6). Improvements are smaller for the *prototype* ensembles. The reliability indicates that the global hindcasts are highly underconfident, in particular *prototype2*. An analysis of the individual components of the reliability [ensemble spread and RMSE, see eq. (5)] reveals that for nearly all lead times the ensemble spread of the global hindcasts clearly exceeds the RMSE (cf. Supplementary Fig. 1). The regionalisation improves both the ensemble spread and the RMSE for most lead times and in all three generations. Since the relative reduction of the spread is larger than that of the RMSE, the two values are now much closer to each other (Supplementary Fig. 1). As a consequence, the SDD ensembles are nearly well calibrated for short lead times in *baseline1* and p*rototype1* and all lead times in *prototype2*. In summary, an added value of downscaling for wind speed can be identified in the ensemble generations. This added value depends on the lead time and the initialisation.

3.2. Forecast skill for different wind percentiles

After identifying the added value of our downscaling approach, we focus on the decadal predictability of regional wind speeds. RPSSs are derived for three different percentiles averaged over Germany: mean wind, 75th percentile and 90th percentile (Fig. 3). Positive skill scores are found for all lead times in all three ensemble generations, except for yr1 (first year after initialisation) for mean wind speed (Fig. 3a). Skill scores are highest for short lead times (yr1-3 and yr1-4), with the best skill of 0.34 for *prototype1* for yr1-3 for the 90th percentile (Fig. 3c). In this case, the initialisation improves the performance of the decadal prediction system against the uninitialised historical runs by 34 %. Skill scores decrease with increasing time after the initialisation (longer lead times) and are often enhanced for higher percentiles. Differences between the three ensembles are rather small, revealing that no initialisation is clearly superior to the other. Overall, the positive skill scores indicate that the hindcasts are closer to the verification dataset DD_{era} than the uninitialised historical runs. This is valid not only for the mean wind speed but also for higher percentiles, which are in particular relevant for the wind energy potentials.

4. Decadal predictability of wind energy potentials

In this section, we assess the decadal predictability of wind energy potentials on the regional scale. Therefore, we first derive forecast skill scores for wind energy output and compare them to skill scores for regional wind speed (Section 4.1). Further, the seasonal dependency of the forecast accuracy is investigated (Section 4.2). Finally, we evaluate potential large-scale sources of forecast skill for wind energy potentials (Section 4.3).

4.1. Forecast skill for Germany and Central Europe

First, RPSSs and MSESSs are calculated for annual *Eout* anomalies averaged over Germany for seven different lead times. The RPSSs for *Eout* (Fig. 4a) are analogue to the RPSSs for mean wind speed (cf. Fig. 3a): skill scores are positive for almost all lead times in all three ensembles, highest skill scores are found for short lead times (with the highest value of 0.28 for *prototype1* and yr1-3), and skill scores decrease slightly with increasing time since initialisation. However, the forecast skill for *Eout* and mean wind speed may differ, which is particularly true for longer lead times. This indicates that the decadal predictability of the wind energy output depends on a wider wind speed range, and particularly on the higher percentiles (see Section 3.2).

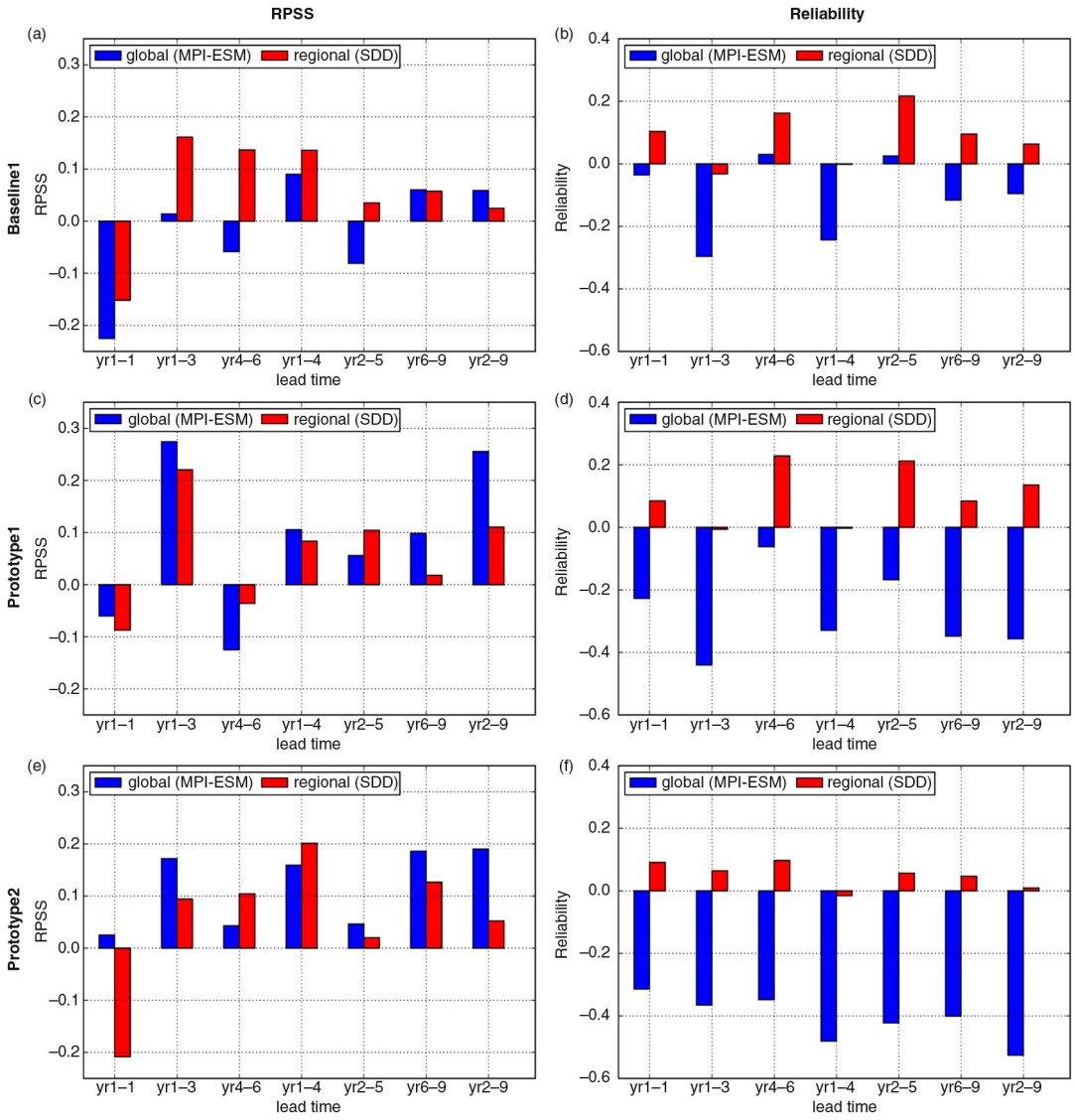

Fig. 2. (a) Ranked probability skill scores (RPSSs) for large-scale MPI-ESM mean wind (blue) and SDD-simulated regional mean wind (red) for seven different lead times for the whole year, averaged over Germany (box 2 in Fig. 1d), for the *baseline1* ensemble. (b) Reliability for large-scale MPI-ESM mean wind (blue) and SDD-simulated regional mean wind (red) for seven different lead times for the whole year, averaged over Germany (box 2 in Fig. 1d), for the *baseline1* ensemble. (c)–(d) as (a)–(b), but for the *prototype1* ensemble. (e)–(f) as (a)–(b), but for the *prototype2* ensemble.

Highest positive MSESS values are found for short lead times, with the best skill of 0.47 for *prototype1* for yr1-3 (Fig. 4b). MSESSs decrease with increasing time since initialisation and are negative for yr2-9. The positive skill found for yr1 for *baseline1* and *prototype1* is maintained for the second year after initialisation (yr2; not shown) and increases considerably for *prototype2* (from -0.03 to 0.3; not shown). For most lead times, both the RPSSs and the MSESSs vary little between the three ensemble generations. However, *prototype1* seems to outperform the other two generations for yr1-3, a period that is supposed to be strongly influenced by the initialisation.

Despite a general agreement between RPSSs and MSESSs, some differences between these two skill scores are detected not only in terms of the magnitude but also in terms of the sign (e.g. yr2-5 and yr2-9; see Fig. 4a and b). Hence, a higher probability of the hindcasts to forecast an observed anomaly category (RPSS) compared to the uninitialised historical runs does not necessarily imply a higher forecast accuracy (MSESS) against the observed anomaly values.

For the following investigations, we focus on MSESS to quantify the differences between ensemble mean predictions and observations, which are directly measured by the mean

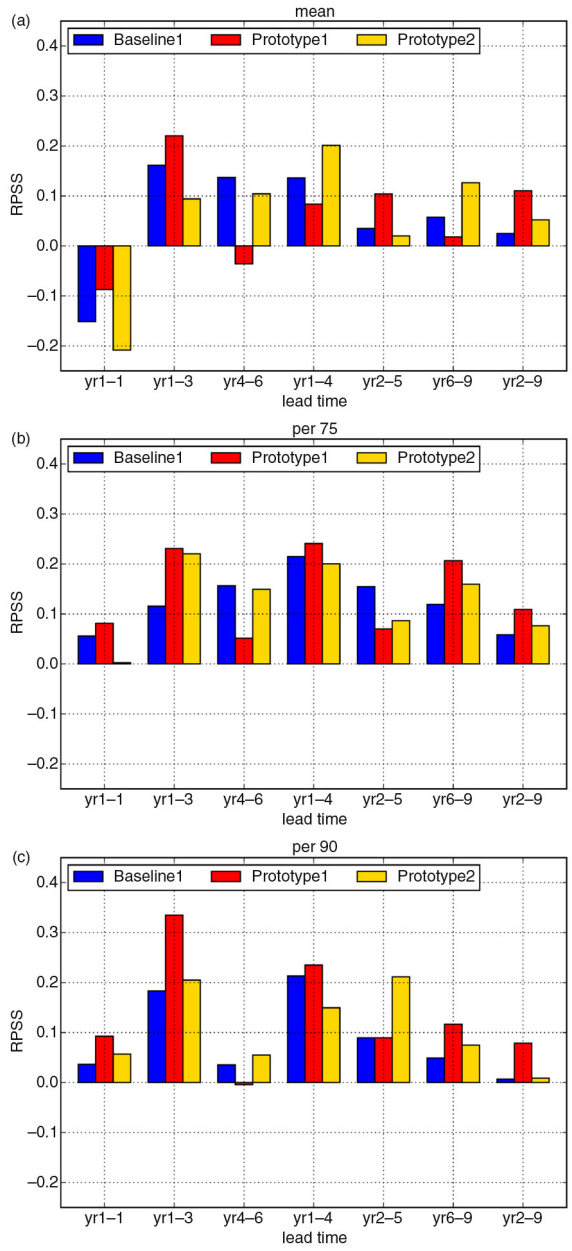

Fig. 3. RPSSs for SDD-simulated wind speed for seven different lead times for the whole year, averaged over Germany (box 2 in Fig. 1d), for the ensemble generations *baseline1* (blue), *prototype1* (red) and *prototype2* (yellow), for different percentiles: (a) mean wind, (b) 75th percentile and (c) 90th percentile.

square error (see Section 2.4). The spatial distributions of MSESS over Central Europe for the annual mean wind energy output are shown in Fig. 5. The three MPI-ESM ensembles are compared for the four exemplary lead times yr1, yr1-3, yr2-5 and yr6-9. Generally, MSESS reveals highest positive values over Northern and Western Germany and the Benelux countries. Differences between the three ensembles are rather small. For yr1 (first year after initialisation), all three ensemble generations show positive skill scores of up to 0.25 for the Benelux countries and large parts of Germany. In these regions, the initialisation of the hindcasts improves their performance against the uninitialised historical runs by 25 %. Negative skill scores of up to −0.5 cover most parts of Poland, the Czech Republic and Eastern Germany, especially for *prototype2*. For yr1-3 and yr2-5, all three generations show similar distributions of MSESS. For yr1-3, the ensembles show positive skill scores of up to 0.6 over most parts of Central Europe. Skill scores are highest for *prototype1* over Germany. For yr2-5, skill scores decline in all three ensembles. They now range from −0.2 (over parts of Poland and the Czech Republic) to 0.4 (over Germany), with highest positive values for *prototype2*. For yr6-9, skill scores are smallest compared to the other lead times (−0.5 to 0.3).

In summary, the three MPI-ESM ensemble generations show an added value of the initialisation compared to the uninitialised simulations and therefore a decadal forecast skill for wind energy output. However, this skill is mostly limited to the first years after initialisation and seems to depend slightly on the initialisation of the different ensemble generations.

4.2. *Seasonal dependency of forecast skill*

Previous studies (e.g. Müller et al., 2012; Mieruch et al., 2014) found a seasonal dependence of forecast skill in the MPI-ESM in terms of temperature and/or precipitation. Given the strong seasonal variations in wind speed, we calculated MSESSs and RPSSs for *Eout* for different multi-year seasonal means (Fig. 6 and Supplementary Figs. 2–5 in the appendix).

For winter (DJF) means, MSESSs are much weaker than for annual means for all three generations and all lead years. Negative values are found over Germany, the Benelux region, and most parts of Poland and the Czech Republic for almost all lead times (Fig. 6a and Supplementary Fig. 2). MSESS values around zero are only found for short lead times (yr1-3 and yr1-4). As for annual *Eout*, the MSESS for spring (MAM) means reaches its maximum for lead time yr1-3, in particular over Western Germany and Benelux (Fig. 6c and Supplementary Fig. 3). For all other lead times, skill scores are small or below zero. The strongest negative MSESS values are found for summer (JJA) means of *Eout* over Germany (Fig. 6e). At the same time, the MSESS reveals the most pronounced spatial heterogeneity for this season, with strong negative values over Northern Germany, while positive skill is identified over Poland and parts of the Czech Republic for nearly all lead times (Supplementary Fig. 4). For autumn (SON) means, positive MSE skill scores persist longest in all three

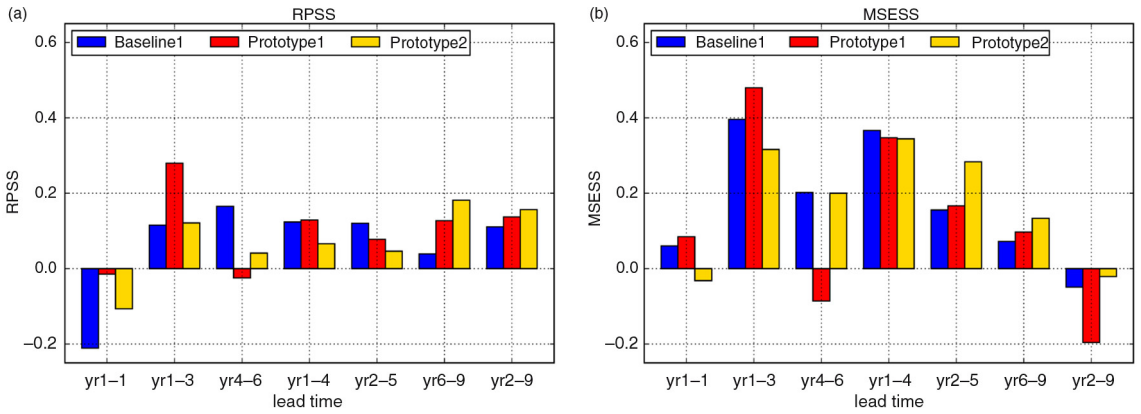

Fig. 4. Forecast skill scores for SDD-simulated *Eout* for seven different lead times for the whole year, averaged over Germany (box 2 in Fig. 1d), for the ensemble generations *baseline1* (blue), *prototype1* (red) and *prototype2* (yellow). (a) RPSSs and (b) mean square error skill scores (MSESSs).

MPI-ESM ensemble generations (Fig. 6g and Supplementary Fig. 5), and even increase for longer lead times. Highest skill scores can be observed over North-Eastern Germany and Western Poland for yr6-9 in all three generations. However, as for the other seasons a negative MSESS is found for yr2-9 over Germany (Fig. 6g).

The probabilistic RPSSs for *Eout* over Germany for the spring, summer and autumn seasons (Fig. 6d, f and h) are mostly comparable to the MSESSs in terms of the sign of the values, with lowest skill in the summer months and highest and most persistent skill scores for autumn. Large discrepancies between both skill scores are found for winter. Winter RPSSs clearly exceed the winter MSESSs (cp. Fig. 6a and b). Positive values are even found for the longer lead times (e.g. yr6-9) as well as for the multi-year mean yr2-9, especially for *baseline1* and *prototype2*. The differences between RPSSs and MSESSs may on the one hand be attributed to the higher variability and absolute values of wind speed and wind energy output in winter, which has a stronger impact in MSESSs than RPSSs. The decadal hindcasts are apparently not able to forecast this high variability, resulting in large discrepancies between prediction and observation. These differences are directly captured by the MSE, leading to negative MSESS values (see Section 2.4). On the other hand, the decadal hindcasts are to some extent able to capture the observed category (below normal, normal, above normal) of the anomalies, resulting in positive RPSS values.

Overall, the decadal forecast skill for wind energy output over Germany and Central Europe shows a strong seasonal dependency, with best skill for autumn and worst skill for summer. Differences between the three MPI-ESM ensemble generations are generally small for all seasons, especially in terms of the sign of the skill scores. Further, the results reveal that the three ensemble generations have generally a higher potential in predicting annual than seasonal wind energy potentials (cf. Figs. 4 and 6).

4.3. *Potential source of forecast skill*

The previous results provided evidence that the decadal forecast skill for wind energy potentials is given primarily for short lead times in all three MPI-ESM ensemble generations. Given the SDD approach for the regionalisation, we assume that the predictive skill for regional *Eout* might originate from the predictive skill for the frequencies of large-scale weather types over Europe (step 1 of SDD; see Section 2.2). Sensitivity studies revealed that *Eout* depends strongly on the occurrence of CWT West, especially those with large pressure gradients, which corresponds to a strong zonal flow over Central Europe (not shown). Figure 7a exemplary shows anomaly time series of annual frequencies of the large-scale CWT West with pressure gradients above 10 hPa per 1000 km (hereafter CWT W+) and of annual *Eout* (averaged over Germany) for ERA-Interim. Both time series show similar year-to-year in-phase variations of the anomalies. They agree particularly well for years 1987–2010. The correlation of 0.62 emphasises the high dependence of *Eout* on the occurrence of CWT W+, although the climatological fraction of this weather type to all CWTs is less than 8 % (see also Reyers et al., 2015; their figure 3). Similar and in some cases even higher correlations are found for the historical runs of MPI-ESM (0.63 to 0.84 for the individual ensemble members), indicating that such a strong relationship between regional *Eout* and the large-scale CWT W+ also exists in the MPI-ESM.

We therefore hypothesise that decadal forecast skill for regional *Eout* is high, if the MPI-ESM on the global scale is able to forecast the frequency of CWT W+ well. Figure 7b shows the MSESSs for annual CWT W+ frequencies for

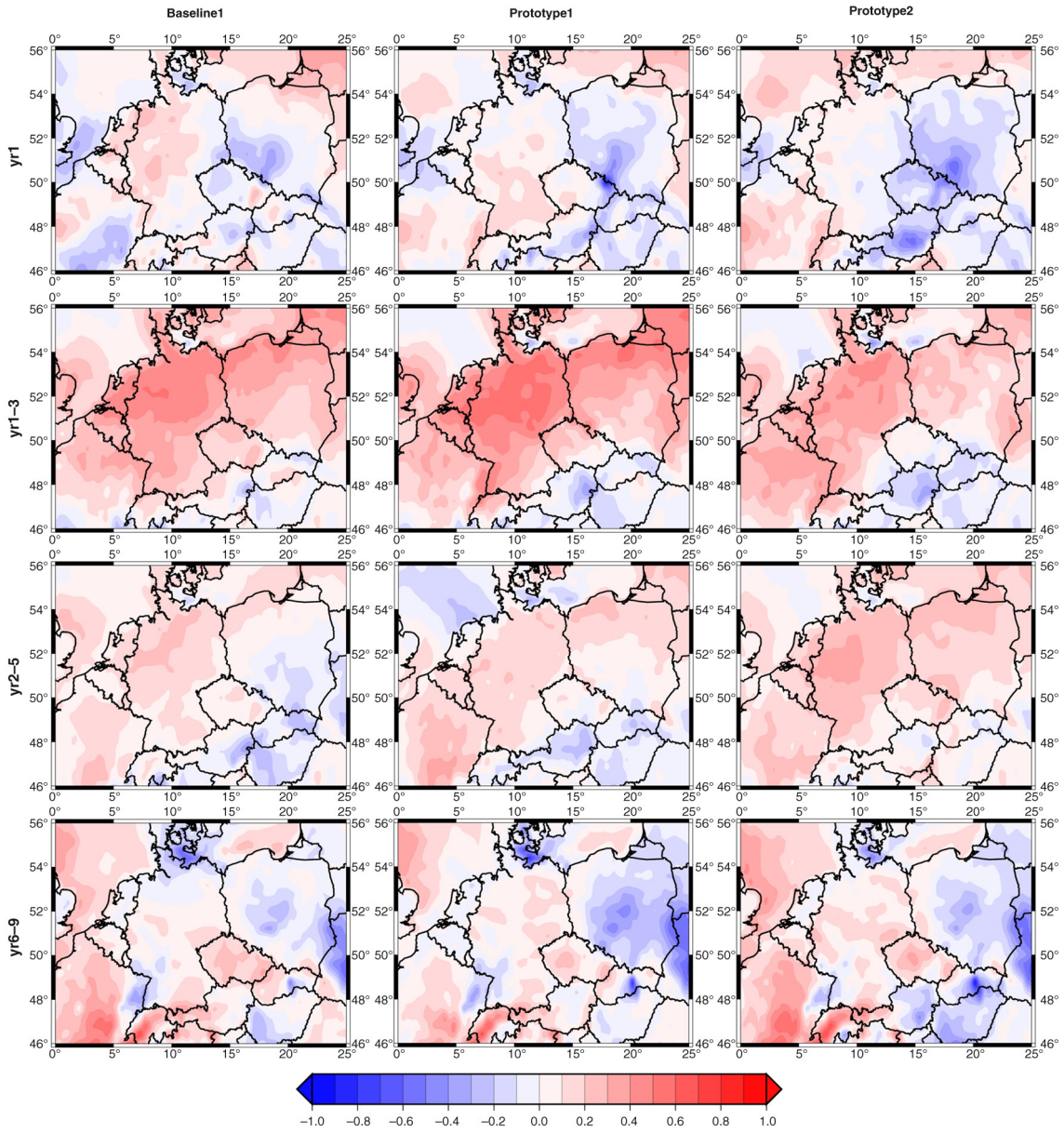

Fig. 5. MSESSs for SDD-simulated *Eout* for four exemplary lead times for the whole year for the ensemble generations *baseline1* (left column), *prototype1* (middle column) and *prototype2* (right column). Reference forecast is the ensemble mean of the uninitialised historical runs.

seven different lead times. Skill scores are positive for all lead times except yr2-9 in all three MPI-ESM ensemble generations. The skill scores for CWT W+ frequencies are similar to MSESSs for *Eout* (see Fig. 4b) and RPSSs for wind speed, with highest skill scores for short lead times and a decrease with increasing time since initialisation. As for wind energy, the highest positive skill score is found for yr1-3 for *prototype1* (added value of initialisation of 60 %), while the highest value for yr2-5 is detected for *prototype2*. As a consequence, the decadal forecast skill for wind energy potentials can to some extend be attributed to an adequate forecast of the frequencies of strong westerly flow over Central Europe. Therefore, a potential source of forecast skill for regional wind energy potentials over Central Europe could be identified.

5. Summary and discussion

The decadal forecast skill for regional wind speed and wind energy potentials over Central Europe was investigated for

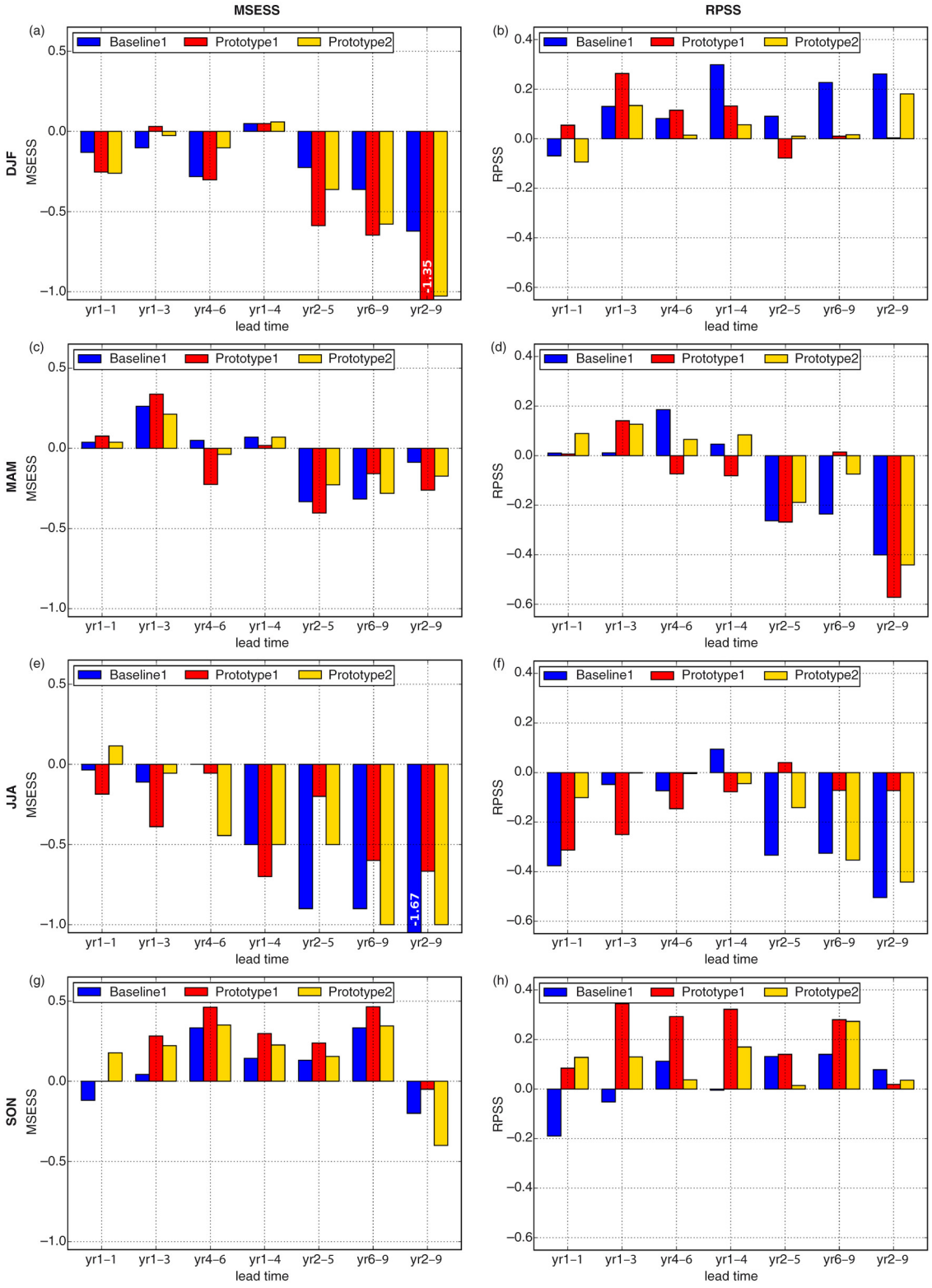

Fig. 6. MSESSs (left column) and RPSSs (right column) for SDD-simulated *Eout* for seven different lead times for the four seasons, averaged over Germany (box 2 in Fig. 1d), for the ensemble generations *baseline1* (blue), *prototype1* (red) and *prototype2* (yellow). (a) and (b) Winter (DJF), (c) and (d) spring (MAM), (e) and (f) summer (JJA), (g) and (h) autumn (SON). MSESS values under −1.0 are displayed in the corresponding bar. Note that yr1 for winter corresponds to months 12–14 after initialisation.

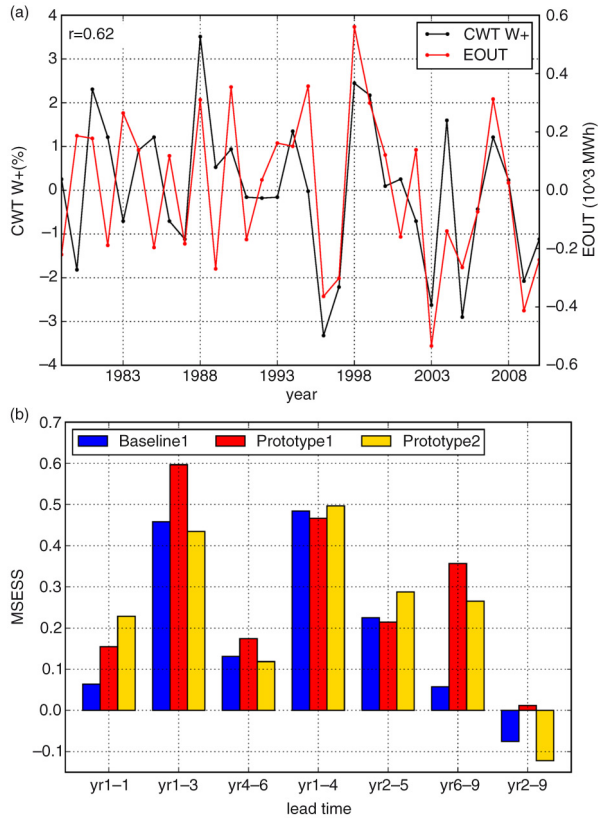

Fig. 7. (a) Time series of annual frequency-anomalies for CWT W+ in % (black line) and of annual *Eout* anomalies in 10^3 MWh (red line) for the ERA-Interim period 1979–2010. The correlation between both time series is given in the upper left corner. (b) MSESSs for CWT W+ for seven different lead times for the whole year for the MPI-ESM ensemble generations *baseline1* (blue), *prototype1* (red) and *prototype2* (yellow). For details, see main text (Section 4.3).

three ensemble generations of the MiKlip decadal prediction system. The MPI-ESM ensembles have the same atmosphere initialisation but differ in their ocean initialisation. The performance of the global MPI-ESM and the regionalised hindcast ensembles was tested in terms of decadal predictability using different skill metrics (MSESS, RPSS and reliability). The main results of this study can be summarised as follows:

- All three ensemble generations show forecast skill for annual wind speeds and *Eout* over Central Europe. This skill is mostly limited to short lead times, with highest values for yr1-3, and is best for North-Western Germany and Benelux.
- In seasonal terms, forecast skill is best for autumn and worst for summer. The predictive skill for seasonal *Eout* is typically lower than for annual *Eout*.
- The differences between the three MiKlip ensemble generations are generally small. However, *prototype1* slightly outperforms the other two generations for yr1-3.
- A dominant westerly weather type with a strong zonal flow (CWT W +) is identified as a potential source for the forecast skill of *Eout* over Central Europe. MSESSs for CWT W+ are similar to MSESSs for *Eout* for almost all lead times.
- The added value of downscaling for mean winds is identified in terms of both RPSSs and reliability but depends on the lead time and the hindcast generation.

The added value of downscaling was quantified in terms of mean wind speeds rather than wind energy output. This choice is motivated by the fact that only 6-hourly wind speeds are available for MPI-ESM, which does not enable an adequate computation of *Eout* (which requires hourly data).

The results of the presented forecast skill assessment depend strongly on the choice of the verification dataset. We have chosen a DD simulation of reanalysis data, since no gridded observations for wind and wind energy are available for Central Europe. Thereby, we assume that the high-resolution wind speeds simulated with DD are a good proxy for observed gridded wind speeds. Nevertheless, skill scores may change if gridded observations are used as a verification dataset.

The present results indicate that the decadal forecast skill for wind energy originates mainly from the initialisation, since high positive skill scores are mostly limited to the first years after initialisation. For longer lead times, this skill disappears. These findings are in line with Haas et al. (2015), who evaluated the decadal predictability of regional peak winds in the MiKlip ensemble *baseline1* and also found highest skill scores for short lead times. The enhanced skill scores for higher percentiles are also consistent with results by Haas et al. (2015), who showed, for example, that the enhanced storminess over Central Europe in the early nineties (leading to enhanced peak winds at the surface) could be identified in the *baseline1* hindcasts. Such skill is not found for lower percentiles (Haas et al., 2015; their figure 7).

We could not find a systematic improvement from the *baseline1* ensemble to the *prototype* versions, thus giving evidence that there is generally no superior initialisation strategy in terms of anomaly- or full-field-initialisation for wind energy applications. This assessment agrees with Kruschke et al. (2015), who found no significant differences between the MiKlip generations for winter storm frequencies over the North Atlantic and Europe.

In this study, we have used the characteristics of one exemplary wind turbine. The consideration of power curves from other wind turbines would result in different *Eout*

values. However, since these differences would be systematic for both the initialised hindcasts and the uninitialised historical runs, we assume that the results presented here are similar for other wind turbines and that the choice of turbine has only a small impact on our conclusions with respect to the decadal predictability (see also Reyers et al., 2016).

The detected decadal forecast skill for regional wind energy output exhibited a strong dependence on the representation of westerly CWTs (the dominant weather types for strong wind situations) in the MPI-ESM. If the occurrence of westerly CWTs, especially those with high pressure gradients, is forecasted well by the global hindcasts, predictive skill is found for both regional wind speeds and regional *Eout*.

For future work, the coupling of this large-scale weather type with low-frequency components like teleconnection patterns could be investigated. This may help to understand the mechanisms behind the decadal predictability for wind energy potentials. Another issue, which could be addressed, is the large uncertainties in the decadal predictability in the MPI-ESM, particularly in terms of the non-systematic skill dependency on lead times and seasons. Further investigations on the influence of the ensemble size and of the different initialisation strategies on the decadal predictability are also necessary. In this study, we considered only 10 of the 15 available members of the two *prototype* ensembles in order to compare the skill scores with the *baseline1* ensemble (which only has 10 ensemble members). Future work could consider all 15 realisations by using the 'fair' variant of the RPSS (e.g. Ferro, 2014), which takes into account ensembles with a different number of members. Further, wind power generation statistics taking the wind farm distribution and installed power into account (e.g. Cannon et al., 2015; Drew et al., 2015) should be analysed.

The present results are encouraging regarding the establishment of a decadal prediction system for Central Europe. They clearly show that there is a potential for forecasts of wind energy potentials up to several years ahead. In addition, the used SDD approach proved to be adequate for an application to large datasets and could easily be applied to operational decadal prediction systems. The regionalisation preserves and sometimes increases the forecast skill of the global runs and improves the ensemble spread in some cases. This opens a wide range of options for end-user application.

6. Acknowledgements

This research was supported by the German Federal Ministry of Education and Research (BMBF) under the project 'Probabilistic Decadal Forecasts for Central and Western Europe' (MiKlip-PRODEF, contract 01LP1120A), which is part of the MiKlip consortium ('Mittelfristige Klimaprognosen', http://www.fona-miklip.de). We thank the ECMWF for the ERA-Interim reanalysis dataset and the Max-Planck-Institute (Hamburg, Germany) for providing the GCM data (MPI-ESM). We thank the German Climate Computer Centre (DKRZ, Hamburg) for computer and storage resources and the Climate Limited-area Modelling Community (CLM Community; http://www.cosmo-model.org) for providing the COSMO-CLM model. We thank the members of MiKlip Module C (Regionalisation) for discussions, and Simona Höpp for help with data processing. We are grateful for the comments of the two anonymous reviewers, which helped to improve the manuscript.

References

Balmaseda, M. A., Mogensen, K. and Weaver, A. T. 2013. Evaluation of the ECMWF ocean reanalysis system ORAS4. *Q. J. Roy. Meteorol. Soc.* **139**, 1132–1161. DOI: http://dx.doi.org/10.1002/qj.2063

Barstad, I., Sorteberg, A. and dos-Santos Mesquita, M. 2012. Present and future offshore wind power potential in Northern Europe based on downscaled global climate runs with adjusted SST and sea ice cover. *Renewable Energy* **44**, 398–405.

Cannon, D. J., Brayshaw, D. J., Methven, J., Coker, P. J. and Lenaghan, D. 2015. Using reanalysis data to quantify extreme wind power generation statistics: a 33 year case study in Great Britain. *Renewable Energy* **75**, 767–778. DOI: http://dx.doi.org/10.1016/j.renene.2014.10.024

Dee, D. P., Uppala, S. M., Simmons, A. J., Berrisford, P., Poli, P. and co-authors. 2011. The ERA-Interim reanalysis: configuration and performance of the data assimilation system. *Q. J. Roy. Meteorol. Soc.* **137**, 553–597. DOI: http://dx.doi.org/10.1002/qj.828

Doblas-Reyes, F. J., Andreu-Burillo, I., Chikamoto, Y., Garcia-Serrano, J., Guemas, V. and co-authors. 2013. Initialized near-term regional climate change prediction. *Nat. Commun.* **4**, 1715. DOI: http://dx.doi.org/10.1038/ncomms2704

Drew, D. R., Cannon, D. J., Brayshaw, D. J., Barlow, J. F. and Coker, P. J. 2015. The impact of future offshore wind farms on wind power generation in Great Britain. *Resour. Policy* **4**, 155–171. DOI: http://dx.doi.org/10.3390/resources4010155

Eade, R., Smith, D., Scaife, A., Wallace, E., Dunstone, N. and co-authors. 2014. Do seasonal-to-decadal climate predictions underestimate the predictability of the real world? *Geophys. Res. Lett.* **41**, 5620–5628. DOI: http://dx.doi.org/10.1002/2014GL061146

Ferro, C. A. T. 2007. Comparing probabilistic forecasting systems with the brier score. *Weather Forecast.* **22**, 1076–1088. DOI: http://dx.doi.org/10.1175/WAF1034.1

Ferro, C. A. T. 2014. Fair scores for ensemble forecasts. *Q. J. Roy. Meteorol. Soc.* **140**, 1917–1923. DOI: http://dx.doi.org/10.1002/qj.2270

Fuentes, U. and Heimann, D. 2000. An improved statistical-dynamical downscaling scheme and its application to the Alpine

precipitation climatology. *Theor. Appl. Climatol.* **65**, 119–135. DOI: http://dx.doi.org/10.1007/s007040070038

General Electric. 2010. 2.5 MW wind turbine series GEA17007B. Online at: http://site.ge-energy.com/prod_serv/products/wind_turbines/en/downloads/GEA17007A-Wind25Brochure.pdf

Giorgetta, M. A., Jungclaus, J., Reick, C. H., Legutke, S., Bader, J. and co-authors. 2013. Climate and carbon cycle changes from 1850 to 2100 in MPI-ESM simulations for the coupled model intercomparison project phase 5. *J. Adv. Model. Earth Syst.* **5**, 572–597. DOI: http://dx.doi.org/10.1002/jame.20038

Giorgi, F., Jones, C. and Asrar, G. R. 2006. Addressing climate information needs at the regional level: the CORDEX framework. *Bull. World Meteorol. Organ.* **58**, 175–183.

Goddard, L., Kumar, A., Solomon, A., Smith, D., Boer, G. and co-authors. 2013. A verification framework for interannual-to-decadal prediction experiments. *Clim. Dyn.* **40**, 245–272. DOI: http://dx.doi.org/10.1007/s00382-012-1481-2

Haas, R. and Pinto, J. G. 2012. A combined statistical and dynamical approach for downscaling large-scale footprints of European windstorms. *Geophys. Res. Lett.* **39**, L23804. DOI: http://dx.doi.org/10.1029/2012GL054014

Haas, R., Reyers, M. and Pinto, J. G. 2015. Decadal predictability of regional-scale peak winds over Europe using the Earth System Model of the Max-Planck-Institute for Meteorology. *Meteorol. Z.* DOI: http://dx.doi.org/10.1127/metz/2015/0583 (in press).

Hueging, H., Born, K., Haas, R., Jacob, D. and Pinto, J. G. 2013. Regional changes in wind energy potential over Europe using regional climate model ensemble projections. *J. Appl. Meteorol. Climatol.* **52**, 903–917.

Ilyina, T., Six, K. D., Segschneider, J., Maier-Reimer, E., Li, H. and Núnez-Riboni, I. 2013. Global ocean biogeochemistry model HAMOCC: model architecture and performance as component of the MPI-Earth system model in different CMIP5 experimental realizations. *J. Adv. Model. Earth Syst.* **5**, 287–315. DOI: http://dx.doi.org/10.1029/2012MS000178

International CLIVAR Project Office (ICPO). 2011. *Data and Bias Correction for Decadal Climate Predictions*. Online at: http://www.wrcp-climate.org/decadal/references/DCPP_Bias_Correction.pdf, compiled by CMIP-WGCM-WGSIP Decadal Climate Prediction Panel.

IPCC. 2012. Managing the risks of extreme events and disasters to advance climate change adaptation. In: *A Special Report of Working Groups I and II of the Intergovernmental Panel on Climate Change* (eds. C. B. Field, V. Barros, T. F. Stocker, D. Qin, D. J. Dokken, K. L. Ebi, M. D. Mastrandrea, K. J. Mach, G.-K. Plattner, S. K. Allen, M. Tignor and P. M. Midgley). Cambridge University Press, Cambridge, 582 pp.

Jones, P. D., Hulme, M. and Briffa, K. R. 1993. A comparison of lamb circulation types with an objective classification scheme. *Int. J. Climatol.* **13**, 655–663.

Jungclaus, J. H., Fischer, N., Haak, H., Lohmann, K., Marotzke, J. and co-authors. 2013. Characteristics of the ocean simulations in the Max Planck Institute Ocean Model (MPIOM) the ocean component of the MPI-Earth system model. *J. Adv. Model. Earth Syst.* **5**, 422–446. DOI: http://dx.doi.org/10.1002/jame.20023

Kharin, V. V., Boer, G. J., Merryfield, W. J., Scinocca, J. F. and Lee, W. S. 2012. Statistical adjustment of decadal predictions in a changing climate. *Geophys. Res. Lett.* **39**, L19705. DOI: http://dx.doi.org/10.1029/2012GL052647

Köhl, A. 2015. Evaluation of the GECCO2 ocean synthesis: transports of volume, heat and freshwater in the Atlantic. *Q. J. Roy. Meteor. Soc.* **141**, 166–181. DOI: http://dx.doi.org/10.1002/qj.2347

Kruschke, T., Rust, H. W., Kadow, C., Leckebusch, G. C. and Ulbrich, U. 2014. Evaluating decadal predictions of northern hemispheric cyclone frequencies. *Tellus A* **66**, 22830. DOI: http://dx.doi.org/10.3402/tellusa.v66.22830

Kruschke, T., Rust, H. W., Kadow, C., Müller, W. A., Pohlmann, H. and co-authors. 2015. Probabilistic evaluation of decadal predictions of Northern Hemisphere winter storms. *Meteorol. Z.* DOI: http://dx.doi.org/10.1127/metz/2015/0641

Marotzke, J., Müller, W. A., Vamborg, F. S. E., Becker, B., Cubasch, U. and co-authors. Submitted. MiKlip – a national research project on decadal climate prediction. *Bull. Am. Meteorol. Soc.*

Meehl, G. A., Goddard, L., Boer, G., Burgman, R., Branstator, G. and co-authors. 2014. Decadal climate prediction: an update from the trenches. *Bull. Am. Meteorol. Soc.* **95**, 243–267. DOI: http://dx.doi.org/10.1175/BAMS-D-12-00241.1

Meehl, G. A., Goddard, L., Murphy, J., Stouffer, R. J., Boer, G. and co-authors. 2009. Decadal Prediction – Can it be skilful? *Bull. Amer. Meteor. Soc.* **90**, 1467–1485. DOI: http://dx.doi.org/10.1175/2009BAMS2778.1

Mieruch, S., Feldmann, H., Schädler, G., Lenz, C.-J., Kothe, S. and co-authors. 2014. The regional MiKlip decadal forecast ensemble for Europe: the added value of downscaling. *Geosci. Model. Dev.* **7**, 2983–2999. DOI: http://dx.doi.org/10.5194/gmd-7-2983-2014

Moccia, J., Wilkes, J., Pineda, I. and Corbetta, G. 2014. Wind energy scenarios for 2020. European Wind Energy Association Report, EWEA, 3p. Online at: http://www.ewea.org/fileadmin/files/library/publications/reports/EWEA-Wind-energy-scenarios-2020.pdf

Müller, W. A., Baehr, J., Haak, H., Jungclaus, J. H., Kröger, J. and co-authors. 2012. Forecast skill of multi-year seasonal means in the decadal prediction system of the Max Planck Institute for Meteorology. *Geophys. Res. Lett.* **39**, L22707. DOI: http://dx.doi.org/10.1029/2012GL053326

Müller, W. A., Pohlmann, H., Sienz, F. and Smith, D. 2014. Decadal climate predictions for the period 1901–2010 with a coupled climate model. *Geophys. Res. Lett.* **41**, 2100–2107. DOI: http://dx.doi.org/10.1002/2014GL059259

Najac, J., Lac, C. and Terray, L. 2011. Impact of climate change on surface winds in France using a statistical-dynamical downscaling method with mesoscale modelling. *Int. J. Climatol.* **31**, 415–430.

Pineda, I., Azau, S., Moccia, J. and Wilkes, J. 2014. Wind in power – 2013 European statistics. European Wind Energy Association Report, EWEA, 3p. Online at: http://www.ewea.org/fileadmin/files/library/publications/statistics/EWEA_Annual_Statistics_2013.pdf (accessed 12 February 2015).

Pinto, J. G., Neuhaus, C. P., Leckebusch, G. C., Reyers, M. and Kerschgens, M. 2010. Estimation of wind storm impacts over Western Germany under future climate conditions using a statistical-dynamical downscaling approach. *Tellus A* **62**, 188–201. DOI: http://dx.doi.org/10.1111/j.1600-0870.2009.00424.x

Pohlmann, H., Müller, W. A., Kulkarni, K., Kameswarrao, M., Matei, D. and co-authors. 2013. Improved forecast skill in the tropics in the new MiKlip decadal climate predictions. *Geophys. Res. Lett.* **40**, 5798–5802. DOI: http://dx.doi.org/10.1002/2013GL058051

Pryor, S. C. and Barthelmie, R. J. 2010. Climate change impacts on wind energy: a review. *Renew. Sustain. Energy Rev.* **14**, 430–437. DOI: http://dx.doi.org/10.1016/j.rser.2009.07.028

Pryor, S. C., Barthelmie, R. J., Claussen, N. E., Drews, M., MacKellar, N. and co-authors. 2012. Analyses of possible changes in intense and extreme wind speeds over Northern Europe under climate change scenarios. *Clim. Dyn.* **38**, 189–208. DOI: http://dx.doi.org/10.1007/s00382-010-0955-3

Pryor, S. C., Schoof, J. T. and Barthelmie, R. J. 2005. Climate change impacts on wind speeds and wind energy density in Northern Europe: empirical downscaling of multiple AOGCMs. *Clim. Res.* **29**, 183–198.

Raddatz, T. J., Reick, C. H., Knorr, W., Kattge, J., Roeckner, E. and co-authors. 2007. Will the tropical land biosphere dominate the climate-carbon cycle feedback during the twenty-first century? *Clim. Dyn.* **29**, 565–574.

Reyers, M., Moemken, J. and Pinto, J. G. 2016. Future changes of wind energy potentials over Europe in a large CMIP5 multi-model ensemble. *Int. J. Climatol.* **36**, 783–796. DOI: http://dx.doi.org/10.1002/joc.4382

Reyers, M., Pinto, J. G. and Moemken, J. 2015. Statistical-dynamical downscaling for wind energy potentials: evaluation and applications to decadal hindcasts and climate change projections. *Int. J. Climatol.* **35**, 229–244. DOI: http://dx.doi.org/10.1002/joc.3075

Rockel, B., Will, A. and Hense, A. 2008. Special issue: regional climate modelling with COSMO-CLM (CCLM). *Meteorol. Z.* **17**, 347–348.

Sillmann, J. and Croci-Maspoli, M. 2009. Present and future atmospheric blocking and its impact on European mean and extreme climate. *Geophys. Res. Lett.* **36**, L10702. DOI: http://dx.doi.org/10.1029/2009GL038259

Smith, D. M., Cusack, S., Colman, A., Folland, C., Harris, G. and co-authors. 2007. Improved surface temperature prediction for the coming decade from a global circulation model. *Science* **317**, 796–799.

Solomon, A., Goddard, L., Kumar, A., Carton, J., Deser, C. and co-authors. 2011. Distinguishing the roles of natural and anthropogenically forced decadal climate variability implications for predictions. *Bull. Am. Meteorol. Soc.* **92**, 141–156. DOI: http://dx.doi.org/10.1175/2010BAMS2962.1

Solomon, S., Qin, D., Manning, M., Chen, Z., Marquis, M and co-authors (eds.). 2007. *Climate Change 2007: The Physical Science Basis*. Cambridge University Press, Cambridge, 996 p.

Stevens, B., Giorgetta, M., Esch, M., Mauritsen, T., Crueger, T. and co-authors. 2013. Atmospheric component of the MPI-M Earth System Model: ECHAM6. *J. Adv. Model. Earth Syst.* **5**, 146–172.

Taylor, K. E., Stouffer, R. J. and Meehl, G. A. 2012. An overview of CMIP5 and the experiment design. *Bull. Am. Meteorol. Soc.* **93**, 485–498. DOI: http://dx.doi.org/10.1175/BAMS-D-11-00094.1

Tobin, I., Vautard, R., Balog, I., Bréon, F. M., Jerez, S. and co-authors. 2014. Assessing climate change impacts on European wind energy from ENSEMBLES high-resolution climate projections. *Clim. Change* **128**, 99–112. DOI: http://dx.doi.org/10.1007/s10584-014-1291-0

Uppala, S. M., Kallberg, P. W., Simmons, A. J., Andrae, U., da Costa Bechthold, V. and co-authors. 2005. The ERA-40 re-analysis. *Q. J. Roy. Meteor. Soc.* **131**, 2961–3012. DOI: http://dx.doi.org/10.1256/qj.04.176

Valcke, S., Claubel, A., Declat, D. and Terray, L. 2003. *OASIS Ocean Atmosphere Seas Ice Soil User's Guide*. Technical Report. TR/CMGC/03/69, CERFACS, Toulouse, p. 85.

Van Oldenborgh, G. J., Doblas-Reyes, F. J., Wouters, B. and Hazeleger, W. 2012. Decadal prediction skill in a multi-model ensemble. *Clim. Dyn.* **38**, 1263–1280. DOI: http://dx.doi.org/10.1007/s00382-012-1313-4

Weigel, A. P., Liniger, M. A. and Appenzeller, C. 2009. Seasonal ensemble forecast: are recalibrated single models better than multi-models? *Mon. Wea. Rev.* **137**, 1460–1479.

Wilks, D. S. 2011. *Statistical Methods in the Atmospheric Sciences*. 3rd ed. Academic Press, Oxford; Waltham, MA.

Supplementary Material

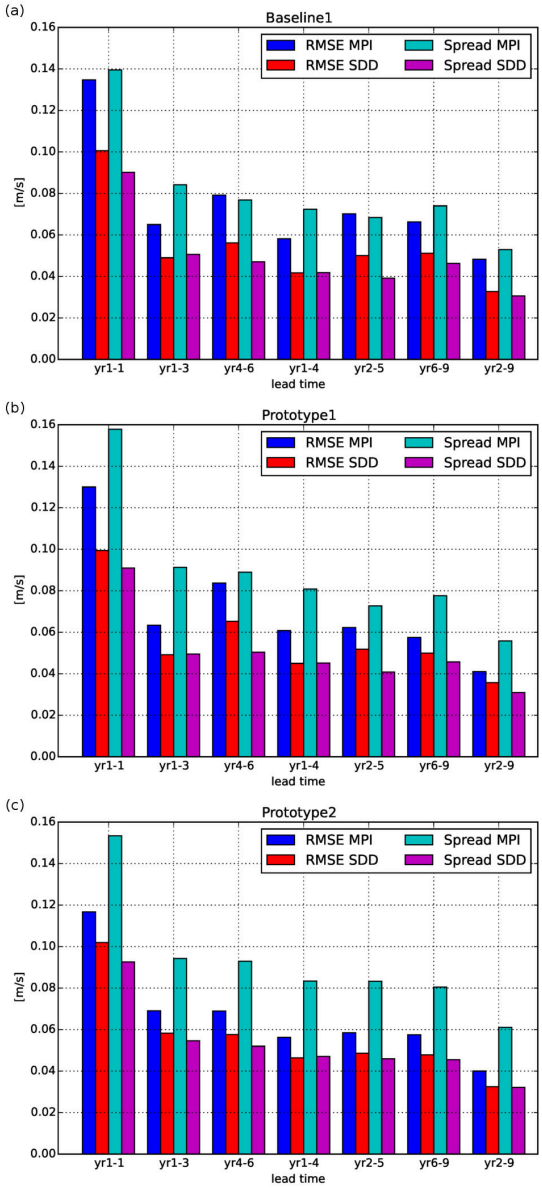

Fig.S 1: (a) RMSE and ensemble spread (components of reliability, see Eq. (5)) for large-scale MPI-ESM mean wind (blue and cyan coloured bars) and SDD simulated regional mean wind (red and magenta coloured bars) for seven different lead times for the whole year, averaged over Germany (box 2 in Fig. 1d), for the baseline1 ensemble. (b) as (a), but for the prototype1 ensemble. (c) as (a), but for the prototype2 ensemble.

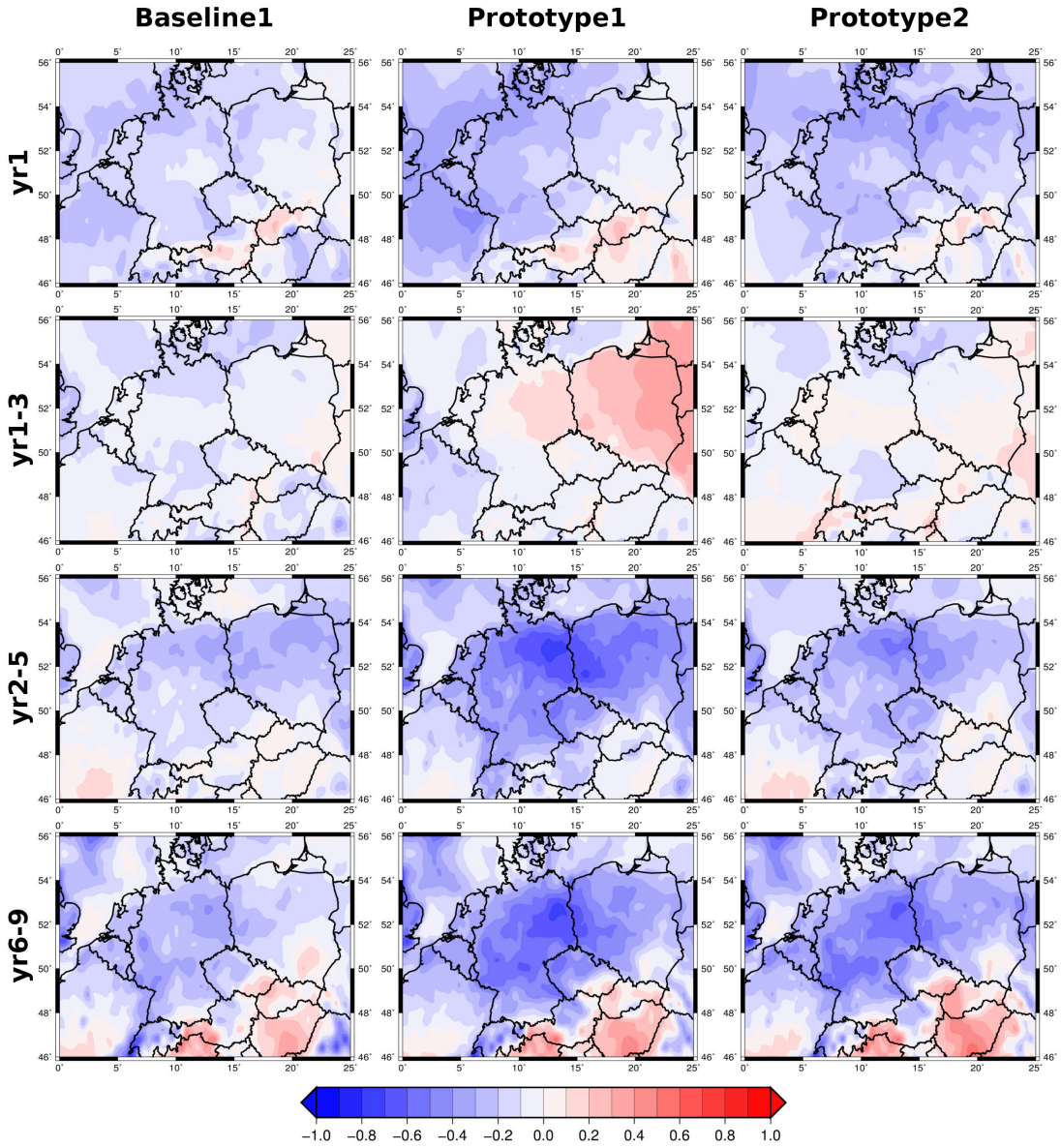

Fig.S 2: MSESS for SDD simulated *Eout* for four exemplary lead times for the winter months DJF (dec1978-dec2000) for the ensemble generations baseline1 (left column), prototype1 (middle column) and prototype2 (right column). Note that yr1 corresponds to months 12 to 14 after initialisation. Reference forecast is the ensemble mean of the uninitialised historical runs.

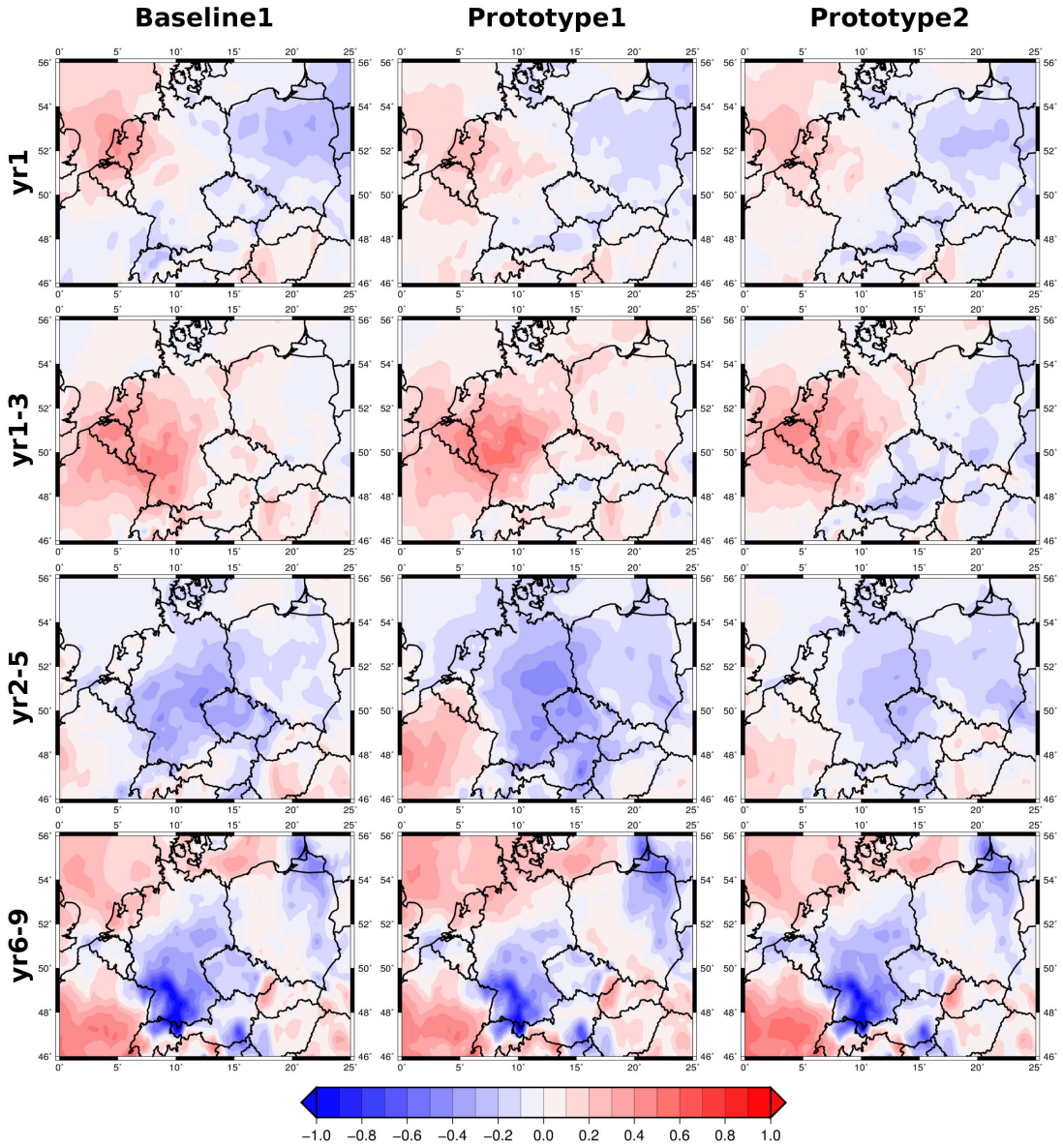

Fig.S 3: MSESS for SDD simulated *Eout* for four exemplary lead times for the spring months MAM (dec1978-dec2000) for the ensemble generations baseline1 (left column), prototype1 (middle column) and prototype2 (right column). Reference forecast is the ensemble mean of the uninitialised historical runs.

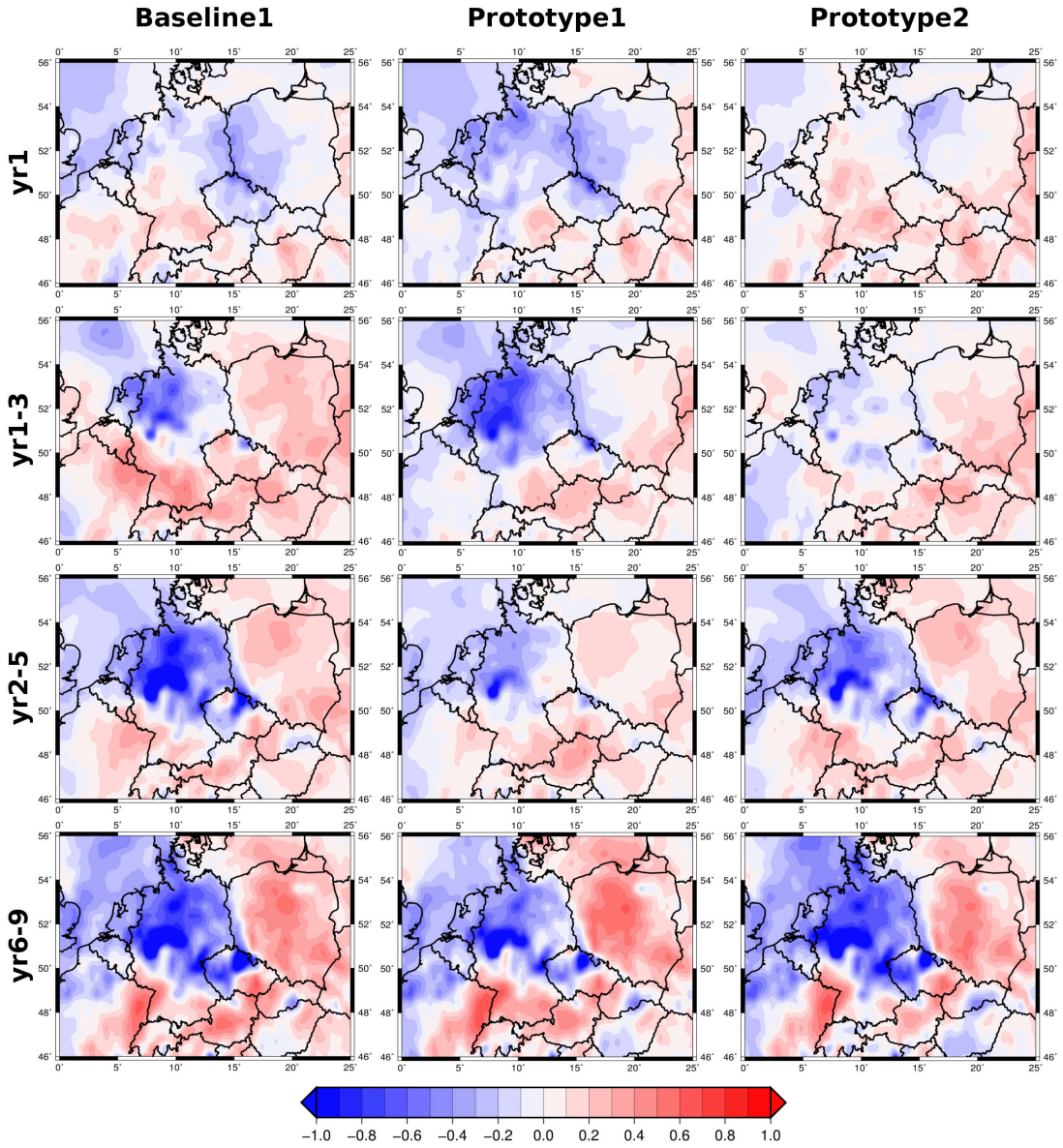

Fig.S 4: MSESS for SDD simulated *Eout* for four exemplary lead times for the summer months JJA (dec1978-dec2000) for the ensemble generations baseline1 (left column), prototype1 (middle column) and prototype2 (right column). Reference forecast is the ensemble mean of the uninitialised historical runs.

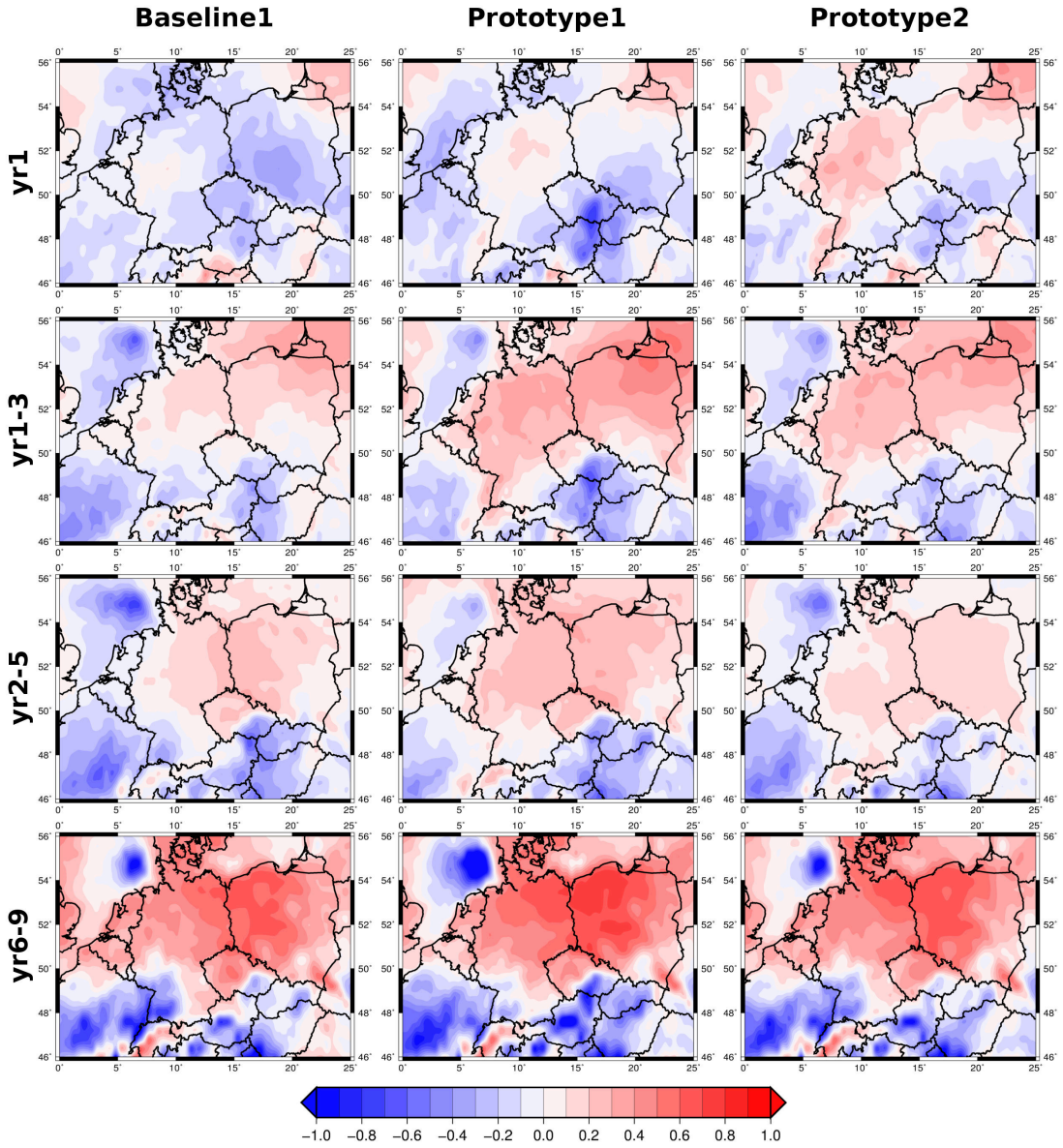

Fig.S 5: MSESS for SDD simulated *Eout* for four exemplary lead times for the autumn months SON (dec1978-dec2000) for the ensemble generations baseline1 (left column), prototype1 (middle column) and prototype2 (right column). Reference forecast is the ensemble mean of the uninitialised historical runs.

8 Development and prospects of the regional MiKlip decadal prediction system over Europe: Predictive skill, added value of regionalization and ensemble size dependency

The previous study (chapter 7) dealing with the decadal predictability of regional scale wind energy potentials represents a specialised application of decadal climate predictions. In the framework of the German MiKlip project, focus is also given to the decadal predictability of primary meteorological parameters like temperature, precipitation and wind speed both on the global and on the regional scale. Within this context, a regional decadal prediction system for Europe is developed, based on dynamical downscaling. Reyers et al. (2017) analysed the current state and the prospects of this regional prediction system. The used data and the main results from this study are presented here (see Appendix for full publication).

Reyers et al. (2017) examined two ensemble generations (baseline0, baseline1) of the regional component of the MiKlip decadal prediction system over Europe. The two generations consist of 10-member hindcast ensembles computed with the global coupled model MPI-ESM-LR. The hindcasts are dynamically downscaled with CCLM to a horizontal grid resolution of 0.22°. The decadal forecast skill is investigated for regional scale tempera-

ture, precipitation and wind speed for lead years 1-5 after initialisation focussing on the eight European PRUDENCE regions. Skill scores are computed by using an ERA-Interim driven CCLM simulation and E-OBS as verification datasets, and uninitialised historical runs as reference dataset. Additionally, the added value of regionalisation is examined by comparing the regional results to the forecast skill of the global ensemble.

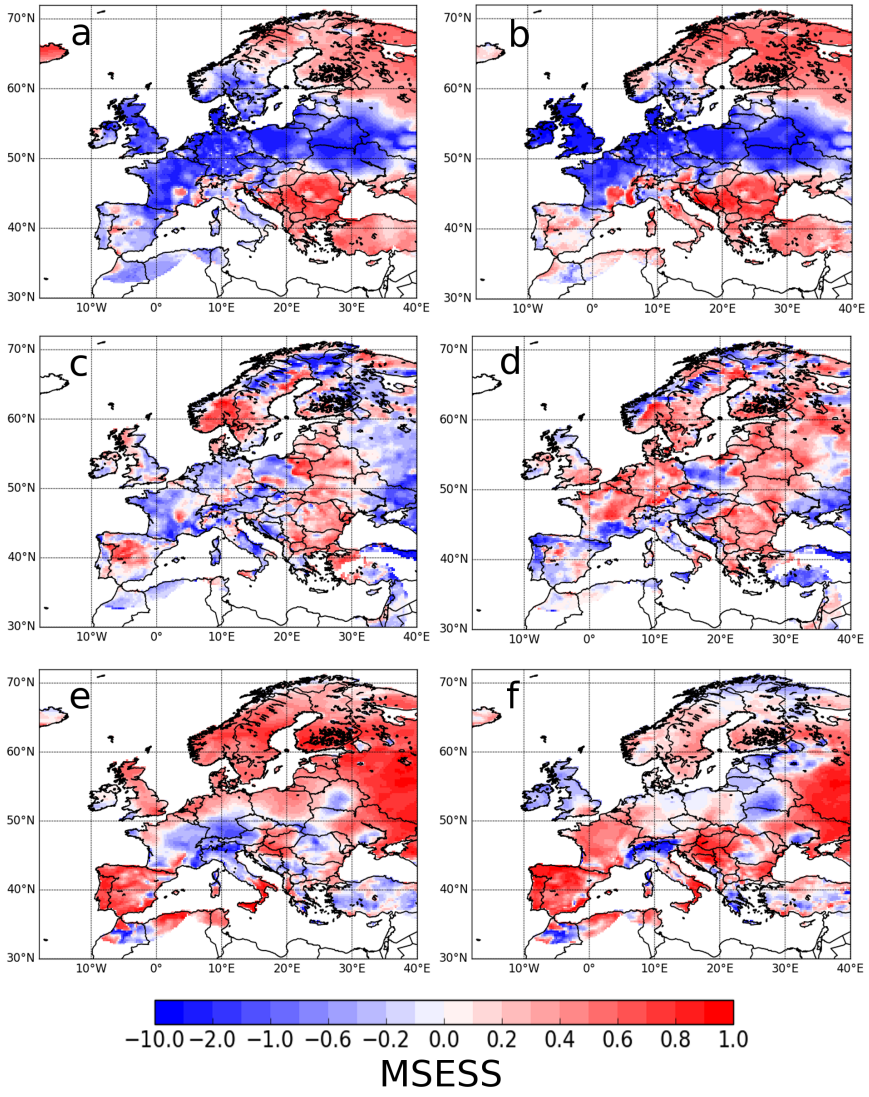

Fig. 8.1: Spatial distribution of the MSE-based skill score (MSESS) for the multi-annual mean of lead years 1-5 for (a) temperature in the downscaled baseline0 ensemble, (b) temperature in the downscaled baseline1 ensemble, (c) precipitation in baseline0, (d) precipitation in baseline1, (e) wind speed in baseline0, and (f) wind speed in baseline1. Source: Reyers et al. (2017), Figure 2 (revised version).

Both ensemble generations show some potential for skilful decadal predictions of regional scale temperature, precipitation and wind speed over Europe. However, the forecast skill depends on the variable, region and hindcast generation (Figure 8.1). For example, the two generations agree well for temperature skill scores over Scandinavia and the Mediterranean (positive skill), as well as the British Isles and Central Europe (negative skill), while deviations are largest for Iberia, Italy and parts of France (Figure 8.1a, b). For precipitation and wind speed, differences between the ensemble generations are generally larger. The improvement of the initialisation from the baseline0 generation to baseline1 increases the predictive skill for some regions, e.g. Mediterranean and Scandinavia for temperature, and Mid-Europe and France for precipitation. For wind speed, there is no systematic improvement detectable.

Compared to the forecast skill of the global model, the regionalisation may provide an added value for decadal predictions. This added value is especially evident for regions with complex topography, but it depends on the variable and the used skill metrics. For instance, the regional downscaling improves the accuracy and reliability for temperature over the British Isles, Scandinavia and the Mediterranean, and for precipitation over the British Isles, Scandinavia, France and Mid-Europe in the baseline1 ensemble (not shown).

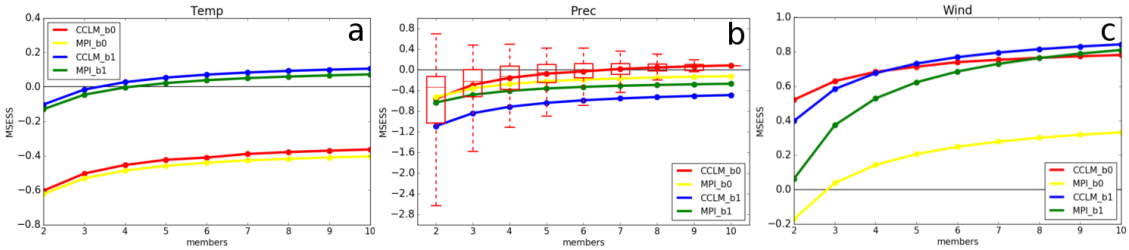

Fig. 8.2: Skill scores for the multi-annual mean of lead years 1-5 of the regional basline0 (red), the global baseline0 (yellow), the regional baseline1 (blue), and the global baseline1 (green) ensembles depending on the ensemble size (ranging from 2 to 10 members, x-axis) for PRUDENCE region IP (Iberian Peninsula). MSESS for (a) temperature, (b) precipitation, and (c) wind speed. Source: Reyers et al. (2017), Figure 6 (revised version).

For all variables and regions, skill scores increase with a stepwise increased ensemble size (as exemplarily shown for the Iberian Peninsula in Figure 8.2). In some cases, skill scores even shift from negative to positive values. A number of 10 ensemble members is identified to be suitable for both global and regional decadal predictions. These results indicate that larger ensemble sizes are beneficial for decadal prediction systems, either through an increase of forecast skill and reliability or through a reduction of bias and uncertainty.

Reyers et al. (2017) concluded that a decadal prediction system would profit from a regional component. The presented results are promising for the development of a regional decadal prediction system for Europe. Additionally, they are relevant for further investigations of wind energy potentials over Europe, which could e.g. focus on inter-daily variability. The identified skill scores for wind speed are comparable to skill scores for *Eout* as identified by Moemken et al. (2016, chapter 7), while predictive skill is lower for temperature and precipitation compared to *Eout*.

9 Summary and discussion

"Limiting climate change will require substantial and sustained reductions of greenhouse gas emissions" (IPCC, 2013).

Currently, the energy supply sector is one of the largest contributors to global greenhouse gas emissions affecting the earth's climate (Bruckner et al., 2014). Therefore the mitigation of climate change requires the transition from a fossil fuel-driven energy system to one with a higher share of renewable energy sources. For Europe, wind energy production shows a large potential, since it is already highly developed and comparatively cheap to run. However, wind energy generation depends on weather and climate conditions (e.g. Pryor and Barthelmie, 2010, 2013) and thus is affected by climate change itself.
In this thesis, different aspects of European wind speeds and wind energy potentials at the regional scale and the potential impact of climate change are analysed. With this aim a uniquely large ensemble of GCMs and GCM-RCM chains is used, considering different downscaling approaches and different timescales. The results are summarised in three scientific publications, focussing on

1. Future changes of wind energy potentials in a statistical-dynamically downscaled CMIP5 multi-model ensemble.

2. Future changes of wind speeds and wind energy potentials in a dynamically downscaled ensemble conducted as part of EURO-CORDEX.

3. The decadal predictability of wind speed and wind energy potentials over Central Europe in a statistical-dynamically downscaled decadal prediction system.

The results aim to improve our understanding of the impact of different model ensembles and different downscaling approaches on the estimation of future wind energy potentials. Additionally, they may help to adjust the planning strategies to optimize the energy system towards climate change adaptation. In the following, the main results of the publications

are summarised in more detail. Afterwards, the results are discussed and an outlook is presented.

9.1 Paper I

Reyers et al. (2016, chapter 4) analysed future changes of regional wind energy output of an exemplary wind turbine. An ensemble of 22 GCMs from CMIP5 is regionalised for Europe using a statistical-dynamical downscaling approach (see chapter 3). Climate change signals are computed for the near future decades (2021-2060) and the end of the 21st century (2061-2100) following the two emission scenarios RCP4.5 and RCP8.5. The paper gives an overview on the ensemble mean changes and quantifies the uncertainties between the individual ensemble members.

The evaluation of the historical runs compared to ERA-Interim reveals an overestimation of westerly weather types over Europe in most CMIP5 models, which is in particular evident for weather classes with strong pressure gradients. In general, the overestimation of westerly weather types results in an overestimation of *Eout* for most parts of Europe in the ensemble mean. The intra-annual variability of *Eout* (difference of winter *Eout* minus summer *Eout*) in the historical CMIP5 ensemble agrees well to ERA-Interim.

The ensemble mean projects an increase of mean annual *Eout* over Northern and Central Europe and a decrease for the Mediterranean region in future decades. In general, signals are more pronounced for the RCP8.5 scenario and the end of the century. For 2061-2100, more than 15 models agree on the sign of change for large parts of Europe. However, responses can strongly differ between the individual ensemble members, not only in terms of magnitude but also in the sign of change. This results in low signal-to-noise ratios for nearly the entire European sector. In seasonal terms, future changes are more robust, especially for the end of the 21st century. For most parts of Europe, increasing *Eout* is simulated for winter, while a decrease is likely for the summer months. These changes result in an increase of the intra-annual variability of *Eout*, which in turn leads to a higher irregularity of wind energy production and could impede a future wind-driven energy system. The climate change signals for the inter-annual variability of *Eout* reveal a high uncertainty between the individual ensemble members. This makes it impossible to conclude whether a changing climate also affects the reliability of wind energy production in future decades.

To summarize, the results from Reyers et al. (2016) clearly reveal a connection between a changing climate and the European wind energy potential under future climate condi-

tions. However, the results show quite wide-ranged future changes between the individual models, with partly large differences from the ensemble mean. This highlights the strong dependency of climate change signals on the choice of GCM and thus the need to consider large ensembles. While the ensemble mean increase of wind energy output over Northern and Central Europe is generally consistent with other recent studies dealing with future changes of wind energy potentials (e.g. Cradden et al., 2012; Nolan et al., 2012, 2014; Hueging et al., 2013; Tobin et al., 2015), some ensemble members simulate a decrease over Northern Europe, which is in line with Pryor et al. (2005b). These findings emphasise the importance to consider multi-model-ensembles as well as different downscaling approaches for impact studies on wind energy.

9.2 Paper II

Moemken et al. (2018, chapter 5) investigated future changes of wind speed and wind energy output in an ensemble conducted within the framework of EURO-CORDEX. Five (respective four) GCMs from CMIP5 are dynamically downscaled with two RCMs, resulting in an ensemble of nine GCM-RCM model chains. Potential future changes are estimated for the near future (2021-2050) and the end of the 21st century (2071-2100) using the two climate change scenarios RCP4.5 and RCP8.5. All analyses are based on three-hourly 10m-wind speeds at 12 km spatial resolution. This high temporal resolution allows insights on several timescales (from annual to sub-daily) and can be used to address stakeholder needs. Results focus on the ensemble mean responses of the two RCMs, but also consider the differences between the individual ensemble members.

The historical EURO-CORDEX runs show substantial biases in 10m-wind velocities when compared to ERA-Interim driven evaluation runs of the same RCMs, both in terms of climatology and intra-annual variability. These biases result from the driving GCMs and the RCMs, but differences between the individual GCMs are larger than those between the RCMs. Since these biases may influence the climate change signals especially when considering wind speed thresholds relevant for wind energy generation, a bias correction based on probability mapping is performed before computing future projections.

The RCM ensemble means project a small decrease of mean annual *Eout* for most of Europe in future decades. Increasing *Eout* is only simulated for the Baltic and the Aegean Sea. In these regions, the climate change signals are relatively robust, while the ensemble spread can be quite large for Central Europe and Scandinavia. Climate change signals are generally more pronounced for the end of the 21st century and in the RCP8.5 scenario. For winter,

an increase of *Eout* is depicted for Western and Central Europe, while *Eout* is projected to decrease for the Mediterranean region. For summer, a decline is simulated for most parts of Europe, especially for Central Europe. As for annual *Eout*, differences between the individual ensemble members are large for Central and parts of Eastern Europe, while the agreement is good for the Baltic and the Aegean Sea. In general, the models agree better for the summer months. The seasonal changes cause an increase of intra-annual variability of *Eout* for Northern, Central and Eastern Europe in the ensemble mean. In addition, a higher inter-daily variability is projected for these regions resulting in an overall higher volatility of wind energy production in future decades. The signals are quite robust for inter-daily variability, while the ensemble spread is rather large for intra-annual variability. No clear future trends are found for the inter-annual variability, revealing a high uncertainty between the individual ensemble members. In terms of specific wind speed characteristics relevant for wind energy production, the RCM ensembles agree on a higher occurrence of low wind speeds at hub height (100m) under future climate conditions for large parts of Europe except the Baltic Sea.

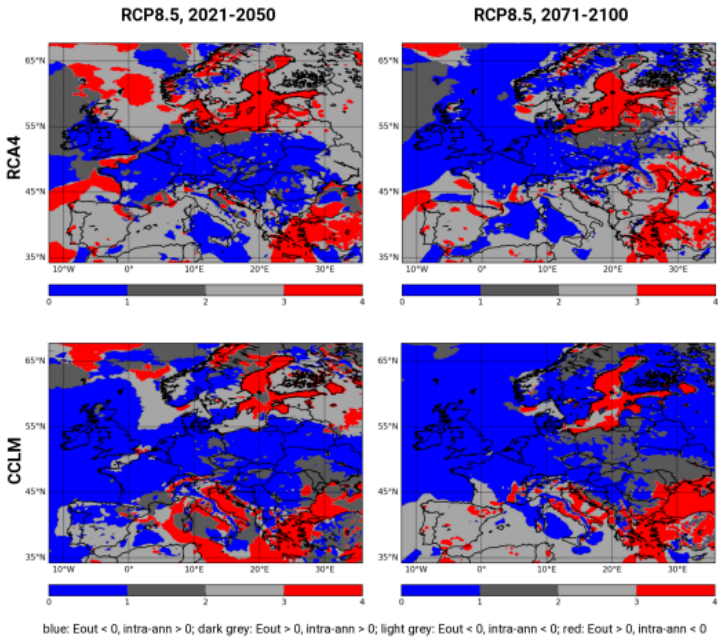

Fig. 9.1: Combined changes of mean annual *Eout* and intra-annual variability of *Eout* for the ensemble mean of RCA4 (top) and CCLM (bottom) for RCP8.5 2021-2050 (left) and 2071-2100 (right). Blue: decreasing *Eout* and increasing intra-annual variability. Dark grey: increasing *Eout* and increasing variability. Light grey: decreasing *Eout* and decreasing variability. Red: increasing *Eout* and decreasing variability.

Thus, Moemken et al. (2018) identified a clear impact of climate change on future wind energy potentials over Europe. In some regions like the Baltic and the Aegean Sea (red areas in Figure 9.1), the wind energy sector could profit from climate change due to an increase of mean *Eout* and a simultaneous decrease in variability. In other areas like France, Germany or the British Isles (blue areas in Figure 9.1), impacts are mostly negative due to decreasing mean *Eout* and higher seasonal variability. The identified climate change signals are comparable to other studies investigating EURO-CORDEX simulations (e.g. Tobin et al., 2016), but generally weaker compared to some studies analysing different model ensembles (Hueging et al., 2013; Reyers et al., 2016). These differences can be attributed to the choice of GCM as well as the downscaling approach (see also section 9.4).

9.3 Paper III

Moemken et al. (2016, chapter 7) applied the statistical-dynamical downscaling approach introduced in chapter 3 to three ensemble generations of the MiKlip decadal prediction system (baseline1, prototype1, protoype2). This system is based on the global Max-Planck-Institute Earth System Model (MPI-ESM). The three generations differ in their ocean initialisation, while they share the same atmosphere initialisation. The decadal forecast skill of regional wind speed and wind energy output over Central Europe is investigated for several lead times using different skill metrics. Skill scores are computed by using uninitialised historical and yearly-initialised hindcast experiments. In addition, the added value of regionalisation is evaluated by comparing skill scores for large-scale wind speeds simulated by MPI-ESM and SDD-simulated regional wind speeds.

The three ensemble generations show some decadal forecast skill for annual wind speeds and *Eout* over Central Europe. This skill is mostly limited to the first years after initialisation (short lead times). Highest values are depicted for yr1-3 and over North-western Germany and the Benelux countries. For seasonal *Eout*, skill scores are generally lower than for annual means. Forecast skill persists longest in autumn and is lowest in the summer months. In general, differences between the three ensemble generations are small, showing no systematic improvement from baseline1 to the prototype generations. Only for yr1-3, prototype1 slightly outperforms the other two generations. The decadal forecast skill for regional *Eout* shows a strong dependence on the representation of westerly weather types in the MPI-ESM. In particular, a dominant westerly weather type with strong pressure gradients over Central Europe is identified as potential source for this skill, showing similar MSE-based skill scores as *Eout* for almost all lead times. This implies, that predictive skill

can be found for regional wind speeds and *Eout*, if the occurrence of westerly weather types is captured well by the global hindcasts. The downscaling of the global hindcasts is able to preserve and sometimes even increase the forecast skill. Also the ensemble spread is often improved by the regionalisation. However, the added value depends on lead times and the ensemble generation.
The results from Moemken et al. (2016) are promising regarding the establishment of a decadal prediction system for wind energy applications for Central Europe. They show a clear potential for forecasts of regional wind speed and regional *Eout* up to several years ahead. In line with e.g. Haas et al. (2016), the decadal forecast skill seems to arise mainly from the initialisation of the prediction system.

9.4 Discussion and outlook

The three publications, which form the core of this thesis, are connected with each other either through the analysed datasets or the applied downscaling approach (see Figure 9.2). The first paper analyses a statistical-dynamically downscaled multi-model ensemble from CMIP5. Paper II is also based on a CMIP5 ensemble, but this one is regionalised with a dynamical downscaling approach in the framework of EURO-CORDEX. Paper III uses the same SDD approach as Paper I to investigate the decadal predictability of wind energy potentials. These connections enable a comparison of the different downscaling techniques and their applicability to different datasets regarding wind energy potentials over Europe. In addition, the impact of different model ensembles and different downscaling approaches on future wind energy potentials can be analysed.

	Statistical-dynamical downscaling	Dynamical downscaling
Climate change projections	Paper I	Paper II
Decadal climate predictions	Paper III	Future work

Fig. 9.2: Schematic illustration of the connection between the individual parts of this thesis.

Paper I and Paper II both reveal a clear impact of climate change on wind energy potentials over Europe under future climate conditions. However, the projected future changes in the

two studies can show some discrepancies. In general, climate change signals identified in Moemken et al. (2018, Paper II) for the EURO-CORDEX ensemble are weaker compared to the signals in Reyers et al. (2016, Paper I) for the CMIP5 ensemble. Moreover, for mean annual *Eout* the ensemble mean changes have different signs of change for Northern and Central Europe, with decreasing *Eout* in Moemken et al. (2018) and increasing *Eout* in Reyers et al. (2016). These differences seem to emerge mainly from the choice of GCM and the different ensemble sizes. The five GCMs used in Moemken et al. (2018) belong to the models with the weakest signals from the 22-member ensemble in Reyers et al. (2016). When comparing the climate change signals from the common five models directly (Figure 9.3), differences are rather small. The individual ensemble members agree well in terms of the spatial pattern and the magnitude of change for most parts of Europe. The small differences arise primarily from the different downscaling methods and from the different analysed time periods. Reyers et al. (2016) computed climate change signals for 2061-2100 compared to 1961-2000, while Moemken et al. (2018) used 2071-2100 compared to 1971-2000. In terms of variability, both studies agree on an increase of intra-annual variability of *Eout* over Northern, Central and Eastern Europe, and a decline of variability for large parts of Southern Europe in future decades. For changes in the inter-annual variability of *Eout*, both publications reveal large uncertainties between the individual ensemble members allowing no clear conclusions on the reliability of wind energy production in future decades. In both studies, results for the regional scale can be related to future trends in the large-scale atmospheric conditions, in particular mean sea level pressure, circulation patterns, and global mean wind speeds.

These results emphasise that the choice of GCM has a larger impact on the climate change signals for wind energy potentials than the downscaling technique. The statistical-dynamical downscaling approach used in Reyers et al. (2016) is thus an adequate method to investigate regional changes of wind energy potentials in large multi-model ensembles. It is a suitable and computationally inexpensive alternative to a pure DD approach for wind energy applications. However, the application of SDD has some limitations due to its composition. The simulations based on SDD are not able to resolve daily or sub-daily processes since only a limited number of representative days is simulated with the RCM (cp. chapter 3). Therefore the SDD application is restricted to seasonal-to-multi-decadal timescales. The dynamical downscaling enables simulations at a very high temporal resolution, e.g. inter- and sub-daily timescales. This allows insights in timescales that cannot be addressed with the SDD approach but could be of interest for decision makers in politics and economy. For example, Moemken et al. (2018) analysed future trends in inter-daily

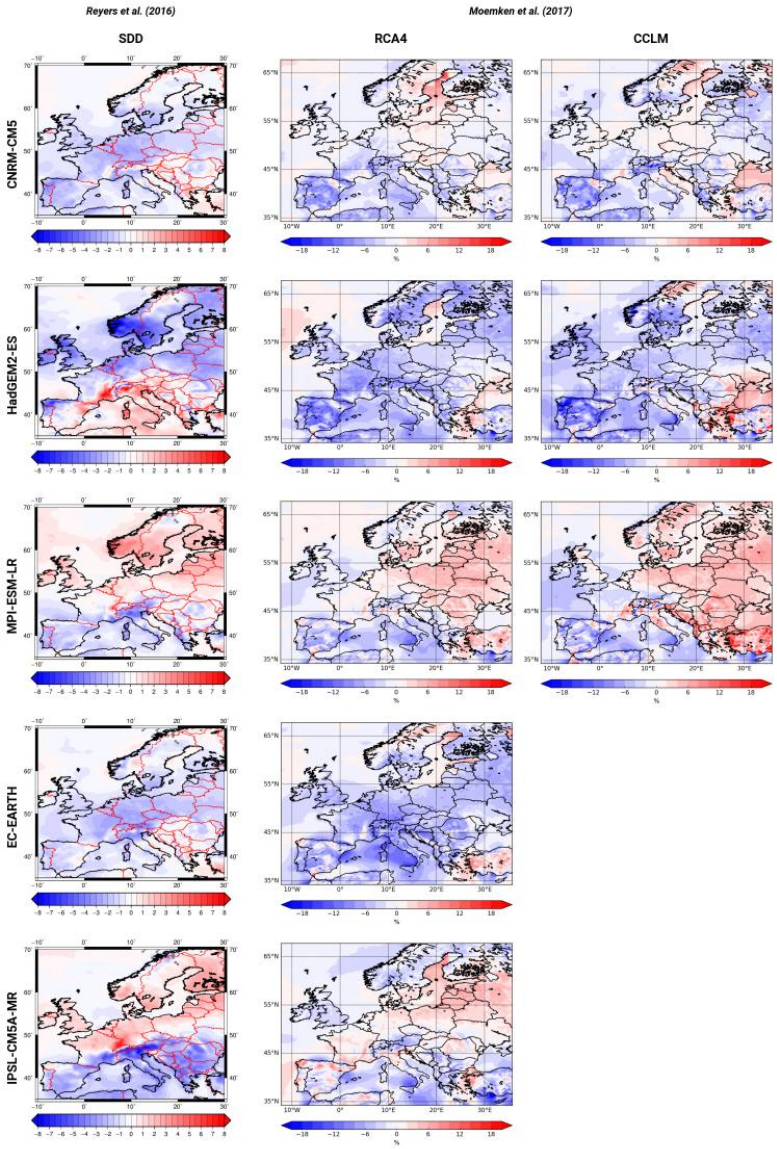

Fig. 9.3: Changes of mean annual *Eout* in % for RCP8.5 for the end of the century (2061-2100 for CMIP5, respectively 2071-2100 for EURO-CORDEX). Left column: results from Reyers et al. (2016). Middle column: results for the RCA4-ensemble from Moemken et al. (2018). Right column: results for the CCLM-ensemble from Moemken et al. (2018). The driving GCMs are depicted in the first column.

variability of *Eout*, which could affect the volatility of a wind-driven energy system. On the other hand, the SDD can be easily applied to large ensembles considering different emission scenarios and periods. Reyers et al. (2016) downscaled 22 GCMs from CMIP5 for two scenarios and two periods. In the meantime, studies based on DD are often limited

to single GCMs and/or emission scenarios. The larger dynamically downscaled ensemble used in Moemken et al. (2018) is only available since several institutions shared their simulations in the framework of EURO-CORDEX.

Therefore both downscaling techniques are needed for future studies analysing the impact of climate change on regional wind speed and wind energy potentials. The decision for one of the two methods depends on the aim and focus of the study. Analyses focussing on seasonal or longer timescales might rather consider a statistical-dynamically downscaled ensemble. This enables the assessment of the uncertainty of climate change projections, which arise not only from different scenarios but also from different GCMs (see Reyers et al., 2016). For studies interested in future changes on sub-seasonal to sub-daily timescales, a dynamically downscaled ensemble is more suitable. In addition, the results from both Reyers et al. (2016) and Moemken et al. (2018) are important for advanced impact studies, which could e.g. analyse the influence of the projected changes of *Eout* on the European energy system. Such an impact study developed from a successful collaboration with colleagues from Forschungszentrum Jülich: Weber et al. (2018, chapter 6) used a five-member ensemble from EURO-CORDEX to analyse the impact of climate change on storage and backup needs in a European renewable energy system focussing on wind energy. They uncovered an increase of storage and backup needs for most of Central, Northern and North-western Europe, and a decrease for the Iberian Peninsula, Greece and Croatia. In their study, two reasons were identified for this increase: an increase of seasonal wind variability and a longer duration of low-wind periods in future decades as found in Moemken et al. (2018) and Reyers et al. (2016). Weber et al. (2018) suggest that the increase in backup needs may to some extend be compensated by using an appropriate mix of wind energy generation and solar energy. Therefore future work should also include potential changes of other renewable energy sources like solar power (e.g. Jerez et al., 2015) to account for an optimal energy mix. This is crucial for the adaptation of the existing energy system to climate change. Wohland et al. (2017) simulated the operation of a fully renewable European electricity model based on EURO-CORDEX data. In line with Weber et al. (2018) they find an increase of backup needs. This increase is connected to more homogeneous wind conditions over Europe under future climate conditions.

Both Reyers et al. (2016) and Moemken et al. (2018) assume that a wind turbine is placed at every model grid point. To account for the wind farm distribution and installed power capacity, future work should also analyse wind power generation statistics (e.g. Cannon et al., 2015; Drew et al., 2015; Tobin et al., 2016). In fact, a widespread distribution of wind farms could be beneficial for the wind energy sector (Grams et al., 2017).

In addition to climate change projections, the demand for predictions focussing on the near future on timescales from one year up to one decade has strongly increased over the last years, particularly in politics and economy (Goddard et al., 2013). Moemken et al. (2016, Paper III) is the first study that analyses the decadal predictability of regional scale wind speed and wind energy potentials. The results reveal a potential decadal predictability of wind speed and wind energy potentials over Central Europe in the MiKlip decadal prediction system that is based on MPI-ESM (Marotzke et al., 2016). Although the decadal forecast skill is limited to the first years after initialisation, it could allow the investigation of future trends of wind energy potentials for the next one to five years. This may be of high importance for the future development of wind power generation in Europe. As in Reyers et al. (2016), the SDD method (section 3.2) is used to downscale three ensemble generations of the global decadal prediction system. Each generation comprises ten ensemble members, which cover 52 respectively 54 decadal hindcasts resulting in 1600 hindcasts with a length of ten years. The downscaling of such a large ensemble is difficult to realise with purely DD methods, assuming a simulation time of approximately five days per hindcast with a RCM. Therefore the SDD is an adequate tool for the regionalisation of the global model data and could also easily be applied to operational decadal prediction systems. The regionalisation with SDD preserves and sometimes increases the decadal forecast skill of the global runs. Additionally, it improves the ensemble spread in some cases. This provides a wide range of opportunities for end-user applications.

The identified skill scores for *Eout* are comparable to skill scores for wind speed as detected by Reyers et al. (2017, chapter 8) for a small dynamically downscaled MiKlip ensemble, while predictive skill for *Eout* is higher compared to temperature and precipitation. In general, differences between the individual hindcast generations are smaller in Moemken et al. (2016) compared to Reyers et al. (2017). This could indicate that signals are more robust for wind energy applications.

Moemken et al. (2016) detected a strong dependency of the decadal forecast skill of *Eout* on the representation of westerly weather types in the MPI-ESM. This may enhance the understanding of the mechanisms behind decadal predictability, for example through further investigations of the coupling between these large-scale weather types and teleconnection patterns. Another topic that needs to be addressed in future work is the large uncertainties in the decadal predictability of wind energy potentials in the MPI-ESM. In particular, focus should be given to the non-systematic dependence of the forecast skill on seasons and hindcast generation. Additionally, the influence of the initialisation strategy and the ensemble size requires further investigations.

The applied SDD approach has limitations regarding the temporal resolution (see also Reyers et al., 2016). A DD method is necessary to analyse the decadal predictability of e.g. the inter-daily variability of *Eout* or the duration of low-wind periods. Therefore, future work should investigate the decadal predictability in a dynamically downscaled decadal prediction system ("future work" part in Figure 9.2). As part of the second phase of the national MiKlip project (*www.fona-miklip.de*), a regional component of the MiKlip decadal prediction system is established. With this aim, the newest generation of the decadal prediction system (preop) is currently downscaled for Europe using COSMO-CLM. This opens a wide range of options for future work. First, a basic evaluation of the new regional prediction system is required, focussing on primary meteorological variables like temperature, pressure, precipitation, and wind speed (cp. Reyers et al., 2017). In a next step, the decadal predictability of wind speed and wind energy potentials in the regional system will be analysed. Additionally, the global preop ensemble is going to be downscaled with the SDD to assess the decadal predictability of wind energy. The comparison of the results from both downscaling methods enables the analysis of the influence of the chosen downscaling technique on the decadal forecast skill for wind energy. The comparison should also include the older ensemble generations (Moemken et al., 2016). This may allow a better estimation of uncertainties. Furthermore, composite analyses could help to understand the mechanisms of decadal predictability. Finally, the decadal predictions produced within MiKlip need to be analysed, with special focus on user applications. So far, most studies focus on the hindcast ensembles to investigate the potential predictive skill of different variables. A first decadal forecast for 2017-2026 focussing on global temperature was analysed and released on the MiKlip webpage (*http://www.fona-miklip.de/decadal-forecast-2017-2026/decadal-forecast-for-2017-2026/*). This analysis will be complemented with other variables, also considering the regional ensemble and potential end-user needs.

To conclude, the results of this thesis extend the current knowledge on wind speed and wind energy potentials over Europe. They provide a substantial basis for the understanding of climate change impacts on different timescales and give a new insight on the influence of different downscaling approaches for wind energy applications. Additionally, the results on decadal predictability are promising regarding the establishment of an operational decadal prediction system for wind energy applications. The outcomes of this thesis are relevant for the successful integration of wind energy into the energy system to enable the transition from a fossil fuel driven energy system to one with a higher share of renewables.

10 Appendix

10.1 Reyers et al. (2015)

Reference:

Reyers, M., Pinto, J. G., and Moemken, J. (2015). Statistical-dynamical downscaling for wind energy potentials: evaluation and applications to decadal hindcasts and climate change projections. *Int. J. Climatol.*, 35:229–244. doi:10.1002/joc.3975

Page numbers are as published in *International Journal of Climatology*.

INTERNATIONAL JOURNAL OF CLIMATOLOGY
Int. J. Climatol. **35**: 229–244 (2015)
Published online 8 April 2014 in Wiley Online Library
(wileyonlinelibrary.com) DOI: 10.1002/joc.3975

RMetS
Royal Meteorological Society

Statistical–dynamical downscaling for wind energy potentials: evaluation and applications to decadal hindcasts and climate change projections

Mark Reyers,[a]* Joaquim G. Pinto[a,b] and Julia Moemken[a]
[a] *Institute for Geophysics and Meteorology, University of Cologne, Germany*
[b] *Department of Meteorology, University of Reading, UK*

ABSTRACT: A statistical–dynamical downscaling (SDD) approach for the regionalization of wind energy output (E_{out}) over Europe with special focus on Germany is proposed. SDD uses an extended circulation weather type (CWT) analysis on global daily mean sea level pressure fields with the central point being located over Germany. Seventy-seven weather classes based on the associated CWT and the intensity of the geostrophic flow are identified. Representatives of these classes are dynamically downscaled with the regional climate model COSMO-CLM. By using weather class frequencies of different data sets, the simulated representatives are recombined to probability density functions (PDFs) of near-surface wind speed and finally to E_{out} of a sample wind turbine for present and future climate. This is performed for reanalysis, decadal hindcasts and long-term future projections. For evaluation purposes, results of SDD are compared to wind observations and to simulated E_{out} of purely dynamical downscaling (DD) methods.

For the present climate, SDD is able to simulate realistic PDFs of 10-m wind speed for most stations in Germany. The resulting spatial E_{out} patterns are similar to DD-simulated E_{out}. In terms of decadal hindcasts, results of SDD are similar to DD-simulated E_{out} over Germany, Poland, Czech Republic, and Benelux, for which high correlations between annual E_{out} time series of SDD and DD are detected for selected hindcasts. Lower correlation is found for other European countries. It is demonstrated that SDD can be used to downscale the full ensemble of the Earth System Model of the Max Planck Institute (MPI-ESM) decadal prediction system.

Long-term climate change projections in Special Report on Emission Scenarios of ECHAM5/MPI-OM as obtained by SDD agree well to the results of other studies using DD methods, with increasing E_{out} over northern Europe and a negative trend over southern Europe. Despite some biases, it is concluded that SDD is an adequate tool to assess regional wind energy changes in large model ensembles.

KEY WORDS wind energy; statistical–dynamical downscaling; decadal forecasts; climate change projections; ensembles

Received 11 November 2013; Revised 10 January 2014; Accepted 11 February 2014

1. Introduction

In recent years, the demand for renewable energy sources as alternative to fossil sources has increased due to the imperative need to reduce greenhouse gas emissions (Solomon *et al.*, 2007). In Europe, wind energy production has emerged as a promising energy source to mitigate the climate change resulting from anthropogenic greenhouse gas emission. A main challenge for political and economical decision makers is the installation of an effective network of wind power plants (Manwell *et al.*, 2009; Wilkes *et al.*, 2012) to meet the goal of the European Commission to produce 15.7% of the EU's electricity usage from wind energy resources by 2020 (Moccia *et al.*, 2011).

Near-surface winds, and thus wind energy production, strongly depend on the synoptic scale variability (2–6 days, e.g. passage of low- and high-pressure centres), seasonality, and on climate variability on different timescales (e.g. Pryor and Barthelmie, 2010). Furthermore, conditions for wind energy production are strongly influenced by local characteristics (e.g. Ouammi *et al.*, 2012). Hence, suitable predictions of regional changes of wind energy potentials on inter-annual to decadal and on centennial timescales are essential for future planning.

A set of global decadal prediction hindcasts have been recently made available through the Coupled Model Intercomparison Project Phase 5 (CMIP5; Taylor *et al.*, 2012). In these experiments, initial conditions for decadal hindcasts and predictions are taken from assimilation runs using analysis data from the past and present for the relaxation towards gridded observational values. Since small initialization perturbations, which reflect the observational uncertainties, might rapidly grow, differences between ensemble members may be large because of these uncertainties (Merryfield *et al.*, 2013). Therefore, large ensembles of decadal hindcasts are required for the assessment of the predictive skill. In CMIP5, most decadal prediction

* Correspondence to: M. Reyers, Institute for Geophysics and Meteorology, University of Cologne, Pohligstr. 3, 50923 Cologne, Germany.
E-mail: mreyers@meteo.uni-koeln.de

systems comprise up to ten realizations of yearly initialized hindcasts and thus several of hundreds of simulations, which can hardly be downscaled by a purely dynamical downscaling (hereafter DD) with regional climate models (RCMs). Therefore, an alternative downscaling approach for the regionalization of large ensembles of decadal hindcasts is required.

The same line of thought also applies to the regionalization of long-term climate change projections, where global climate model's (GCMs) output needs to be downscaled to the regional and local scales. With this aim, several downscaling techniques have been developed and applied in recent years. They can be roughly classified as statistical, dynamical or statistical–dynamical approaches (Hewitson and Crane, 1996; Wilby and Wigley, 1997; Fuentes and Heimann, 2000; Maraun *et al.*, 2010). In terms of the regional impact of climate change on wind energy potentials, Nolan *et al.* (2012) analyse possible changes in wind energy resources of Ireland with a DD approach (ECHAM5/MPI-OM1 GCM ensemble simulations and one RCM). Hueging *et al.* (2013) investigated regional changes in wind energy potential for Europe by considering ensemble projections from two RCMs driven by ECHAM5/MPI-OM1 simulations (A1B scenario). An empirical downscaling method has been employed by, for example, Pryor *et al.* (2005) to estimate the future change in wind energy, using wind observations as predictands and large-scale atmospheric fields of ECHAM4/OPYC3 as predictors. In these and other studies, the analysis focuses typically on single emission scenarios or a single GCM/RCM. In case of the DD methods, this is surely due to the very time-consuming high-resolution simulations of the RCMs. At the same time, several studies reveal that uncertainties in the future projections of synoptic variability in GCMs arise not only from different greenhouse gas forcings but also from discrepancies between individual GCMs using the same scenario that may be quite large, e.g. because of different parameterizations or uncertainties in ocean circulation changes (e.g. Ulbrich *et al.*, 2008; Harvey *et al.*, 2012; Woollings *et al.*, 2012). Because of these uncertainties, a downscaling methodology for wind energy, which can easily be applied to large (multi-model) ensembles of long-term future projections, would be beneficial. A useful method for downscaling multiple GCMs is the expansion of DD applications by statistical approaches (e.g. Fuentes and Heimann, 2000). For wind applications, for example, Najac *et al.* (2011) have recently combined mesoscale modelling with statistical transfer functions between large-scale and local winds to infer the impact of climate change on surface winds over France.

In this study, a statistical–dynamical downscaling (SDD) approach for wind energy applications on the regional scale in Europe with special focus on Germany is proposed and evaluated. The aim of the study is to investigate in how far:

- SDD is able to simulate realistic near-surface wind distributions for recent climate conditions;
- SDD produces comparable results to the time-consuming DD with respect to the simulation of wind energy output on different timescales;
- SDD is efficient for the application to large ensembles of both decadal hindcasts and long-term climate change projections to assess the changes of wind energy in near future and to the end of the 21st century in multi-model ensembles.

This study is organized as follows. The methodology of SDD and the used data sets are introduced in Section 2. Results of SDD as applied to different exemplary global data sets are discussed in the following sections: Section 3 describes the evaluation of SDD based on ERA-Interim Reanalysis data, Section 4 describes the application on the Earth System Model of the Max Planck Institute (MPI-ESM) decadal hindcasts, and Section 5 describes investigations based on climate change projections with the ECHAM5 model. A short discussion concludes this paper.

2. Methods and data

The proposed SDD approach (following Fuentes and Heimann, 2000; Pinto *et al.*, 2010) for the simulation of highly-resolved wind energy output consists of four crucial steps (see Figure 1). These steps will be introduced and described in detail in the following. For convenience, the stepwise application of SDD to a reanalysis data set is presented. The application to other data sets, such as decadal hindcasts, is quite similar and will be described later in this section (see below).

Step 1: In the first step of SDD approach, a weather typing approach is used to characterize the large-scale circulation of each day (see Figure 1). With this aim, the circulation weather type (CWT) approach from Jones *et al.* (1993) is considered. This approach follows the manual Lamb weather types (Lamb, 1972; Jenkinson and Collinson, 1977) and has been widely used in many applications (e.g. Jones *et al.*, 2012). Daily mean sea level pressure (MSLP) fields of the ERA-Interim reanalysis project (Dee *et al.*, 2011) are used as input data. This data set comprises the period 1979–2010 and is interpolated on a 2.5° grid for the computation of the CWTs. By regarding instantaneous MSLP values at 16 points around the central point at 10°E, 50°N (near Frankfurt, Germany; cf. Figure 2), the near-surface atmospheric flow for each day is determined and assigned to one of the ten basic CWTs: northeast, NE; east, E; southeast; SE; south, S; southwest, SW; west, W; northwest, NW; north, N; cyclonic, C; anti-cyclonic, A. In addition, the mixed type anti-cyclonic/west A/W is considered as its frequency is comparable to the values of some of the basic CWTs and should, therefore, not be neglected. For wind energy, a further crucial factor is the strength of the geostrophic flow. Therefore, aside from the direction of flow, a f-parameter representing the gradient of the instantaneous MSLP field at the central point is calculated. Depending on the CWT, the f-parameter ranges from ca. 45 hPa per

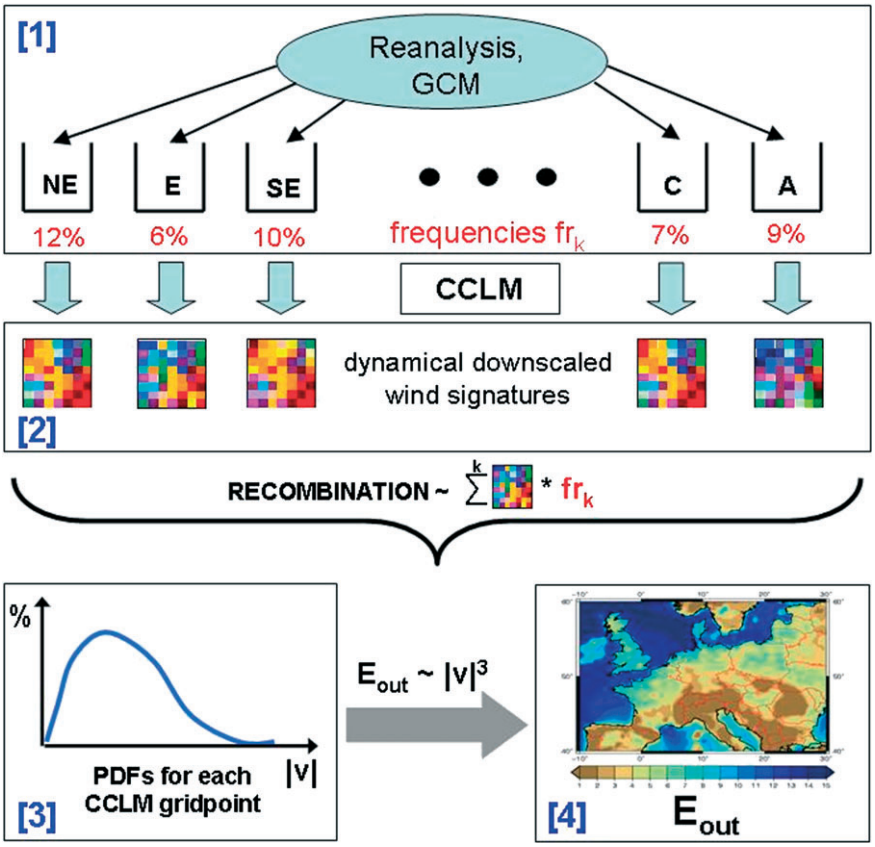

Figure 1. Schematic illustration of the SDD with its four crucial steps: 1 – large-scale weather type analysis; 2 – DD of representative days for each weather class; 3 – recombination of simulated wind signatures for the representatives to PDFs of 10-m wind speed for each CCLM grid point; 4 – determination of spatial distributions of regional E_{out} by applying wind turbine characteristics to the PDFs. The single steps are described in detail in Section 2.

1000 km (strong MSLP gradient) to values below 5 hPa per 1000 km (slack MSLP gradient). To capture the full spectrum of potential wind velocities within a CWT, each of the 11 CWTs is subdivided into classes of f-parameters with 5 hPa per 1000 km intervals (0–5 to 40–45 hPa per 1000 km). Altogether, a total of 77 classes have been identified (see Table 1). As an example, Figure 2 shows climatological MSLP fields for class W, with f-parameter 0–5 *versus* 35–40 hPa per 1000 km, and for class C, with f-parameter 0–5 *versus* 20–25 hPa per 1000 km. As expected, classes with high f-parameters (Figure 2(b) and (d)) show a much stronger MSLP gradient around the central point and thus higher geostrophic wind speeds than classes with low f-parameters (Figure 2(a) and (c)).

Step 2: To obtain highly resolved wind signatures of the different classes, in the second step of SDD, representative days for each of the 77 classes are simulated with the regional COSMO model of the German Weather Forecast Service Deutscher Wetterdienst (DWD) (http://www.cosmo-model.org) in its *CL*imate *M*ode (version 4.8, hereafter CCLM). CCLM is a three-dimensional, non-hydrostatic atmospheric circulation model with generalized terrain-following height level on a rotated coordinate system (Rockel *et al.*, 2008). CCLM simulations are performed with a horizontal resolution of 0.22° × 0.22°, using ERA-Interim data as initial and boundary conditions. The model domain is consistent with the domain used in the EURO-CORDEX project (Giorgi *et al.*, 2006), comprising the European-East Atlantic sector with 226 grid points in south–north and 232 grid points in west–east direction. It roughly ranges from 20°N to 70°N and from 30°W to 50°E.

For each of the 77 classes, ten representative days were selected (see Appendix S1), if available, and simulated with CCLM. If a class occurs on <10 days within the ERA-Interim period 1979–2010, the full set of days is used as representatives. A total of 669 representative days have been simulated. The choice of the representative days within a class is random, but we have selected representatives from all four seasons if possible. As this is a quite large number of selected days, it can be assumed that the full spectrum of potential representatives is largely covered by this method and thus the variability of the target parameter (wind) both for each weather class and climatology.

Step 3: In the third step, CCLM-simulated hourly 10-m winds of the representative days are recombined to wind velocity distributions [probability density functions (PDFs)] for the full ERA-Interim period 1979–2010. The PDFs are determined for each CCLM grid point, separately: for a given wind velocity (0.1 m s^{-1} velocity ranges), the respective occurrence is calculated as sum of the contributions of all classes weighted by

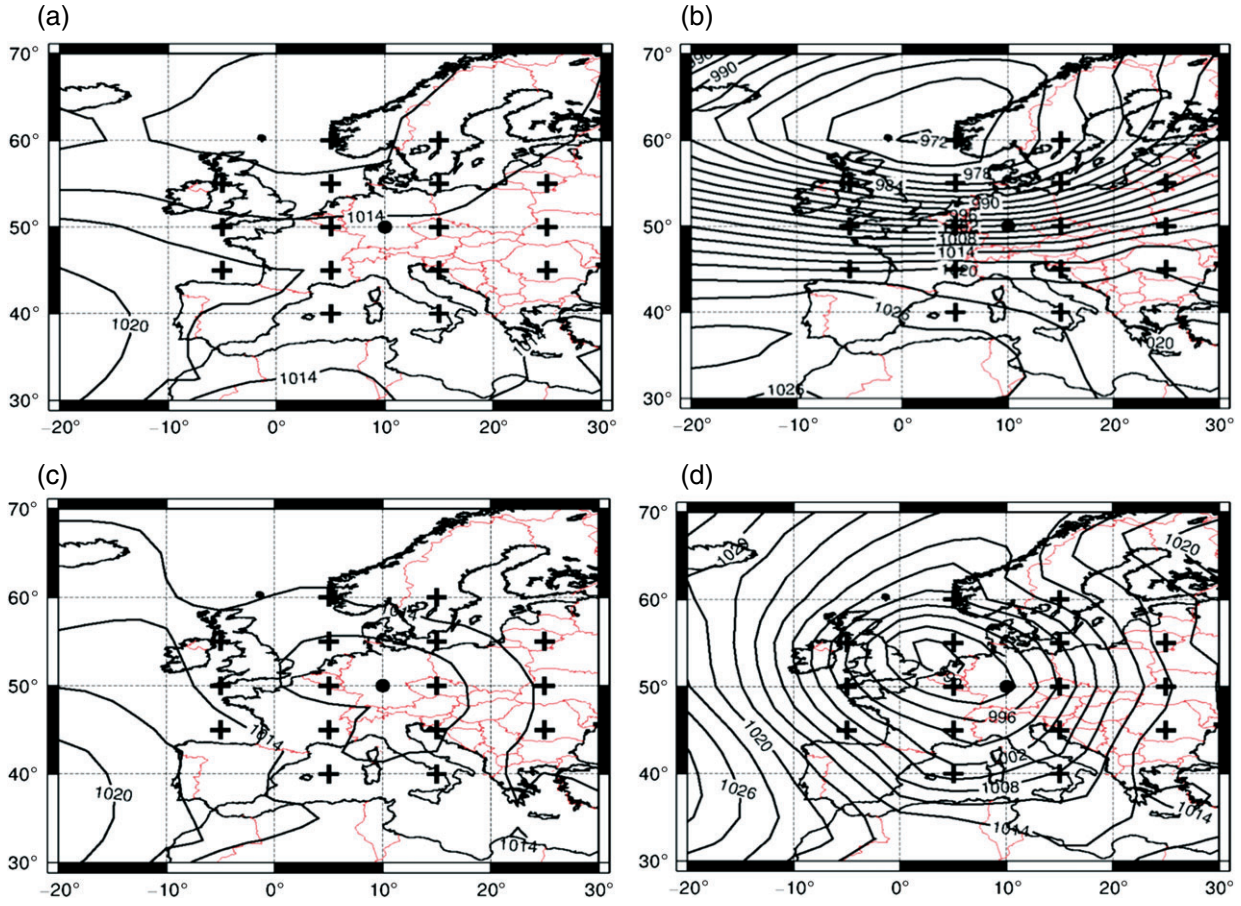

Figure 2. Climatological means of exemplary CWT classes as obtained from MSLP fields of ERA-Interim. (a) CWT W with f-parameter between 0 and 5 hPa per 1000 km. (b) CWT W with f-parameter between 35 and 40 hPa per 1000 km. (c) CWT C with f-parameter between 0 and 5 hPa per 1000 km. (d) CWT C with f-parameter between 20 and 25 hPa per 1000 km. The black point represents the central point for the CWT analysis, the black crosses the surrounding ERA-Interim grid points used for the computation of the CWTs. For more details, see text.

Table 1. Relative frequency, range of f-parameter (in hPa per 1000 km), and number of classes of each CWT. The last row shows the total of identified CWT classes.

CWT	Frequencies (%)	f-Range	No. of classes
NE	4.01	0–30	6
E	4.34	0–30	6
SE	4.93	0–35	7
S	5.36	0–35	7
SW	9.86	0–45	9
W	9.58	0–45	9
NW	8.17	0–45	9
N	5.29	0–35	7
C	12.02	0–25	5
A	32.16	0–25	5
A/W	4.30	0–35	7
Total no. of classes			77

the climatological class frequency and the number of simulated representatives.

Step 4: The climatological 10-m wind speed PDFs form the basis for the determination of mean wind energy output (E_{out}) following Hueging *et al.* (2013). First, 10-m wind velocities are extrapolated to a height of 80 m, which is assumed to be the average hub height of onshore wind turbines (EEA, 2009). For the extrapolation, the power law is used:

$$\frac{v(z)}{v(z_{\mathrm{r}})} = \left(\frac{z}{z_{\mathrm{r}}}\right)^{\alpha}, \tag{1}$$

with $v(z)$ and $v(z_{\mathrm{r}})$ being the wind velocities in 80 m (z) and 10 m (z_{r}), respectively. The parameter α is the power law exponent, which is set to 0.2 for onshore areas and to 0.14 for offshore sites (IEC, 2005a, 2005b). Wind velocities of 80 m are then used to compute E_{out}, using wind turbine characteristics of an idealized 2.5 MW wind turbine from General Electric (2010):

- No energy output is produced below 80-m wind velocities of 3.5 m s^{-1} (cut-in velocity) and for velocities higher than 25 m s^{-1} (cut-out velocity).
- Between wind velocities of 3.5 m s^{-1} (cut-in velocity) and 12.5 m s^{-1} (rated velocity), E_{out} can be determined as follows:

$$E_{\mathrm{out}} = c_{\mathrm{p}} \frac{1}{2} \rho \pi R^2 v_{80}^3, \tag{2}$$

where c_{p} is the power coefficient (0.35), ρ is the air density (constant value of 1.225 kg m^{-3}), R is the rotor radius of

the idealized wind turbine (50 m), and v_{80} is the 80-m wind velocity.

- Between wind velocities of 12.5 m s^{-1} (rated velocity) and 25 m s^{-1} (cut-out velocity), a constant energy output of 2.5 MW is assumed.

To obtain spatial distributions of mean annual wind energy output for the period 1979–2010, for each CCLM grid point, computed E_{out} is integrated over all wind velocity ranges of the gridded PDFs, using the respective climatological velocity frequencies as weighting factors.

For the application of SDD method to shorter time periods or to other data sets, only the weather typing analysis (step 1) has to be adapted to these new data sets. If, for example, E_{out} is to be simulated on annual timescales, the CWT analysis is carried out for single years. In steps 2–4, the resulting weather class frequencies (e.g. for single years) are then used in the same manner as for ERA-Interim climatology to obtain 10-m wind speed PDFs and finally spatial distributions of regional E_{out}, using the same simulated representative days as for the full ERA-Interim period. This assumes that the selected days are also representative for the weather classes in other data sets, only the frequencies of the classes will change (e.g. in future projections).

In this study, the SDD approach is applied to three different data sets. For evaluation purposes, the SDD approach is applied to ERA-Interim as described above. To calculate adequate E_{out} values, realistic simulations of 10-m wind speed PDFs are required (see step 3). In this respect, SDD-simulated PDFs are compared to PDFs as derived from observations. Hourly 10-m wind velocities from stations of the German Weather Forecast Service (DWD) are used. We have only regarded stations with a height below 800 m asl, where measurements cover more than 98% of the period 1979–2010. Furthermore, SDD-simulated E_{out} is compared to E_{out} simulations of a purely DD method. The DD run is simulated with CCLM, using continuous ERA-Interim data from 1979 to 2010 as boundary conditions (hereafter DD_{era}). For DD_{era}, E_{out} is computed from hourly 10-m wind velocity output and then summed up for certain periods, using the same turbine characteristics as for SDD (see Equations 1 and 2). Aside from climatological means, results of SDD for selected time periods are compared to DD_{era} results.

In terms of applications, the SDD approach is applied to the decadal prediction system of the coupled MPI-ESM (Mueller *et al.*, 2012). The latest experiment version is used (MPI-ESM Baseline1), where initial conditions for decadal hindcasts and predictions are taken from assimilation runs forced by sea surface temperature and salinity anomalies of the operational ECMWF ocean reanalysis system (ORAs4; Balmaseda *et al.*, 2013). This experiment comprises ten realizations of yearly initialized decadal hindcasts and predictions from 1960 to 2011 (hereafter dec1960 to dec2011; altogether $52 \times 10 = 520$ realizations), each of them covering a period of 10 years. SDD results are compared to outcomes as obtained by the DD method. Four DD runs are simulated with CCLM, using atmospheric fields of four selected decadal hindcasts as boundary conditions: first realization of dec1980 (initialized at 01.01.1981; hereafter DD_{1980_1}), first realization of dec2000 (initialized at 01.01.2001; hereafter DD_{2000_1}), and the first and tenth realization of dec1990 (initialized at 01.01.1991, respectively; hereafter DD_{1990_1} and DD_{1990_10}).

To demonstrate that SDD is appropriate for the application to ensembles of long-term climate change projections, we employ the method also to simulations with the GCM ECHAM5/MPI-OM of the Max-Planck-Institute Hamburg (hereafter ECHAM5; Jungclaus *et al.*, 2006; Roeckner *et al.*, 2006). SDD is applied to an ensemble for recent climate conditions (20C scenario, 1961–2000) and to the three scenarios B1, A1B, and A2 (2061–2100, respectively) of the Special Report on Emission Scenarios (SRES; Nakicenovic and Swart, 2000) to estimate regional changes of wind energy by the end of the 21st century. As the projected changes for pressure gradients and winds under future climate conditions for Europe on the regional scale are comparatively small (e.g. Hueging *et al.*, 2013), it can be assumed that primarily only the frequencies of the weather classes will change in future climate, while the wind characteristics within each class will remain largely unchanged. Therefore, the selected representatives are considered as suitable also for the climate conditions during the second half of the 21st century. The CO_2 concentration increases from 367 ppm in the year 2000 to 540, 703, and 836 ppm by the year 2100 for B1, A1B, and A2, respectively. For the A1B scenario, results of SDD are compared to Hueging *et al.* (2013), who have employed two different RCMs (inter alia the CCLM) to simulate regional changes in wind energy potential over Europe using the first two realizations of ECHAM5 20C and A1B as boundary conditions.

3. Evaluation and application to ERA-Interim

In this section, results of the single steps of the SDD application to ERA-Interim are presented and evaluated against observations and DD_{era}. Figure 3 shows the climatological frequencies of the 77 classes for the period 1979–2010 as obtained from the weather typing approach (step 1). The most dominating CWTs are A, C, and the westerly types (SW, W, NW). While for CWT A, the observed f-parameter range is mainly restricted to low values (0–5 and 5–10 hPa per 1000 km), frequencies of the CWTs SW, W, and NW are highest for f-parameter ranges of 5–10 to 20–25 hPa per 1000 km. These results reflect that anti-cyclonic conditions are generally related to weak MSLP gradients, and that westerly flows are predominantly connected with stronger near-surface winds. Lowest frequencies are found for the easterly CWTs (SE, E, NE).

As described in Section 2, the frequencies of the 77 weather classes are used for the recombination of

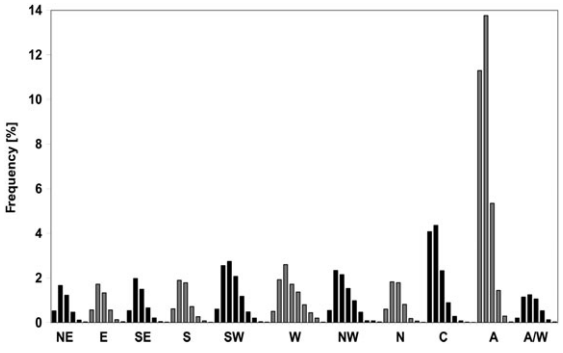

Figure 3. Climatological frequencies of all weather classes for ERA-Interim (1979–2010). For each CWT, weather classes are shown for ascending f-parameter (5 hPa per 1000 km intervals) from left to right (0–5, 5–10, 10–15 hPa per 1000 km, etc.). For better indication, the CWTs are separated by black and grey colouring.

simulated representative days (step 2) to downscaled PDFs of 10-m wind velocities per COSMO-CLM grid point (step 3). According to the wind turbine characteristics used in this study (see Equations 2), the majority of E_{out} is produced by upper wind percentiles. Figure 4 exemplary shows the 75th and 90th percentiles for the period 1979–2010 as derived from SDD and DD_{era}. Differences between SDD- and DD_{era}-simulated percentiles are quite small for the entire European sector (see Figure 4(a)–(d)). Both SDD and DD_{era} reveal highest percentiles over sea surfaces and at the northern coasts, and smallest percentiles over the Alps and in southeast Europe.

Compared to observations, the 75th and 90th percentiles are overestimated by SDD for some stations in Mid-Germany, whereas for most stations in western and southern Germany as well as in the coastal area, SDD-simulated percentiles agree well to observations (see Figure 5). In general, the north–south gradient observed for Germany, with strongest percentiles at the coasts and lowest percentiles near the Alps, is matched well by the SDD approach.

For eight exemplary stations (for location of the stations, see Figure 5(a)), full PDFs are compared to PDFs for the respective nearest CCLM grid point as derived by SDD (1979–2010, see Figure 6). Please note that frequencies for the six stations in former West Germany are shown in 0.5 m s^{-1} intervals, whereas frequencies for Schwerin (SW) and Leipzig (LE) are given in 1 m s^{-1}

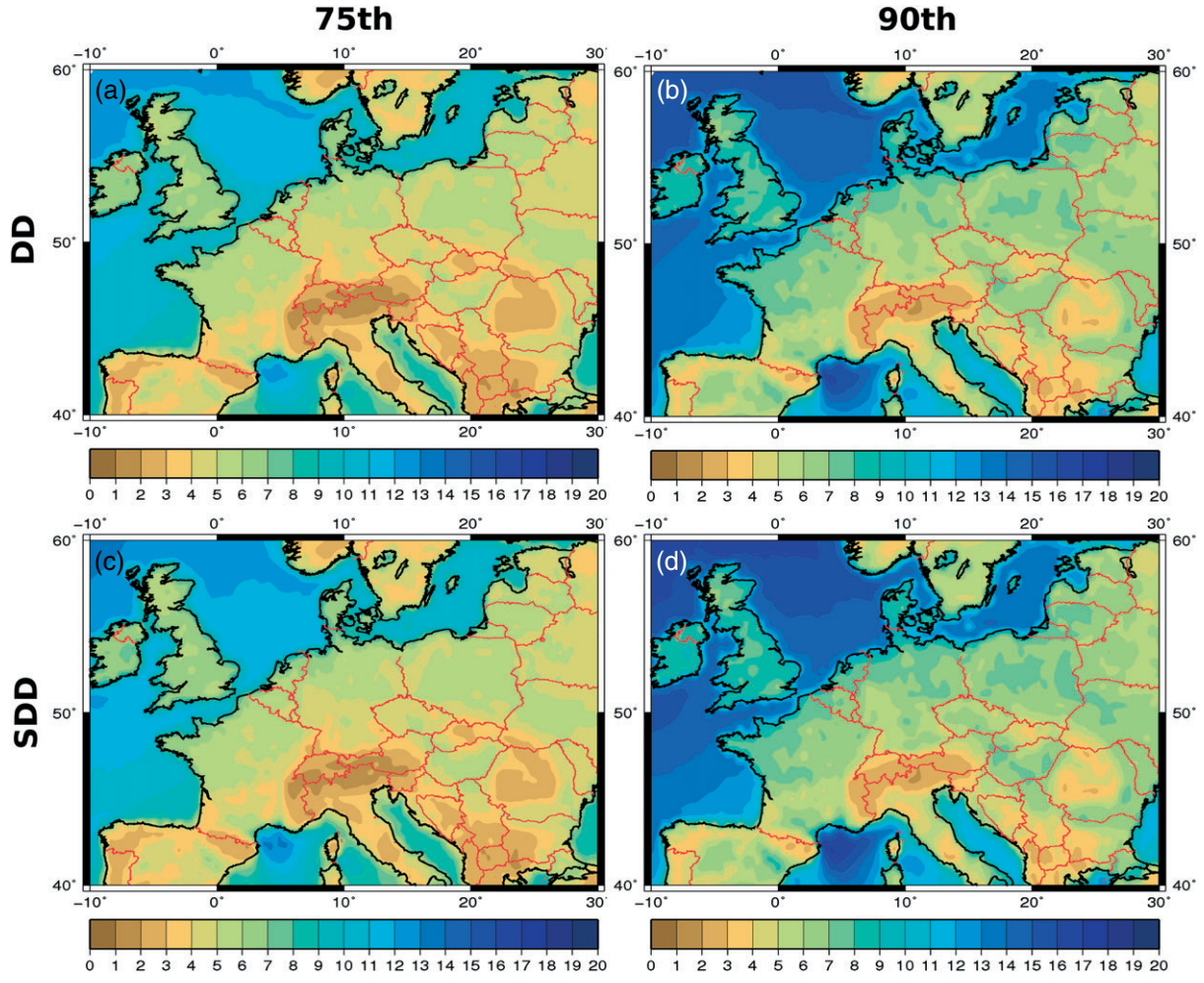

Figure 4. 75th (left column) and 90th (right column) percentiles in m s^{-1} of the 10-m wind velocity for the period 1979–2010. Upper row, DD; lower row, SDD.

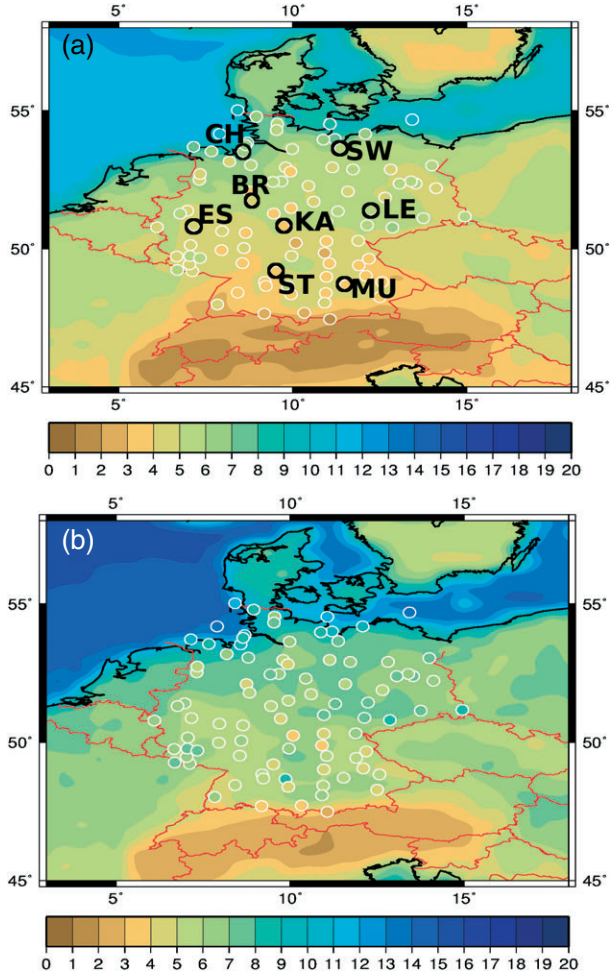

Figure 5. (a) 75th and (b) 90th percentiles in $m\,s^{-1}$ of the 10-m wind velocity for the period 1979–2010 as obtained by SDD (shaded) and observations (small circles). Note that (a) shows a zoom of Figure 4(c), and (b) shows a zoom of Figure 4(d). The black circles in (a) mark the locations of the stations shown in Figure 6: CH, Cuxhaven; BR, Bremen; SW, Schwerin; ES, Essen; KA, Kassel; LE, Leipzig; ST, Stuttgart; MU, Munich.

intervals (due to different measurement accuracy in former east Germany before 1990). Discrepancies between SDD-simulated and observed PDFs are largest for the coastal and near-coastal stations Cuxhaven (CH), Bremen (BR), and Schwerin (SW), while PDFs are simulated quite realistic for the non-coastal stations. However, the general observed wind distributions are captured well by the SDD approach, with highest wind speeds occurring in the North and frequent low wind velocities in southern Germany. The same PDFs have been derived from DD_{era} simulations. These PDFs are for most stations similar to the PDFs as obtained by the SDD approach. Only for few stations, results from DD_{era} show a slightly higher agreement to observations than SDD-simulated PDFs (e.g. Essen and Munich).

The gridded PDFs of the 10-m wind velocity for the period 1979–2010 are used to compute climatological annual means of E_{out} per CCLM model grid point (step 4). The spatial pattern of E_{out} as obtained by the SDD approach is realistic and quite similar to DD_{era}-simulated E_{out}, with highest values over ocean surfaces and rather small output over mountainous areas and southeast Europe (see Figure 7(a) and (b)). Only the magnitudes between both downscaling methods slightly differ. For most regions, SDD simulates higher E_{out} values than DD_{era}, but deviations are quite small compared with absolute magnitudes (see Figure 7(c)). The main positive bias of SDD compared to DD_{era} results from a slight overestimation of the frequencies of high wind speeds by SDD, as can be seen for most of the eight stations in Germany presented in Figure 6. Although the differences between the PDFs of SDD and DD_{era} are actually very small, they still lead to a slight but visible overestimation of wind energy output by SDD, as E_{out} is proportional to v^3.

For the application to decadal predictions, SDD should be able to simulate suitable E_{out} anomalies on timescales from several years down to single years. This is first tested for ERA-Interim by comparing annual time series of E_{out} anomalies as simulated by SDD to time series derived from DD_{era}. Figure 8 shows such a comparison for six exemplary sub-regions in central Europe (for location of the sub-regions, see Figure 7(a)). For Belgium, central Germany, northern Germany, and Poland, the time series of both methods are quite similar. Despite a slight underestimation of the general variability by SDD compared to DD_{era}, the year-to-year variation is captured well. Larger discrepancies between the two methods of up to $800\,MWh\,year^{-1}$ can be seen for a sub-region in northern France, where the annual variability is clearly underestimated by SDD. Nevertheless, for most years, the anomalies of both methods have the same sign. Differences between SDD and DD_{era} are largest for a sub-region in the North Sea. Comparisons of time series of 5-year running means and for other sub-regions also reveal a good accordance between SDD and DD_{era} for land surfaces in central Europe and a lower agreement over ocean surfaces (not shown). Even over the Baltic States, SDD-simulated time series of E_{out} are similar to DD_{era}. An overview of the regions with a high agreement between SDD and DD_{era} is given by Figure 9(a), which shows the correlation between annual E_{out} time series of both downscaling methods for all CCLM grid points. Very high correlations of more than 0.8 can be seen for Germany, Benelux, and Poland. Significant positive correlations of up to 0.8 are found for Great Britain, Czech Republic, and parts of the Baltic States, while correlation is low for southern Europe and the North Sea. This is due to the used weather typing approach, which is only representative for the large scale flow at the surrounding of the central point (in this case Germany and nearby areas) but not for areas far away from it (e.g. Italy). A physical explanation for the comparable low correlation over the North Sea is the high roughness length variability over sea surfaces due to varying heights of the water waves, which cannot be fully captured by SDD on timescales down to single years (unlike DD), as the same simulated representatives are used every time (see Section 2).

Figure 9(b) shows the RMSE of the SDD time series relative to the time series as obtained by DD_{era}. To take into

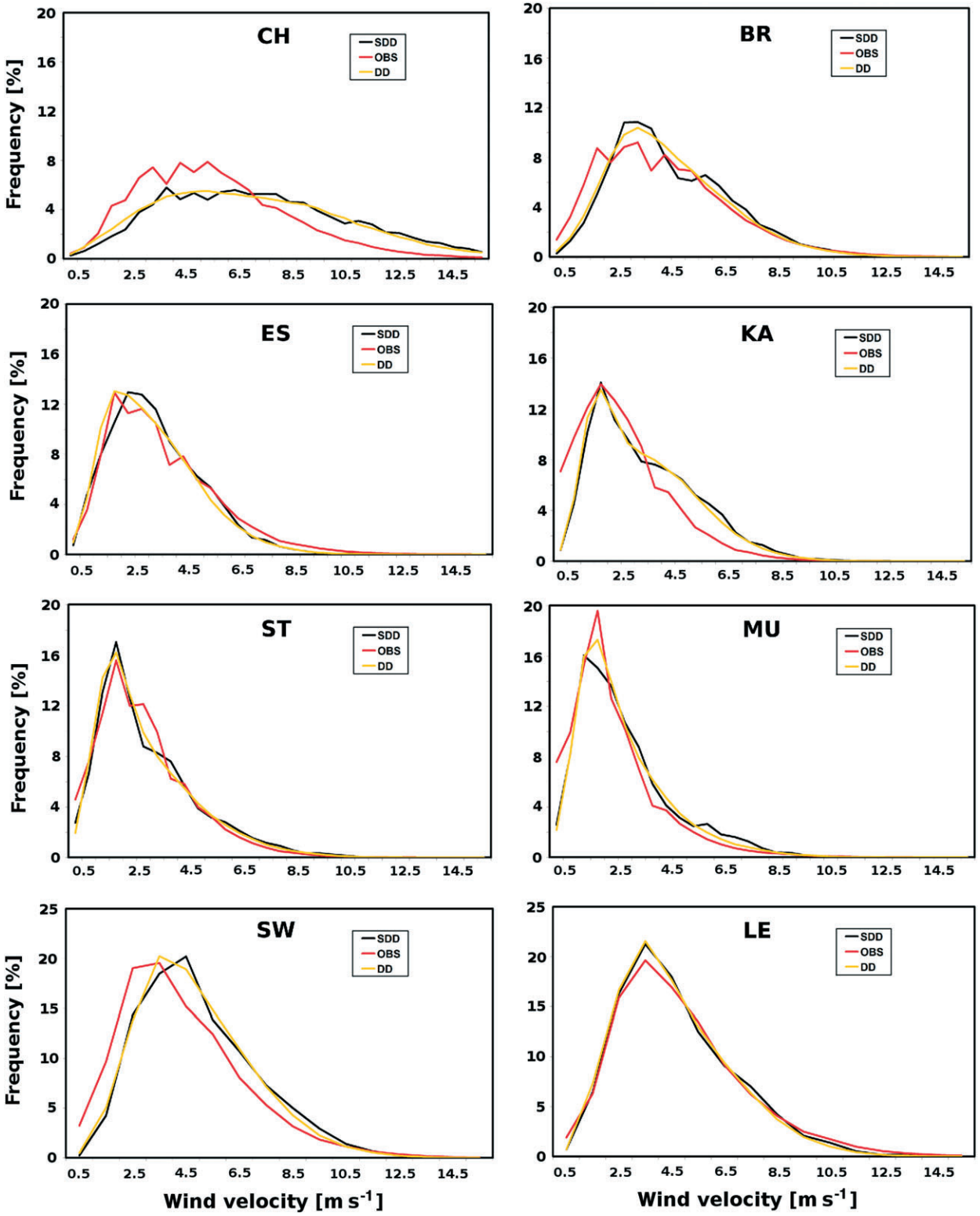

Figure 6. PDFs of the 10-m wind velocity for the period 1979–2010 at eight exemplary stations and at the corresponding CCLM grid points. Black line, SDD; dark grey line, observations; bright grey line, DD. Locations of the stations are shown in Figure 5(a). Please note that frequencies for the upper six stations are shown in 0.5 m s^{-1} intervals, and for the lower two stations in 1 m s^{-1} intervals.

account that the RMSE is inherently small over regions with low E_{out} and thus low variability (like e.g. the Alps) and vice versa, the RMSE is normed by the standard deviation of DD_{era}. Over central Europe, regions with small RMSE correspond well to regions with a high correlation between both time series (cf. Figure 9(a)). This implies that for these areas, SDD is not only able to capture the year-to-year variation in wind energy output (Figure 9(a)), but also simulates magnitudes of E_{out}, which are similar to that of DD_{era} (Figure 9(b)).

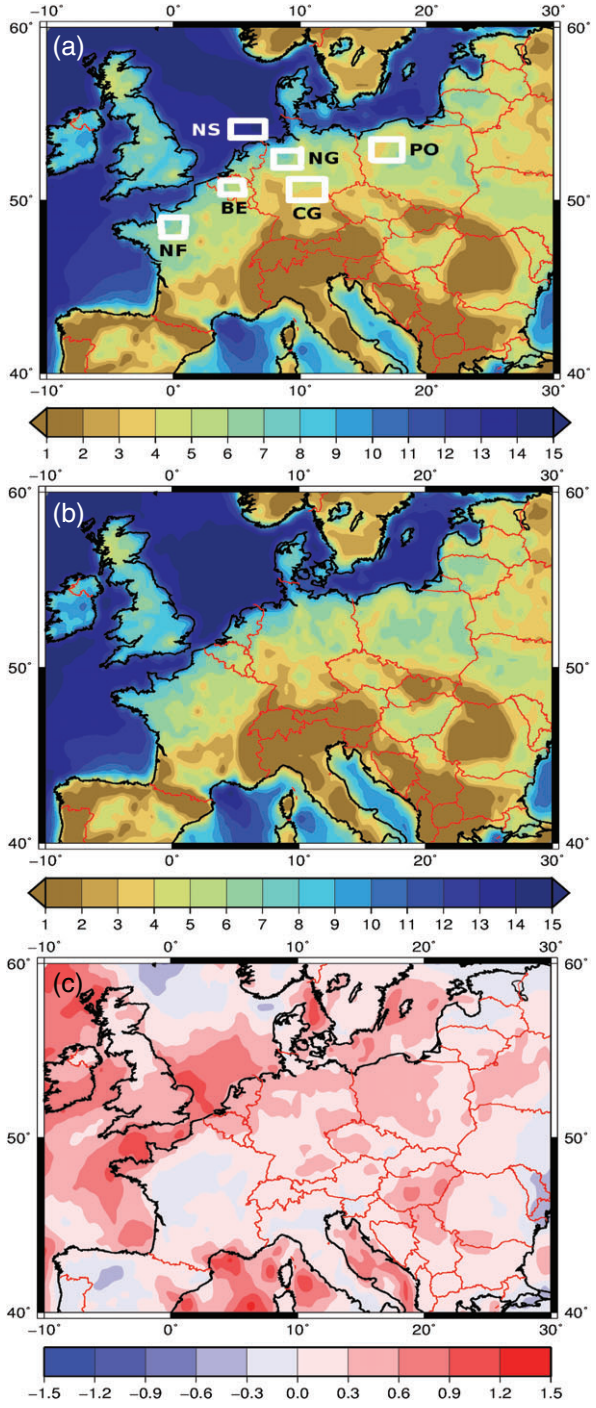

Figure 7. (a) Annual mean of E_{out} in 10^3 MWh year^{-1} for ERA-Interim (1979–2010) as obtained by DD_{era}. (b) Annual mean of E_{out} in 10^3 MWh year^{-1} for ERA-Interim (1979–2010) as obtained by SDD. (c) Difference between E_{out} from SDD and from DD_{era} in 10^3 MWh year^{-1}. The boxes in (a) represent sub-regions for the computation of E_{out} time series as shown in Figures 8 and 10.

4. Application to decadal hindcasts and predictions

The objective of this subsection is to investigate whether SDD is appropriate for the application to the full ensemble of the decadal prediction system of the MPI-ESM (520 decadal hindcasts and predictions with a length of 10 years). It should be kept in mind that a detailed evaluation of a potential predictive skill of the MPI-ESM on the regional scale is still ongoing and is not the purpose of this study. This will be analysed in a separate study.

Like for ERA-Interim, results of SDD application to MPI-ESM are compared to the outcomes of DD. Here, four selected decadal hindcasts are regarded. Again, simulated annual time series of E_{out} anomalies of both methods are compared. Figure 10 exemplary shows the annual E_{out} anomalies of both methods for the first realization of dec1980 (1 January 1981 to 31 December 1990). Despite a slightly lower variability of SDD, time series of both methods are quite similar. The accordance between SDD and DD_{1980_1} is highest for Belgium (BE), sub-regions in Germany, and Poland, while discrepancies are stronger for the sub-region in northern France and over the North Sea. Similar results are found for the first and tenth realization of dec1990 and the first realization of dec2000 (not shown). These outcomes are confirmed when regarding the correlation per grid point between the simulated time series of SDD and DD methods (Figure 11). For all four analysed hindcasts, correlations between SDD and DD are highest for grid points over Germany, for which the 77 weather classes were defined (see Section 2). High and, in most cases, significant correlations are also found for Poland and the Benelux. Also for the coastal areas of these countries, where high energy output is produced, SDD simulations agree well to the DD method. Compared to ERA-Interim (cf. Figure 9(a)) correlation between SDD and DD is lower at grid points over the Baltic States. Like for ERA-Interim, we have also computed the RMSE of the SDD time series relative to the time series as obtained by DD (not shown). Again, regions with small RMSE correspond well to regions with high correlations (cf. Figure 11), which means that the magnitudes of E_{out} as simulated by SDD are similar to those of DD for these areas (particularly Germany). To summarize, these results reveal that for onshore areas in central Europe, SDD is an appropriate alternative to time-consuming DD and can therefore be used as an applicable tool to analyse the full ensemble of the decadal prediction system of the MPI-ESM. An example for a potential application of SDD to determine a predictive skill of the MPI-ESM is given in Figure 12. For each realization of all yearly initialized decadal hindcasts and predictions, PDFs of the 10-m wind velocity for years 1–4 after initialisation are determined to generate 4-year running mean time series of E_{out}. Time series of the ensemble mean E_{out} as well as the standard deviation (SD) between the ten realisations for the sub-region in central Germany (CG) are shown in Figure 12(a). For comparison, the corresponding 4-year running mean time series as simulated by DD_{era} is presented. Not surprisingly, the ensemble mean time series of the MPI-ESM show a lower variability than time series from DD_{era}. At the same time, the spread between the different realisations is quite large, revealing that the uncertainty arising from different initialisations is very high in the MPI-ESM decadal prediction system. The correlations between the 4-year running mean time series of DD_{era} and

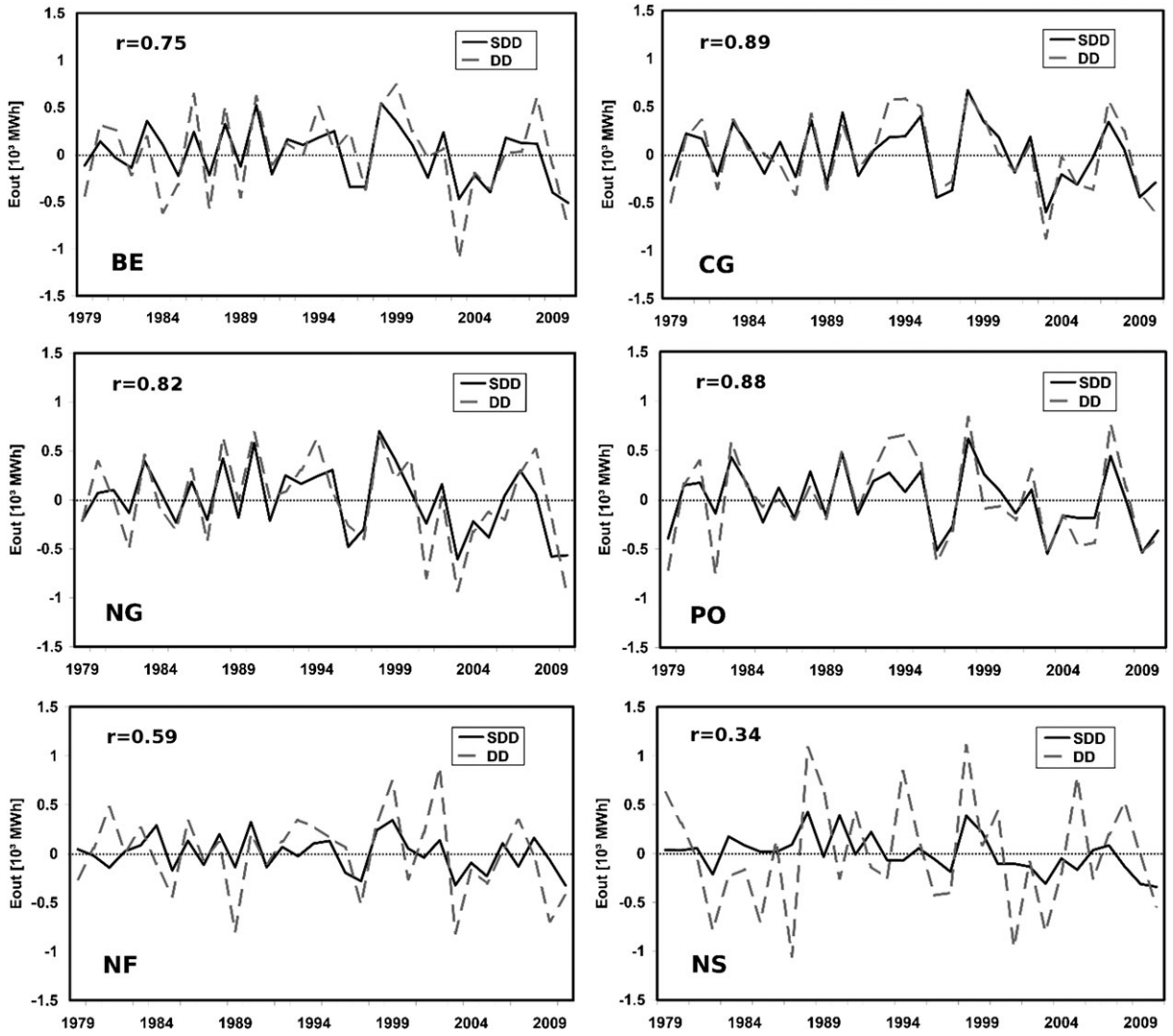

Figure 8. Time series of annual E_{out} anomalies in 10^3 MWh for the ERA-Interim period 1979–2010 as obtained by SDD (black solid line) and by DD_{era} (grey dashed line) for sub-regions in Belgium (BE), central Germany (CG), northern Germany (NG), Poland (PO), northern France (NF), and the North Sea (NS). For location of the sub-regions, see Figure 7(a). The correlations between SDD and DD time series are given in the upper left corner of each panel.

of the MPI-ESM ensemble mean for years 1–4 after initialisation are rather low or in some cases even negative for most grid points over central Europe (see Figure 12(b)). For countries in central Europe, only over The Netherlands and for a small region in Czech Republic, a significant positive correlation is found. These preliminary results suggest that with respect to wind energy on the regional scale, the predictive skill of the MPI-ESM decadal prediction system for short lead times is rather small, but a much deeper analysis is required to quantify the forecast skill.

5. Application to climate change projections

Finally, SDD is applied to different scenarios from the ECHAM5 model. The weather typing approach is applied to large-scale daily MSLP fields of the different ECHAM5 scenarios to obtain climatological PDFs of the 10-m wind velocity for the recent climate (20C, 1961–2000) and for the second half of the 21st century (A1B, B1, and A2 scenarios; 2061–2100, respectively). Then, the differences between the resulting E_{out} climatologies of the greenhouse gas scenarios and the 20C scenario are computed to determine climate change signals for wind energy (2061–2100 minus 1961–2000). For the A1B scenario, results are compared to Hueging *et al.* (2013), who used DD methods for their analysis. For consistency, ensemble means of the first and second realization of the scenarios are regarded.

The climatological regional E_{out} patterns for the ECHAM5 20C scenario (1961–2000) as obtained by SDD are comparable to the results of Hueging *et al.* (2013, cf. their figure 1(e)), with highest values over ocean surfaces and near the coasts and low energy output for southeast Europe (not shown).

The regional changes of E_{out} for 2061–2100 in the three SRES are shown in Figure 13. For the A1B scenario, annual changes as simulated by SDD (Figure 13(a)) are similar to the changes detected by Hueging *et al.*

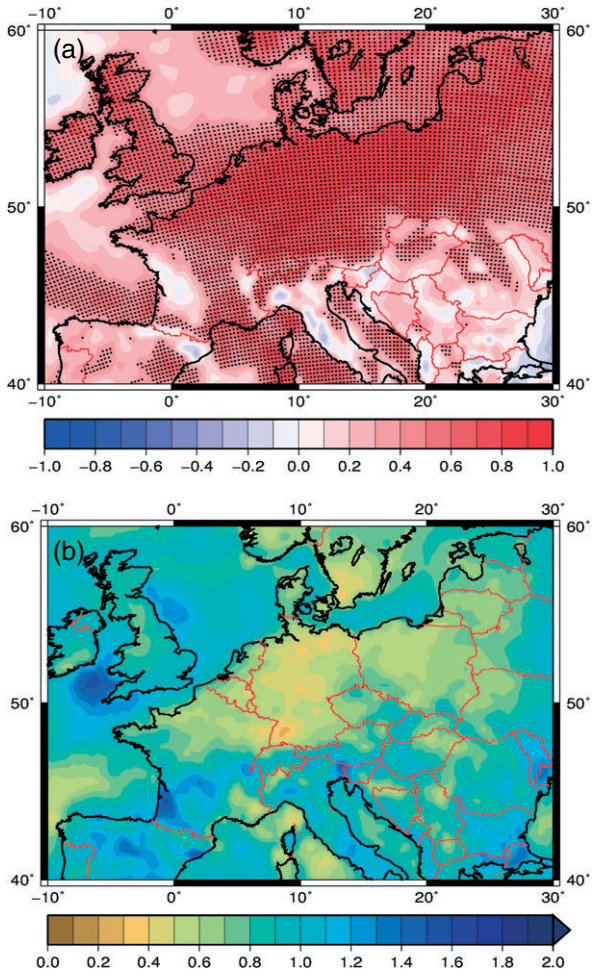

Figure 9. (a) Correlation between annual E_{out} time series of SDD and DD_{era} per CCLM grid point for the ERA-Interim period 1979–2010. Grid points with a significant correlation are dotted (*t*-test, 95% confidence level). (b) RMSE of annual E_{out} time series of SDD relative to DD_{era} time series per CCLM grid point for the ERA-Interim period 1979–2010, normed by the standard deviation of DD_{era}.

(2013, see their figure 3(g)). Although the magnitudes of the signals are somewhat weaker for SDD, regional trends of annual E_{out} are the same as in Hueging *et al.* (2013). Both, results of SDD and of Hueging *et al.* (2013), reveal increasing annual energy output over northern and northeast Europe and a decrease in E_{out} over southern Europe. Similar results are observed for changes in E_{out} during the winter months (December, January, February; see Figure 13(b)). Again, climate change signals as simulated by SDD are weaker than in Hueging *et al.* (2013, see their figure 3(i)), but regional patterns agree well in terms of the sign of the trend. Higher E_{out} for 2061–2100 is observed over northern and central Europe, whereas less energy output is simulated for the Mediterranean countries. Clear regional differences between SDD and Hueging *et al.* (2013) occur only for the climate change signals of the summer months (June, July, and August). While Hueging *et al.* (2013) detected a positive trend of E_{out} over the Baltic Sea (see their figure 3(k)), reduced E_{out} for 2061–2100 is simulated by SDD (Figure 13(c)). However, both methods reveal a decrease in E_{out} for Germany, Poland, Great Britain, and most parts of the Mediterranean countries.

The advantage of SDD is that it can also be applied to other greenhouse gas scenarios. Climate change signals of B1 are weaker than for the A1B scenario (Figure 13(d)–(f)), as one would expect. Apart from that, both scenarios show similar regional trends by the end of the 21st century, i.e. increasing E_{out} over northern Europe and decreasing E_{out} over southern Europe for the whole year and for the winter months, and a negative trend over central and western Europe for summer.

Regional changes of annual E_{out} in the A2 scenario have the same magnitude as in the A1B scenario (Figure 13(g)). Interestingly, differences between both scenarios are stronger in terms of the intra-annual changes. While the trend of E_{out} for the winter months is stronger in the A2 scenario over most parts of the central and northern Europe, in particular over Germany (Figure 13(h)), the decrease in E_{out} for June, July, and August is slightly weaker than in the A1B scenario (Figure 13(i)).

Despite slight discrepancies in the climate change projections for the A1B scenario compared to Hueging *et al.* (2013), these results reveal that the proposed SDD is an adequate downscaling tool for the analysis of wind energy changes in large ensembles of climate change scenarios, providing results consistent to DD methods in a cost-efficient way.

6. Summary and discussion

In this study, a SDD approach for the analysis of regional changes of wind energy output in large ensembles of decadal prediction systems and long-term climate projections is proposed and evaluated for different data sets. Here, SDD has been generated for applications to central Europe with special focus on Germany, for which the weather typing approach has been performed.

Regarding the verification of the SDD methodology and the comparison to observational data, SDD is able to derive realistic near-surface wind distributions for most stations in Germany. Some deficits can be observed for coastal stations, where simulated and observed PDFs of 10-m wind velocities differ. These discrepancies may in part be associated with the resolution of the model chain. At a horizontal resolution of 0.22° (~25 km), grid cells that correspond to stations at the coasts consist of not only land surfaces but also ocean surfaces, thus comprising unrealistic surface characteristics. Results for coastal areas would be improved by increasing the horizontal resolution of the simulated representative episodes by, for example, using a double nesting procedure. Despite these deficits, we conclude that SDD simulates realistic near-surface wind speeds and regional E_{out} patterns for recent climate conditions, and provides comparable results to the time-consuming pure DD approach. This assessment is valid for the entire European sector.

Regarding the application of SDD to decadal hindcasts, a good accordance between the SDD approach and DD

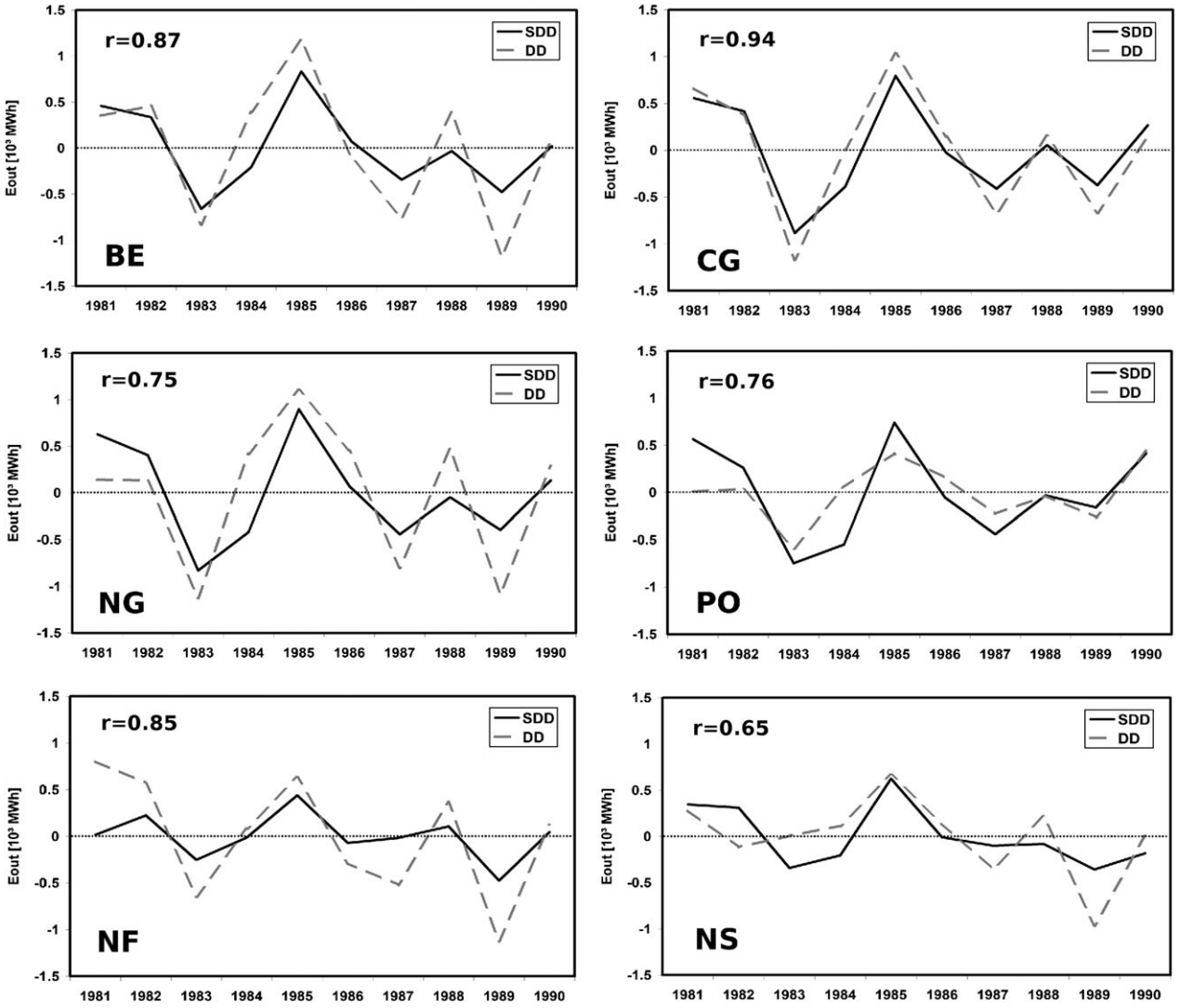

Figure 10. Time series of annual E_{out} anomalies in 10^3 MWh for the first realization of dec1980 (1981–1990) as obtained by SDD (black solid line) and by DD_{1980_1} (grey dashed line) for sub-regions in Belgium (BE), central Germany (CG), northern Germany (NG), Poland (PO), northern France (NF), and the North Sea (NS). For location of the sub-regions, see Figure 7(a). The correlations between SDD and DD time series are given in the upper left corner of each panel.

methods on timescales down to single years is found for Germany and nearby areas, particularly Poland, Czech Republic, and the Benelux countries. For four exemplary decadal hindcasts, high correlations between SDD- and DD-simulated annual E_{out} time series are found for these onshore areas. Lower correlations are detected for other European countries (e.g. France and Scandinavia) and for offshore areas, which implies that the applicability of SDD for decadal prediction systems as used in this study is limited to Germany and the surrounding countries. This is due to the considered weather typing approach that is representative for the large-scale flow over an area of roughly 20° by 30° centred over Germany (see Figure 2). The approach could also be applied for decadal predictions of wind energy in other regions of Europe simply by choosing different central points for the CWT classification, e.g. in Scandinavia or in southern Europe. For Germany and nearby areas, annual E_{out} time series as obtained by SDD show a slightly lower variability than DD-simulated time series. The consequences of this deficit for the detection of a predictive skill of decadal hindcasts (e.g. in terms of anomaly correlations) can be considered negligible, as for almost every year SDD simulates similar anomalies as DD in terms of the sign of E_{out}, as this effect can be easily scaled up. SDD has been employed to downscale the full ensemble of MPI-ESM that comprises 520 decadal hindcasts and predictions of a length of 10 years. Assuming a simulation time of ∼5 days per hindcast when using transient simulations with RCMs even on fast supercomputers, the regionalization of such a large ensemble can hardly be accomplished by purely DD methods. SDD, therefore, forms a suitable tool to analyse the predictive skill of decadal prediction systems with respect to wind energy on regional scales.

In this study, simulated representative days of the 77 classes have been forced with ERA-Interim. In a sensitivity study, we have repeated the procedure as applied to decadal hindcasts with a new set of representatives using

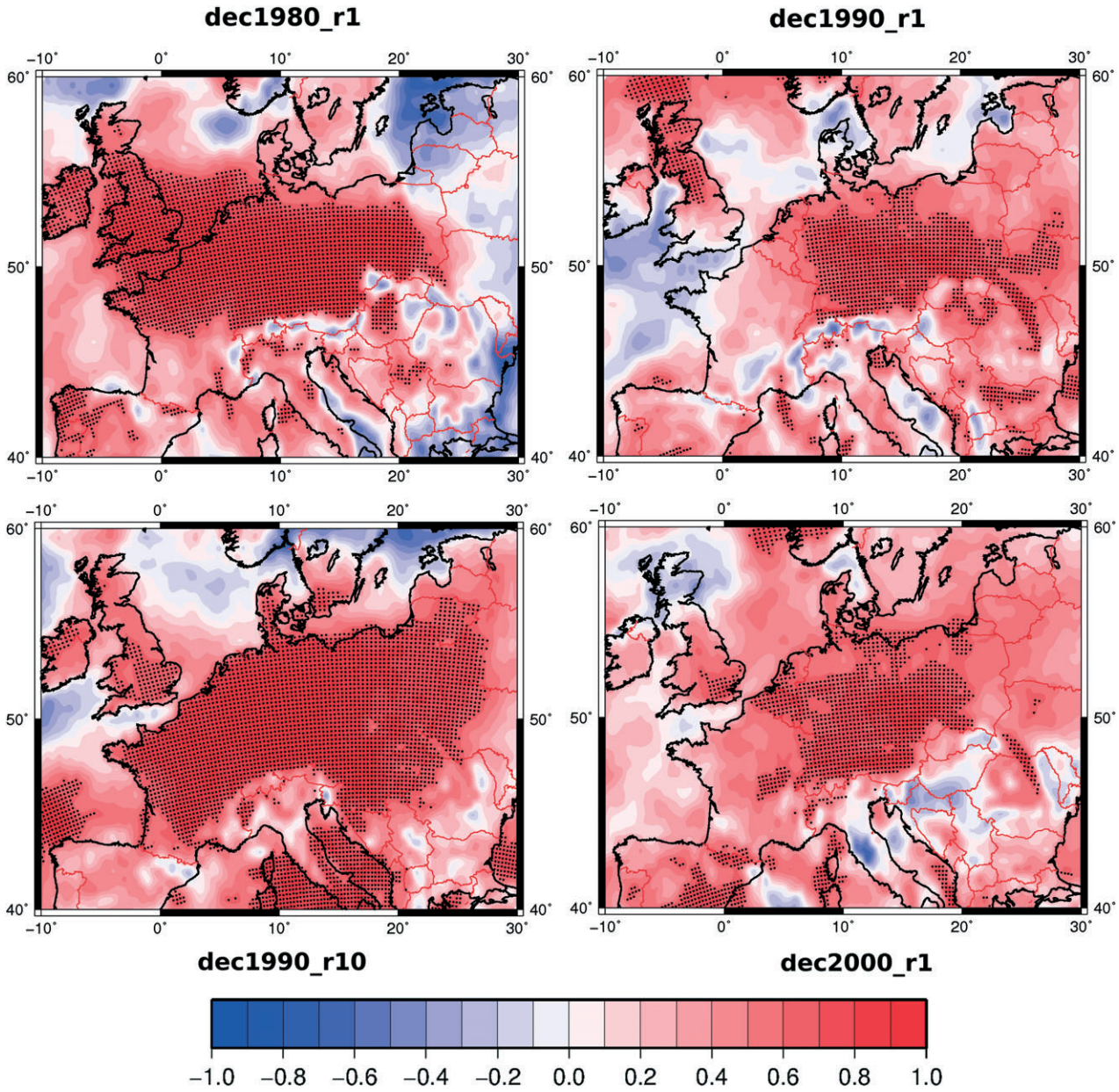

Figure 11. Correlation per CCLM grid point between annual E_{out} time series simulated by SDD and by DD for exemplary hindcasts dec1980_r1 (1981–1990), dec1990_r1 (1991–2000), dec1990_r10 (1991–2000), and dec2000_r1 (2001–2010). Grid points with a significant correlation are dotted (*t*-test, 95% confidence level).

large-scale fields of the MPI-ESM as boundary conditions. For Germany and nearby areas, results of the sensitivity study are quite similar to the results presented in this paper (e.g. annual E_{out} time series). Hence, the SDD method seems to be quite robust and the downscaled ERA-Interim-forced representatives used in this study can also be employed for the application of SDD to decadal prediction systems of other institutions contributing to CMIP5.

Regarding climate change applications, the SDD method performs well for the entire European sector, including Scandinavia and southern Europe. For example, long-term climate change projections of wind energy potentials as obtained by SDD agree well to the results of other studies using DD methods, with mean annual wind energy increasing over countries in northern Europe and decreasing over southern Europe in a future climate (cf. Hueging *et al.*, 2013). Furthermore, several studies reveal positive trends over the regions in northern Europe for future winter months and a decline in wind energy during the summer months (Nolan *et al.*, 2012; Hueging *et al.*, 2013), which is consistent with the findings of this study. These results suggest that ten representatives per class (see also Appendix S1) are sufficient to cover the main spectrum of potential European-wide spacious wind patterns that may occur within a class in climatological time periods. Compared to Hueging *et al.* (2013), the climate change signals of SDD are slightly weaker for most parts of Europe, hence the magnitude of the wind energy trends as simulated by SDD should be regarded with care. Here,

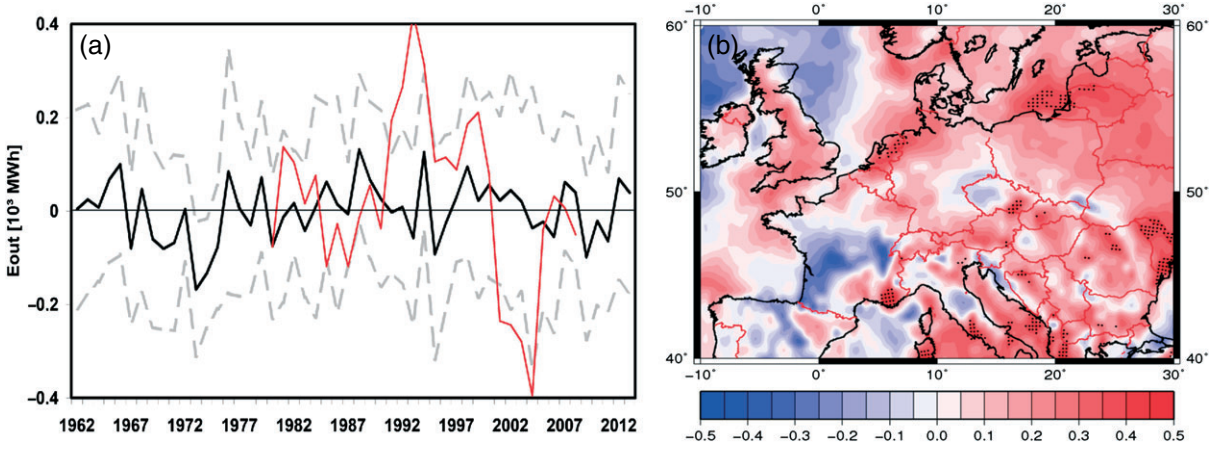

Figure 12. (a) Four-year running mean time series of E_{out} for years 1–4 after initialization for the MPI-ESM decadal hindcasts and predictions from dec1960 to dec2011 as obtained by the SDD method for a sub-region in central Germany (cf. Figure 7(a)). Shown is the ensemble mean over the ten realizations (black solid line), and the ensemble mean ± 1 SD of the ten ensemble members (grey dashed line). The thin grey line shows the 4-year running mean time series of DD_{era}. (b) Correlation between the 4-year running mean time series of DD_{era} (thin grey line in (a)) and of the MPI-ESM ensemble mean for years 1–4 after initialization (black solid line in (a)). Grid points with a significant correlation are dotted (*t*-test, 95% confidence level).

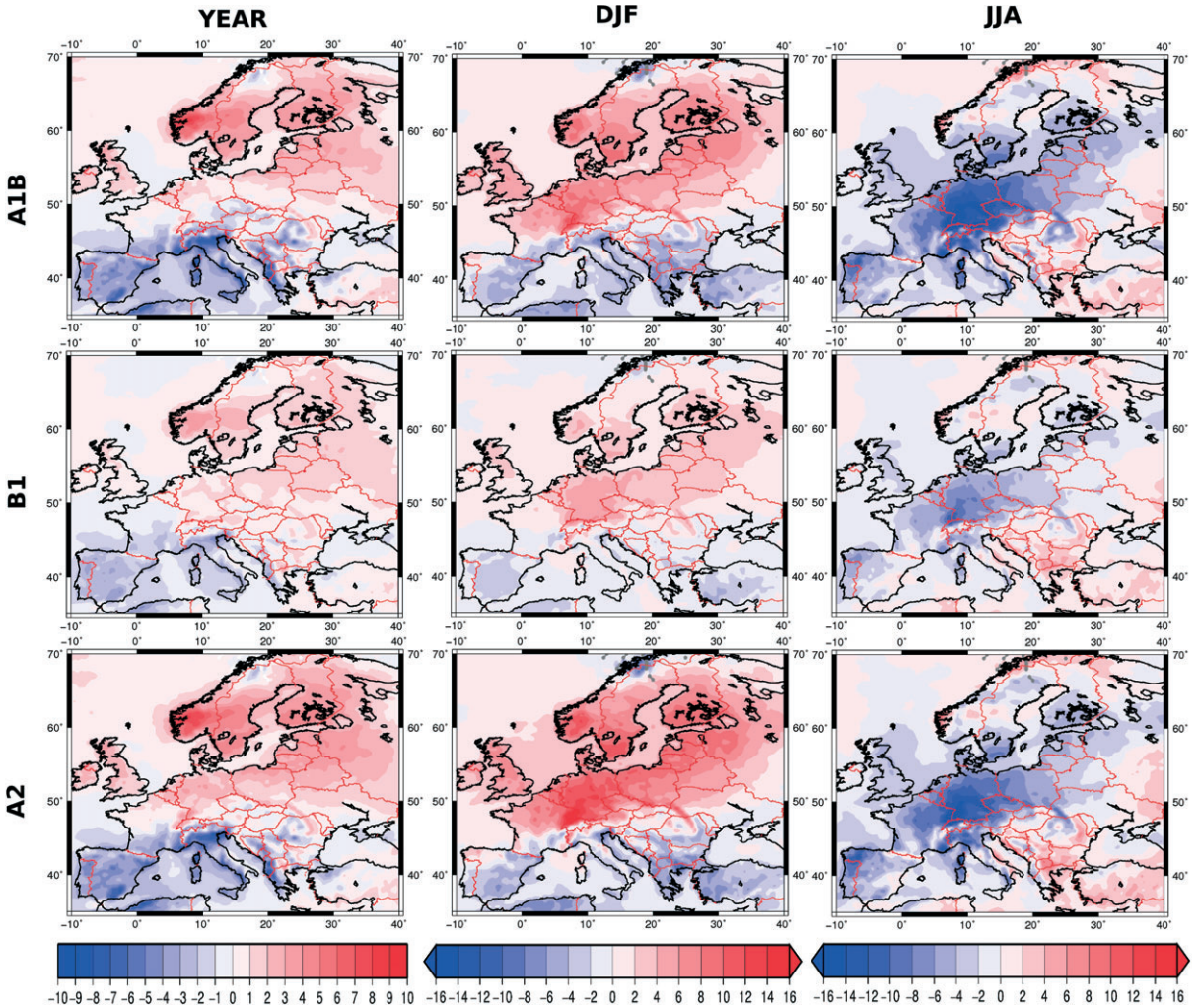

Figure 13. Regional changes (%) in E_{out} between ECHAM5 SRES (2061–2100) and the ECHAM5 20C scenario (1961–2000) as obtained by SDD for all year (annual, left column), winter (DJF, middle column), and summer (JJA, right column). Differences are shown for ensemble means of the first two realizations of the scenarios A1B (upper row), B1 (middle row), and A2 (lower row).

SDD has been employed to SRES of the GCM ECHAM5. As its application to other data sets requires only a new employment of the CWT analysis on global MSLP fields, while the other steps of the downscaling procedure are in principle the same as for ECHAM5, SDD can easily be applied to other GCMs. This enables an assessment of the uncertainty of long-term climate change projections that may arise not only from different scenarios but also from different GCMs. SDD is therefore an adequate tool to analyse regional wind energy changes in multi-model ensembles such as those released in the new CMIP5 (Taylor *et al.*, 2012), which includes current GCM data of 29 institutions.

We conclude that SDD is a suitable and inexpensive alternative to DD and that it can be easily applied for large ensemble of global runs. Although the current application focused on wind energy potentials for Germany, decadal hindcasts and climate change projections, the methodology has the potential for use in many other applications. Another potential valuable application could be, for example, the investigation of changes of surface wind percentiles in near- and long-term future. As PDFs of 10 m winds are computed in the third step of SDD (see Section 2), the same procedure and simulated representatives as used in this study could be employed for this purpose.

The here presented SDD methodology has been developed primarily for applications within the ongoing MiKlip consortium ('Mittelfristige Klimaprojektion', http://www.fona-miklip.de) and a detailed analysis of the forecast skill of the MPI-ESM decadal prediction system with respect to wind energy on the regional scale is still ongoing. With this aim, different deterministic and probabilistic metrics (see, for example, Goddard *et al.*, 2013) for estimating the predictive skill and the forecast uncertainty will be employed.

Acknowledgements

This research was supported by the German Federal Ministry of Education and Research (BMBF) under the project Probabilistic Decadal Forecast for central and western Europe (MiKlip -PRODEF, contract 01LP1120A), which is part of the MiKlip consortium ("Mittelfristige Klimaprojektion", http://www.fona-miklip.de). We thank the ECMWF for the ERA-Interim Reanalysis data set and the DWD for providing the wind speed data. We acknowledge the Max-Planck-Institute (Hamburg, Germany) for providing the GCM (ECHAM5 and MPI-ESM). We thank the German Climate Computer Centre (DKRZ, Hamburg) for computer and storage resources (project number 785 PRODEF). We thank the COSMO-CLM community and the members of MIKLIP-Module C (Regionalization) for discussions. We also thank Patrick Ludwig, Rabea Haas, and Hanna Hueging (University of Cologne) for discussions. Finally, we would like to thank the two anonymous reviewers for their helpful comments.

Supporting Information

The following supporting information is available as part of the online article:

Appendix S1. Sensitivity of the SDD to the number of simulated representatives.

Figure S1. PDFs of 10-m wind velocity for the period 1979–2010 at the two exemplary CCLM grid points corresponding to the stations Bremen (BR) and Stuttgart (ST). Thin black line: DD_{era}. Blue line: SDD with five simulated representative days per weather class (5repr). Red line: SDD with ten simulated representative days per weather class (10repr). Green line: SDD with 20 simulated representative days per weather class (20repr). Locations of the stations are shown in Figure 5(a).

References

Balmaseda MA, Mogensen K, Weaver AT. 2013. Evaluation of the ECMWF ocean reanalysis system ORAS4. *Q. J. R. Meteorol. Soc.* **139**: 1132–1161.

Dee DP, Uppala SM, Simmons AJ, Berrisford P, Poli P, Kobayashi S, Andrae U, Balmaseda MA, Balsamo G, Bauer P, Bechtold P, Beljaars ACM, van de Berg L, Bidlot J, Bormann N, Delsol C, Dragani R, Fuentes M, Geer AJ, Haimberger L, Healy SB, Hersbach H, Holm EV, Isaksen L, Kallberg P, Kohler M, Matricardi M, McNally AP, Monge-Sanz BM, Morcrette JJ, Park BK, Peubey C, de Rosnay P, Tavolato C, Thepaut JN, Vitart F. 2011. The ERA-Interim reanalysis: configuration and performance of the data assimilation system. *Q. J. R. Meteorol. Soc.* **137**: 553–597.

EEA. 2009. Europe's onshore and offshore wind energy potential: an assessment of environmental and economic constraints. EEA Tech. Rep. 6/2009, European Environmental Agency, Copenhagen, 88 p.

Fuentes U, Heimann D. 2000. An improved statistical–dynamical downscaling scheme and its application to the Alpine precipitation climatology. *Theor. Appl. Climatol.* **65**: 119–135.

General Electric. 2010. 2.5 MW wind turbine series. GE Brochure GEA17007B, General Electric, Fairfield, CT, 16 p, http://www.geenergy.com/content/multimedia/_files/downloads/GEA17007AWind25Brochure.pdf.

Giorgi F, Jones C, Asrar GR. 2006. Adressing climate information needs at the regional level: the CORDEX framework. *Bull. World Meteorol. Organ.* **58**: 175–183.

Goddard L, Kumar A, Solomon A, Smith D, Boer G, Gonzale P, Kharin V, Merryfield W, Deser C, Mason SJ, Kirtman BP, Msadek R, Sutton R, Hawkins E, Fricker T, Hegerl G, Ferro CAT, Stephenson DB, Meehl GA, Stockdale T, Burgman R, Greene AM, Kushnir Y, Newman M, Carton J, Fukumori I, Delworth T. 2013. A verification framework for interannual-to-decadal predictions systems. *Clim. Dyn.* **40**: 245–272.

Harvey BJ, Shaffrey LC, Woollings TJ, Zappa G, Hodges KI. 2012. How large are projected 21st century storm track changes? *Geophys. Res. Lett.* **39**: L18707, DOI: 10.1029/2012GL052873.

Hewitson BC, Crane RG. 1996. Climate downscaling: techniques and application. *Climate Res.* **7**: 85–95.

Hueging H, Born K, Haas R, Jacob D, Pinto JG. 2013. Regional changes in wind energy potential over Europe using regional climate model ensemble projections. *J. Appl. Meteorol. Climatol.* **52**: 903–917.

IEC. 2005a. Wind turbines – part 1: design requirements. IEC 61400-1, International Electrotechnical Commission. Geneva, Switzerland, 179 p.

IEC. 2005b. Wind turbines – part 3: design requirements for offshore wind turbines. IEC 61400-3, International Electrotechnical Commission. Geneva, Switzerland, 263 p.

Jenkinson AF, Collinson FP. 1977. An initial climatology of gales over the North Sea. In *Synoptic Climatology Branch Memorandum, No. 62*. Meteorological Office: Bracknell, UK.

Jones PD, Hulme M, Briffa KR. 1993. A comparison of lamb circulation types with an objective classification scheme. *Int. J. Climatol.* **13**: 655–663.

Jones PD, Harpham C, Briffa KR. 2012. Lamb weather types derived from reanalysis products. *Int. J. Climatol.* **33**: 1129–1139.

Jungclaus JH, Keenlyside N, Botzet M, Haak H, Luo J-J, Latif M, Marotzke J, Mikolajewicz U, Roeckner E. 2006. Ocean circulation and tropical variability in the coupled model ECHAM5/MPI-OM. *J. Clim.* **19**: 3952–3972.

Lamb HH. 1972. British Isles weather types and a register of the daily sequence of circulation patterns 1981–1971. In *Geophysical Memoir, No. 116*. HMSO, 85 p: London.

Manwell JF, McGrown JG, Rogers AL. 2009. *Wind Energy Explained, Theory, Design and Application*, 2nd edn. Wiley, 704 p: Chichester, UK.

Maraun D, Wetterhall F, Ireson AM, Chandler RE, Kendon EJ, Goodess CM, Jones RG, Onof C, Vrac M, Thiele-Eich I. 2010. Precipitation downscaling under climate change: recent developments to bridge the gap between dynamical models and the end user. *Rev. Geophys.* **48**: RG3003, DOI: 10.1029/2009RG000314.

Merryfield WJ, Lee WS, Boer GJ, Kharin VV, Scinocca JF, Flato GM, Ajayamohan RS, Fyfe JC, Tang M, Polavarapu S. 2013. The Canadian Seasonal to Interannual Prediction System. Part I: models and initialization. *Mon. Weather Rev.* **141**: 2910–2945.

Moccia J, Arapogianni A, Wilkes J, Kjaer C, Gruet R. 2011. Pure power – wind energy targets for 2020 and 2030. European Wind Energy Association Report, EWEA, Brussels, 98 p, http://www.ewea.org/fileadmin/files/library/publications/reports/Pure_Power_III.pdf.

Mueller WA, Baehr J, Haak H, Jungclaus JH, Kroeger J, Matei D, Notz D, Pohlmann H, von Storch JS, Marotzke J. 2012. Forecast skill of multi-year seasonal means in the decadal prediction system of the Max Planck Institute for Meteorology. *Geophys. Res. Lett.* **39**: L22707, DOI: 10.1029/2012GL053326.

Najac J, Lac C, Terray L. 2011. Impact of climate change on surface winds in France using a statistical-dynamical donwscaling method with mesoscale modelling. *Int. J. Climatol.* **31**: 415–430, DOI: 10.1002/joc.2075.

Nakicenovic N, Swart R. 2000. Emission scenarios. A Special Report of Working Group III of the Intergovernmental Panel on Climate Change, Cambridge University Press. Cambridge, UK, 599 p.

Nolan P, Lynch P, McGrath R, Semmler T, Wang SY. 2012. Simulating climate change and its effect on the wind energy resource of Ireland. *Wind Energy* **15**: 593–608.

Ouammi A, Ghigliotti V, Robba M, Mimet A, Sacile R. 2012. A decision support system for the optimal exploitation of wind energy on regional scale. *Renew. Energy* **37**: 299–309.

Pinto JG, Neuhaus CP, Leckebusch GC, Reyers M, Kerschgens M. 2010. Estimation of wind storm impacts over West Germany under future climate conditions using a statistical-dynamical downscaling approach. *Tellus A* **62**: 188–201, DOI: 10.1111/j.1600-0870.2009.00424.x.

Pryor SC, Barthelmie RJ. 2010. Climate change impacts on wind energy: a review. *Renew. Sustain. Energy Rev.* **14**: 430–437.

Pryor SC, Schoof JT, Barthelmie RJ. 2005. Empirical downscaling of wind speed probability distributions. *J. Geophys. Res.* **110**: D19109, DOI: 10.1029/2005JD005899.

Rockel B, Will A, Hense A. 2008. Special issue: regional climate modelling with COSMO-CLM (CCLM). *Meteorol. Z.* **17**: 347–348.

Roeckner E, Brokopf R, Esch M, Giorgetta M, Hagemann S, Kornblueh L, Manzini E, Schlese U, Schulzweida U. 2006. Sensitivity of simulated climate to horizontal and vertical resolution in the ECHAM5 atmosphere model. *J. Clim.* **19**: 3771–3791.

Solomon S, Qin D, Manning M, Chen Z, Marquis M, Averyt K, Tignor MMB, Miller JR, Eds HL. 2007. *Climate Change 2007: The Physical Science Basis*. Cambridge University Press: Cambridge, UK, 996 p.

Taylor KE, Stouffer RJ, Meehl GA. 2012. An overview of CMIP5 and the experiment design. *Bull. Am. Meteorol. Soc.* **93**: 485–498.

Ulbrich U, Pinto JG, Kupfer H, Leckebusch GC, Spangehl T, Reyers M. 2008. Changing northern hemisphere storm tracks in an ensemble of IPCC climate change simulations. *J. Clim.* **21**: 1669–1679.

Wilby RL, Wigley TML. 1997. Downscaling general circulation model output: a review of methods and limitations. *Prog. Phys. Geogr.* **21**: 530–548.

Wilkes J, Moccia J, Dragan M. 2012. Wind in power – 2011 European statistics. European Wind Energy Association Report, EWEA, Brussels, 11 p, http://www.ewea.org/fileadmin/files/library/publications/statistics/Wind_in_power_2011_European_statistics.pdf.

Woollings T, Gregory JM, Pinto JG, Reyers M, Brayshaw DJ. 2012. Response of the North Atlantic storm track to climate change shaped by ocean-atmosphere coupling. *Nat. Geosci.* **5**: 313–317.

10.2 Weber et al. (2018)

Reference:

Weber, J., Wohland, J., Reyers, M., Moemken, J., Hoppe, C., Pinto, J. G., and Witthaut, D. (2018). Impact of climate change on backup energy and storage needs in wind-dominated power systems in Europe. *PLOS ONE*. doi:10.1371/journal.pone.0201457, accepted

Page numbers are as submitted to *PLOS ONE*.

Impact of climate change on backup energy and storage needs in wind-dominated power systems in Europe

Juliane Weber[1,2*], Jan Wohland[1,2], Mark Reyers[3], Julia Moemken[4], Charlotte Hoppe[5,6], Joaquim G. Pinto[4], Dirk Witthaut[1,2]

1 Forschungszentrum Jülich, Institute of Energy and Climate Research – Systems Analysis and Technology Evaluation (IEK-STE), Jülich, Germany

2 University of Cologne, Institute for Theoretical Physics, Cologne, Germany

3 University of Cologne, Institute for Geophysics and Meteorology, Cologne, Germany

4 Karlsruhe Institute of Technology, Institute of Meteorology and Climate Research, Karlsruhe, Germany

5 Forschungszentrum Jülich, Institute of Energy and Climate Research – Troposphere (IEK-8), Jülich, Germany

6 University of Cologne, Rhenish Institute for Environmental Research, Cologne, Germany

* ju.weber@fz-juelich.de

Abstract

The high temporal variability of wind power generation represents a major challenge for the realization of a sustainable energy supply. Large backup and storage facilities are necessary to secure the supply in periods of low renewable generation, especially in countries with a high share of renewables. We show that strong climate change is likely to impede the system integration of intermittent wind energy. To this end, we analyze the temporal characteristics of wind power generation based on high-resolution climate projections for Europe and uncover a robust increase of backup energy and storage needs in most of Central, Northern and North-Western Europe. This effect can be

traced back to an increase of the likelihood for long periods of low wind generation and an increase in the seasonal wind variability.

Introduction

The mitigation of climate change requires a fundamental transformation of our energy system. Currently, the generation of electric power with fossil fuel-fired power plants is the largest source of carbon dioxide emissions with a share of approximately 35 % of the global emissions [1]. These power plants must be replaced by renewable sources such as wind turbines and solar photovoltaics (PV) within at most two decades to meet the 2°C or even the 1.5°C goal of the Paris agreement [2–4]. While wind and solar power have shown an enormous progress in efficiency and costs [5, 6], the large-scale integration into the electric power system remains a great challenge.

The operation of wind turbines is determined by weather and climate and thus strongly depends on the regional atmospheric conditions. Hence, the generated electric power is strongly fluctuating on different time scales. These fluctuations are crucial for system operation [6–11]. In particular, large storage and backup facilities are needed to guarantee supply also during periods of low wind generation [12–14]. How does climate change affect these fluctuations and the challenges of system integration? Previous studies have addressed the impact of climate change on the availability of cooling water [15, 16], the energy demand [17, 18], the combination of run-of-river and PV [19] or the change of global energy yields of wind and solar power [20–27]. However, the potentially crucial impact of climate change on temporal wind fluctuations has not yet been considered in the literature. In this article, we provide an in-depth analysis of the temporal statistics of wind generation in a changing climate and we assess their potential impact on energy system operation.

A consensus exists about general changes in the mean sea level pressure and circulation patterns in the European/North Atlantic region [28–31]. A projected increase of the winter storminess over Western Europe [32, 33] leads to enhanced wind speeds over Western and Central Europe, while in summer a general decrease is identified [23–25, 34]. This can lead to a strong increase of the seasonal variability of wind power generation and thus impede system integration, even though the annual

mean changes are comparatively small.

In this article, we study how climate change affects the temporal characteristics of wind power generation and the necessity for backup and storage infrastructures in wind-dominated power systems in individual European countries and for a perfectly interconnected European power system. Our analysis is based on five state-of-the-art global circulation models (GCMs) downscaled by the EURO-CORDEX initiative [35,36]. We complement our results with an assessment of the large ensemble of the Coupled Model Intercomparison Project Phase 5 (CMIP5, [37]) based on circulation weather types [38]. The paper is organized as follows. We first introduce our model to derive the backup need of a country as a function of the storage capacity. Additionally, we present the methods to analyze the CMIP5 ensemble. Afterwards we report our results. The article closes with a discussion.

Methods

The operation of future renewable power systems with large contributions of wind crucially depends on weather and climate. GCMs are used to simulate the dynamics of the earth system on coarse spatial scales for different scenarios of future greenhouse gas concentrations (representative concentration pathways, RCPs [39]). To analyze the operation of the electric power system, a high spatial and temporal resolution is required. Our analysis is thus based on a subset of the EURO-CORDEX ensemble which provides dynamically downscaled climate change data at high resolution (0.11° and 3 hours). Time series for the aggregated wind power generation in a country are obtained from the near-surface wind speed (see Fig 1a, b).

Backup and storage infrastructures are needed when renewable generation drops below load. In order to quantify the necessary amount of backup and storage to ensure a stable supply, we adopt a coarse-grained model of the electric power system (see Fig 1c, d). Backup and storage needs crucially depend on the temporal characteristics of wind power generation, in particular the length of periods with low wind generation and the seasonal variability. In the present paper, we thus focus on temporal characteristics and their potential alteration due to climate change.

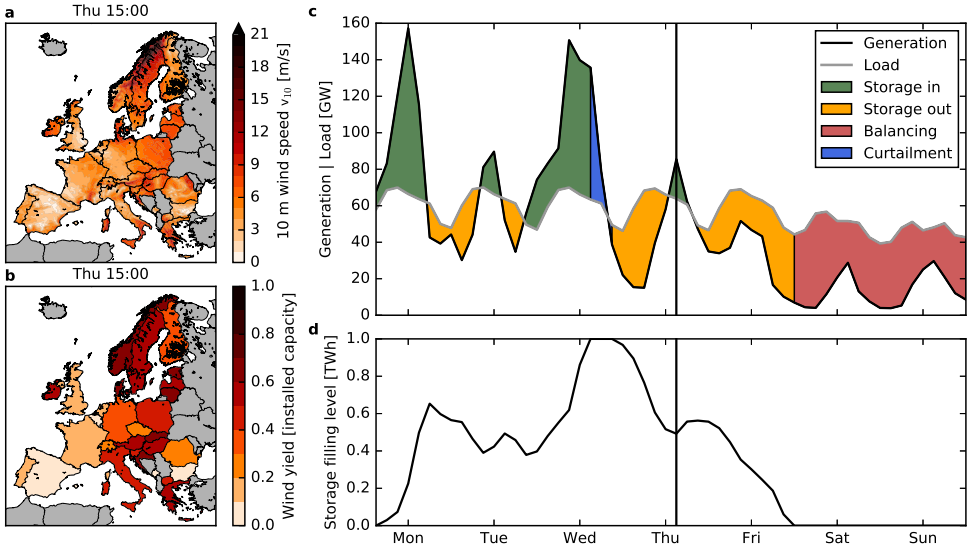

Fig 1. Conversion of near-surface wind speeds to country-wise aggregated wind power generation combined with backup and storage infrastructures. **a**, Near-surface wind velocities of the downscaled ERA-Interim data over Europe for one exemplary point in time. **b**, Corresponding estimated wind power yield for each country in units of the installed capacity at this exemplary time step. **c**, Renewable generation (black) and load (grey) in Germany for one exemplary week in spring assuming a power system with 100 % wind power on average. The vertical line denotes the time selected in panels **a** and **b**. The color indicates the operation of the storage system. Green: Excess power is stored. Yellow: Residual load is covered by the storage. Red: Residual load is covered by backup power plants as the storage is empty. Blue: Excess power must be curtailed as the storage is fully charged. **d**, Evolution of the storage filling level $S(t)$.

Wind power generation time series

Our analysis is based on a subset of the EURO-CORDEX regional climate simulations which provides dynamically downscaled climate change data at high resolution for Europe based on five GCMs: CNRM-CM5, EC-EARTH, HadGEM2-ES, IPSL-CM5A-MR, MPI-ESM-LR [35] (see also Table A in S1 Appendix). All data is freely available for example at the ESGF (Earth System Grid Federation) node at DKRZ (German Climate Computing Centre) [40]. The five models are downscaled using the hydrostatic Rossby Centre regional climate model RCA4 [41, 42]. The downscaling provides continuous surface (10 m) wind data from 1970 to 2100 with a spatial resolution of 0.11° and a temporal resolution of $T = 3$ hours. Unfortunately, downscaled data at this high spatial and temporal resolution is not yet available for more GCMs or for different regional climate models at ESGF [40]. Considering the use of only one regional climate model, Moemken *et al.* [25] show that differences between different

GCMs are usually larger than differences between different regional climate models.

We analyze a strong climate change scenario (RCP8.5) using a rising radiative forcing pathway leading to additional 8.5 W/m^2 (∼1370 ppm CO_2 equivalent) by 2100 and a medium climate change scenario (RCP4.5, ∼650 ppm CO_2 equivalent, see S3 Appendix) [39]. We compare two future time frames, 2030-2060 (mid century, 'mc') and 2070-2100 (end of century, 'eoc'), to a historical reference time frame (1970-2000, 'h').

The calculation of wind power generation requires wind speeds at the hub height of wind turbines. As the high resolution wind velocities are only available at a height of $z_0 = 10$ m, they must be extrapolated to a higher altitude. We choose a hub height of $z = 90$ m as in [22] and extrapolate the surface wind velocities v_{z_0} using a power law formula: $v_z = v_{z_0}\,(z/z_0)^{1/7}$ [43]. Although widely used, this simple formula is only valid for smooth open terrain and only applies for a neutrally stable atmosphere [44, 45]. Unfortunately, the available data set does not allow to assess the stability of the atmosphere. Thus, it is unclear how to improve the scaling law with the present data available. Tobin *et al.* [22] show in a sensitivity study that their results hardly depend on the extrapolation technique or on the chosen hub height. They further state that the "uncertainty related to climate model formulation prevails largely over uncertainties lying in the methodology used to convert surface wind speed into power output".

The wind generation is derived using a standardized power curve with a cut-in wind speed of $v_i = 3.5$ m/s, a rated wind speed of $v_r = 12$ m/s and a cut-out wind speed of $v_o = 25$ m/s as in [22]. The capacity factor $CF(t)$ (i.e. the generation normalized to the rated capacity) then reads

$$CF(t) = \begin{cases} 0 & \text{if } v_z(t) < v_i \text{ or } v_z(t) \geq v_o. \\ \frac{v_z^3(t) - v_i^3}{v_r^3 - v_i^3} & \text{if } v_i \leq v_z(t) \leq v_r \\ 1 & \text{else.} \end{cases} \tag{1}$$

In order to account for wind farms and regional (or sub-cell) velocitiy variations, the power curve is smoothed using a gaussian kernel (see Fig A in S1 Appendix)

$$\mathrm{Ker}(v) = \frac{1}{\sqrt{2\pi\sigma^2}} \exp\left[\frac{-\left(v_0 - v\right)^2)}{2\sigma^2}\right], \tag{2}$$

where we chose $v_0 = v_{\max}/2 + 0.3$ m/s and $\sigma = 1$ m/s with $v_{\max}$ being the maximum of

the occurring wind velocities v at hub height. The parameters were chosen such that the rated wind power output is reached for wind speeds which are a little bit higher than the chosen rated wind speed [43, 46].

To obtain the gross generation per country, we equally distribute wind farms on grid points for which the local average wind yield is higher than the country average (see Fig B in S1 Appendix) [47]. The distribution is fixed using historical reanalysis data from ERA-Interim [48] downscaled by the EURO-CORDEX initiative [35, 41] to guarantee consistency (cf. Fig 1b). We do not use the wind farm distribution as of today because installed capacities in a fully-renewable power system will be much higher and also more widespread than they are today such that wind parks will be built in yet unused locations. Furthermore, it was shown in [47, 49] that different wind farm distributions do not significantly affect the results (see also Figs D-F in S4 Appendix where we tested a homogeneous wind farm distribution within each country).

Wind power generation is aggregated using two approaches: (a) aggregation per country neglecting transmission constraints, assuming an unlimited grid within each country; (b) aggregation over the whole European continent, assuming a perfectly interconnected European power system (copperplate). If we find the same results for both cases, we can assume that these results also hold for the intermediate case. The intermediate case is discussed elsewhere [50, 51] for current climatic conditions and in Wohland *et al.* [52] for a changing climate but without considering storage.

As the temporal characteristics of offshore and onshore wind power highly differ from each other, it is important to assess the impact of climate change on offshore and onshore wind separately – at least in a first step. Therefore, in this study, offshore sites are not considered.

For the load time series $L(t)$ we use data of the year 2015 provided by the European Network of Transmission System Operators for Electricity (ENTSO-E, [53]) and repeat this year 31 times. The load time series have been adapted to the calendars of the individual models, if necessary, by e.g. removing the 31st of a month for HadGEM2-ES, which uses a 30-day calendar, or by constructing an additional day for leap years by repeating the 28th of February. In order to avoid trends in the load timeseries, we consider a single year only. Furthermore, we show in a sensitivity study assuming constant loads that our results dominantly depend on the generation timeseries and are

hardly affected by the load time series (see Fig C in S4 Appendix). Throughout all time frames we assume that wind power provides a fixed share γ of the load $L(t)$ per country [12]. Hence, the fluctuating wind power generation $R(t)$ is scaled such that

$$R(t) = \gamma \frac{CF(t)}{\langle CF(t) \rangle} \langle L(t) \rangle, \tag{3}$$

where the brackets denote the average over the respective time frame for a given model. This procedure normalizes out a possible change of the gross wind power yield, and thus allows to isolate the effects of a change in the temporal distribution of the renewable generation. As a consequence, in all considered time frames (historical, mid century and end of century), the total amount of energy generated by wind power plants is the same. Only changes in the temporal aspects such as the duration of low-wind periods or the seasonal wind variability can lead to changes in backup energy and storage needs (see the following sections). For the copperplate assumption, the wind power generation is scaled such that each country provides a fixed share γ of the country-specific load. Afterwards, the country-specific wind power generation is summed-up to one aggregated time series. In the main manuscript, we focus on a fully renewable power system per country, i.e., $\gamma = 1$. Results for different values of γ are shown in Figs A and B in S4 Appendix.

Calculation of backup energy needs

Country-wise aggregated wind generation and load data are used to derive the backup energy need of a country given different storage capacities. At each point of time t power generation and consumption of a country must be balanced [12, 50, 54]

$$R(t) + B(t) = \Delta(t) + L(t) + C(t), \tag{4}$$

where $R(t)$ and $B(t)$ denote the generation by fluctuating renewables and dispatchable backup generators, respectively, $L(t)$ is the load and $C(t)$ denotes curtailment (cf. Fig 1c). $\Delta(t)$ is the generation ($\Delta(t) < 0$) or load ($\Delta(t) > 0$) of the storage facilities,

such that the storage filling level evolves according to (cf. Fig 1d)

$$S(t+T) = S(t) + \Delta(t) \cdot T. \tag{5}$$

where T is the duration of one time step (here: 3 hours). The storage filling level must satisfy $0 \leq S(t) \leq S_{\max}$ with $S_{\max}$ being the storage capacity. We decide to minimize the total backup energy

$$\min B_{\text{tot}} = \sum_t B(t) \cdot T \tag{6}$$

which also minimizes fossil-fuel usage and hence greenhouse gas emissions. One option to minimize B_{tot} is to consider a storage-first strategy [54], which we apply sequentially: In the case of overproduction (i.e. $R(t) > L(t)$) excess energy is stored until the storage device is fully charged,

$$\Delta(t) = \min[R(t) - L(t); (S_{\max} - S(t))/T]. \tag{7}$$

To ensure power balance, we may need curtailment

$$C(t) = R(t) - L(t) - \Delta(t). \tag{8}$$

In the case of scarcity (i.e. $R(t) < L(t)$) energy is provided by the storage infrastructures until they are empty,

$$\Delta(t) = -\min[L(t) - R(t); S(t)/T]. \tag{9}$$

The missing energy has to be provided by backup power plants,

$$B(t) = L(t) - R(t) + \Delta(t). \tag{10}$$

The backup power B is not restricted in our model and can be interpreted as the aggregated amount of backup power per country, not differentiating between different technologies. In order to keep the storage neutral, a periodic boundary condition is applied [55]: We run the above algorithm twice. First, we choose $S(t=0) = S_{\max}/2$. In the second run, we set $S(t=0)$ to $S(t=t_{\max})$ of the first run. This way, the storage

filling level at $t = t_{\max}$ equals the initial storage filling level at $t = 0$. We emphasize that by the term 'storage' we mean storage regardless of the technical realization. Hence, $S_{\max}$ describes the total accumulated storage capacity, including virtual storage. For simplicity, we neglect losses in the storage process.

In the figures we show the average backup energy per year $E = \langle B \rangle / \langle L \rangle \cdot L_{\text{year}}$. L_{year} is the average yearly gross electricity demand of the respective country. Thus, E/L_{year} gives the share of energy that has to be provided by dispatchable backup generators [54].

Persistence of low wind situations

We measure the probability for long low-wind periods during which a high amount of energy is required from storage devices and backup power plants. Therefore, we identify all periods for which the wind power generation is continuously smaller than average (i.e. $R(t) < \langle R \rangle$) and record their duration τ. We decided to choose $\langle R \rangle$ as threshold value because we are interested in long periods of underproduction, which cause the storage to become depleted such that backup energy is required. From the single durations τ, we can estimate a probability distribution. Extreme events are quantified by the 95 % quantile of the distribution.

Seasonal wind variability

The wind yield in Europe is usually higher in winter than in summer. An increasing seasonal wind variability would refer to higher wind yields in the winter months and/or lower wind yields in the summer months and would lead to higher backup energy needs during summer.

We define the winter-summer ratio of the country-wise aggregated wind power generation as the ratio of the average winter wind generation $\langle R \rangle_{\text{DJF}}$ and the average summer wind generation $\langle R \rangle_{\text{JJA}}$:

$$R_{\text{winter}-\text{summer}} = \frac{\langle R \rangle_{\text{DJF}}}{\langle R \rangle_{\text{JJA}}}, \tag{11}$$

with 'DJF': December, January, February, and 'JJA': June, July, August. $\langle R \rangle_{\text{DJF}}$ and $\langle R \rangle_{\text{JJA}}$ are the mean generations within a certain time frame (historical, mid century,

end of century).

Analysis of low wind periods using a statistical analysis of a large CMIP5 ensemble

Our analysis is complemented with lower resolution data of 22 GCMs contributing to the Coupled Model Intercomparison Project Phase 5 (CMIP5, [37]). The GCM output is analyzed with a statistical method developed by Reyers *et al.* [23, 24]. We characterize the large-scale circulation over Central Europe by determining the prevalent circulation weather type (CWT, [38]) using instantaneous daily mean sea level pressure (MSLP) fields around a central point at 10°E and 50°N (near Frankfurt, Germany) at 00 UTC (see also Fig 2 in Reyers *et al.* [23]). The different CWT classes are either directional ('North', 'North-East', 'East', 'South-East', 'South', 'South-West', 'West', 'North-West') or rotating ('Cyclonic', 'Anti-cyclonic'). Additionally, a proxy for the large-scale geostrophic wind (denoted as f-parameter) is derived using the gradient of the instantaneous MSLP field. Higher geostrophic wind values (i.e. higher f-parameters) correspond to larger wind power yields in Central Europe [56].

In order to compare the CMIP5 and the EURO-CORDEX data, we test whether the f-parameter derived using the coarse ERA-Interim reanalysis data [23] is capable to reproduce the characteristics of German low-wind generation periods as determined from the downscaled ERA-Interim dataset [48]. We classify days with below-average wind power generation (scarcity) for each CWT by a low value of the f-parameter, $f(t) \leq f_{\mathrm{th}}$. Thus, for each day, we can analyze whether the classifier ($f(t) \leq f_{\mathrm{th}}$) correctly predicts that the wind power generation is below average ($R(t) < \langle R \rangle$) or erroneously predicts that the wind power generation is above average ($R(t) \geq \langle R \rangle$). The quality of this classification is quantified by the fraction of true predictions, called sensitivity

$$\mathrm{SEN} = \frac{n[R < \langle R \rangle \,\&\, f \leq f_{\mathrm{th}}]}{n[R < \langle R \rangle \,\&\, f \leq f_{\mathrm{th}}] + n[R < \langle R \rangle \,\&\, f > f_{\mathrm{th}}]} \tag{12}$$

and the fraction of false predictions

$$\mathrm{FFP} = \frac{n[R \geq \langle R \rangle \,\&\, f \leq f_{\mathrm{th}}]}{n[R \geq \langle R \rangle \,\&\, f \leq f_{\mathrm{th}}] + n[R \geq \langle R \rangle \,\&\, f > f_{\mathrm{th}}]}, \tag{13}$$

where n denotes the number of days where the conditions are satisfied [57]. A compromise must be found between a maximum sensitivity for high values of f_{th} and a minimum fraction of false predictions for low values of f_{th}. A common choice is to choose the value f_{th} which minimizes $(1 - \mathrm{SEN})^2 + \mathrm{FFP}^2$ [57] (see also Fig C in S1 Appendix (ROC-curve)). Under the assumption that the meaning of the f-parameter does not depend on GCM and time frame, we use the derived f_{th} to estimate the duration of low wind periods as described in above.

Results

Increase of backup and storage needs

We assess the impact of climate change on the average backup energy per year E as a function of the storage capacity S_{max}. The storage capacity is given in units of the yearly load L_{year} of a country and is shown on a range between $S_{\mathrm{max}} = 10^{-5}$ to $S_{\mathrm{max}} = 10^{-1}$. The case of $S_{\mathrm{max}} = 10^{-5}$ can be regarded as the no-storage case. Results hardly differ for even smaller storage capacities. It should be noted that storage capacities above about 10^{-3} correspond to a scenario with massive extension of (effective) storage capacities. This could include the large-scale deployment of novel technologies, in particular chemical storage and/or virtual storage. As in highly renewable power systems huge amounts of storage will be necessary (see e.g. [54, 55]), we decided to consider also these highly optimistic cases.

All models in the EURO-CORDEX ensemble predict an increase of the necessary backup energy in most of Central Europe (i.e. Germany, Poland, Czech Republic, Switzerland, Austria, the Netherlands and Belgium), France, the British Isles and Scandinavia for a strong climate change scenario (RCP8.5) by the end of the century relative to the historical time frame (see Fig 2c and d). This implies that even though the same amount of energy is produced by renewables in both time frames, less renewable energy can actually be used. Relative changes are highest in Switzerland and the United Kingdom with a range between 12.2 to 24.2 % (ensemble mean: 15.6 %) and 7.1 to 16.5 % (ensemble mean: 12.1 %), respectively for a storage capacity of $S_{\mathrm{max}} = 0.01 \cdot L_{\mathrm{year}}$. However, results for mountainous regions like Switzerland should be

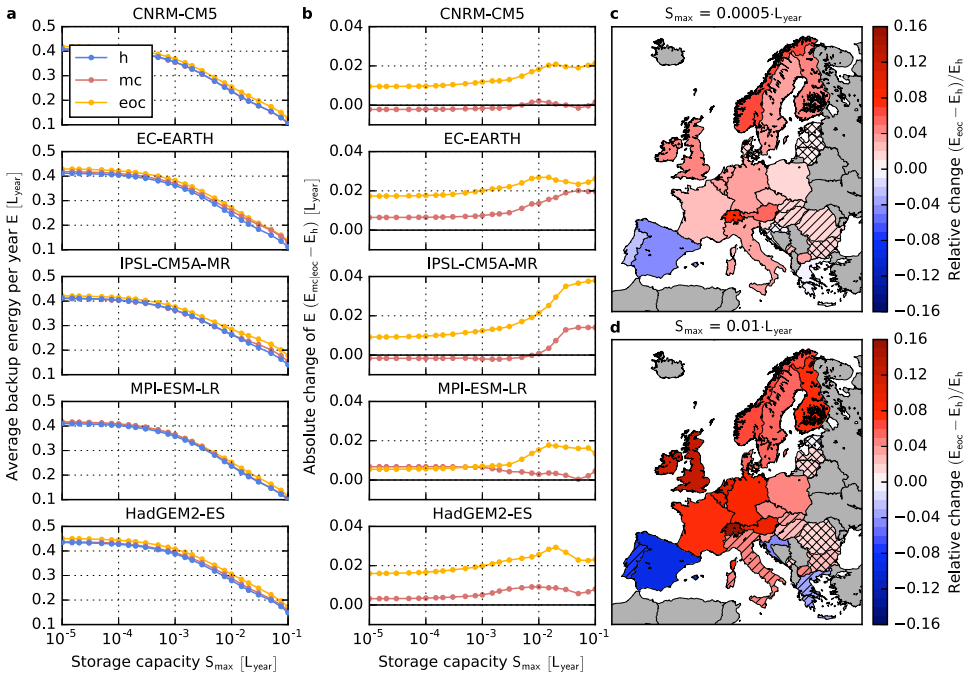

Fig 2. Impact of strong climate change on backup energy needs in Europe. **a,** Amount of energy that has to be provided by dispatchable backup generators in Germany as a function of the storage capacity $S_{\max}$ for the five models in the EURO-CORDEX ensemble and a strong climate change scenario (RCP8.5). Energy is given in units of the average yearly gross electricity consumption L_{year}. Blue: 1970-2000 (h), Red: 2030-2060 (mc), Yellow: 2070-2100 (eoc). **b,** Absolute change of the average backup energy as a function of $S_{\max}$ in Germany. Colors are the same as in panel **a**. **c, d,** Relative change of the average backup energy needs by the end of the century with respect to the historical time frame for 29 European countries and two values of the storage capacity $S_{\max}$. The color code corresponds to the average of the five models and the hatching indicates the robustness of the results. No hatching: 5/5, striped: 4/5, crossbred: 3/5 models agree on the sign of change.

regarded with caution as wind farms might be placed at sites which are unsuitable. In addition, climate model results over complex terrain are known to have large uncertainties. An opposite effect is observed for the Iberian Peninsula, Greece and Croatia where the need for backup energy decreases (e.g., Spain: -4.7 to -15.5 %; ensemble mean: -9.1 % for $S_{\max} = 0.01 \cdot L_{\text{year}}$). These results hold for a variety of scenarios for the development of storage infrastructures leading to different values of the storage size $S_{\max}$, being more pronounced for larger storage sizes. The latter partly results from a change in the seasonal variability of the wind power generation (cf. below). In the Baltic region and South-Eastern Europe, relative changes are weaker and the models most often do not agree on the sign of change and can therefore be

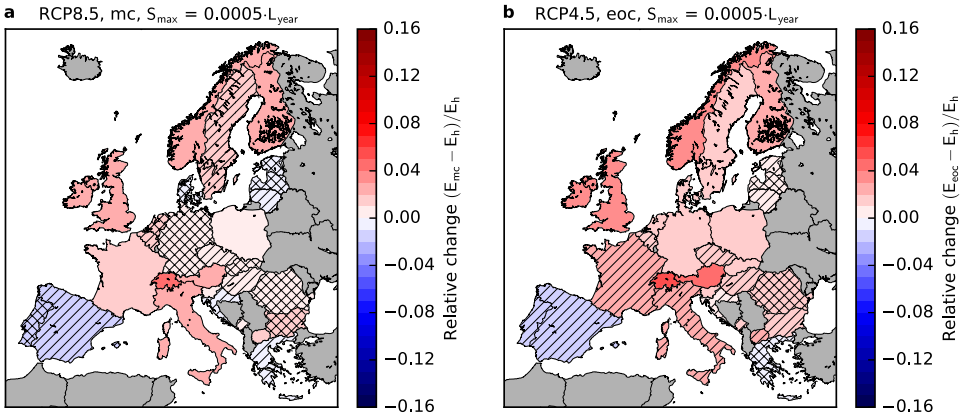

Fig 3. Impact of climate change on backup energy needs in Europe for different time frames and scenarios. a, mid century and strong climate change (RCP8.5). b, end of century and medium climate change (RCP4.5). Further parameters and presentation as in Fig. 2c.

regarded as not robust [58, 59].

Similar changes are observed already at mid century (2030-2060, see Fig 3a and Fig A in S2 Appendix) and for RCP4.5 (see Fig 3b and Fig A in S3 Appendix). However, the results are less pronounced and often not robust.

For Germany (Fig 2a and b), the absolute increase of the average backup energy per year E amounts to 0.6-3.8 % of the average yearly consumption L_{year} by the end of the century. Assuming a yearly consumption of the order of $L_{\text{year}} = 600$ TWh [60], this corresponds to an additional need of 4-23 TWh of backup energy per year.

In a perfectly interconnected Europe, the average relative backup energy per year is much smaller than for individual countries (e.g., for Germany, cf Fig 2a and Fig 4a). This is because the balancing takes place over a large spatial scale with many different wind patterns at the same time step. For all five models and all storage capacities, we find an increase of the average backup energy per year E by the end of the century (see Fig 4). Values range from 0.3 to 2.2 % of the average yearly consumption L_{year}. For high storage capacities, the change depends strongly on the seasonal wind variability (cf. below). Hence, we find increasing backup energy needs for many single European countries as well as for a perfectly interconnected Europe. This implies that, even though balancing takes place over large spatial scales, certain wind situations occur simultaneously in many countries. In fact, Wohland *et al.* [52] find that wind conditions become more homogeneous within Europe in a future climate, which decreases

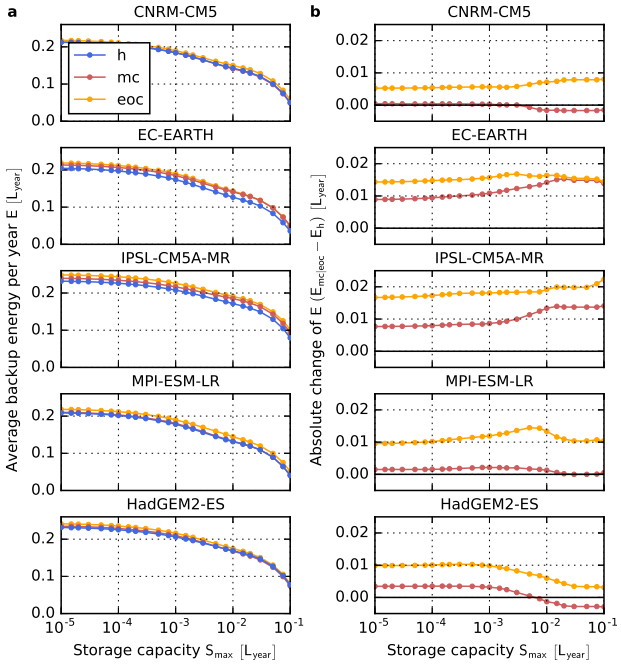

Fig 4. Impact of strong climate change on backup energy needs for a perfectly interconnected European power system. a, Amount of energy that has to be provided by dispatchable backup generators in Europe as a function of the storage capacity $S_{\max}$ for the five models in the EURO-CORDEX ensemble and a strong climate change scenario (RCP8.5). Energy is given in units of the average yearly gross electricity consumption L_{year}. Blue: 1970-2000 (h), Red: 2030-2060 (mc), Yellow: 2070-2100 (eoc). **b,** Absolute change of the average backup energy as a function of $S_{\max}$. Colors are the same as in panel **a**.

inter-state balancing of electricity. For mid century, the same effect albeit at a weaker magnitude can be observed.

Two main drivers for the increase in the backup energy can be identified: a higher probability for long periods with low wind power generation and a higher seasonal wind variability.

Challenges by long low-wind periods

During long periods of low renewable generation, the storage facilities get depleted with a high probability such that the residual load has to be covered by backup power plants leading to a high backup energy need. In Fig 5 we show the duration distribution of periods for which wind power generation is continuously lower than average (i.e. $R(t) < \langle R \rangle$) for Germany (panel a) and the relative change of the 95 % quantile (panel

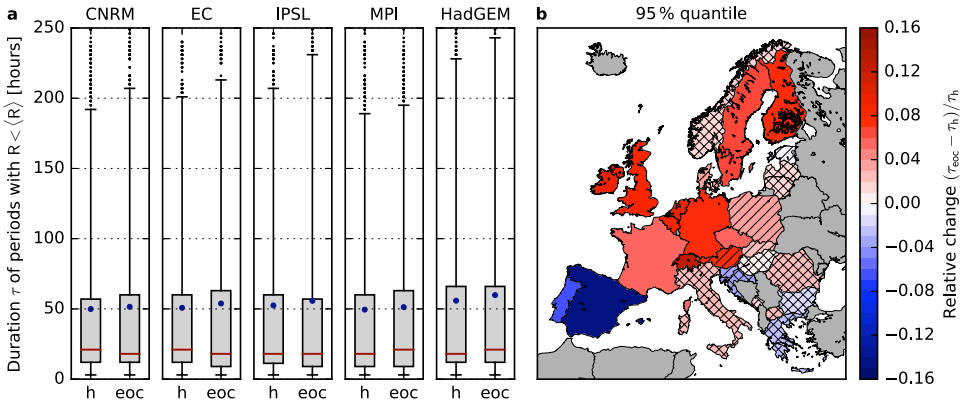

Fig 5. Change of the duration of periods with low wind generation. a, Distribution of the duration of periods during which the wind generation is continuously lower than average ($R(t) < \langle R \rangle$) in Germany for the five models in the EURO-CORDEX ensemble. Boxes represent the 25 % to 75 % quantiles, whiskers indicate the 5 % and 95 % quantiles, the red line is the median, the blue dot shows the mean and black dots represent outliers. Results are shown for the historical time frame (h, 1970-2000) and the end of the century (eoc, 2070-2100) for a strong climate change scenario (RCP8.5). **b**, Relative change of the duration assigned to the 95 % quantile by the end of the century with respect to the historical time frame for 29 European countries. The color code corresponds to the average of the five models and the hatching indicates the robustness of the results. No hatching: 5/5, striped: 4/5, crossbred: 3/5 models agree on the sign of change.

b). The 95 % quantile shifts to longer durations in most of Central Europe, France, the British Isles, Sweden and Finland and decreases on the Iberian Peninsula by the end of the century. These findings are robust in the sense that all five models in the EURO-CORDEX ensemble agree on the sign of change as illustrated for Germany in Fig 5a.

Long low-wind periods are crucially difficult for the operation of future renewable power systems [13]. An increasing magnitude for such extreme events thus represents a serious challenge for renewable integration. In Eastern Europe, Italy, Greece and Norway relative changes are weaker and not robust. The effect develops mostly in the second half of the century (cf. Fig B in S2 Appendix) and for strong climate change (RCP8.5, cf. Fig B in S3 Appendix).

The complete distribution of durations is shown in Fig 6. We find that for Germany (panels a) not only the duration associated with the 95 %-quantile tends to increase but also the probability for particularly long durations (except for CNRM-CM5). Considering the perfectly interconnected European power system (panels b), we also

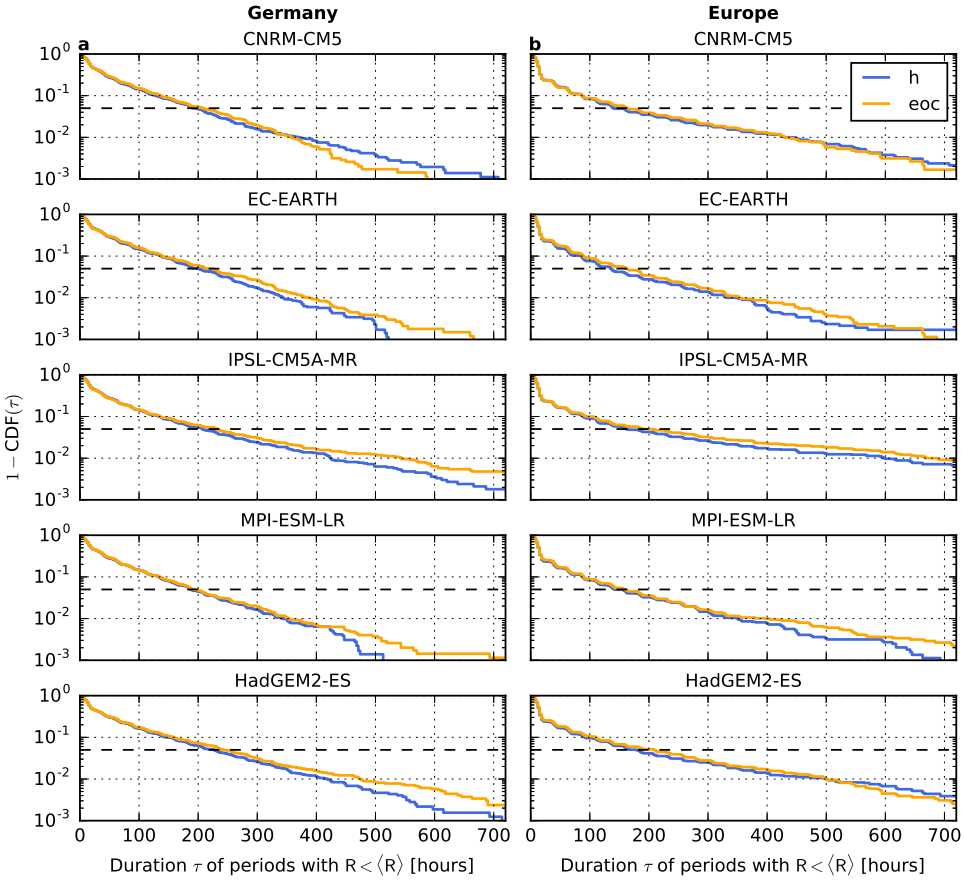

Fig 6. Change of the duration of periods with low wind generation. a, One minus the cumulative distribution function (CDF) of periods having a duration τ during which the wind generation is continuously lower than average ($R(t) < \langle R \rangle$) for Germany and **b,** for the European copperplate. Results are shown for the historical time frame (h, 1970-2000) and the end of the century (eoc, 2070-2100) for a strong climate change scenario (RCP8.5) for the five models in the EURO-CORDEX ensemble. The dashed vertical line represents the 95 %-quantile of the CDF.

find that the 95 % quantile shifts to higher values by the end of the century. Furthermore, the probability for low-wind periods having a duration of up to about 500 hours increases (again except for CNRM-CM5). For longer durations, the curves often cross. However, it is difficult to evaluate such extreme events appropriately in the context of climate change given the finite duration of the time series. All in all, this analyis indicates that long lasting low-wind conditions, which extend over the whole European continent, are projected to become more likely (see also [52]).

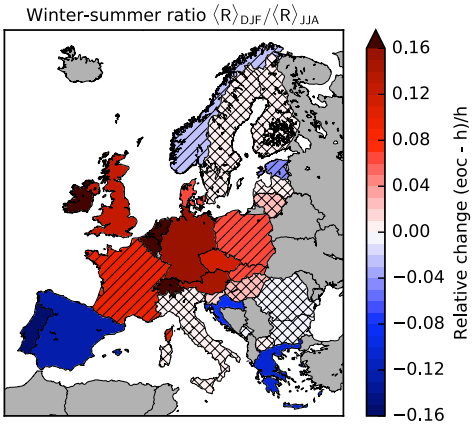

Fig 7. Impact of strong climate change on the seasonal variability of wind power generation. Relative change of the winter-summer ratio of the average wind power yield $\langle R\rangle_{\mathrm{DJF}}/\langle R\rangle_{\mathrm{JJA}}$ (DJF: December-February vs. JJA: June-August) by the end of the century (eoc, 2070-2100) with respect to the historical time frame (h, 1970-2000). The brackets denote the temporal average over the respective winter and summer months. Results are shown for a strong climate change scenario (RCP8.5) for 29 European countries. The color code corresponds to the average of the five models and the hatching indicates the robustness of the results. No hatching: 5/5, striped: 4/5, crossbred: 3/5 models agree on the sign of change.

Higher seasonal wind variability

The second reason for an increase of backup and storage needs is an increasing intensity of the seasonal wind variability. Typically, the wind power yield is highest in the winter months such that backup power plants are needed mostly in summer.

The winter-summer ratio increases for most of Central and North-Western Europe, and decreases for the Iberian Peninsula, Greece and Croatia (see Fig 7) for four or all five models in the EURO-CORDEX ensemble. In these countries the seasonal variability therefore contributes to the observed changes of backup needs. Changes are small and not robust in Italy, most of Eastern Europe and Scandinavia (except Denmark). Hence, the increase of backup needs in Northern Europe is attributed solely to the higher probability for long periods with low wind power generation. For mid century (see Fig C in S2 Appendix), and for medium climate change (RCP4.5, see Fig C in S3 Appendix), results are comparable but less robust for some countries.

For the perfectly interconnected European power system, four of the five models predict an increasing seasonal wind variability in the range of 4.1 to 10.4 %. Thus, the lower seasonal wind variability on the Iberian Peninsula, Greece and Croatia cannot

totally compensate the higher seasonal wind variability in the other European countries. In contrast, HadGEM2-ES predicts a decrease of -2.8 %.

The higher seasonal wind variability also explains the relative increase of the backup energy for higher storage capacities (cf. Fig 2). A high storage capacity allows to store some part of the energy for several months. However, as the storage capacity is still limited, a higher seasonal wind variability implies that the storage is fully charged earlier in winter and that it is depleted earlier in summer. Thus, less excess energy can be transferred from the winter to the summer months if the seasonal variability of wind power generation increases.

The duration of low-wind periods is strongly associated with the seasonal wind variability, e.g. low-wind periods are more frequent over Western Europe in summer than in winter. To assess the implications of this connection in a changing climate, we evaluated the distribution of durations of low-wind periods also per season, and computed the changes between the distributions for the end of the century vs. recent climate conditions. We found that in countries where the seasonal wind variability increases, the duration of low-wind periods also increases (in most cases) in all seasons, but primarily in summer . This result is robust for all five models. The same effect, albeit in the reverse direction, is observed for e.g. Spain, where a decreasing duration of low-wind periods is coupled to the decreasing seasonal wind variability and hence to shorter durations of low-wind periods in summer. We note that there are also countries where the probability for long low-wind periods increases, but no change in the seasonal wind variability is observed (e.g. Finland). Hence, we conclude that the change of seasonality and duration are indeed highly coupled, but one effect is not simply the consequence of the other.

Low-wind periods in a large CMIP5 ensemble

To substantiate our findings, we analyze a large CMIP5 ensemble [37] consisting of 22 GCMs with a much coarser resolution than the EURO-CORDEX ensemble as explained in the methods section.

The typical duration of periods with $f(t) \leq f_{\mathrm{th}}$ in Central Europe increases by the end of the century for most GCMs in the CMIP5 ensemble. 19 of the 22 models predict

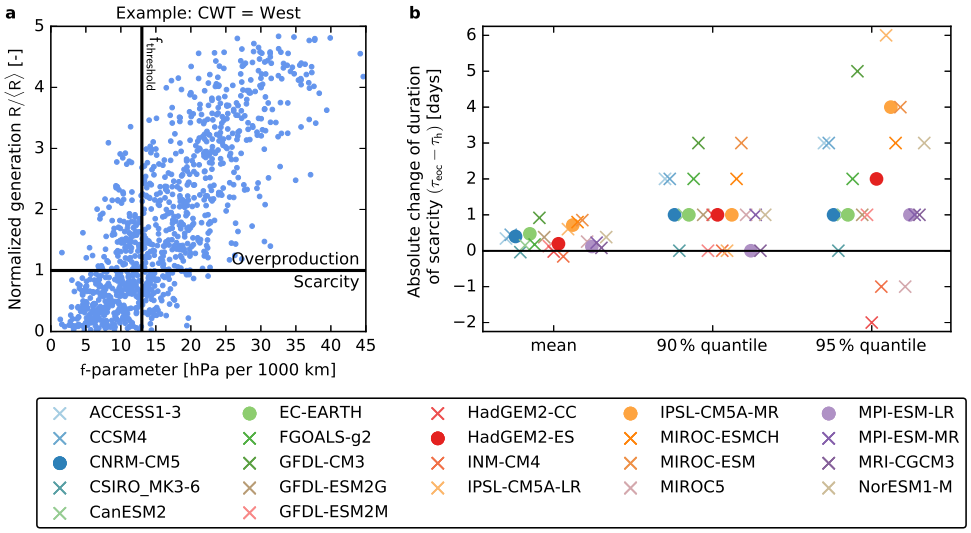

Fig 8. Assessment of long low-wind periods in a large CMIP5 ensemble. a, Days with below average wind power generation in Central Europe are identified by a low value of the f-parameter ($f(t) \leq f_{\mathrm{th}}$) in the GCM output. To determine the optimal value of the threshold f_{th}, for each circulation weather type (CWT, here, the western type is shown) we compare the f-parameter to the German wind power output $R(t)$, calculated from the dynamically downscaled ERA-Interim reanalysis dataset [48]. **b,** Absolute change of the duration of periods with $f(t) \leq f_{\mathrm{th}}$ by the end of the century (eoc, 2070-2100) compared to the historical time frame (h, 1970-2000) for a strong climate change scenario (RCP8.5) for 22 GCMs in the CMIP5 ensemble. The change of the mean duration, the 90 % quantile and the 95 % quantile of the duration distribution are shown. Filled circles represent the five GCMs which are also downscaled by the EURO-CORDEX initiative.

an increase of the mean duration (Fig 8b). The 90 % quantile of the duration increases for 16 models and remains unchanged for the remaining six models, while the 95 % quantile increases for 18 of the 22 models. Fig 8b shows that the five models of the EURO-CORDEX ensemble (shown as filled circles) form a representative subset of the CMIP5 ensemble since their results are well distributed within the range of the majority of all models and thus do not contain outliers. Hence, the large CMIP5 ensemble corroborates our previous findings, predicting an increase of the likelihood for long periods with low wind power output for a strong climate change scenario.

To assess the sensitivity of the choice of f_{th}, we repeated our analysis by determining one value for f_{th} which is independent of the underlying CWT. This does not change the results as shown in Fig I in S4 Appendix.

Climatologic developments driving enhanced seasonality

The identified increase in the seasonal variability of wind power generation has been discussed in terms of the projected changes of large-scale atmospheric circulation and regional wind conditions. A consensus exists about general changes in the large-scale circulation patterns in the Eastern North Atlantic region and Europe, which is however dependent on the time of the year [28]. During winter, the eddy-driven jet stream and cyclone intensity are extended towards the British Isles [29]. Accordingly, winter storminess is projected to increase over Western Europe [32, 33], leading to enhanced winds over Western and Central Europe. The signal in summer corresponds rather to a northward shift of the eddy driven jet stream, cyclone activity and lower tropospheric winds, together with an increase in anticyclonic circulation over Southern Europe [30]. The latter is associated with an expansion of the Hadley circulation due to enhanced radiative forcing [31]. These developments are projected to decrease wind speeds during summer [23–25, 34].

These seasonal changes have strong implications not only on temperature and precipitation patterns, but also in the seasonal wind regimes and intra-annual variability. The seasonal variability of wind power generation increases under future climate conditions [23, 25, 34] even though the annual mean changes are comparatively small [21, 22, 24, 25, 34]. The impact may be large for the operational systems, and thus needs to be quantified adequately based on state-of-the-art climate model projections.

Discussion

Wind power, PV and other renewable sources can satisfy the majority of the global energy demand [5, 6, 61]. However, system integration remains a huge challenge: The operation of wind turbines and PV relies on weather and climate and thus shows strong temporal fluctuations [7–10, 12–14, 51, 62]. The impact of climate change on the global energy yields of wind and solar power has been addressed previously [21–26], but the impact on fluctuations and system integration has been addressed only recently [52, 63, 64].

In this paper, we analyzed the change of the temporal characteristics of wind power generation in a strong (RCP8.5) and a medium climate change scenario (RCP4.5, see

Fig 3a and S3 Appendix). Backup and storage needs increase in most of Central, Northern and North-Western Europe and decrease over the Iberian Peninsula, Greece and Croatia. As these effects are observed for both aggregation approaches used in this study (approach (a): aggregation per country, approach (b): European copperplate), we hypothesize that the effect will also be observed in intermediate scenarios with restricted interconnection between countries. By mid century and for medium climate change, results are less pronounced and often not robust. Two main climatologic reasons for the observed increase were identified: a higher probability for long periods of low wind power generation and a stronger seasonal wind variability.

Wohland *et al.* [52] examined climate change impacts for different levels of European grid integration. Since the same climatic input data was used, their results can complement the interpretation of the findings in the current study. Neglecting energy storage, they report an increase of backup energy irrespective of the grid design by the end of the century and RCP8.5.

The projected increase in backup energy needs may partly be compensated in some countries by using an appropriate mix of wind and PV (see also Fig H in S4 Appendix). Furthermore, wind generation from offshore wind farms is often more persistent and installed capacities are strongly increasing. In a further study, climate projections for onshore and offshore wind and PV should thus be analyzed together in order to account for possible changes in the temporal variations of the combined system of renewables.

To isolate the change of the temporal characteristics of wind power generation, we made several simplifications. First of all, we assumed that wind provides a fixed share γ of the load for all time frames. This procedure normalizes out a possible change of global wind yields (previously discussed [21–25]). In S4 Appendix Figs A-C, we evaluated the impact of a higher or lower renewable penetration γ and of the exact load time series on our results and found the same tendencies, albeit at different magnitude. Technological progress of the wind turbines and changes of typical hub heights were not considered in a detailed way. However, a different siting of wind farms or a higher hub height of 120 m hardly impacts our results (see Figs D-G in S4 Appendix). For an integrated assessment, technological progress should be taken into account, but our approach reveals the impact of climate change on the temporal characteristics clearly.

A reliable interpretation of climate projections should be based on multi-model

ensembles [22, 37]. Our analysis of the small EURO-CORDEX ensemble consisting of five models shows robust results regarding the sign of change for several regions in Europe. A statistical analysis of the output of 22 GCMs from the CMIP5 ensemble supports our findings, as the duration of periods with low values of the f-parameter over Central Europe is likely to increase. Large-scale climatologic developments leading to an increase of the seasonal wind variability were previously discussed [23, 25, 28–34]. For future research, it would be highly desirable if larger ensembles of dynamically downscaled models would be provided. Furthermore, data at turbine hub height should be made available. Ongoing downscaling experiments within the new CMIP6 CORDEX initiative [65] will allow to assess the impact of climate change on system integration of intermittent renewables for various regions in the same manner. This should include a detailed and explicit analysis on the projected changes of both wind and PV. In conclusion, our work contributes to highlight the importance of integrated energy and climate research to enable a sustainable energy transition.

Supporting information

S1 Appendix. Supporting figures and tables for the methods section.

S2 Appendix. Mid century (2030-2060).

S3 Appendix. RCP4.5.

S4 Appendix. Sensitivity studies.

Acknowledgments

We acknowledge the World Climate Research Programme's Working Group on Regional Climate, and the Working Group on Coupled Modelling, former coordinating body of CORDEX and responsible panel for CMIP5. We also thank the climate modelling groups (listed in Table A in S1 Appendix) for producing and making available their model output. We also acknowledge the Earth System Grid Federation infrastructure an international effort led by the U.S. Department of Energy's Program for Climate

Model Diagnosis and Intercomparison, the European Network for Earth System Modelling and other partners in the Global Organisation for Earth System Science Portals (GO-ESSP). We thank H. Elbern, G. B. Andresen, S. Kozarcanin, T. Brown, and J. Hoersch for stimulating discussions. We gratefully acknowledge support from the Helmholtz Association (via the joint initiative "Energy System 2050 – A Contribution of the Research Field Energy" and the grant no. VH-NG-1025) and the Federal Ministry for Education and Research (BMBF grant no. 03SF0472) to D. W.. For M. R., J. M. and J. G. P. contributions were partially funded by the the Helmholtz-Zentrum Geesthacht/German Climate Service Center (HZG/GERICS). J.G.P. thanks the AXA Research Fund for support.

References

1. T Bruckner et al . Energy Systems. In: O Edenhofer et al , editor. Climate Change 2014: Mitigation of Climate Change. Contribution of Working Group III to the Fifth Assessment Report of the Intergovernmental Panel on Climate Change. Cambridge University Press, Cambridge, United Kingdom; 2014.

2. UNFCCC. Adoption of the Paris Agreement. Report No. FCCC/CP/2015/L.9/Rev.1; 2015. http://unfccc.int/resource/docs/2015/cop21/eng/l09r01.pdf.

3. Rogelj J, Luderer G, Pietzcker RC, Kriegler E, Schaeffer M, Krey V, et al. Energy system transformations for limiting end-of-century warming to below 1.5°C. Nature Climate Change. 2015;5(6):519–527.

4. Rogelj J, Den Elzen M, Höhne N, Fransen T, Fekete H, Winkler H, et al. Paris Agreement climate proposals need a boost to keep warming well below 2°C. Nature. 2016;534(7609):631–639.

5. Jacobson MZ, Delucchi MA. Providing all global energy with wind, water, and solar power, Part I: Technologies, energy resources, quantities and areas of infrastructure, and materials. Energy Policy. 2011;39(3):1154–1169.

6. R Sims et al . Integration of Renewable Energy into Present and Future Energy Systems. In: O Edenhofer et al , editor. IPCC Special Report on Renewable Energy Sources and Climate Change Mitigation. Cambridge University Press, Cambridge, United Kingdom; 2011.

7. Bloomfield H, Brayshaw DJ, Shaffrey LC, Coker PJ, Thornton H. Quantifying the increasing sensitivity of power systems to climate variability. Environmental Research Letters. 2016;11(12):124025.

8. Olauson J, Ayob MN, Bergkvist M, Carpman N, Castellucci V, Goude A, et al. Net load variability in Nordic countries with a highly or fully renewable power system. Nature Energy. 2016;1:16175.

9. Davidson MR, Zhang D, Xiong W, Zhang X, Karplus VJ. Modelling the potential for wind energy integration on China's coal-heavy electricity grid. Nature Energy. 2016;1:16086.

10. Huber M, Dimkova D, Hamacher T. Integration of wind and solar power in Europe: Assessment of flexibility requirements. Energy. 2014;69:236–246.

11. Weber J, Zachow C, Witthaut D. Modeling long correlation times using additive binary Markov chains: Applications to wind generation time series. Physical Review E. 2018;97(3):032138.

12. Heide D, von Bremen L, Greiner M, Hoffmann C, Speckmann M, Bofinger S. Seasonal optimal mix of wind and solar power in a future, highly renewable Europe. Renewable Energy. 2010;35:2483.

13. Elsner P, Fischedick M, Sauer DU. Flexibilitätskonzepte für die Stromversorgung 2050. Muenchen: Acatech; 2015.

14. Díaz-González F, Sumper A, Gomis-Bellmunt O, Villafáfila-Robles R. A review of energy storage technologies for wind power applications. Renewable and Sustainable Energy Reviews. 2012;16(4):2154–2171.

15. Van Vliet MT, Yearsley JR, Ludwig F, Vögele S, Lettenmaier DP, Kabat P. Vulnerability of US and European electricity supply to climate change. Nature Climate Change. 2012;2(9):676–681.

16. Van Vliet MT, Wiberg D, Leduc S, Riahi K. Power-generation system vulnerability and adaptation to changes in climate and water resources. Nature Climate Change. 2016;6:375–380.

17. Allen MR, Fernandez SJ, Fu JS, Olama MM. Impacts of climate change on sub-regional electricity demand and distribution in the southern United States. Nature Energy. 2016;1:16103.

18. Auffhammer M, Baylis P, Hausman CH. Climate change is projected to have severe impacts on the frequency and intensity of peak electricity demand across the United States. Proceedings of the National Academy of Sciences. 2017;114(8):1886–1891.

19. François B, Hingray B, Borga M, Zoccatelli D, Brown C, Creutin JD. Impact of Climate Change on Combined Solar and Run-of-River Power in Northern Italy. Energies. 2018;11(2):290.

20. Pryor S, Barthelmie R. Climate change impacts on wind energy: a review. Renewable and sustainable energy reviews. 2010;14(1):430–437.

21. Tobin I, Vautard R, Balog I, Bréon FM, Jerez S, Ruti PM, et al. Assessing climate change impacts on European wind energy from ENSEMBLES high-resolution climate projections. Climatic Change. 2015;128(1-2):99–112.

22. Tobin I, Jerez S, Vautard R, Thais F, Van Meijgaard E, Prein A, et al. Climate change impacts on the power generation potential of a European mid-century wind farms scenario. Environmental Research Letters. 2016;11(3):034013.

23. Reyers M, Pinto JG, Moemken J. Statistical–dynamical downscaling for wind energy potentials: evaluation and applications to decadal hindcasts and climate change projections. International Journal of Climatology. 2015;35(2):229–244.

24. Reyers M, Moemken J, Pinto JG. Future changes of wind energy potentials over Europe in a large CMIP5 multi-model ensemble. International Journal of Climatology. 2016;36(2):783–796.

25. Moemken J, Reyers M, Feldmann H, Pinto JG. Future changes of wind speed and wind energy potentials in EURO-CORDEX ensemble simulations. Journal of Geophysical Research: Atmospheres. 2018;123(12):6373–6389.

26. Jerez S, Tobin I, Vautard R, Montávez JP, López-Romero JM, Thais F, et al. The impact of climate change on photovoltaic power generation in Europe. Nature Communications. 2015;6:10014.

27. Stanton MCB, Dessai S, Paavola J. A systematic review of the impacts of climate variability and change on electricity systems in Europe. Energy. 2016;109:1148–1159.

28. Demuzere M, Werner M, Van Lipzig N, Roeckner E. An analysis of present and future ECHAM5 pressure fields using a classification of circulation patterns. International Journal of Climatology. 2009;29(12):1796–1810.

29. Woollings T, Gregory JM, Pinto JG, Reyers M, Brayshaw DJ. Response of the North Atlantic storm track to climate change shaped by ocean-atmosphere coupling. Nature Geoscience. 2012;5(5):313–317.

30. Zappa G, Hoskins BJ, Shepherd TG. Improving climate change detection through optimal seasonal averaging: the case of the North Atlantic jet and European precipitation. Journal of Climate. 2015;28(16):6381–6397.

31. Lu J, Vecchi GA, Reichler T. Expansion of the Hadley cell under global warming. Geophysical Research Letters. 2007;34(6).

32. Pinto JG, Karremann MK, Born K, Della-Marta PM, Klawa M. Loss potentials associated with European windstorms under future climate conditions. Climate Research. 2012;54(1):1–20.

33. Feser F, Barcikowska M, Krueger O, Schenk F, Weisse R, Xia L. Storminess over the North Atlantic and northwestern Europe – A review. Quarterly Journal of the Royal Meteorological Society. 2015;141(687):350–382.

34. Hueging H, Haas R, Born K, Jacob D, Pinto JG. Regional changes in wind energy potential over Europe using regional climate model ensemble projections. Journal of Applied Meteorology and Climatology. 2013;52(4):903–917.

35. Jacob D, Petersen J, Eggert B, Alias A, Christensen OB, Bouwer LM, et al. EURO-CORDEX: new high-resolution climate change projections for European impact research. Regional Environmental Change. 2014;14(2):563–578.

36. Giorgi F, Gutowski Jr WJ. Regional dynamical downscaling and the CORDEX initiative. Annual Review of Environment and Resources. 2015;40:467–490.

37. Taylor KE, Stouffer RJ, Meehl GA. An overview of CMIP5 and the experiment design. Bulletin of the American Meteorological Society. 2012;93(4):485–498.

38. Jones P, Hulme M, Briffa K. A comparison of Lamb circulation types with an objective classification scheme. International Journal of Climatology. 1993;13(6):655–663.

39. Van Vuuren DP, Edmonds J, Kainuma M, Riahi K, Thomson A, Hibbard K, et al. The representative concentration pathways: an overview. Climatic change. 2011;109:5–31.

40. ESGF (Earth System Grid Federation) node at DKRZ (German Climate Computing Centre). EURO-CORDEX data; accessed August 16, 2016. `https://esgf-data.dkrz.de/projects/esgf-dkrz/`.

41. Strandberg G, Bärring L, Hansson U, Jansson C, Jones C, Kjellström E, et al. CORDEX scenarios for Europe from the Rossby Centre regional climate model RCA4. SMHI, Sveriges Meteorologiska och Hydrologiska Institut; 2015.

42. Samuelsson P, Jones CG, Willén U, Ullerstig A, Gollvik S, Hansson U, et al. The Rossby Centre Regional Climate model RCA3: model description and performance. Tellus A. 2011;63(1):4–23.

43. Manwell JF, McGowan JG, Rogers AL. Wind Energy Explained. John Wiley & Sons, Ltd; 2009.

44. Kubik M, Coker PJ, Barlow JF, Hunt C. A study into the accuracy of using meteorological wind data to estimate turbine generation output. Renewable Energy. 2013;51:153–158.

45. Bratton DC, Womeldorf CA. The Wind Shear Exponent: Comparing Measured Against Simulated Values and Analyzing the Phenomena That Affect the Wind Shear. In: ASME 2011 5th International Conference on Energy Sustainability. American Society of Mechanical Engineers; 2011. p. 2245–2251.

46. Andresen GB, Søndergaard AA, Greiner M. Validation of Danish wind time series from a new global renewable energy atlas for energy system analysis. Energy. 2015;93:1074–1088.

47. Monforti F, Gaetani M, Vignati E. How synchronous is wind energy production among European countries? Renewable and Sustainable Energy Reviews. 2016;59:1622–1638.

48. Dee D, Uppala S, Simmons A, Berrisford P, Poli P, Kobayashi S, et al. The ERA-Interim reanalysis: Configuration and performance of the data assimilation system. Quarterly Journal of the royal meteorological society. 2011;137(656):553–597.

49. Becker S, Frew BA, Andresen GB, Zeyer T, Schramm S, Greiner M, et al. Features of a fully renewable US electricity system: Optimized mixes of wind and solar PV and transmission grid extensions. Energy. 2014;72:443–458.

50. Rodriguez RA, Becker S, Andresen GB, Heide D, Greiner M. Transmission needs across a fully renewable European power system. Renewable Energy. 2014;63:467–476.

51. Schlachtberger D, Becker S, Schramm S, Greiner M. Backup flexibility classes in emerging large-scale renewable electricity systems. Energy Conversion and Management. 2016;125:336–346.

52. Wohland J, Reyers M, Weber J, Witthaut D. More homogeneous wind conditions under strong climate change decrease the potential for inter-state balancing of electricity in Europe. Earth System Dynamics. 2017;8(4):1047.

53. European Network of Transmission System Operators for Electricity (ENTSO-E). Hourly load values; accessed December 10, 2016. `https://www.entsoe.eu/db-query/consumption/mhlv-all-countries-for-a-specific-month`.

54. Rasmussen MG, Andresen GB, Greiner M. Storage and balancing synergies in a fully or highly renewable pan-European power system. Energy Policy. 2012;51:642–651.

55. Jensen TV, Greiner M. Emergence of a phase transition for the required amount of storage in highly renewable electricity systems. The European Physical Journal Special Topics. 2014;223(12):2475–2481.

56. Bakker AM, van den Hurk BJ. Estimation of persistence and trends in geostrophic wind speed for the assessment of wind energy yields in Northwest Europe. Climate dynamics. 2012;39(3-4):767–782.

57. Egan JP. Signal detection theory and ROC analysis. Cambridge: Academic Press; 1975.

58. IPCC. Climate Change 2013: The Physical Science Basis. Contribution of Working Group I to the Fifth Assessment Report of the Intergovernmental Panel on Climate Change. Cambridge University Press, Cambridge, United Kingdom; 2013.

59. Hawkins E, Sutton R. The potential to narrow uncertainty in regional climate predictions. Bulletin of the American Meteorological Society. 2009;90(8):1095–1107.

60. AG Energiebilanzen e V . Energieverbrauch in Deutschland im Jahr 2016; 2017. http://www.ag-energiebilanzen.de/.

61. Lu X, McElroy MB, Kiviluoma J. Global potential for wind-generated electricity. Proceedings of the National Academy of Sciences. 2009;106(27):10933–10938.

62. Grams CM, Beerli R, Pfenninger S, Staffell I, Wernli H. Balancing Europe's wind-power output through spatial deployment informed by weather regimes. Nature Climate Change. 2017;7:557–562.

63. Kozarcanin S, Liu H, Andresen GB. Climate change impacts on large-scale electricity system design decisions for the 21st Century. arXiv preprint arXiv:180501364. 2018.

64. Schlott M, Kies A, Brown T, Schramm S, Greiner M. The Impact of Climate Change on a Cost-Optimal Highly Renewable European Electricity Network. arXiv preprint arXiv:180511673. 2018.

65. Eyring V, Bony S, Meehl GA, Senior CA, Stevens B, Stouffer RJ, et al. Overview of the Coupled Model Intercomparison Project Phase 6 (CMIP6) experimental design and organization. Geoscientific Model Development. 2016;9(5):1937–1958.

10.3 Reyers et al. (2017)

Reference:

Reyers, M., Feldmann, H., Mieruch, S., Pinto, J. G., Uhlig, M., Ahrens, B., Früh, B., Kameshvar, M., Laube, N., Moemken, J., Müller, W. A., Schädler, G., and Kottmeier, C. (2017). Development and prospects of the regional MiKlip decadal prediction system over Europe: Predictive skill, added value of regionalization and ensemble size dependency. *Earth Syst. Dynam. Discussions.* doi:10.5194/esd-2017-70, in review

Page numbers are as submitted to *Earth System Dynamics*.

Earth Syst. Dynam. Discuss., https://doi.org/10.5194/esd-2017-70
Manuscript under review for journal Earth Syst. Dynam.
Discussion started: 4 September 2017

Earth System Dynamics Discussions
Open Access
EGU

Development and prospects of the regional MiKlip decadal prediction system over Europe: Predictive skill, added value of regionalization and ensemble size dependency

Mark Reyers[1], Hendrik Feldmann[2], Sebastian Mieruch[2,3], Joaquim G. Pinto[2], Marianne Uhlig[2,4], Bodo Ahrens[5], Barbara Früh[6], Kameswarrao Modali[7], Natalie Laube[2], Julia Mömken[1,2], Wolfgang Müller[7], Gerd Schädler[2], Christoph Kottmeier[2]

[1]Institute for Geophysics and Meteorology, University of Cologne, Cologne, Germany
[2]Institute for Meteorology and Climate Research (IMK-TRO), Karlsruhe Institute of Technology (KIT), Karlsruhe, Germany
[3]Alfred-Wegener Institute for Polar and Marine Sciences, Bremerhaven, Germany
[4]School of Geography, Environment and Earth Sciences, Victoria University of Wellington, Wellington, New Zealand
[5]Institute for Atmospheric and Environmental Sciences, Goethe-University Frankfurt a.M., Frankfurt a.M., Germany
[6]Deutscher Wetterdienst (DWD), Offenbach, Germany
[7]Max Planck Institute for Meteorology, Hamburg, Germany

Correspondence to: M. Reyers, (mreyers@meteo.uni-koeln.de)

Abstract. The current state of development and prospects of the regional MiKlip decadal prediction system for Europe are analysed. The Miklip regional system consists of two 10-member hindcast ensembles computed with the global coupled model MPI-ESM-LR downscaled for the European region with COSMO-CLM to a horizontal resolution of 0.22° (~25km). Prediction skills are computed for temperature, precipitation, and wind speed using E-OBS and an ERA-Interim driven COSMO-CLM simulation as verification datasets. Focus is given to the eight European PRUDENCE regions and to lead years 1-5 after initialization. Evidence of the general potential for regional decadal predictability for all three variables is provided. For example, the initialized hindcasts outperform the uninitialized historical runs for some key regions in Europe and for some variables both in terms of accuracy and reliability. However, forecast skill is not detected in all cases, but it depends on the variable, the region, and the hindcast generation. A comparison of the downscaled hindcasts with the global MPI-ESM-LR runs reveals that the MiKlip prediction system may distinctly benefit from regionalization, in particular for parts of Southern Europe and for Scandinavia. The forecast accuracy and the reliability of the MiKlip ensemble is systematically enhanced when the ensemble size is stepwise increased, and a number of 10 members is found to be suitable for decadal predictions. This result is valid for all variables and European regions in both the global and regional MiKlip ensemble. The predictive skill improves distinctly, particularly for temperature, when retaining the long-term trend in the time series. The present results are encouraging towards the development of a regional decadal prediction system.

Earth Syst. Dynam. Discuss., https://doi.org/10.5194/esd-2017-70
Manuscript under review for journal Earth Syst. Dynam.
Discussion started: 4 September 2017

Earth System Dynamics Discussions
Open Access
EGU

1. Introduction

In recent years, the interest in climate predictions on time-scales from one year up to a decade has increased in the climate science community, since this time span falls within the planning horizon for a wide variety of decision makers (Meehl et al., 2009; 2014). A large ensemble of initialised decadal hindcasts has been consolidated in a component of the Coupled Model Intercomparison Project Phase 5 (CMIP5; Taylor et al., 2012), and the number of studies aiming at decadal predictions has strongly increased in recent years (for a review see Meehl et al., 2014). Typically, the North Atlantic is a key region for decadal predictions and forecast skill is found for various quantities such as heat content and SST (e.g. Kröger et al, 2012; Yaeger et al., 2012), CO2 uptake (Li et al., 2016) and integrated quantities such as the AMOC (Pohlmann et al., 2013a) and sub-polar gyre (Matei et al., 2012; Yaeger et al., 2012; Robson et al., 2013). Other studies focus on primary meteorological parameters on the global scale, in particular surface temperature (e.g Chikamoto et al., 2012; Doblas-Reyes et al., 2013; Ho et al., 2013; Corti et al., 2015), while few studies analyse storm tracks (Kruschke et al., 2014, 2016), Atlantic tropical cyclones (Dunestone et al., 2011), intense or extreme events (e.g. Benestad and Mezghani, 2015) or zoom into a certain region of the world (e.g. Guemas et al., 2015). For example, Sutton and Hodson (2005) found a downstream impact of the Atlantic Multidecadal Oscillation (AMO; SST anomalies over the North Atlantic) on decadal time scales, with higher temperatures and increased precipitation over Europe in an AMO warm phase compared to a cold phase.

In the German research consortium MiKlip (http://www.fona-miklip.de), a global decadal prediction system was developed based on the Max-Planck-Institute Earth System Model (MPI-ESM) (for an overview see Marotzke et al., 2016). Within the first phase of the project, three hindcast generations were produced. The skill of the MiKlip System for decadal predictions was analysed in a wide variety of recent studies. For example, Müller et al. (2012) investigated global surface air temperature in the first generation of the global MiKlip system (baseline0) and found that the initialized hindcasts have predictive skill over the North-Atlantic region, while negative skill scores are identified for the tropics. A modified initialization in the second global MiKlip system generation (baseline1) considerably improves the performance in the tropics, but brings only limited skill improvement over the North-Atlantic and Europe (Pohlmann et al., 2013b). Significant positive skill scores for cyclone frequencies over the Central North-Atlantic were identified by Kruschke et al. (2014) in the global baseline0 and baseline1 generations, but no significant skill was detected over the Eastern North-Atlantic and Europe. Furthermore, Kadow et al. (2016) evaluated the global MiKlip system with respect to temperature and precipitation, giving evidence that an enlargement of the hindcast ensemble generally leads to an improvement of the prediction system.

The MiKlip consortium is to our best knowledge the first institution worldwide which has established a decadal prediction system for the regional scale. With this aim considerable efforts were made to downscale the global MPI-ESM hindcasts by developing and/or employing different regionalisation techniques. Previous experiences reveal that a skill for regional decadal predictions exists but that the interpretation of the results is quite complex due to their non-linear relationship to the global prediction skill. For example, Mieruch et al. (2014) found rather heterogeneous predictive skill for precipitation and temperature over Europe in the baseline0 generation. The skill differs over space, season, variable, and lead time after

initialisation. However, a general feature is an improved model spread for precipitation in the downscaled hindcasts when compared to their global counterparts. A potential for predicting regional peak winds and wind energy potentials over Central Europe several years ahead was identified in Haas et al. (2016) and Moemken et al. (2016). Particularly, they found highest skill scores for the first years after initialisation. However, these studies consider different variables, lead times, skill metrics, and downscaling and data pre-processing methods, which makes it difficult to identify general conclusions for the decadal predictability over Europe in the MiKlip decadal prediction system.

In this study, the decadal predictive skill for temperature, precipitation, and wind speed over Europe is analysed for the baseline0 and baseline1 generation of the MiKlip system. With this aim, we used the same methodologies for all three variables to ensure comparability. Global MPI-ESM and downscaled hindcast ensembles are considered to address the following three key questions:

- Is there a potential for skilful regional decadal predictions in Europe, and does this skill depend from the long-term trend?
- Does regional downscaling provide an added value for decadal predictions?
- How does the regional decadal predictive skill depend on the ensemble size?

The main topics of this paper are to demonstrate the potential of skilful regional decadal climate prediction for Europe for specific key climate variables to assess the added value compared to the respective global predictions and the impact of the ensemble size on the skill estimates. Thus, our focus lies on the methodological development and not on the physical mechanisms leading to the predictive skill.

The datasets used in this study are described in section 2, followed by the methodologies for data pre-processing and skill analysis in section 3. The results for the three key questions are shown in section 4. Section 5 summarizes the results of a sensitivity analysis with respect to different pre-processing methodologies. A summary and discussion, as well as an outlook for future work are given in section 6.

2. Data

The analysed global hindcasts were simulated with the coupled model MPI-ESM in low-resolution (MPI-ESM-LR; Giorgetta et al., 2013). Its atmospheric component is based on the ECHAM6 model (Stevens et al., 2013) with a horizontal resolution of T63 and 47 vertical levels, which is coupled to the MPIOM ocean model (Jungclaus et al., 2013) with a horizontal resolution of 1.5° and 40 vertical levels. Two hindcast generations are considered here, both computed with the MPI-ESM-LR but with different initialisation strategies. The first generation (baseline0; Müller et al., 2012) is initialised with oceanic conditions from an assimilation experiment, where the model state is nudged towards temperature and salinity anomalies from NCEP/NOAA reanalysis (Kalnay et al., 1996). For the second generation (baseline1; Pohlmann et al., 2013b), temperature and salinity anomalies from the ocean reanalysis system 4 (ORAS4; Balmaseda et al., 2013) are used instead, together with a full-field 3-D atmospheric initialisation using fields from ERA40 (Uppala et al., 2005) and ERA-

Interim (Dee et al., 2011). For both generations, yearly initialised hindcasts are available, each of them comprising a 10-year period. For the downscaling experiment, global forcing for hindcasts of five starting dates are used (1 January 1961, 1971, 1981, 1991, and 2001; hereafter referred to as dec1960, dec1970, dec1980, dec1990, and dec2000) to cover the whole period from 1961-2010. For each starting date, an ensemble of 10 members was generated using 1-day lagged initialisation from the assimilation experiments (cf. Marotzke et al., 2016 for more details). This resulted in an ensemble of 50 global hindcasts per generation (baseline0 and baseline1; hereafter MPI_b0 and MPI_b1).

In this study, we analyzed global hindcasts dynamically downscaled to the EURO-CORDEX domain (Giorgi et al., 2006; cf Figure 1) at a horizontal grid resolution of 0.22° using the mesoscale non-hydrostatic regional climate model COSMO-CLM (CCLM; Rockel et al., 2008) on a rotated grid. The model version COSMO4.8-clm17 is employed. By using the MPI-ESM-LR ensemble as driving data, the global "initial condition" perturbation strategy is simply passed to the regional model. Analog to the global data, the experiment includes MPI_b0 and MPI_b1 downscaled hindcasts for dec1960, dec1970, dec1980, dec1990, and dec2000, with 10 members per decade (hereafter CCLM_b0 and CCLM_b1).

To evaluate the performance of both the global MPI-ESM and the regional CCLM hindcasts, a CCLM simulation run with reanalysis boundary conditions and observational datasets are used for verification. For temperature and precipitation we consider the observational dataset E-OBS (Haylock et al., 2008) based on the ECA&D (European Climate Assessment & Dataset; http://eca.knml.nl/) at a regular 0.25°x0.25° grid. As no gridded dataset is available for wind, a CCLM simulation forced with boundary conditions from ERA40 and ERA-Interim is employed as verification dataset for wind speed. For this reanalysis driven simulation CCLM is applied in the same model setup as for the regionalisation of the global hindcast ensemble (see above).

In this study, we want to quantify if the initialisation with observed climate states improves the performance of decadal predictions. To address this issue, uninitialised model simulations started from historical CMIP5 runs are usually considered as reference dataset (see also section 3.2). With this aim, a 10-member ensemble of uninitialised MPI-ESM-LR historical runs started from a pre-industrial control simulation are used, which are only forced by the aerosol and greenhouse gas concentrations for the period 1850-2005 (e.g. Müller et al., 2012).

3. Methods

3.1 Data processing

All datasets considered in this study are pre-processed in an analogous manner to enable a direct comparison. First, all data is interpolated to the same regular 0.25°x0.25° grid, which corresponds to the resolution of the E-OBS data. At each grid point, monthly anomaly time series are computed by subtracting the long-term means for the period 1961-2010 from the interpolated raw datasets.

In this study, we are primarily interested in anomalies on inter-annual to decadal timescales, which can be associated with the natural variability. Thus, to exclude responses to external radiative forcing, all monthly anomaly time series are de-

Earth Syst. Dynam. Discuss., https://doi.org/10.5194/esd-2017-70
Manuscript under review for journal Earth Syst. Dynam.
Discussion started: 4 September 2017

trended. We use a simple linear regression approach for all variables at each grid point to remove the long-term trend for the period 1961-2010, as the trend for the different variables over Europe cannot be uniformly defined but depends on the considered region (Christensen et al., 2007b). Finally, annual values are derived and multi-annual means for lead years 1-5 are built for further evaluation. In order to assess the impact of the de-trending on the predictive skill, the data processing steps as described above are repeated without de-trending for a sensitivity study.

Following the suggestion of Goddard et al. (2013), the skill analysis is mainly performed for spatial means. Spatial averaging of the de-trended anomaly time series is performed for eight PRUDENCE regions over Europe (see Fig. 1; Christensen and Christensen, 2007a). Note that we only used grid points over land surfaces for the spatial means, as E-OBS data are not available over the oceans. Additionally, we calculated the predictive skill on the basis of all individual grid points for specific exercises.

3.2 Skill metrics

The following three metrics are used to evaluate the performance of the global and regional hindcast ensembles and to address the three key questions: the continuous ranked probability skill score (CRPSS), the mean squared error skill score (MSESS), and the anomaly correlation coefficient (ACC). The skill metrics are applied to the pre-processed time series described in section 3.1 and are computed for multi-annual means for lead time years 1-5 after initialisation. Recent studies analysing the MiKlip decadal prediction system demonstrated that the MiKlip ensemble performs best for the first years after initialisation for a wide range of variables, while the skill diminishes for longer forecast periods. For example, Müller et al. (2012) found highest skill scores for years 1-4 and 2-5 for annual mean surface temperature both for the North Atlantic region and global means. The same is true for annual wind speed and wind energy potentials over Central Europe, for which skilful predictions are mainly restricted to the first years after initialisation (1-4 years), while negative skill scores are found for longer lead time periods (Moemken et al., 2016). Kruschke et al. (2014) provided evidence that the prediction skill for winter cyclones over the North Atlantic region is best for years 2-5 and reduced for longer time periods. Following the recommendation by Goddard et al. (2013), we focus in the following on the lead-time 1-5 years after initialisation, for which possible skill should originate mainly from the initialisation.

The CRPSS (e.g. Goddard et al., 2013) is often used to assess the reliability of probabilistic forecast models and defined as

$$CRPSS = 1 - \frac{CRPS_{hind}}{CRPS_{ref}}$$

with

$$CRPS = \int_{-\infty}^{\infty} [F(y) - F_o(y)]^2 \, dy$$

$CRPS_{hind}$ is the continuous ranked probability score (CRPS; Wilks, 2011), comparing cumulative distribution functions (CDFs) of the initialised hindcast experiments with CDFs of the verification dataset (observations). $CRPS_{ref}$ is the CRPS of a

Earth Syst. Dynam. Discuss., https://doi.org/10.5194/esd-2017-70
Manuscript under review for journal Earth Syst. Dynam.
Discussion started: 4 September 2017

reference dataset, which are in this study the uninitialized MPI-ESM-LR historical simulations. In case of a positive CRPSS the reliability in terms of the probabilistic quality of the forecast spread is higher in the initialised hindcasts than in the reference dataset, which is in this case the uninitialised historical ensemble. It can thus be used to test if the model ensemble spread adequately represents the forecast uncertainty.

The deterministic MSESS (Goddard, 2013) is defined as

$$MSESS = 1 - \frac{MSE_{hind}}{MSE_{ref}}$$

with

$$MSE = \frac{1}{N}\sum_{n}^{N}(\bar{X}_{\iota} - O_i)^2$$

where MSE_{hind} is the mean squared error (MSE) between the ensemble mean of the initialised hindcasts (X_i) and the verification data, and MSE_{ref} is the mean squared error of the uninitialised reference dataset versus the verification data (O_i). A positive MSESS means that the hindcasts are closer to the verification dataset than the uninitialised runs, indicating that the initialisation leads to higher accuracy in predicting observed values. Note that independently from the ensemble size of the hindcast ensembles, the same historical 10-member ensemble is always used as reference dataset for the computation of CRPSS and MSESS.

The ACC (e.g. Wilks, 2011) is computed as the Pearson correlation between the ensemble mean of the hindcasts at a certain location i and the corresponding observations (Obs):

$$ACC_i = \frac{1}{N}\frac{\sum_t hind_t\, Obs_t}{\sigma_{hind}\,\sigma_{Obs}}$$

where $t = 1, \ldots, N$ is the time index. The ACC quantifies the accuracy of the predictions only in terms of the temporal course, while it is independent from the mean bias.

4. Results

4.1 Is there a potential for skilful regional decadal predictions in Europe?

In this section we address the key question of the general potential for skilful regional decadal predictions over Europe. With this aim, we analyse both the potential added value of initialization compared to the (uninitialized) historical runs and the implications of removing the long-term trend for the predictive skill. Skilful in this context means an improvement of the skill metrics, e.g., when comparing de-trended decadal hindcasts to the uninitialised climate simulations. We therefore analyse the ability of the forecast system to better predict the climate variations up to five years ahead due to the initialization with observations using different skill metrics (see section 3.2). To determine the predictive skill over Europe,

the three skill scores were calculated for all individual land grid points of the Euro-CORDEX domain on the 0.25° grid (see section 3.1).

Fig. 2 shows MSESS plots for the de-trended time-series of temperature, precipitation and surface wind speed in CCLM_b0 and CCLM_b1. For temperature (Fig. 2a and 2b), positive skill scores are found in both ensembles over Scandinavia and for the Mediterranean, while a stripe of negative values occurs over the British Isles and Central Europe. The largest deviations between CCLM_b0 and CCLM_b1 are found for Iberia, parts of southern France and Italy, where the MSESS is positive for CCLM_b1 but neutral to negative for CCLM_b0. To determine the effect of the trend on the predictive skill, we compare the data with (tr) and without trend (dtr) for the example of CCLM_b1 (first and second column of Table 1 and Table 2), keeping all other post-processing steps the same (see section 3.1). With trend included, the correlation improves (Table 1). It shows high positive values between 0.68 - 0.96 in all regions, thus indicating that a predictive skill for temperature arises at least partially from a realistic prediction of the climate trend. The MSESS (Table 2) increases for all but the north-western regions (BI, FR, ME), but is less improved than the correlation.

Larger deviations between both ensembles are revealed for precipitation (Fig. 2c and 2d), where the MSESS fields are distinctly patchier when compared to temperature (Fig. 2a and 2b), reflecting the local character of rainfall. Both ensembles show positive MSESS values for regions in Scandinavia, Eastern Europe, Iberia, and the British Isles (Fig. 2c and 2d). In CCLM_b1, predictive skill is also identified over Western Central Europe. Thus for CCLM_b1 positive skill is found for larger areas indicating an added value of the improved initialization procedure in baseline1 compared to baseline0. Like for temperature the skill scores for precipitation benefit from including the trends (column 3 and 4 of Table 1 and Table 2), although not as uniformly and strongly as for temperature. MSESS is improved only in the southern and eastern regions by including the trend.

Regarding wind speed, the predictive skill in CCLM_b0 (Fig. 2e) shows high MSESS values over Scandinavia, Iberia, Southern Italy and along the coasts of the North and the Baltic Sea, while strongly negative values are found e.g. over most of France, southern Germany and the Alpine region. In CCLM_b1, the MSESS depicts low but positive values over most of Western and Central Europe, while strong negative values are now identified over parts of Eastern Europe (Fig. 2f). Overall the predictive skill of CCLM_b0 is slightly higher and affects a larger area, indicating that the changes in the initialization method do not improve the results for wind speed. Including the trend leads to higher skill scores in most regions for CCLM_b1 (fifth and sixth column of Table 1 and Table 2). Here, the MSESS improves more distinctly than for the other variables.

We conclude that in terms of the MSESS accuracy there generally is a potential for skilful decadal predictions over Europe in the regional MiKlip ensembles. However, the skill pattern is not uniformly found as it depends on the region and the variable, i.e. for individual regions the initialisation of the hindcasts and decadal predictions lead to an added value for accurate (retrospective) forecasts several years ahead, while for some regions the uninitialized historical runs deliver more reliable predictions. Further, the discrepancies between the two hindcast generations (CCLM_b0 and CCLM_b1), seem to indicate a slight shift in the pattern due to the different initialization methods for the global predictions.

Earth Syst. Dynam. Discuss., https://doi.org/10.5194/esd-2017-70
Manuscript under review for journal Earth Syst. Dynam.
Discussion started: 4 September 2017

The skill of a prediction was also quantified using CRPSS and ACC. The spatial distribution of the CRPSS is very similar to that of the MSESS, while large deviations may arise for the ACC. This is exemplary shown in Fig. 3 for wind speed. For example, positive MSESS values are obtained for CCLM_b1 for Scandinavia and the coast of the North Sea (Fig. 2f), while the ACC is mainly negative for this domain (Fig. 3b). On the other hand, the spatial CRPSS patterns (Fig. 3c and 3d) agree well to MSESS for both ensembles (Fig. 2e and 2f). Again, there are strong differences in the prediction skill for wind speed between CCLM_b0 and CCLM_b1, in particular for ACC (Fig. 3a and 3b). These differences might to some extent be associated with the different representation of the cyclone track density in the two ensembles. Kruschke et al. (2014) showed that the skill for winter cyclones is rather low in b1, while positive skill scores are detected in b0 over some parts of Europe and southeast of Iceland.

For the better understanding of the skill scores and their relation the different skill metrics are compared in scatter plots. Fig. 4a exemplary shows scatter diagrams of CRPSS vs the MSESS for temperature on individual grid point basis for CCLM_b1 for the mean over the lead-time 1–5 years. Generally, the accuracy and the reliability can vary highly with geographical position. However, and for the majority of the individual land grid points over Europe, positive MSESS are concurrent with positive CRPSS values (upper right quadrant). Both skill scores are linked to each other, as a quasi linear dependency between CRPSS and MSESS is found. This is not only the case for CCLM_b1 (Fig. 4a) but also for MPI_b1 (Fig. 4b). In particular, we found that positive values for CRPSS often accompany with a high accuracy of the decadal predictions. This is generally true for all variables and both ensembles considered here (not shown).

On the other hand, no such linear relationship between ACC vs MSESS is found (see Fig. 4c for temperature). The ACC vs MSESS combination is clearly stronger scattered than for CRPSS vs MSESS, both in terms of the general spread and the peak values of the number of grid points with a given skill score combination. Hence, a low mean bias of decadal predictions (resulting in positive MSESS values) does not necessarily imply a realistic temporal evolution. Still, positive MSESS values correspond to positive ACC values for most of the individual grid points, indicating a high potential for skilful regional decadal predictions over Europe. There are similar findings for precipitation (Fig. 4 e) with a broad distribution of the correlation values and a narrower range of the core area for the MSESS.

For ACC, keeping the original time series leads to enhanced predictability, while the impact of de-trending on the MSESS is less clear. In fact, the removal of a linear trend may in some cases be problematic. For example, if this trend is associated with a changing AMO phase, this may lead to an underestimation of the skill. During the investigation period, the AMO phase has indeed changed from cold to a warm (Sutton and Hodson, 2005). A proper attribution of the detected trends to greenhouse-gas induced climate change versus natural variability pattern is thus difficult.

4.2 Does regional downscaling provide an added value for decadal predictions?

Recent studies document that the application of regional climate models may improve climate simulations, in particular over complex terrain (Berg et al., 2013; Feldmann et al., 2013; Hackenbruch et al., 2016). This is mainly due to a more realistic

Earth Syst. Dynam. Discuss., https://doi.org/10.5194/esd-2017-70
Manuscript under review for journal Earth Syst. Dynam.
Discussion started: 4 September 2017

representation of the topography (e.g. mountain ranges or coast lines) in the RCMs compared to global-scale GCMs. In this section we analyse whether the downscaling with a regional climate model also leads to an added value for decadal predictions over Europe.

Figure 4 already indicates a shift of the overall distribution of skill scores from regionalised hindcasts towards higher values compared to the global ones for the baseline1 ensemble. For temperature the core area of the skill values from the regional hindcasts (Fig 4a) is more confined to the upper right quadrant compared to the global ensemble (Fig 4b). This indicates an added value of downscaling for the accuracy as well as for the reliability. For the temperature correlation, the patterns are quite similar (Fig4 c, d), whereas for precipitation there is a clear shift towards an improved correlation and for a higher MSESS from the downscaling (Fig. 4 e,f). No or only a marginally low added value of regionalization on grid point scale is observed for CCLM_b1 wind speed and for the majority of the variables and skill metrics in the baseline0 ensemble (not shown).

Ideally, an added value of downscaling should be accompanied by a positive absolute skill. Figure 5 depicts these two aspects for the three variables (2m temperature, precipitation, near-surface wind), the three verification metrics (MSESS, ACC, CRPSS), and the two ensemble generations (b0 and b1), as derived for the spatial means over the eight PRUDENCE regions (cf. Fig. 1). Green dots indicate an added value of the CCLM results compared to MPI-ESM-LR and red dots no added value. Red background color indicates a negative skill score and green color a positive skill for the respective metric. This figure can be interpreted along several dimensions: (i) the skill for the different climate variables (background color), (ii) the improvement by downscaling (dot color), (iii) the improvement from b0 to b1, (iv) the skill for different regions, (v) and the different skill metrics.

For temperature, CCLM_b1 mostly shows an added value compared to MPI_b1 as well as compared to CCLM_b0. For most regions, this is particularly expressed in the MSESS and the anomaly correlation. For instance, with respect to the accuracy (MSESS and ACC) CCLM_b1 has higher skill in 6 of 8 PRUDENCE regions compared to MPI_b1. No added value of downscaling in both ensemble generations is found only for France (FR – region 3 from Fig. 1). Additionally, no benefit from downscaling could be detected with CCLM_b0 for the British Isles (BI – 1), Mid-Europe (ME - 4) and the Mediterranean Area (MD - 7), where CCLM_b1 performs better. In general, in CCLM_b1 there are more regions with positive skill scores in southern Europe (IP - 2, AL - 6) and in Scandinavia (SC- 5). In the Mediterranean region both ensemble generations depict only positive skill scores.

For precipitation, an improvement from downscaling is detected particularly for CCLM_b1 over the majority of metrics and regions. In addition, CCLM_b1 is clearly superior to CCLM_b0 with respect to skill and added value. This indicates a positive effect of the improved initialization procedures in b1 compared to b0 (Pohlmann, 2013b). However, this improvement does not affect all regions. CCLM_b0 performs better than its successor for the Iberian Peninsula, whereas skill and/or added value are higher in CCLM_b1 for the regions in the North-West (BI, FR, ME) and North (SC). With respect to the reliability CCLM_b1 outperforms CCLM_b0 for precipitation (CCLM_b0: 4 regions with positive CRPSS,

CCLM_b1: 7 regions with positive CRPSS), while for temperature both ensembles are equivalent (2 regions with positive CRPSS in CCLM_b0 and in CCLM_b1).

For the near surface wind Fig. 5 shows heterogeneous results. CCLM_b0 has an added value of downscaling in more regions than CCLM_b1. On the other hand CCLM_b1 provides an added value for the CRPSS in 4 regions, while for CCLM_b0 no added value of downscaling is found with respect to the reliability. CCLM_b0 has a positive skill in the Northern parts of the domain (BI, SC), whereas positive skill scores are found for CCLM_b1 over most other PRUDENCE regions at least for one skill metric. For Eastern Europe (EA - 8) none of the metrics are positive for both generations.

The detected shift in the skill patterns between CCLM_b0 and CCLM_b1 can be expected due to the different initialization procedures of the two generations. However, there also seem to be regions with more stable skill properties: The Mediterranean area shows positive skill for all variables and metrics (except wind in CCLM_b0).

An added value of regionalization over the majority of variables and metrics can be found for Southern Europe (MD, IP) and Scandinavia. As these areas have complex coastlines and orography, this result may be indicative of a better representation of small-scale processes in the CCLM. On the other hand, for the Alps (AL) only the ACC shows skill and added value from downscaling for temperature in both generations. The PRUDENCE region AL is the smallest of the regions, with the steepest orography. It might be that for the Alps an even higher resolution for the downscaling would be advantageous to improve the accuracy and reliability of the hindcasts.

We conclude that regional downscaling indeed may provide an added value for decadal predictions over Europe. However, while for some complex regions like MD, IP or SC this added value is to some extent systematic, for other areas in Europe the analysis reveals a mixed picture for the different variables and the skill metrics.

4.3 How does the regional decadal predictive skill depend on the ensemble size?

Past studies suggest that the ensemble size of a prediction system has an impact on the forecast skill of a model (Richardson, 2001; Ferro et al., 2008). Generally, there is consensus that the prediction skill for both seasonal and decadal predictions is enhanced when the number of ensemble members is increased. Kadow et al. (2014) analysed the global MiKlip baseline1 generation and concluded that the forecast accuracy for surface temperature for lead year 1 and 2-9 is improved for nearly the whole globe when the ensemble size is increased from 3 to 10 members. This is in line with the findings of Sienz et al. (2016), who examined the prediction skill for North Atlantic sea surface temperature in the same hindcast ensemble. Also for seasonal predictions of the North Atlantic Oscillation a forecast system profits from increasing size (e.g. Scaife et al., 2014). However, it is still open how a regional decadal forecast system does depend on the quantity of ensemble members. With this aim we analysed the impact of the ensemble size in the predictive skill for the eight PRUDENCE regions in Europe in both the regional and the global MiKlip ensembles. In the following, results are only exemplary shown for the Iberian Peninsula (IP), as the findings are similar for the other PRUDENCE regions. Figure 6 exhibits the dependency of CRPSS, MSESS, and ACC for lead years 1-5 (y-axis) on the ensemble size (x-axis) for all three variables spatially averaged over IP.

Earth Syst. Dynam. Discuss., https://doi.org/10.5194/esd-2017-70
Manuscript under review for journal Earth Syst. Dynam.
Discussion started: 4 September 2017

For each ensemble size *n* (*n* varying between 2 and 10), the solid coloured lines depict the averaged skill scores for all permutations of *n*-member ensemble combinations for each of the four individual hindcast ensembles (MPI_b0, MPI_b1, CCLM_b0, and CCLM_b1). Ranked probability skillscores may be negatively biased for small ensembles sizes (e.g. Ahrens and Walser, 2008), while such a bias is not reported for MSESS and ACC. To ensure a direct comparability of the results for the three skill metrics we therefore decided not to use a de-biased version of the CRPSS in this study.

Enhanced predictive skill can be observed when the number of members is stepwise increased for both the global and the regional hindcast ensembles. MSESS and CRPSS show a rather logarithmic relationship with increasing n, depicting the highest skill scores for the 10 member ensembles for all three variables (Figure 6a-c and 6g-i). On the other hand, the lowest skill scores (often with negative values for CRPSS and MSESS) are always found for the 2-member ensembles. This ensemble size dependency of MSESS and CRPSS is systematic and is found in both hindcast generations for all variables over all eight PRUDENCE regions (not shown), regardless whether the skill scores are negative or positive. In some cases, the ensemble size increase even leads to a shift from negative MSESS and CRPSS values to positive values (e.g. Fig. 6c, 6h, and 6i). In contrast, no systematic conclusion can be stated for the ACC, as the ensemble size dependency of the predictive skill depends on the variable and the considered MiKlip ensemble (Fig. 6d-f). But even here a larger ensemble size is advantageous, as negative skill scores become more robust (cf. Fig. 6e, f). Nevertheless, there are also examples for the ACC where the ensemble size dependency is similar to that of MSESS and CRPSS, like e.g. for temperature (Fig. 6d). These results suggest that a decadal prediction system generally benefits from larger ensemble sizes, either in terms of more skilful and reliable decadal forecasts or at least of a reduction of the bias or the uncertainty, depending on the variable and the hindcast generation. Note that for most variables and skill scores the hindcast generation is more important for the skill than the resolution. In additions, most diagrams indicate an added value of downscaling. For the reliability of wind speed both generations of CCLM surpass their MPI counterparts, indicating a systematic added value of downscaling.

For ensembles with less than 10 members, the skill scores of all possible *n*-member ensemble combinations are averaged. This is exemplary illustrated for the MSESS for precipitation in the CCLM_b0 ensemble (see box-whisker plots in Fig. 6b). While the spread between the individual *n*-member ensembles declines with an increasing number of members *n*, it is quite large for small ensemble sizes: for instance, the MSESS varies between -1.5 and +0.8 for the 2-member ensembles (Fig. 6b). In fact, even for the 7-member ensemble quite different results can be found depending on the selection of the ensemble members, ranging from high positive MSESS values to zero. These results clearly demonstrate the necessity of using large ensembles to reduce these uncertainties.

We conclude that the predictive skill with respect to both accuracy and model spread is generally improved when the size of the hindcast ensembles increases. This is valid for all variables, regions, and hindcast ensembles considered in this study. The skill scores converge towards a certain value in most cases for MSESS and CRPSS in all hindcasts (see Fig. 6a-c and 6g-i). The increments in added value by increasing the number of ensemble members decrease for more than 5 members. Nevertheless, it is recommended to use ten members or more for the skill assessment of decadal predictions on the regional scale.

Earth Syst. Dynam. Discuss., https://doi.org/10.5194/esd-2017-70
Manuscript under review for journal Earth Syst. Dynam.
Discussion started: 4 September 2017

Earth System Dynamics Discussions
Open Access
EGU

5. Summary and discussion

In this study the decadal predictability in the regional MiKlip decadal prediction system is analysed for temperature, precipitation, and wind speed over Europe and compared to the forecast skill of the global ensemble. The goal is to assess the prospect of such a system for the application in forecasts on decadal timescales. Focus is given to years 1-5 after initialization. Three skill scores are used to quantify the accuracy and the reliability of the two different MiKlip hindcast generations. The main findings of our study can be summarized as follows:

- There is a potential for regional decadal predictability over Europe for temperature, precipitation, and wind speed in the MiKlip system, but the predictive skill depends on the variable, the region, and the hindcast generation.
- The MiKlip prediction system may distinctly benefit from regional downscaling. An added value in terms of accuracy and reliability is particularly revealed for temperature over the British Isles (BI), Scandinavia (SC), the Mediterranean (MD), and for precipitation over the British Isles (BI), Scandinavia (SC), Mid-Europe (ME), and France (FR) for the b1 generation. Most of these regions are characterized by complex coastlines and orography, which indicates that the better representation of topographic structures in the regionalised hindcasts may improve the predictive skill.
- The improvement of the initialization procedure from baseline0 to baseline1 as described in Pohlmann et al. (2013b) increases the overall predictive skill in the downscaled MiKlip hindcasts over Europe, at least for precipitation and temperature. But improvement of the skill varies between variable and region. The skill for temperature increases around the Mediterranean Sea and parts of Scandinavia from b0 to b1. For precipitation the skill of b1 compared to b0 is higher in all regions but the Iberian Peninsula. Only for wind speed there is mostly no benefit from the improved initialization in most regions.
- A systematic enhancement of MSESS and CRPSS skill scores is found with increasing ensemble size, and a number of 10 members is found to be suitable for decadal predictions. This is valid for all variables and European regions in the global and regional MiKlip ensembles.
- The predictive skill may increase when keeping the original time series including the long-term trend. A linear de-trending may remove parts of the signal since the climate trend and the AMO teleconnection pattern are in phase both contributing to ascending trends over the hindcast period 1960 – 2010.

Müller et al. (2012) and Pohlmann et al. (2013b) had found systematic prediction skills for surface temperature over large parts of the North-Atlantic and Europe in both global generations (baseline0, baseline1). From the results of our study, it is apparent that key European regions for decadal predictability (beyond the climate trend) with the regional prediction system seem to be the Mediterranean Area and the Iberian Peninsula. This is in line with findings from Guemas et al. (2015). This finding may be related with skilful predictions of the AMO (Garcia-Serrano et al., 2012; Guemas et al., 2015). Due to the rather non-linear relationship of these large-scale North Atlantic features to regional atmospheric conditions over Europe, the mechanisms steering the decadal variability and predictability of climate variables in European regions are thus more

complex. The decadal variability of regional precipitation, temperature, and wind speed over most parts of Europe is largely affected by the North Atlantic oscillation, but its skilful decadal predictability over the continent is still under debate. With this respect, a better understanding of the mechanisms relevant for the regional climate over Europe on the decadal time scale is required, as was for example obtained for the tropical Atlantic (Dunstone et al., 2011). This is an objective of the ongoing 2nd phase of the MiKlip project.

The skill scores may strongly vary between neighbouring grid points. Comparable results were found by e.g. Guemas et al. (2015), who detected a rather diffuse pattern for the accuracy of decadal predictions over Europe for seasonal temperature and precipitation. This might at least partly be due to spatial and temporal inhomogeneity of the gridded observational references. A more realistic assessment of the prediction skill can be made by considering spatial means (Goddard et al., 2013) which was mostly considered in this study. In line with e.g. Kadow et al. (2016), we could show that an enlargement of the ensemble size up to 10 members results in an improvement of the prediction skill over Europe. However, prediction skill could further benefit from even larger ensemble sizes, especially in areas with low signal-to-noise ratio (cf. Sienz et al., 2016).

Bias and drift adjustment (e.g., Boer et al., 2016) provide prospect in skill improvement not only for GCMs but also for RCMs. This is particularly the case for ensemble simulations run with full-field initialization (prototype, not analysed here; cf. Marotzke et al., 2016). While bias and drift adjustment methods have improved the forecast skill of near-term climate prediction (e.g., Kruschke et al., 2016), such corrections are less important for the baseline0 and baseline1 ensembles analysed here as they were generated with anomaly initialisation (Marotzke et al., 2016). Nevertheless, bias correction and calibration are an important topic in the second phase of MiKlip.

Due to the high computational costs of dynamical downscaling, only five starting dates (one per decade) are available for the regional MiKlip ensemble generation b0 (see section 2). This is a shortcoming regarding the statistical significance of the results and some of the statements presented in this study. The statistical significance will be easier to quantify when the regional simulations for the newest Miklip ensemble generation are available with annual starting dates over more than 50 years. On the other hand, regional decadal forecasts may have advantages beyond the examples discussed in this paper. For example, RCMs enables the integration of improved components of the hydrological cycle or climate-system components with memory on multi-year time-scales like soil moisture (Khodaya et al., 2014; Sein et al., 2015). Kothe et al. (2016) has shown that extracting the initial state of the deep soil in the RCMs from regional data assimilation schemes may improve decadal predictions. Further, Akhtar et al. (2017) demonstrated that the regional feedback between large water bodies and the atmosphere play a major in the regional climate system. This feedback can only be captured in regionalized climate predictions by a dynamic RCM-ocean coupling. Most of the approaches mentioned above are ongoing within the 2nd phase of MiKlip and are expected to enhance the decadal predictability over Europe. We thus conclude that a decadal prediction system would clearly benefit from a regional forecast ensemble.

The regional decadal prediction system generated by the MiKlip consortium comprises altogether 1000 years (two hindcast generations, each of them comprising ten hindcast members for five starting years) of simulations with 0.22° for the entire

EURO-CORDEX region, which is a to our best knowledge unprecedented. Hence, this ensemble enabled us to gain important insights into different aspects and the prospects of regional downscaling for decadal predictions, and serve as a good basis for future studies. In the ongoing 2nd phase of MiKlip it is planned to downscale a complete ensemble hindcast generation with ten members for more than 50 starting years, giving altogether more than 5000 years.

Author Contributions

MR, HF, SM and MU developed the concept of the paper; MR, HF and JGP wrote the first manuscript draft. MR, HF, SM, MU, NL and JM contributed with data analysis and analysis tools. HF, SM, MR, BA, BF contributed with RCM simulations. MK and WM contributed with the global MPI-ESM-LR simulations and prepared boundary conditions for RCM simulations. CK leads the MiKlip-C consortium, with CO-Is BA, BF, JGP, GS. All authors contributed with ideas, interpretation of the results and manuscript revisions.

Acknowledgments

MiKlip is funded by the German Federal Ministry for Education and Research (BMBF, contracts: 01LP1518 A-D and 01LP1519) All simulations were carried out at the German Climate Computing Centre (DKRZ), which also provided all major data services. We acknowledge the E-OBS data set from the EU-FP6 project ENSEMBLES (http://ensembles-eu.metoffice.com) and the data providers in the ECA&D project (http://www.ecad.eu). We thank the European Centre for Medium-Range Weather Forecasts (ECMWF) for their ERA-40 and ERA-Interim Reanalysis data (http://apps.ecmwf.int/datasets/). JGP thanks the AXA Research Fund for support. We thank past and present members of the MiKlip –C (Regionalization) group for discussions and comments.

References

Akhtar, N., Brauch, J., and Ahrens, B.: Climate Modeling over the Mediterranean Sea: Impact of Resolution and Ocean Coupling, Clim. Dynam., doi:10/1007/s00382-017-3570-8, 2017.

Balmaseda, M. A., Mogensen, K., and Weaver, A. T.: Evaluation of the ECMWF ocean reanalysis system ORAS4, Q. J. R. Meteor. Soc., 139, 1132-1161., doi:10.1002/qj.2063, 2013.

Benestad, R. E. and Mezghani, A.: On downscaling probabilities for heavy 24-hour precipitation events at seasonal-to-decadal scales, Tellus A, 67, 25954, doi:10.3402/tellusa.v67.25954, 2015.

Berg, P., Wagner, S., Kunstmann, S., and G. Schaedler: High resolution regional climate model simulations for Germany: part I – validation, Clim. Dynam., 40, 401-414, 2013.

Boer, G. J., Smith, D. M., Cassou, C., Doblas-Reyes, F., Danabasoglu, G., Kirtman, B., Kushnir, Y., Kimoto, M., Meehl, G. A., Msadek, R., Mueller, W. A., Taylor, K. E., Zwiers, F., Rixen, M., Ruprich-Robert, Y., and Eade, R.: The Decadal Climate Prediction Project (DCPP) contribution to CMIP6, Geosci. Model Dev., 9, 3751-3777, doi:10.5194/gmd-9-3751-2016, 2016.

Chikamoto Y., Kimoto, M., Ishii, M., Mochizuki, T., Sakamoto, T. T., Tatebe, H., Komuro, Y., Watanabe, M., Nozawa, T., Shiogama, H., Mori, M., Yasunaka, S., and Imada, Y.: An overview of decadal climate predictability in a multi-model ensemble by climate model MIROC, Clim. Dynam., 40, 1201-1222, doi:10.1007/s00382-012-1351-y, 2012.

Christensen, J.H. and Christensen, O.B.: A summary of the PRUDENCE model projections of changes in European climate by the end of this century, Climate Change, 81, 7-30, doi:10.1007/s10584-006-9210-7, 2007a.

Christensen, J.H., Hewitson, B., Busuioc, A., Chen, A., Gao, X., Held, I., Jones, R., Kolli, R.K., Kwon, W.-T., Laprise, R., Magaña Rueda, V., Mearns, L., Menéndez, C.G., Räisänen, J., Rinke, A., Sarr, A., and Whetton, P.: Regional Climate Projections, in: Climate Change 2007: The Physical Science Basis. Contribution of Working Group I to the Fourth Assessment Report of the Intergovernmental Panel on Climate Change, Cambridge University Press, Cambridge, United Kingdom and New York, NY, USA, 2007b.

Corti S., Palmer, T., Balmaseda, M., Weisheimer, A., Drijfhout, S., Dunstone, N., Hazeleger, W., Kröger, J., Pohlmann, H., Smith, D., von Storch. J.-S., and Wouters, B.: Impact of Initial Conditions versus External Forcing in Decadal Climate Predictions: A Sensitivity Experiment, J. Climate, 28, 4454–4470, doi:10.1175/JCLI-D-14-00671.1, 2015.

Dee, D. P., Uppala, S. M., Simmons, A. J., Berrisford, P., Poli, P., Kobayashi, S., Andrae, U., Balmaseda, M. A., Balsamo, G., Bauer, P., Bechtold, P., Beljaars, A. C. M., van de Berg, L., Bidlot, J.,Bormann, N., Delsol, C., Dragani, R., Fuentes, M., Geer, A. J., Haimberger, L., Healy, S. B., Hersbach, H., Holm, E. V., Isaksen, L., Kallberg, P., Köhler, M., Matricardi, M., McNally, A. P., Monge-Sanz, B. M., Morcrette, J.-J., Park, B.-K., Peubey, C., de Rosnay, P., Tavolato, C., Thepaut, J.-N., and Vitart, F.: The ERA-Interim reanalysis: configuration and performance of the data assimilation system, Q. J. R. Meteor. Soc., 137, 553-597, doi:10.1002/qj.828, 2011.

Doblas-Reyes, F. J., Andreu-Burillo, I., Chikamoto, Y., García-Serrano, J., Guemas, V., Kimoto, M., Mochizuki, T., Rodrigues, L. R. L. and van Oldenborgh, G. J.: Initialized near-term regional climate change prediction, Nature Commun., 4, 1715, doi:10.1038/ncomms2704, 2013.

Dunstone, N. J., Smith, D. M., and Eade, R.: Multi-year predictabilityof the tropical Atlantic atmosphere driven by the high latitude North Atlantic Ocean, Geophys. Res. Lett., 38, L14701, doi:10.1029/2011GL047949, 2011.

Feldmann, H., Schaedler, G., Panitz, H.-J., and Kottmeier, C.: Near future changes of extreme precipitation over complex terrain in Central Europe derived from high resolution RCM ensemble simulations, Int. J. Climatol., 33, 1964-1977, 2013.

Ferro, C. A. T., Richardson, D. S., and Weigel, A. P.: On the effect of ensemble size on the discrete and continuous ranked probability scores, Meteorol. Appl., 15, 1, 19-24, doi:10.1002/met.45, 2008.

Garcia-Serrano, J., Doblas-Reyes, F. J., and Coelho, C. A. S.: Understanding Atlantic multi-decadal variability prediction skill, Geophys. Res. Lett., 39, L18708, doi:10.1029/2012GL053283, 2012.

Giorgetta, M. A., Jungclaus, J. J., Reick, C. H., Legutke, S., Bader, J., Böttinger, M. and Brovkin, V., Crueger, T., Esch, M., Fieg, K., Glushak, K., Gayler, V., Haak., H., Hollweg, H.-D., Ilyina, T., Kinne, S., Kornblueh, L., Matei, D., Mauritsen, T., Mikolajewicz., U., Mueller, W. A., Notz, D., Pithan, F., Raddatz, T., Rast, S., Redler, R., Roeckner, E., Schmidt, H., Schnur, R., Segschneider, J., Six, K. D., Stockhause, M., Timmreck, C., Wegner, J., Widmann, H., Wieners, K.-H., Claussen, M., Marotzke, J., and Stevens, B.: Climate and carbon cycle changes from 1850 to 2100 in MPI-ESM simulations for the Coupled Model Intercomparison Project phase 5, J. Adv. Model. Earth Sy., 5, 572–597, doi:10.1002/jame.20038, 2013.

Giorgi, F., Jones, C., and Asrar, G. R.: Addressing climate information needs at the regional level: the CORDEX framework, Bulletin of the World Meteorological Organization, 58, 175-183, 2006.

Goddard, L., Kumar, A., Solomon, A., Smith, D., Boer, G., Gonzalez, P., Kharin, V., Merryfield, W., Deser, C., Mason, S. J., Kirtman, B. P., Msadek, R., Sutton, R., Hawkins, E., Fricker, T., Hegerl, G., Ferro, C. A. T., Stephenson, D. B., Meehl, G. A., Stockdale, T., Burgman, R., Greene, A. M., Kushnir, Y., Newman, M., Carton, J., Fukumori, I., and Delworth, T.: A verification framework for interannual-to-decadal predictions experiments, Clim. Dynam., 40, 245-272, doi:10.1007/s00382-012-1481-2, 2013.

Guemas V., García-Serrano, J., Mariotti, A., Doblas-Reyes, F., and Caron, L.-Ph.: Prospects for decadal climate prediction in the Mediterranean region, Q. J. R. Meteor. Soc., 141, 580–597, doi:10.1002/qj.2379, 2015.

Hackenbruch, J., Schaedler, G., and Schipper, J. W.: Added value of high-resolution regional climate simulations for regional impact studies, Meteorol. Z., 25, 291-304, doi:10.1127/metz/2016/0701, 2016.

Haas, R., Reyers, M., and Pinto, J. G.: Decadal predictability of regional-scale peak winds over Europe based on MPI-ESM-LR, Meteorol. Z., 25, 739-752, doi:10.1127/metz/2015/0583, 2016.

Haylock, M. R., Hofstra, N., Klein Tank, A. M. G., Klok, E. J., Jones, P. D., and New, M.: A European daily high-resolution gridded data set of surface temperature and precipitation for 1950-2006, J. Geophys. Res., 113, D20119, doi:10.1029/2008JD010201, 2008.

Ho, C. K., Hawkins, E., Shaffrey, L., Bröcker, J., Hermanson, L., Murphy, J. M., Smith, D. M., and Eade, R.: Examining reliability of seasonal to decadal sea surface temperature forecasts: The role of ensemble dispersion, Geophys. Res. Lett., 40, 5770-5775, doi:10.1002/2013GL057630, 2013.

Jungclaus, J. H., Fischer, N., Haak, H., Lohmann, K., Marotzke, J., Matei, D., Mikolajewicz, U., Notz, D., and von Storch, J.-S.: Characteristics of the ocean simulations in MPIOM, the ocean component of the MPI-Earth system model, J. Adv. Model. Earth Sy., 5, 422-446, doi:10.1002/jame.20023, 2013.

Kadow, C., Illing, S., Kunst, O., Rust, H. W., Pohlmann, H., Müller, W. A., and Cubasch, U.: Evaluation of forecasts by accuracy and spread in the MiKlip decadal climate prediction system, Meteorol. Z., 25, 631-643, doi:10.1127/metz/2015/0639, 2016.

Kalnay, E., Kanamitsu, M., Kistler, R., Collins, W., Deaven, D., Gandin, L., Iredell, M., Saha, S., White, G., Woollen, J., Zhu, Y., Leetmaa, A., Reynolds, R., Chelliah, M., Ebisuzaki, W., Higgins, W., Janowiak, J., Mo, K. C., Ropelewski, C.

Wang, J., Jenne, R. and Joseph, D.: The NCEP/NCAR 40-Year Reanalysis Project, B. Am. Meteorol. Soc., 77, 437-471, doi:10.1175/1520-0477(1996)077<0437:TNYRP>2.0.CO;2, 1996.

Khodayar, S., Selinger, A., Feldmann, H., Kottmeier, Ch.: Sensitivity of soil moisture initialization for decadal predictions under different regional climatic conditions in Europe, Int. J. Climatol., 35, 1899-1915, doi: 10.1002/joc.4096, 2014.

Kothe, S., Tödter, J., and Ahrens, B.: Strategies for soil initialisation in regional decadal climate predictions, Meteorol. Z., 25, 775-794, doi:10.1127/metz/2016/0729, 2016.

Kröger, J., Müller, W. A., and von Storch, J.-S.: Impact of different ocean reanalyses on decadal climate prediction, Clim. Dynam., doi:10.1007/s00382-012-1310-7, 2012.

Kruschke, T., Rust, H. W., Kadow, C., Leckebusch, G. C., and Ulbrich, U.: Evaluating decadal predictions of northern hemispheric cyclone frequencies, Tellus A, 66, 22830, doi:10.3402/tellusa.v66.22830, 2014.

Kruschke, T., Rust, H. W., Kadow, C., Müller, W. A., Pohlmann, H., Leckebusch, G. C., and Ulbrich, U.: Probabilistic evaluation of decadal prediction skill regarding Northern Hemisphere winter storms, Meteorol. Z., 25, 721-738, doi:10.1127/metz/2015/0641, 2016.

Li, H., Ilyina, T., Müller, W. A., and Sienz, F.: Decadal predictions of the North Atlantic CO2 uptake, Nature Commun., 7, doi:10.1038/ncomms11076, 2016.

Marotzke J., Müller, W. A., Vamborg, F. S. E., Becker, P., Cubasch, U., Feldmann, H., Kaspar, F., Kottmeier, C., Marini, C., Polkova, I., Prömmel, K., Rust, H. W., Rust, H. W., Stammer, D., Ulbrich, U., Kadow, C., Köhl, A., Kröger, J., Kruschke, T., Pinto, J. G., Pohlmann, H., Reyers, M., Schröder, M., Sienz, F., Timmreck, C., and Ziese, M.: MiKlip – a National Research Project on Decadal Climate Prediction, B. Am. Meteorol. Soc., Early Online Releases, doi:10.1175/BAMS-D-15-00184.1, 2016.

Matei, D., Pohlmann, H., Jungclaus, J. H., Müller, W. A., Haak, H., and Marotzke, J.: Two tales of initializing decadal climate prediction experiments with the ECHAM5/MPI-OM model, J. Climate, 8502-8523, doi:10.1175/JCLI-D-11-00633.1, 2012.

Meehl, G. A., Goddard, L., Murphy, J., Stouffer, R. J., Boer, G., Danabasoglu, G., Dixon, K., Giorgetta, M. A., Greene, A. M., Hawkins, E., Hegerl, G., Karoly, D., Keenlyside, N. S., Kimoto, M., Kirtman, B., Navarra, A., Pulwarty, R., Smith, D., Stammer, D., and Stockdale, T.: Decadal Prediction, B. Am. Meteorol. Soc., 90, 1467-1485, doi:10.1175/2009BAMS2778.1, 2009.

Meehl, G. A., Goddard, L., Boer, G., Burgman, R., Branstator, G., Cassou, C., Corti S., Danabasoglu, G., Doblas-Reyes, F., Hawkins, E., Karspeck, A., Kimoto, M., Kumar, A., Matei, D., Mignot, J., Msadek, R., Navarra, A., Pohlmann, H., Rienecker, M., Rosati, T., Schneider, E., Smith, D., Sutton, R., Teng, H., van Oldenborgh, G. J., Vecchi, G., and Yeager, S.: Decadal Climate Prediction: An Update from the Trenches, B. Am. Meteorol. Soc., 95, 243–267, doi:10.1175/BAMS-D-12-00241.1, 2014.

Mieruch, S., Feldmann, H., Schädler, G., Lenz, C.-J., Kothe, S., and Kottmeier, C.: The regional MiKlip decadal forecast ensemble for Europe: the added value of downscaling, Geosci. Model Dev., 7, 2983-2999, doi:10.5194/gmd-7-2983-2014, 2014.

Moemken, J., Reyers, M., Buldmann, B., and Pinto, J. G.: Decadal predictability of regional scale wind speed and wind energy potentials over Central Europe, Tellus A, 68, 29199, doi:10.3402/tellusa.v68.29199, 2016.

Müller, W. A., Baehr, J., Haak, H., Jungclaus, J. H., Kröger, J., Matei, D., Notz, D., Pohlmann, H., von Storch, J.-S., and Marotzke, J.: Forecast skill of multi-year seasonal means in the decadal prediction system of the Max Planck Institute for Meteorology, Geophys. Res. Lett., 39, L22707, doi:10.1029/2012GL053326, 2012.

Pohlmann, H., Smith, D. M., Balmaseda, M. A., Keenlyside, N. S., Masina, S., Matei, D., Müller, W. A., and P. Rogel, P.: Predictability of the mid-latitude Atlantic meridional overturning circulation in a multi-model system, Clim. Dynam., 41, 775-785, doi:10.1007/s00382-013-1663-6, 2013a.

Pohlmann H., Müller, W. A., Kulkarni, K., Kameswarrao, M., Matei, D., Vamborg, F. S. E., Kadow, C., Illing, S., and Marotzke, J.: Improved forecast skill in the tropics in the new MiKlip decadal climate predictions, Geophys. Res. Lett., 40, 5798–5802, doi:10.1002/2013GL058051, 2013b.

Richardson, D.S.: Measures of skill and value of ensemble predictions systems, their interrelationship and the effect of ensemble size, Q. J. R. Meteor. Soc., 1277, 2473-2489, doi:10.1002/qj.49712757715, 2001.

Robson, J., Sutton, R., and D. Smith: Predictable climate impacts of the decadal changes in the ocean in the 1990s, J. Climate, doi:10.1175/JCLI-D-12-00827.1, 2013.

Rockel, B., Will, A., and A. Hense: The Regional Climate Model COSMO-CLM (CCLM), Meteorol. Z., 17, 347- 348, doi:10.1127/0941-2948/2008/0309, 2008.

Scaife, A. A., Arribas, A., Blockley, E., Brookshaw, A., Clark, R. T., Dunstone, N., Eade, R., Fereday, D., Folland, C. K., Gordon, M., Hermanson, L., Knight, J. R., Lea, D. J., MacLachlan, C., Maidens, A., Martin, M., Peterson, A. K., Smith, D., Vellinga, M., Wallace, E., Waters, J., and Williams, A.: Skillful long-range prediction of European and North American Winters, Geophys. Res. Lett., 41, 2514-2519, doi:10.1002/2014GL059637, 2014.

Sein, D. V., Mikolajewicz, U., Gröger, M., Fast, I., Cabos, W., Pinto, J. G., Hagemann, S., Semmler, T., Izquierdo, A., and Jacob, D.: Regionally coupled atmosphere - ocean – sea ice – marine biogeochemistry model ROM: 1. Description and validation, J. Adv. Model. Earth Sy., 7, 268–304, doi:10.1002/2014MS000357, 2015.

Sienz, F., Müller, W. A., and Pohlmann, H.: Ensemble size impact on the decadal predictive skill assessment, Meteorol. Z., 25, 6, 645–655, 2016.

Stevens, B., Giorgetta, M. A., Esch, M., Mauritsen, T., Crueger, T., Rast, S., Salzmann, M., Schmidt, H., Bader, J., Block, K., Brokopf, R., Fast, I., Kinne, S., Kornblueh, L., Lohmann, U., Pincus, R., Reichler, T., and Roeckner, E.: Atmospheric component of the MPI-M Earth System Model: ECHAM6, J. Adv. Model. Earth Sy., 5, 146-172, doi:10.1002/jame.20015, 2013.

Sutton, R. T., and Dong, B.: Atlantic Ocean influence on a shift in European climate in the 1990s, Nature Geosc., 5, 788-792, doi:10.1038/NGEO1595, 2012.

Sutton, R.T. and Hodson, D.L.R: Atlantic Ocean Forcing of North American and European Summer Climate, Science, 309, 5731, 115-118, doi:10.1126/science.1109496, 2005.

Taylor, K.E., Stouffer, R.J., and Meehl, G.A.: An Overview of CMIP5 and the Experiment Design, B. Am. Meteorol. Soc., 93, 485–498, doi:10.1175/BAMS-D-11-00094.1, 2012.

Uppala, S. M., KÅllberg, P. W., Simmons, A. J., Andrae, U., Bechtold, V. D. C., Fiorino, M., Gibson, J. K., Haseler, J., Hernandez, A., Kelly, G. A., Li, X., Onogi, K., Saarinen, S., Sokka, N., Allan, R. P., Andersson, E., Arpe, K., Balmaseda, M. A., Beljaars, A. C. M., Berg, L. Van De., Bidlot, J., Bormann, N., Caires, S., Chevallier, F., Dethof, A., Dragosavac, M., Fisher, M., Fuentes, M., Hagemann, S., Hólm, E., Hoskins, B. J., Isaksen, L., Janssen, P. A. E. M., Jenne, R., Mcnally, A. P., Mahfouf, J.-F., Morcrette, J.-J., Rayner, N. A., Saunders, R. W., Simon, P., Sterl, A., Trenberth, K. E., Untch, A., Vasiljevic, D., Viterbo, P., and Woollen, J.: The ERA-40 re-analysis. Q. J. R. Meteor. Soc., 131, 2961–3012, doi:10.1256/qj.04.176, 2005.

Wilks, D. S.: Statistical Methods in the Atmospheric Sciences, Academic Press, 3rd revised edition, 2011.

Yeager, S., Karspeck, A., Danabasoglu, G., Tribbia, J., and Teng, H.: A decadal prediction case study: Late twentieth-century North Atlantic Ocean heat content, J. Climate, 25, 5173-5189, doi:10.1175/JCLI-D-11-00595.1, 2012.

Earth Syst. Dynam. Discuss., https://doi.org/10.5194/esd-2017-70
Manuscript under review for journal Earth Syst. Dynam.
Discussion started: 4 September 2017

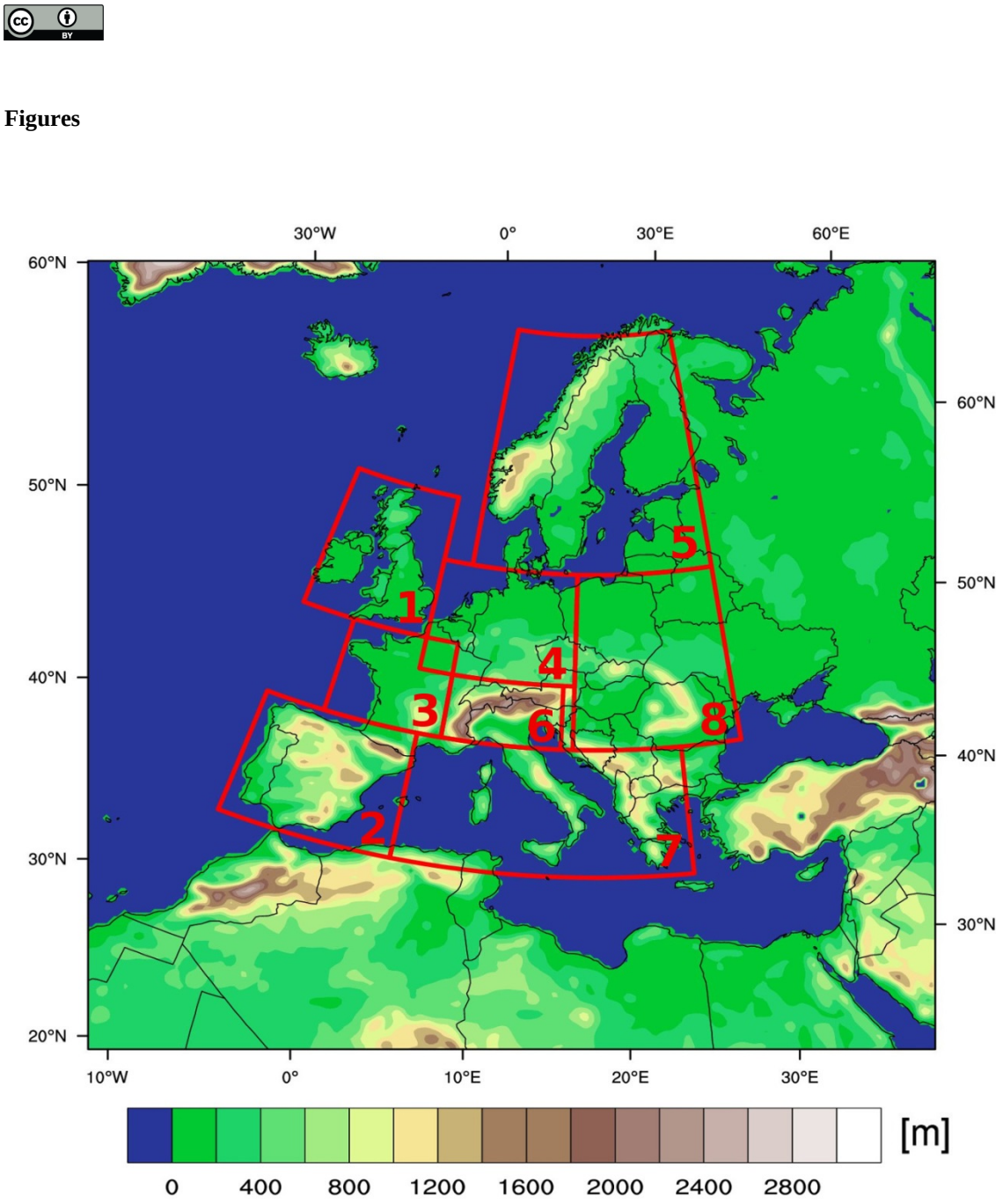

Figures

Figure 1: CCLM modelling domain (= EURO-CORDEX domain): Modell orography and PRUDENCE regions. 1: British Isles BI; 2: Iberian Peninsula IP; 3: France FR; 4: Mid-Europe ME; 5: Scandinavia SC; 6: Alps AL; 7: Mediterranean MD; 8: Eastern Europe EA.

Earth Syst. Dynam. Discuss., https://doi.org/10.5194/esd-2017-70
Manuscript under review for journal Earth Syst. Dynam.
Discussion started: 4 September 2017

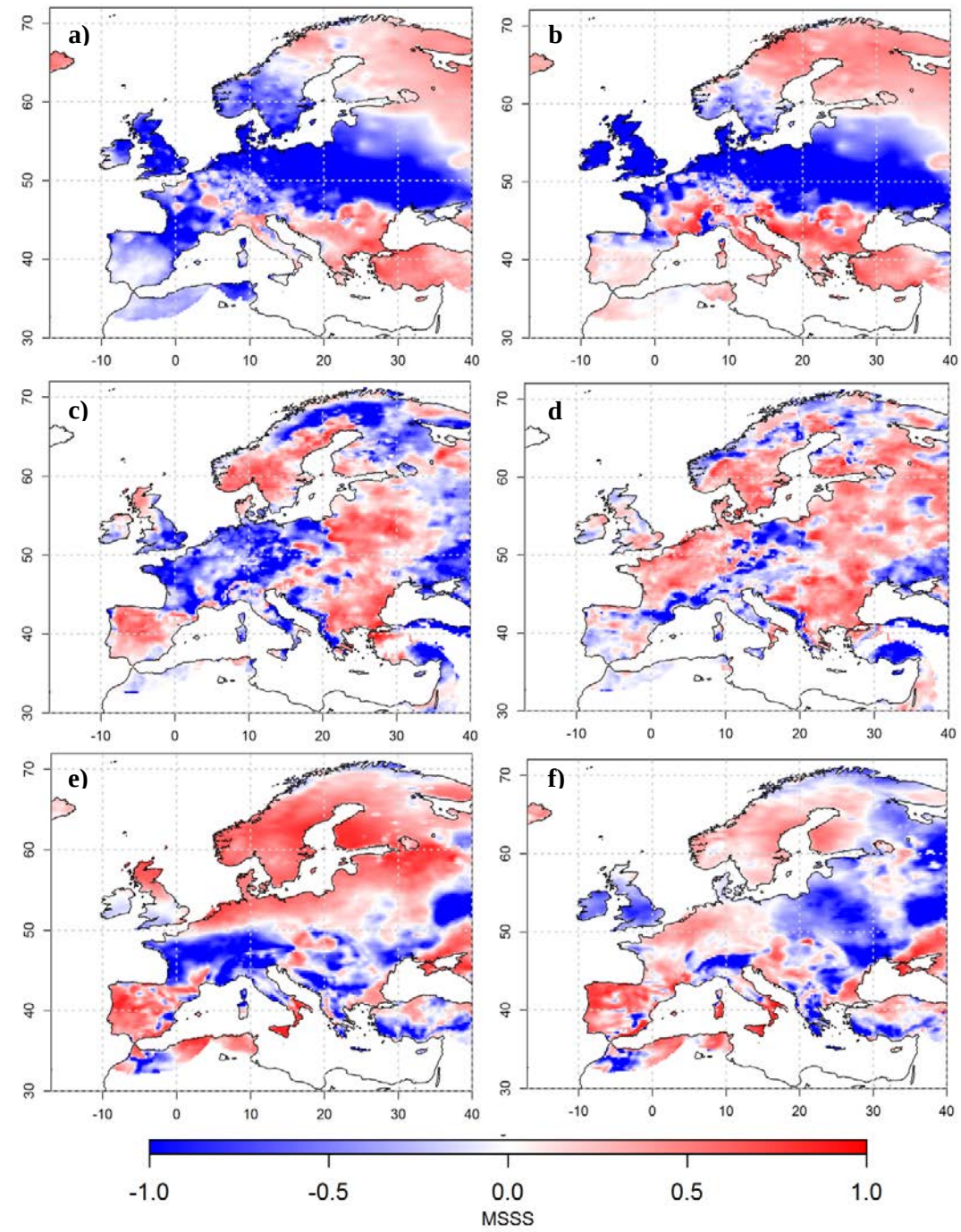

Figure 2: Spatial distribution of the MSESS for the multi-annual mean of lead years 1-5 for (a) temperature in CCLM_b0, (b) temperature in CCLM_b1, (c) precipitation in CCLM_b0, (d) precipitation in CCLM_b1, (e) wind speed in CCLM_b0, and (f) wind speed in CCLM_b1. All datasets have been de-trended, and as reference dataset we have used the uninitialized historical ensemble.

Earth Syst. Dynam. Discuss., https://doi.org/10.5194/esd-2017-70
Manuscript under review for journal Earth Syst. Dynam.
Discussion started: 4 September 2017

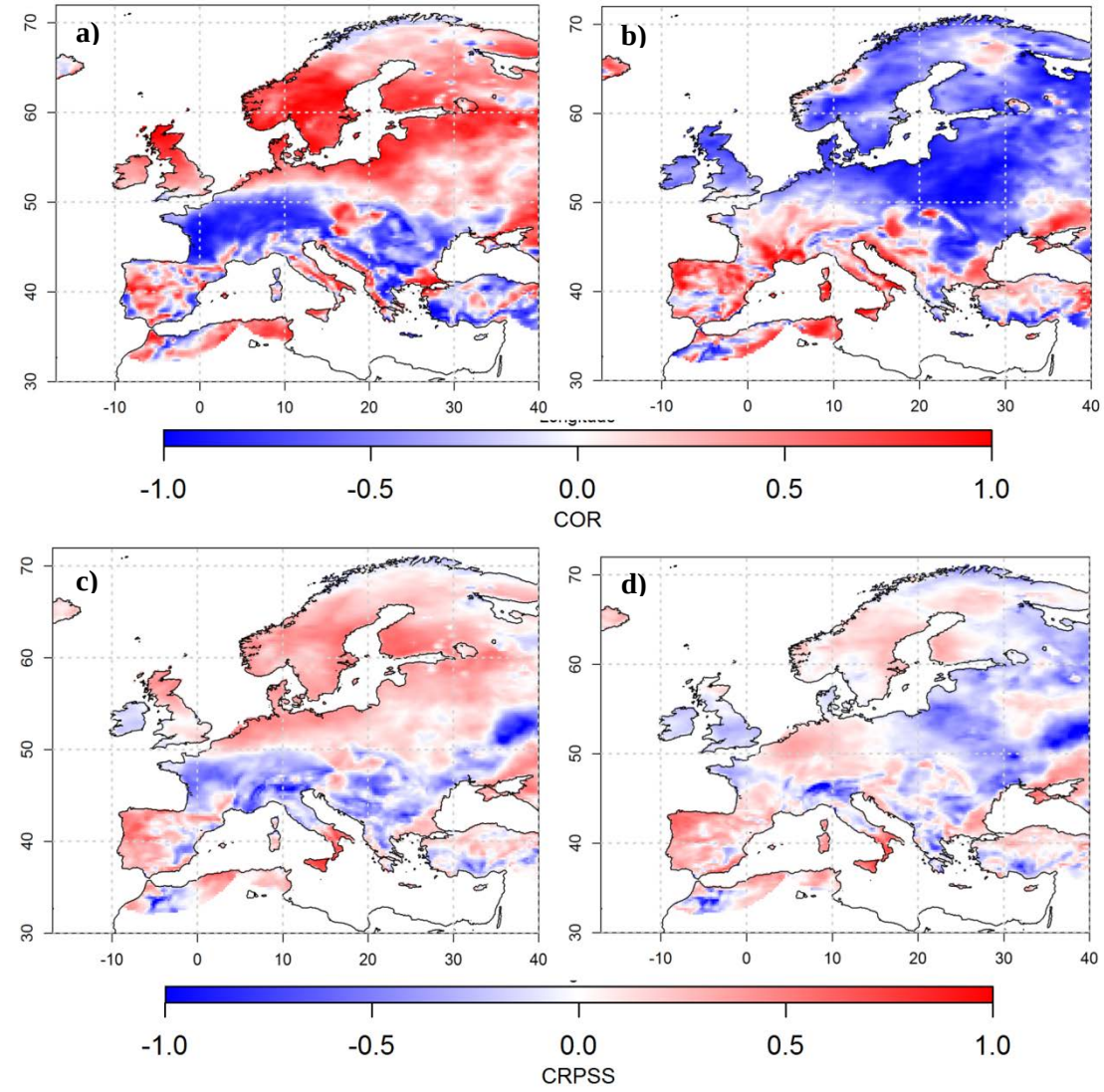

Figure 3: Spatial distribution of the skill scores for the multi-annual mean of lead years 1-5 for wind speed. (a) ACC for CCLM_b0, (b) ACC for CCLM_b1, (c) CRPSS for CCLM_b0, and (d) CRPSS for CCLM_b1. All datasets have been de-trended, and for CRPSS we have used the uninitialized historical ensemble as reference dataset.

Earth Syst. Dynam. Discuss., https://doi.org/10.5194/esd-2017-70
Manuscript under review for journal Earth Syst. Dynam.
Discussion started: 4 September 2017

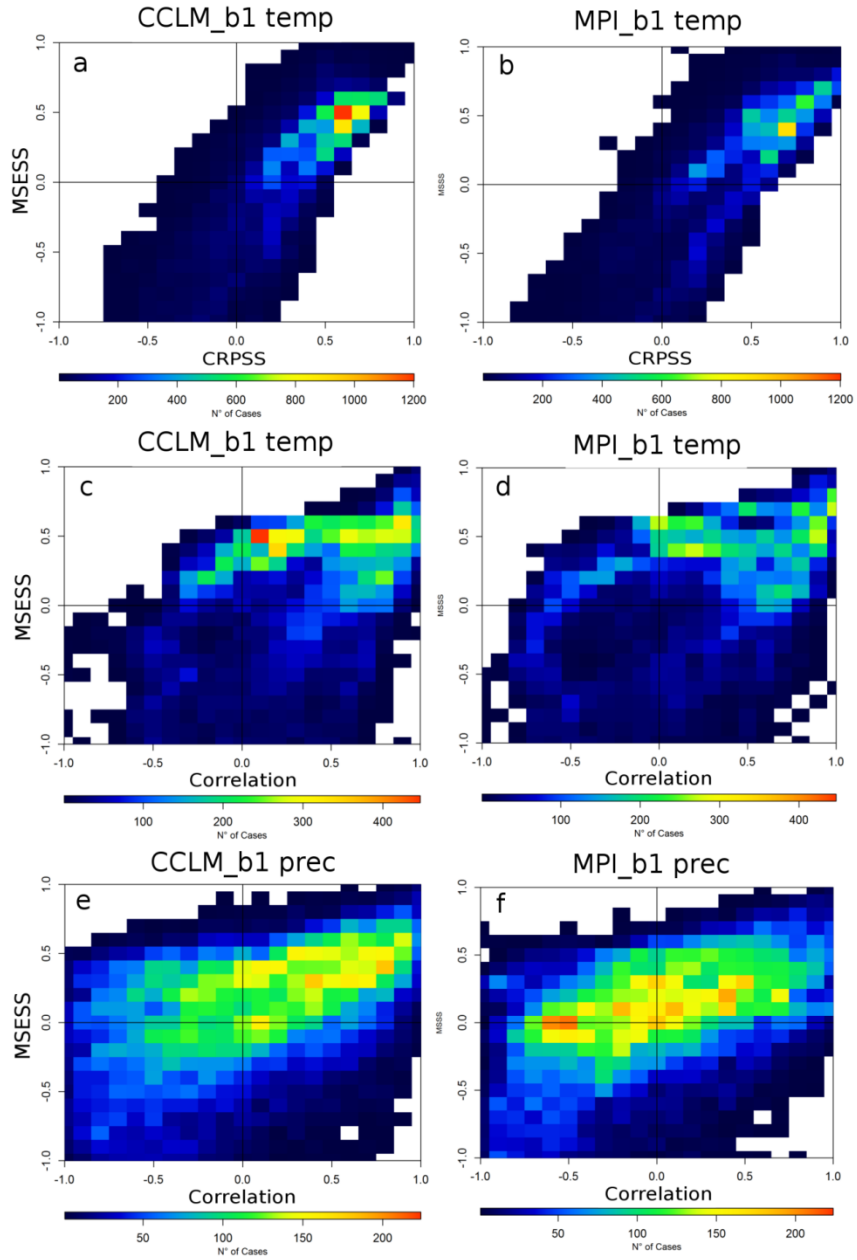

Figure 4: Scatter diagrams for CRPSS (x-axis) vs MSESS (y-axis) for temperature at all individual EURO-CORDEX grid points for the multi-annual mean of lead years 1-5 in (a) CCLM_b1 and (b) MPI_b1. (c), (d) as (a), (b) but for ACC vs MSESS for temperature. (e), (f) as (a), (b) but for ACC vs MSESS for precipitation. Colours denote the number of grid points over Europe with a given skill score combination. All datasets have been de-trended, and for MSESS and CRPSS we have used the uninitialized historical ensemble as reference dataset. Note the different scaling of the colour bars.

Earth Syst. Dynam. Discuss., https://doi.org/10.5194/esd-2017-70
Manuscript under review for journal Earth Syst. Dynam.
Discussion started: 4 September 2017

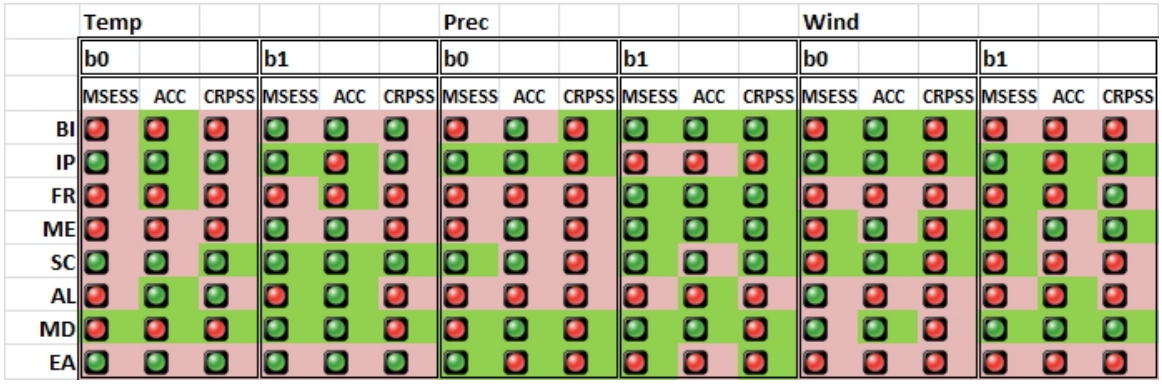

Figure 5: Predictive skill (MSESS, ACC and CRPSS) and added value of the regional MiKlip ensembles (CCLM_b0 and CCLM_b1) over the eight PRUDENCE regions (cf. Fig. 1) for temperature (left columns), precipitation (middle), and 10m-wind (right) for the multi-annual mean of lead years 1-5. Red filled boxes indicate negative skill scores, green filled boxes positive skill scores. Green dots denote an added value compared to the global forcing by MPI-ESM-LR, red dots indicate no added value by regionalization. All datasets have been de-trended, and for MSESS and CRPSS we have used the uninitialized historical ensemble as reference dataset.

Earth Syst. Dynam. Discuss., https://doi.org/10.5194/esd-2017-70
Manuscript under review for journal Earth Syst. Dynam.
Discussion started: 4 September 2017

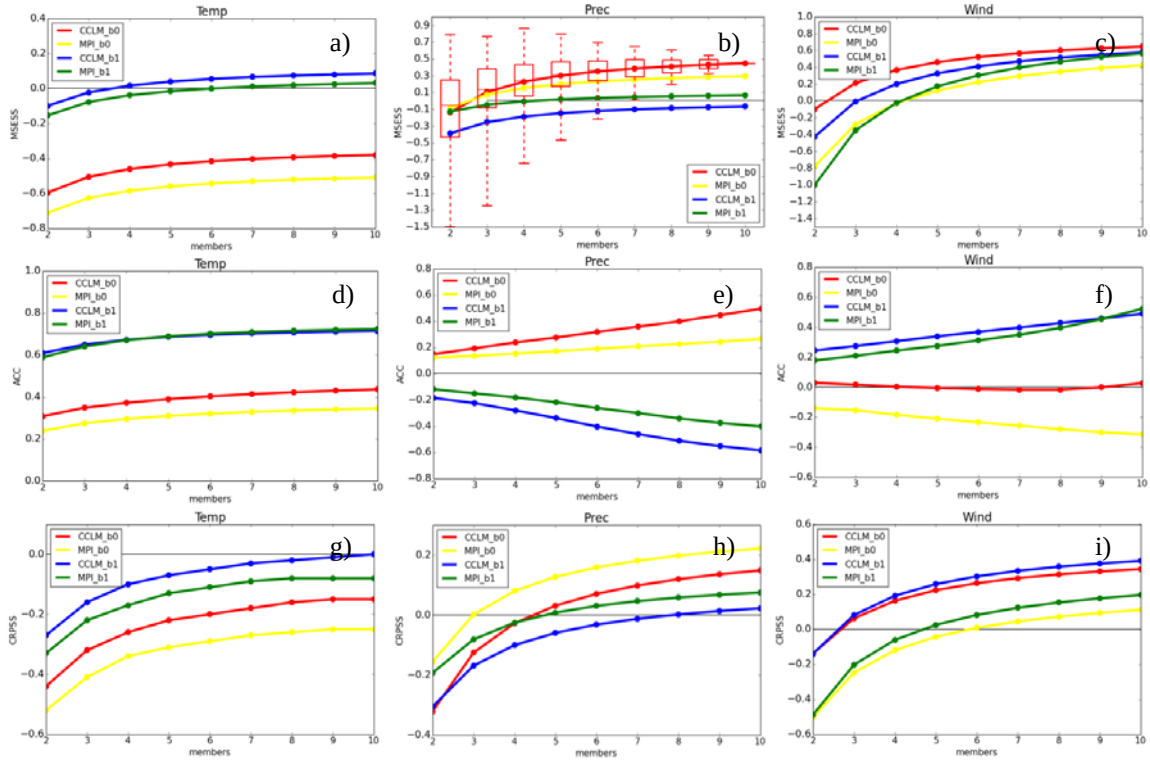

Figure 6: Skill scores for the multi-annual mean of lead years 1-5 of the CCLM_b0 (red), MPI_b0 (yellow), CCLM_b1 (blue), and MPI_b1 (green) ensembles depending on the ensemble size (x-axis, ranging from 2 to 10 members) over IP (cf. Fig. 1). MSESS for (a) temperature, (b) precipitation, and (c) wind speed; ACC for (d) temperature, (e) precipitation, and (f) wind speed; CRPSS for (g) temperature, (h) precipitation, and (i) wind speed. In (b) box-whisker plots for the skill scores of all n-member combinations are shown. All datasets have been de-trended, and for MSESS and CRPSS we have used the uninitialized historical ensemble as reference dataset. Note the different scaling of the y-axis. For details please refer to main text.

Earth Syst. Dynam. Discuss., https://doi.org/10.5194/esd-2017-70
Manuscript under review for journal Earth Syst. Dynam.
Discussion started: 4 September 2017

Earth System Dynamics Discussions
Open Access
EGU

Tables

	Temperature		Precipitation		Wind	
	dtr	tr	dtr	tr	dtr	tr
1 BI	-0.18	**0.68**	0.27	**0.49**	-0.54	-0.57
2 IP	0.71	**0.87**	-0.59	**0.19**	0.49	**0.63**
3 FR	0.69	**0.92**	0.77	0.50	0.15	**0.32**
4 ME	-0.12	**0.80**	0.64	**0.79**	-0.37	**0.04**
5 SC	0.44	**0.69**	-0.07	**0.63**	-0.63	-0.54
6 AL	0.83	**0.97**	0.37	0.18	0.10	**0.44**
7 MD	0.95	**0.96**	0.55	**0.91**	0.48	0.42
8 EA	-0.09	**0.73**	-0.10	-0.04	-0.94	-0.39

Table 1: ACC for temperature, precipitation, and wind speed in the CCLM_b1 ensemble over all eight PRUDENCE regions (cf. Fig. 1) for lead-years 1-5. De-trended 5-year averages (dtr), and 5-year averages with retained trend (tr). Lower skill scores in tr compared to dtr are marked in blue. Higher skill scores in tr compared to dtr are marked in red, and if skill scores of tr are additionally positive they are marked in bold red and underline. The uninitialized historical ensemble has been used as reference dataset. For details see main text.

Earth Syst. Dynam. Discuss., https://doi.org/10.5194/esd-2017-70
Manuscript under review for journal Earth Syst. Dynam.
Discussion started: 4 September 2017

Earth System Dynamics Discussions
Open Access
EGU

	Temperature		Precipitation		Wind	
	dtr	tr	dtr	tr	dtr	tr
1 BI	-4.58	-6.94	0.15	0.15	-0.54	-0.42
2 IP	0.09	0.11	-0.07	-0.49	0.58	**0.84**
3 FR	-0.58	-2.07	0.44	0.34	0.21	**0.56**
4 ME	-1.46	-2.40	0.44	**0.63**	0.18	0.14
5 SC	0.15	**0.32**	0.26	0.21	0.10	0.09
6 AL	0.44	**0.47**	-0.36	-0.18	-0.23	**0.19**
7 MD	0.68	**0.76**	0.68	**0.73**	0.20	**0.43**
8 EA	-1.78	-0.42	0.31	**0.36**	-0.72	**0.22**

Table 2: As Table 1, but for MSESS.

5

References

Bakker, A. H., van den Brink, H., Coelingh, J., and Bessembinder, J. (2007). Wind Energy in North-Western Europe in a changing climate. Technical report, KNMI, The Netherlands.

Barstad, I., Sorteberg, A., and dos-Santos Mesquita, M. (2012). Present and future offshore wind power potential in northern Europe based on downscaled global climate runs with adjusted SST and sea ice cover. *Renew. Energ.*, 44:398–405.

Bett, P. E., Thornton, H. E., and Clark, R. T. (2013). European wind variability over 140 yr. *Adv. Sci. Res.*, 10(1):51–58. doi:10.5194/asr-10-51-2013.

Bloom, A., Kotroni, V., and Lagouvardos, K. (2008). Climate change impact of wind energy availability in the Eastern Mediterranean using the regional climate model PRECIS. *Nat. Hazards Earth Syst. Sci.*, 8:1249–1257.

Bloomfield, H. C., Brayshaw, D. J., Shaffrey, L. C., Coker, P. J., and Thornton, H. E. (2016). Quantifying the increasing sensitivity of power systems to climate variability. *Environ. Res. Lett.*, 11:124025.

Bruckner, T., Bashmakov, I. A., Mulugetta, Y., Chum, H., de la Vega Navarro, A., Edmonds, J., Faaij, A., Fungtammasan, B., Garg, A., Hertwich, E., Honnery, D., Infield, D., Kainuma, M., Khennas, S., Kim, S., Nimir, H. B., Riahi, K., Strachan, N., Wiser, R., and Zhang, X. (2014). Energy Systems. In Edenhofer, O., Pichs-Madruga, R., Sokona, Y., Farahani, E., Kadner, S., Seyboth, K., Adler, A., Baum, I., Brunner, S., Eickemeier, P., Kriemann, B., Savolainen, J., Schlömer, S., von Stechow, C., Zwickel, T., and Minx, J. C., editors, *Climate Change 2014: Mitigation of Climate Change. Contribution of Working Group III to the Fifth Assessment Report of the Intergovernmental Panel on Climate Change*, page 516pp. Cambridge University Press, Cambridge, United Kingdom and New York, NY, USA.

Cannon, D. J., Brayshaw, D. J., Methven, J., Coker, P. J., and Lenaghan, D. (2015). Using reanalysis data to quantify extreme wind power generation statistics: a 33 year case study in Great Britain. *Renew. Energ.*, 75:767–778. doi:10.1016/j.renene.2014.10.024.

Chikamoto, Y., Kimoto, M., Ishii, M., Mochizuki, T., Sakamoto, T. T., Tatebe, H., Komuro, Y., Watanabe, M., Nozawa, T., Shiogama, H., Mori, M., Yasunaka, S., and Imada, Y. (2013). An overview of decadal climate predictability in a multi-model ensemble by climate model MIROC. *Clim. Dyn.*, 40:1201–1222.

Compo, G. P., Whitaker, J. S., Sardeshmukh, P. D., Matsui, N., Allan, R. J., Yin, X., Gleason, B. E., Vose, R. S., Rutledge, G., Bessemoulin, P., Brönniman, S., Brunet, M., Crouthamel, R. I., Grant, A. N., Groisman, P. Y., Jones, P. D., Kruk, M. C., Kruger, A. C., Marshall, G. J., Maugeri, M., Mok, H. Y., Nordli, O., Ross, T. F., Trigo, R. M., Wang, X. L., Woodruff, S. D., and Worley, S. J. (2011). The Twentieth Century Reanalysis Project. *Q. J. R. Meteorol. Soc.*, 137:1–28. doi:10.1002/qj.776.

Cradden, L. C., Harrison, G. P., and Chick, J. P. (2012). Will climate change impact on wind power development in the UK? *Clim. Chang.*, 115:837–852.

Dee, D. P., Uppala, S. M., Simmons, A. J., Berrisford, P., Poli, P., Kobayashi, S., Andrae, U., Balmaseda, M. A., Balsamo, G., Bauer, P., Bechthold, P., Beljaars, A. C. M., van de Berg, L., Bidlot, J., Bormann, N., Delsol, C., Dragani, R., Fuentes, M., Geer, A. J., Haimberger, L., Healy, S. B., Hersbach, H., Holm, E. V., Isaksen, L., Kallberg, P., Kohler, M., Matricardi, M., McNally, A. P., Monge-Sanz, B. M., Morcrette, J. J., Park, B. K., Peubey, C., de Rosnay, P., Tavolato, C., Thepaut, J. N., and Vitart, F. (2011). The ERA-Interim reanalysis: configuration and performance of the data assimilation system. *Q. J. R. Meteorol. Soc.*, 137:553–597.

Devis, A., van Lipzig, N. P. M., and Demuzere, M. (2013). A new statistical approach to downscale wind speed distributions at a site in Northern Europe. *J. Geophys. Res.*, 118(5):2272–2283. doi:10.1002/jgrd.50245.

Doblas-Reyes, F. J., Andreu-Burillo, I., Chikamoto, Y., Garcia-Serrano, J., Guemas, V., Kimoto, M., Mochizuki, T., Rodrigues, L. R. L., and van Oldenborgh, G. J. (2013). Initialized near-term regional climate change prediction. *Nat. Commun.*, 4:1715. doi:10.1038/ncomms2704.

Drew, D. R., Cannon, D. J., Brayshaw, D. J., Barlow, J. F., and Coker, P. J. (2015). The impact of future offshore wind farms on wind power generation in Great Britain. *Resources*, 4:155–171. doi:10.3390/resources4010155.

Eade, R., Smith, D., Scaife, A., Wallace, E., Dunstone, N., Hermanson, L., and Robinson, N. (2014). Do seasonal-to-decadal climate predictions underestimate the predictability of the real world? *Geophys. Res. Lett.*, 41:5620–5628. doi:10.1002/2014GL061146.

Emeis, S. (2013). *Wind Energy Meteorology.* Green Energy and Technology. Springer-Verlag, Berlin and Heidelberg. doi:10.1007/978-3-642-30523-8_1.

EWEA (2016). Wind in power - 2015 European statistics. *European Wind Energy Association Report, EWEA*, page 12p. https://windeurope.org/wp-content/uploads/files/about-wind/statistics/EWEA-Annual-Statistics-2015.pdf (accessed 12 December 2016).

Fischedick, M., Schaeffer, R., Adedoyin, A., Akai, M., Bruckner, T., Clarke, L., Krey, V., Savolainen, I., Teske, S., Ürge-Vorsatz, D., and Wright, R. (2011). Mitigation Potential and Costs. In Edenhofer, O., Pichs-Madruga, R., Sokona, Y., Seyboth, K., Matschoss, P., Kadner, S., Zwickel, T., Eickemeier, P., Hansen, G., Schlömer, S., and von Stechow, C., editors, *IPCC Special Report on Renewable Energy Sources and Climate Change Mitigation. Prepared by Working Group III of the Intergovernmental Panel on Climate Change*, page 840pp. Cambridge University Press, Cambridge, United Kingdom and New York, NY, USA.

Fuentes, U. and Heimann, D. (2000). An improved statistical-dynamical downscaling scheme and its application to the Alpine precipitation climatology. *Theor. Appl. Climatol.*, 65:119–135.

Giorgi, F., Jones, C., and Asrar, G. R. (2009). Addressing climate information needs at the regional level: the CORDEX framework. *Bulletin of the World Meteorologic Organization*, 58(3):175–183.

Goddard, L., Kumar, A., Solomon, A., Smith, D., Boer, G., Gonzalez, P., Kharin, V., Merryfield, W., Deser, C., Mason, S. J., Kirtman, B. P., Msadek, R., Sutton, R., Hawkins, E., Fricker, T., Hegerl, G., Ferro, C. A. T., Stephenson, D. B., Meehl, G. A., Stockdale, T., Burgman, R., Greene, A. M., Kushnir, Y., Newman, M., Carton, J., Fukumori, I., and Delworth, T. (2013). A verification framework for interannual-to-decadal predictions experiments. *Clim. Dyn.*, 40:245–272.

Grams, C. M., Beerli, R., Pfenninger, S., Staffell, I., and Wernli, H. (2017). Balancing Europe's wind-power output through spatial deployment informed by weather regimes. *Nat. Clim. Change*, 7:557–562.

Haas, R. and Pinto, J. G. (2012). A combined statistical and dynamical approach for downscaling large-scale footprints of European windstorms. *Geophys. Res. Lett.*, 39:L23804. doi:10.1029/2012GL054014.

Haas, R., Reyers, M., and Pinto, J. G. (2016). Decadal predictability of regional-scale peak winds over Europe using the Earth System Model of the Max-Planck-Institute for Meteorology. *Meteorol. Z.*, 25(6):739–752. doi:10.1127/metz/2015/0583.

Haugen, J. E. and Iversen, T. (2008). Response in extremes of daily precipitation and wind from a downscaled multi-model ensemble of anthropogenic global climate change scenarios. *TellusA*, 60(3):411–426.

Hewitson, B. C. and Crane, R. G. (1996). Climate downscaling: techniques and application. *Clim. Res.*, 7:85–95.

Huber, M., Dimkova, D., and Hamacher, T. (2014). Integration of wind and solar power in Europe: Assessment of flexibility requirements. *Energy*, 69:236–246.

Hueging, H., Haas, R., Born, K., Jacob, D., and Pinto, J. G. (2013). Regional changes in wind energy potential over Europe using regional climate model ensemble projections. *J. Appl. Meteor. Climatol.*, 52:903–917.

Hurrell, J. W. and van Loon, H. (1997). Decadal variations in climate associated with the North Atlantic Oscillation. *Clim. Chang.*, 36:301–326. doi:10.1023/A:1005314315270.

IEC (2005a). Wind turbines – part 1: design requirements. Technical report, International Electrotechnical Commission, Geneva, Switzerland.

IEC (2005b). Wind turbines – part 3: design requirements for offshore wind turbines. Technical report, International Electrotechnical Commission, Geneva, Switzerland.

IPCC (2012). Managing the risks of extreme events and disasters to advance climate change adaptation. In Field, C. B., Barros, V., Stocker, T. F., Qin, D., Dokken, D. J., Ebi, K. L., Mastrandrea, M. D., Mach, K. J., Plattner, G.-K., Allen, S. K., Tignor, M., and Midgley, P. M., editors, *A Special Report of Working Groups I and II of the*

Intergovernmental Panel on Climate Change, page 582pp. Cambridge University Press, Cambridge, United Kingdom and New York, NY, USA.

IPCC (2013). Summary for Policymakers. In Stocker, T. F., Qin, D., Plattner, G.-K., Tignor, M., Allen, S. K., Boschung, J., Nauels, A., Xia, Y., Bex, V., and Midgley, P. M., editors, *Climate Change 2013: The Physical Science Basis. Contribution of Working Group I to the Fifth Assessment Report of the Intergovernmental Panel on Climate Change*. Cambridge University Press, Cambridge, United Kingdom and New York, NY, USA.

Jenkinson, A. F. and Collinson, F. P. (1977). An initial climatology of gales over the North Sea. *Synoptic Climatology Branch Memorandum*, 62.

Jerez, S., Tobin, I., Vautard, R., Montávez, J. P., López-Romero, J. M., Thais, F., Bartok, B., Christensen, O. B., Colette, A., Déqué, M., Nikulin, G., Kotlarski, S., van Meijgaard, E., Teichmann, C., and Wild, M. (2015). The impact of climate change on photovoltaic power generation in Europe. *Nat. Commun.*, 6:10014. doi:10.1038/ncomms10014.

Jones, P. D., Harpham, C., and Briffa, K. R. (2012). Lamb weather types derived from reanalysis products. *Int. J. Climatol.*, 33:1129–1139.

Jones, P. D., Hulme, M., and Briffa, K. R. (1993). A comparison of Lamb circulation types with an objective classification scheme. *Int. J. Climatol.*, 13:655–663.

Kalnay, E., Kanamitsu, M., Kistler, R., Collins, W., Deaven, D., Gandin, L., Iredell, M., Saha, S., White, G., Woollen, J., Zhu, Y., Chelliah, M., Ebisuzaki, W., Higgins, W., Janowiak, J., Mo, K. C., Ropelewski, C., Wang, J., Leetmaa, A., Reynolds, R., Jenne, R., and Joseph, D. (1996). The NCEP/NCAR 40-Year Reanalysis Project. *Bull. Am. Meteorol. Soc.*, 77:437–471.

Kjellström, E., Nikulin, G., Hansson, U., Strandberg, G., and Ullerstig, A. (2011). 21st century changes in the European climate: uncertainties derived from an ensemble of regional climate model simulations. *TellusA*, 63(1):24–40.

Kraus, H. (2004). *Die Atmosphäre der Erde: Eine Einführung in die Meteorologie*. Springer-Verlag, Berlin and Heidelberg, 3. auflage edition. doi:10.1007/3-540-35017-0.

Kruschke, T., Rust, H. W., Kadow, C., Leckebusch, G. C., and Ulbrich, U. (2014). Evaluating decadal predictions of northern hemispheric cyclone frequencies. *TellusA*, 66:22830. doi:10.3402/tellusa.v66.22830.

Lamb, H. H. (1972). British Isles weather types and a register of the daily sequence of circulation patterns 1981–1971. In *Geophysical Memoir, No. 116*, page 85p. HMSO, London.

Leckebusch, G. C., Weimer, A., Pinto, J. G., Reyers, M., and Speth, P. (2008). Extreme wind storms over Europe in present and future climate: a cluster analysis approach. *Meteorol. Z.*, 17(1):67–82.

Lu, X., McElroy, M. B., and Kiviluoma, J. (2009). Global potential for wind-generated electricity. *PNAS*, 106(27):10933–10938.

Manwell, J. F., McGowan, J. G., and Rogers, A. L. (2009). *Wind Energy Explained: Theory, Design and Application*. John Wiley & Sons, Ltd, Chichester, UK, second edition edition.

Maraun, D., Wetterhall, F., Ireson, A. M., Chandler, R. E., Kendon, E. J., Widman, M., Brienen, S., Rust, H. W., Sauter, T., Themessl, M., Venema, V. K. C., Chun, K. P., Goodess, C. M., Jones, R. G., Onof, C., Vrac, M., and Thiele-Eich, I. (2010). Precipitation downscaling under climate change: Recent developments to brigge the gap between dynamical models and the end user. *Rev. Geophys.*, 48:RG3003. doi:10.1029/2009RG000314.

Marotzke, J., Müller, W. A., Vamborg, F. S. E., Becker, P., Cubasch, U., Feldmann, H., Kaspar, F., Kottmeier, C., Marini, C., Polkova, I., Prömmel, K., Rust, H. W., Stammer, D., Ulbrich, U., Kadow, C., Köhl, A., Kröger, J., Kruschke, T., Pinto, J. G., Pohlmann, H., Reyers, M., Schröder, M., Sienz, F., Timmreck, C., and Ziese, M. (2016). MiKlip: A National Research Project on Decadal Climate Prediction. *Bull. Am. Meteorol. Soc.*, 97:2379–2394. doi:10.1175/BAMS-D-15-00184.1.

Meehl, G. A., Goddard, L., Murphy, J., Stouffer, R. J., Boer, G., Danabasoglu, G., Dixon, K., Giorgetta, M. A., Greene, A. M., Hawkins, E., Hegerl, G., Karoly, D., Keenlyside, N., Kimoto, M., Kirtman, B., Navarra, A., Pulwarty, R., Smith, D., Stammer, D., and Stockdale, T. (2009). Decadal Prediction – Can it be skilful? *Bull. Am. Meteorol. Soc.*, 90:1467–1485.

Mieruch, S., Feldmann, H., Schädler, G., Lenz, C.-J., Kothe, S., and Kottmeier, C. (2014). The regional MiKlip decadal forecast ensemble for Europe: the added value of downscaling. *Geosci. Model. Dev.*, 7:2983–2999. doi:10.5194/gmd-7-2983-2014.

Moccia, J., Wilkes, J., Pineda, I., and Corbetta, G. (2014). Wind energy scenarios for 2020. *European Wind Energy Association Report, EWEA*, page 3p. http://www.ewea.org/fileadmin/files/library/publications/scenarios/EWEA-Wind-energy-scenarios-2020.pdf (accessed 12 December 2016).

Moemken, J., Reyers, M., Buldmann, B., and Pinto, J. G. (2016). Decadal predictability of regional scale wind speed and wind energy potentials over Central Europe. *TellusA*, 68:29199. doi:10.3402/tellusa.v68.29199.

Moemken, J., Reyers, M., Feldmann, H., and Pinto, J. G. (2018). Future changes of wind speed and wind energy potentials in EURO-CORDEX ensemble simulations. *J. Geophys. Res. Atmos.*, 123:6373–6389. doi:10.1029/2018JD028473.

Mömken, J. (2014). Dekadische Vorhersagbarkeit von Windenergiepotentialen für Deutschland. Master's thesis, Institute for Geophysics and Meteorology, University of Cologne, Germany.

Müller, W. A., Baehr, J., Haak, H., Jungclaus, J. H., Kröger, J., Matei, D., Notz, D., Pohlmann, H., von Storch, J.-S., and Marotzke, J. (2012). Forecast skill of multi-year seasonal means in the decadal prediction system of the Max Planck Institute for Meteorology. *Geophys. Res. Lett.*, 39:L22707. doi:10.1029/2012GL053326.

Müller, W. A., Pohlmann, H., Sienz, F., and Smith, D. (2014). Decadal climate predictions for the period 1901-2010 with a coupled climate model. *Geophys. Res. Lett.*, 41:2100–2107. doi:10.1002/2014GL059259.

Nolan, P., Lynch, P., McGrath, R., Semmler, T., and Wang, S. Y. (2012). Simulating climate change and its effect on the wind energy resource of Ireland. *Wind Energy*, 15:593–608. doi:10.1002/we.489.

Nolan, P., Lynch, P., and Sweeney, C. (2014). Simulating the future wind energy resource of Ireland using the COSMO-CLM model. *Wind Energy*, 17:19–37. doi:10.1002/we.1554.

Peixoto, J. P. and Oort, A. H. (1992). *Physics of Climate*. American Institute of Physics, New York.

Petersen, E. L., Mortensen, N. G., Landberg, L., Højstrup, J., and Frank, H. P. (1998). Wind power meteorology. Part I: climate and turbulence. *Wind Energy*, 1:25–45.

Pinto, J. G., Neuhaus, C. P., Leckebusch, G. C., Reyers, M., and Kerschgens, M. (2010). Estimation of wind storm impacts over Western Germany under future climate conditions using a statistical-dynamical downscaling approach. *TellusA*, 62:188–201.

Price, T. J. (2005). James Blyth – Britain's First Modern Wind Power Engineer. *Wind Engineering*, 29(3):191–200. doi:10.1260/030952405774354921.

Pryor, S. C. and Barthelmie, R. J. (2003). Long-term trends in near-surface flow over the Baltic. *Int. J. Climatol.*, 23:271–289. doi:10.1002/joc.878.

Pryor, S. C. and Barthelmie, R. J. (2010). Climate change impacts on wind energy: a review. *Renew. Sustainable Energy Rev.*, 14:430–437. doi:10.1016/j.rser.2009.07.028.

Pryor, S. C. and Barthelmie, R. J. (2013). Assessing the vulnerability of wind energy to climate change and extreme events. *Clim. Chang.*, 121:79–91.

Pryor, S. C., Barthelmie, R. J., Claussen, N. E., Drews, M., MacKellar, N., and Kjellström, E. (2012). Analyses of possible changes in intense and extreme wind speeds over Northern Europe under climate change scenarios. *Clim. Dyn.*, 38:189–208. doi:10.1007/s00382-010-0955-3.

Pryor, S. C., Barthelmie, R. J., and Kjellström, E. (2005a). Analyses of the potential climate change impact on wind energy resources in northern Europe using output from a regional climate model. *Clim. Dyn.*, 25:815–835.

Pryor, S. C., Schoof, J. T., and Barthelmie, R. J. (2005b). Climate change impacts on wind speeds and wind energy density in Northern Europe: empirical downscaling of multiple AOGCMs. *Clim. Res.*, 29:183–198.

Pryor, S. C., Schoof, J. T., and Barthelmie, R. J. (2005c). Empirical downscaling of wind speed probability distributions. *J. Geophys. Res.*, 110:D19109. doi:10.1029/2005JD005899.

Räisänen, J., Hansson, U., Ullerstig, A., Döscher, R., Graham, L. P., Jones, C., Meier, H. E. M., Samuelsson, P., and Willén, U. (2004). European climate in the late twenty-first century: regional simulations with two driving global models and two forcing scenarios. *Clim. Dyn.*, 22:13–31.

Räisänen, J., Rummukainen, M., and Ullerstig, A. (2001). Downscaling of greenhouse gas induced climate change in two GCMs with the Rossby Centre regional climate model for northern Europe. *TellusA*, 53:168–191. doi:10.1034/j.1600-0870.2001.00168.x.

Reyers, M., Feldmann, H., Mieruch, S., Pinto, J. G., Uhlig, M., Ahrens, B., Früh, B., Kameshvar, M., Laube, N., Moemken, J., Müller, W. A., Schädler, G., and Kottmeier, C. (2017). Development and prospects of the regional MiKlip decadal prediction system over Europe: Predictive skill, added value of regionalization and ensemble size dependency. *Earth Syst. Dynam. Discussions*. doi:10.5194/esd-2017-70, in review.

Reyers, M., Moemken, J., and Pinto, J. G. (2016). Future changes of wind energy potentials over Europe in a large CMIP5 multi-model ensemble. *Int. J. Climatol.*, 36:783–796. doi:10.1002/joc.4382.

Reyers, M., Pinto, J. G., and Moemken, J. (2015). Statistical-dynamical downscaling for wind energy potentials: evaluation and applications to decadal hindcasts and climate change projections. *Int. J. Climatol.*, 35:229–244. doi:10.1002/joc.3975.

Rockel, B., Will, A., and Hense, A. (2008). Special issue: regional climate modelling with COSMO-CLM (CCLM). *Meteorol. Z.*, 17:347–348.

Rodriguez, R. A., Becker, S., Andresen, G. B., Heide, D., and Greiner, M. (2014). Transmission needs across a fully renewable European power system. *Renew. Energ.*, 63:467–476.

Seaby, L. P., Refsgaard, J. C., Sonnenborg, T. O., Stisen, S., Christensen, J. H., and Jensen, K. H. (2013). Assessment of robustness and significance of climate change signals for an ensemble of distribution-based scaled climate projections. *J. Hydrol*, 486:479–493.

Smith, D. M., Cusack, S., Colman, A. W., Folland, C. K., Harris, G. R., and Murphy, J. M. (2007). Improved surface temperature prediction for the coming decade from a global circulation model. *Science*, 317:796–799.

Solomon, S., Qin, D., Manning, M., Chen, Z., Marquis, M., Averyt, K., Tignor, M. M. B., and Jr, H. L. M., editors (2007). *Climate Change 2007: The Physical Science Basis*. Cambridge University Press.

Stull, R. B. (1988). *Introduction to Boundary-Layer Meteorology*. Kluwer Academic Publishers, Boston.

Taylor, K. E., Stouffer, R. J., and Meehl, G. A. (2012). An overview of CMIP5 and the experiment design. *Bull. Am. Meteorol. Soc.*, 93:485–498. doi:10.1175/BAMS-D-11-00094.1.

Teixeira, J., Stevens, B., Bretherton, C. S., Cederwall, R., Doyle, J. D., Golaz, J. C., Holtslag, A. A. M., Klein, S. A., Lundquist, J. K., Randall, D. A., Siebesma, A. P., and Soares, P. M. M. (2008). Parameterization of the Atmospheric Boundary Layer: A View from Just Above the Inversion. *Bull. Am. Meteorol. Soc.*, 89:453–458.

Tobin, I., Jerez, S., Vautard, R., Thais, F., van Meijgaard, E., Prein, A., Déqué, M., Kotlarski, S., Maule, C. F., Nikulin, G., Noel, T., and Teichmann, C. (2016). Climate change impacts on the power generation potential of a European mid-century wind farms scenario. *Environ. Res. Lett.*, 11:034013. doi:10.1088/1748-9326/11/3/034013.

Tobin, I., Vautard, R., Balog, I., Bréon, F.-M., Jerez, S., Ruti, P. M., Thais, F., Vrac, M., and Yiou, P. (2015). Assessing climate change impacts on European wind energy from ENSEMBLES high-resolution climate projections. *Clim. Chang.*, 128:99–112.

Trigo, R. M., Osborn, T. J., and Corte-Real, J. M. (2002). The North Atlantic Oscillation influence on Europe: climate impacts and associated physical mechanisms. *Clim. Res.*, 20:9–17. doi:10.3354/cr020009.

Troen, I. and Petersen, E. L. (1989). *European Wind Atlas*. Risø National Laboratory, Roskilde.

Uppala, S. M., Kallberg, P. W., Simmons, A. J., Andrae, U., Bechtold, V. D. C., Fiorino, M., Gibson, J. K., Haseler, J., Hernandez, A., Kelly, G. A., Li, X., Onogi, K., Saarinen, S., Sokka, N., Allan, R. P., Andersson, E., Arpe, K., Balmaseda, M. A., Beljaars, A. C. M., Berg, L. V. D., Bidlot, J., Bormann, N., Caires, S., Chevallier, F., Dethof, A., Dragosavac, M., Fisher, M., Fuentes, M., Hagemann, S., Hölm, E., Hoskins, B. J., Isaksen, L., Janssen, P. A. E. M., Jenne, R., Mcnally, A. P., Mahfouf, J.-F., Morcrette, J.-J., Rayner, N. A., Saunders, R. W., Simon, P., Sterl, A., Trenberth, K. E., Untch, A., Vasiljevic, D., Viterbo, P., and Woollen, J. (2005). The ERA-40 re-analysis. *Q. J. R. Meteorol. Soc.*, 131:2961–3012. doi:10.1256/qj.04.176.

van Oldenborgh, G. J., Doblas-Reyes, F. J., Wouters, B., and Hazeleger, W. (2012). Decadal prediction skill in a multi-model ensemble. *Clim. Dyn.*, 38:1263–1280.

Vautard, R., Cattiaux, J., Yiou, P., Thépaut, J.-N., and Ciais, P. (2010). Northern Hemisphere atmospheric stilling partly attributed to an incease in surface roughness. *Nat. Geosci.*, 3(11):756–761. doi:10.1038/ngeo979.

Vautard, R., Thais, F., Tobin, I., Bréon, F.-M., de Lavergne, J.-G. D., Colette, A., Yiou, P., and Ruti, P. M. (2014). Regional climate model simulations indicate limited climatic impacts by operational and planned European wind farms. *Nat. Commun.*, 5:3196. doi:10.1038/ncomms4196.

von Bremen, L. and Lange, M. (2011). Ensembleprognosen der Windleistung für Anwendungen in der Energiewirtschaft. *Probabilistische Wettervorhersage, promet*, 37:62–71.

Weber, J., Wohland, J., Reyers, M., Moemken, J., Hoppe, C., Pinto, J. G., and Witthaut, D. (2018). Impact of climate change on backup energy and storage needs in wind-dominated power systems in Europe. *PLOS ONE*. doi:10.1371/journal.pone.0201457, accepted.

Wilby, R. L., Charles, S. P., Zorita, E., Timbal, B., Whetton, P., and Mearns, L. O. (2004). Guidelines for Use of Climate Scenarios Developed from Statistical Downscaling Methods. *IPCC Report*. Supporting material, published online.

Wilby, R. L. and Wigley, T. M. L. (1997). Downscaling general circulation model output: a review of methods and limitations. *Prog. Phys. Geog.*, 21:530–548.

Wilkes, J., Moccia, J., and Dragan, M. (2012). Wind in power – 2011 European statistics. *European Wind Energy Association Report, EWEA*, page 11p.

Wiser, R., Yang, Z., Hand, M., Hohmeyer, O., Infield, D., Jensen, P. H., Nikolaev, V., O'Malley, M., Sinden, G., and Zervos, A. (2011). Wind energy. In Edenhofer, O., Pichs-Madruga, R., Sokona, Y., Seyboth, K., Matschoss, P., Kadner, S., Zwickel, T., Eickemeier, P., Hansen, G., Schlömer, S., and von Stechow, C., editors, *IPCC Special Report on Renewable Energy Sources and Climate Change Mitigation*. Cambridge University Press, Cambridge, United Kingdom and New York, NY, USA.

Wohland, J., Reyers, M., Weber, J., and Witthaut, D. (2017). More homogeneous wind conditions under strong climate change decrease the potential for inter-state balancing of electricity in Europe. *Earth Syst. Dynam.*, 8:1047–1060. doi:10.5194/esd-8-1047-2017.

Yan, Z., Bate, S., Chandler, R. E., Isham, V., and Wheater, H. (2002). An Analysis of Daily Maximum Wind Speed in Northwestern Europe Using Generalized Linear Models. *J. Clim.*, 15:2073–2088.

List of Abbreviations

A	anti-cyclonic
AW	anti-cyclonic/west
A1B	emission scenario
C	cyclonic
CCLM	COSMO-CLM
CMIP5	Coupled Model Intercomparison Project Phase 5
CORDEX	Coordinated Regional Downscaling Experiment
COSMO-CLM	Consortium for small scale modelling in climate mode
CWT	circulation weather type
DD	dynamical downscaling
DJF	December, January, February
DWD	German Weather Service, 'Deutscher Wetterdienst'
E	east
Eout	wind energy output
ERA-Interim	ECMWF Reanalysis, INTERIM period 1979-now
ERA-40	ECMWF Reanalysis, period 1957-2002
EURO-CORDEX	European branch of CORDEX
GCM	global climate model
GERICS	German Climate Service Center
HZG	Helmholtz-Zentrum Geesthacht
IEC	International Electrotechnical Commission
IPCC	International Panel on Climate Change
JJA	June, July, August
LWT	Lamb weather type
MAM	March, April, May
MiKlip	decadal climate predictions, 'Mittelfristige Klimaprognosen'
MPI-ESM	Max-Planck-Institute Earth System Model
MSE	mean squared error
MSLP	mean-sea-level pressure

MW	mega watt
MWh	mega watt hours
N	north
NAO	North Atlantic Oscillation
NCEP	National Center for Environmental Prediction
NE	northeast
NW	northwest
N117	N117 wind turbine by Nordex
PDF	probability density function
RCM	regional climate model
RCP	representative concentration pathways, emission scenario
REMO	Regional Modell
S	south
SD	statistical downscaling
SDD	statistical-dynamical downscaling
SE	southeast
SON	September, October, November
SW	southwest
V112	V112 wind turbine by Vestas
W	west
WED	wind energy density
yr1-3	first to third year after initialisation
20C	control simulation for present climate

Danksagung

An dieser Stelle möchte ich mich bei allen bedanken, die mich die letzten Jahre begleitet und unterstützt haben.
Als Erstes danke ich meinem Doktorvater Prof. Dr. Joaquim Pinto sowie Prof. Dr. Yaping Shao für die Betreuung und Begutachtung dieser Arbeit.
Joaquim - vielen Dank für deine Unterstützung und dein Vertrauen, die vielen anregenden Diskussionen und die konstruktive Kritik, und natürlich für die Möglichkeit meine wissenschaftliche Laufbahn in Karlsruhe fortzusetzen.

Des Weiteren möchte ich mich bei Dr. Mark Reyers und Hendrik Feldmann für die Mitbetreuung bedanken.
Mark – vielen Dank für deine Hilfe bei allen Problemen und Fragen (auch über die neue Entfernung hinweg), die Unterstützung/Beteiligung an den Publikationen und natürlich das Korrekturlesen dieser Arbeit.
Hendrik – vielen Dank für alle Erklärungen, die Unterstützung beim letzten Paper und das Korrekturlesen.

Außerdem danke ich Dr. Karin Boessenkool von der Graduiertenschule GSGS, besonders für die Unterstützung bei den Problemen während der letzten Phase dieser Arbeit.

Vielen Dank auch an alle neuen und alten Kollegen in Karlsruhe und Köln für die tolle Arbeitsatmosphäre und die Hilfsbereitschaft.
Melle – vielen Dank für deine Hilfe und das Korrekturlesen dieser Arbeit.
Sven und Gabi – danke für die Unterstützung bei allen (besonders plötzlich auftauchenden) Computer- und Programmierproblemen.
Natalie – dank dir habe ich mich in Karlsruhe direkt willkommen gefühlt.

Schließlich möchte ich mich ganz besonders bei meiner Familie und meinen Freunden bedanken.
Mama – vielen Dank für deine Liebe, dein Vertrauen, deine Geduld, die viele Aufmunterung und Motivation, und so vieles mehr.
Papa – du hast mir so viel mitgegeben und ich weiß, du wärst jetzt sehr stolz.

Beiträge zu den Publikationen

Reyers, M., Moemken, J., and Pinto, J. G. (2016). Future changes of wind energy potentials over Europe in a large CMIP5 multi-model ensemble. *Int. J. Climatol.*, 36:783–796. doi:10.1002/joc.4382

Die Idee zur Untersuchung zukünftiger Änderungen von Windenergiepotentialen in einem großen Ensemble von Globalmodellen und das Konzepts für diese Veröffentlichung wurden in Zusammenarbeit mit M. Reyers und J. G. Pinto entwickelt. Die Auswertung und Analyse der Daten im Rahmen der Veröffentlichung wurden überwiegend von mir durchgeführt. Außerdem wurden die Grafiken und Bilder größtenteils von mir erstellt. Der erste Textentwurf stammt von mir und M. Reyers. Der Text wurde in Zusammenarbeit mit J. G. Pinto fertiggestellt.

Moemken, J., Reyers, M., Feldmann, H., and Pinto, J. G. (2018). Future changes of wind speed and wind energy potentials in EURO-CORDEX ensemble simulations. *J. Geophys. Res. Atmos.*, 123:6373–6389. doi:10.1029/2018JD028473

Die Idee, den Einfluss des Klimawandels auf Windenergiepotentiale in Europa in einem größeren Regionalmodell-Ensemble zu untersuchen, wurde mit J. G. Pinto und M. Reyers entwickelt. Das Konzept der Veröffentlichung wurde mit J. G. Pinto erstellt, sämtliche Auswertungen wurden von mir durchgeführt. Ebenso habe ich alle Grafiken und Bilder erstellt. Die Interpretation der Ergebnisse im Sinne des Multimodell-Ensembles wurde zusätzlich mit H. Feldmann diskutiert, der über starke Expertise in diesem Bereich verfügt. Der Text wurde von mir ausgearbeitet und in Zusammenarbeit mit den Koautoren fertiggestellt.

Moemken, J., Reyers, M., Buldmann, B., and Pinto, J. G. (2016). Decadal predictability of regional scale wind speed and wind energy potentials over Central Europe. *TellusA*, 68:29199. doi:10.3402/tellusa.v68.29199

Die Idee, die dekadische Vorhersagbarkeit von Windgeschwindigkeiten und Windenergiepotentialen in Deutschland zu untersuchen, stammt von J. G. Pinto und mir. Das Konzept für diese Veröffentlichung wurde zusammen mit M. Reyers und J. G. Pinto entwickelt. Die Auswertungen wurden größtenteils von mir durchgeführt, ein Teil wurde von B. Buldmann ergänzt. Die Abbildungen wurden allesamt von mir erstellt. Der Text wurde von mir ausgearbeitet und in Zusammenarbeit mit J. G. Pinto und M. Reyers fertiggestellt.

Reyers, M., Pinto, J. G., and Moemken, J. (2015). Statistical-dynamical downscaling for wind energy potentials: evaluation and applications to decadal hindcasts and climate change projections. *Int. J. Climatol.*, 35:229–244. doi:10.1002/joc.3975

Das Konzept für diesen Artikel wurde von M. Reyers und J. Pinto entwickelt. Die Auswertung und Analyse der Daten wurde von M. Reyers und mir durchgeführt. Der erste Textentwurf stammt von M. Reyers und wurde in Zusammenarbeit mit J. Pinto und mir fertiggestellt.

Weber, J., Wohland, J., Reyers, M., Moemken, J., Hoppe, C., Pinto, J. G., and Witthaut, D. (2018). Impact of climate change on backup energy and storage needs in wind-dominated power systems in Europe. *PLOS ONE*. doi:10.1371/journal.pone.0201457, accepted

Das Konzept für diesen Artikel hat D. Witthaut entwickelt. Die Simulationen und die Datenanalyse stammen von J. Weber und J. Wohland. Die Analyse der CWTs in den globalen Daten wurde von mir und M. Reyers durchgeführt und Daten für weitere Berechnungen J. Weber von mir zur Verfügung gestellt (Publikationen Reyers et al. (2016) und Moemken et al. (2018)). Die meteorologische Interpretation der Ergebnisse stammt ebenfalls von mir und M. Reyers. Der Text ist in enger Zusammenarbeit aller Autoren entstanden.

Reyers, M., Feldmann, H., Mieruch, S., Pinto, J. G., Uhlig, M., Ahrens, B., Früh, B., Kameshvar, M., Laube, N., Moemken, J., Müller, W. A., Schädler, G., and Kottmeier, C. (2017). Development and prospects of the regional MiKlip decadal prediction system over Europe: Predictive skill, added value of regionalization and ensemble size dependency. *Earth Syst. Dynam. Discussions*. doi:10.5194/esd-2017-70, in review

Das Konzept für diesen Artikel stammt von M. Reyers, H. Feldmann, S. Mieruch und M. Uhlig. Die Datenanalyse wurde von M. Reyers, H. Feldmann, S. Mieruch, M. Uhlig, N. Laube und mir durchgeführt, wobei ich die Untersuchungen zur Windgeschwindigkeit übernommen habe. Der erste Textentwurf stammt von M. Reyers, H. Feldmann und J. Pinto. Alle Autoren waren an Ideen, der Interpretation der Ergebnisse und der Fertigstellung des Manuskripts beteiligt.

Erklärung

Ich versichere, dass ich die von mir vorgelegte Dissertation selbstständig angefertigt, die benutzten Quellen und Hilfsmittel vollständig angegeben und die Stellen der Arbeit – einschließlich Tabellen, Karten und Abbildungen – , die anderen Werken im Wortlaut oder dem Sinn nach entnommen sind, in jedem Einzelfall als Entlehnung kenntlich gemacht habe; dass diese Dissertation noch keiner anderen Fakultät oder Universität zur Prüfung vorgelegen hat; dass sie – abgesehen von unten angegebenen Teilpublikationen – noch nicht veröffentlicht worden ist, sowie, dass ich eine solche Veröffentlichung vor Abschluss des Promotionsverfahrens nicht vornehmen werde. Die Bestimmungen der Promotionsordnung sind mir bekannt. Die von mir vorgelegte Dissertation ist von Prof. Dr. Joaquim Pinto betreut worden.

Nachfolgend genannte Teilpublikationen liegen vor:

Reyers, M., Pinto, J. G., and Moemken, J. (2015). Statistical-dynamical downscaling for wind energy potentials: evaluation and applications to decadal hindcasts and climate change projections. *Int. J. Climatol.*, 35:229–244. doi:10.1002/joc.3975

Reyers, M., Moemken, J., and Pinto, J. G. (2016). Future changes of wind energy potentials over Europe in a large CMIP5 multi-model ensemble. *Int. J. Climatol.*, 36:783–796. doi:10.1002/joc.4382

Moemken, J., Reyers, M., Buldmann, B., and Pinto, J. G. (2016). Decadal predictability of regional scale wind speed and wind energy potentials over Central Europe. *TellusA*, 68:29199. doi:10.3402/tellusa.v68.29199

Moemken, J., Reyers, M., Feldmann, H., and Pinto, J. G. (2018). Future changes of wind speed and wind energy potentials in EURO-CORDEX ensemble simulations. *J. Geophys. Res. Atmos.*, 123:6373–6389. doi:10.1029/2018JD028473

Weber, J., Wohland, J., Reyers, M., Moemken, J., Hoppe, C., Pinto, J. G., and Witthaut, D. (2018). Impact of climate change on backup energy and storage needs in wind-dominated power systems in Europe. *PLOS ONE*. doi:10.1371/journal.pone.0201457, accepted

Reyers, M., Feldmann, H., Mieruch, S., Pinto, J. G., Uhlig, M., Ahrens, B., Früh, B., Kameshvar, M., Laube, N., Moemken, J., Müller, W. A., Schädler, G., and Kottmeier, C. (2017). Development and prospects of the regional MiKlip decadal prediction system over Europe: Predictive skill, added value of regionalization and ensemble size dependency. *Earth Syst. Dynam. Discussions*. doi:10.5194/esd-2017-70, in review

Karlsruhe, den 23. Juli 2018

(Julia Mömken)